2012

Development of System Reliability Models for Railway Bridges

Andrzej S. Nowak Ph.D.
University of Nebraska-Lincoln, asn0007@auburn.edu

Anna Maria Rakoczy Ph.D.
University of Nebraska-Lincoln, arakoczy1@gmail.com

MID-AMERICA
TRANSPORTATION CENTER

Report # MATC-UNL: 426

Final Report
25-1121-0001-426

Development of System Reliability Models for Railway Bridges

Andrzej S. Nowak, Ph.D.
Professor
Department of Civil Engineering
University of Nebraska-Lincoln

Anna Maria Rakoczy, Ph.D. Candidate
Graduate Research Assistant

2012

A Cooperative Research Project sponsored by the
U.S. Department of Transportation Research and
Innovative Technology Administration

Development of System Reliability Models for Railway Bridges

Andrzej S. Nowak, Ph.D.
Professor
Civil Engineering
University of Nebraska-Lincoln

Anna M. Rakoczy
Ph.D. Candidate
Civil Engineering
University of Nebraska-Lincoln

A Report on Research Sponsored by

Mid-America Transportation Center

University of Nebraska-Lincoln

July 2012

Technical Report Documentation Page

1. Report No. 25-1121-0001-426	2. Government Accession No.	3. Recipient's Catalog No.
4. Title and Subtitle Development of System Reliability Models for Railway Bridges		5. Report Date July 2012
		6. Performing Organization Code
7. Author(s) Andrzej S. Nowak and Anna M. Rakoczy		8. Performing Organization Report No. 25-1121-0001-426
9. Performing Organization Name and Address Mid-America Transportation Center 2200 Vine St. PO Box 830851 Lincoln, NE 68583-0851		10. Work Unit No. (TRAIS)
		11. Contract or Grant No.
12. Sponsoring Agency Name and Address Research and Innovative Technology Administration 1200 New Jersey Ave., SE Washington, D.C. 20590		13. Type of Report and Period Covered July 2012
		14. Sponsoring Agency Code MATC TRB RiP No. 28686
15. Supplementary Notes		

16. Abstract
Performance of the railway transportation network depends on the reliability of railway bridges, which can be affected by various forms of deterioration and extreme environmental conditions. More than half of the railway bridges in US were built before 1950 and many show signs of distress. There is a need for efficient methods to evaluate the safety reserve in the railway bridges by identification of the most sensitive parts of the bridge. An accurate estimation of remaining fatigue life of a structural component is very important in prioritizing bridge rehabilitation and replacement. However, existing procedures to evaluate the fatigue behavior of bridges are based on estimation rather than the exact formulas because the load and the resistance models contain many uncertainties. Therefore, probabilistic methods are the most convenient way to provide levels of safety for various design cases. The objective of this study is to develop a reliability model for railway bridges, in particular for the fatigue and strength limit states. It will be demonstrated on two through-plate girder structures. The research involved nonlinear finite element method (FEM) analysis of typical railway bridges, development of statistical parameters of live load and resistance, and calculation of a reliability index for various considered conditions. The findings of this research with final conclusions will serve as a basis for the development of more rational provisions for the design and evaluation of railway bridges.

17. Key Words railway bridges, FEM analysis, reliability index		18. Distribution Statement	
19. Security Classif. (of this report) Unclassified	20. Security Classif. (of this page) Unclassified	21. No. of Pages 199	22. Price

Table of Contents

List of Figures

List of Tables

Abstract

Performance of the railway transportation network depends on the reliability of railway bridges, which can be affected by various forms of deterioration and extreme environmental conditions. More than half of the railway bridges in US were built before 1950 and many show signs of distress. There is a need for efficient methods to evaluate the safety reserve in the railway bridges by identification of the most sensitive parts of the bridge.

An accurate estimation of remaining fatigue life of a structural component is very important in prioritizing bridge rehabilitation and replacement. However, existing procedures to evaluate the fatigue behavior of bridges are based on estimation rather than the exact formulas because the load and the resistance models contain many uncertainties. Therefore, probabilistic methods are the most convenient way to provide levels of safety for various design cases.

The objective of this study is to develop a reliability model for railway bridges, in particular for the fatigue and strength limit states. It will be demonstrated on two through-plate girder structures. The research involved nonlinear finite element method (FEM) analysis of typical railway bridges, development of statistical parameters of live load and resistance, and calculation of a reliability index for various considered conditions. The findings of this research with final conclusions will serve as a basis for the development of more rational provisions for the design and evaluation of railway bridges.

Chapter 1 Introduction

1.1 Problem Statement

Performance of the railway transportation network depends on the reliability of railway bridges. They are subjected to static and dynamic loads caused by moving trains. Moreover, railway bridges are vulnerable to extreme environmental exposure and load effect while in service. Special attention should be paid to the evaluation of existing bridges since more than half of those in the US were built before 1950.

Railway bridges constitute a vital part of the transportation infrastructure system and they require special attention to provide safe and economical service. The design and rating procedures for railway bridges are included in the Manual for Railway Engineering published by the American Railway Engineering and Maintenance-of-Way Association (AREMA). According to the AREMA Manual, bridge owners have to perform periodic bridge inspections, at least annually by qualified inspectors, to determine whether the structure satisfies the required design or rating conditions. More detailed instructions of inspections are provided by the Federal Railroad Administration, part 327–Bridge Safety Standards. However, the rating condition for a particular bridge is not sufficient for prioritization of structures for repair or replacement, as it depends on many factors. On one side there are the load rating criteria, and on the other side there is structural deterioration. Additionally, environmental and climate conditions have a considerable influence on structure members.

The question is how to measure the level of safety based on the inspection findings. This involves determining how to prioritize inspection findings; for example, what is a low, medium and high level of corrosion, or how many loose connections can lead to failure. The question is

how to measure the level of safety. Therefore, it is proposed that the probability of failure be used as a prioritization criterion for bridge repair.

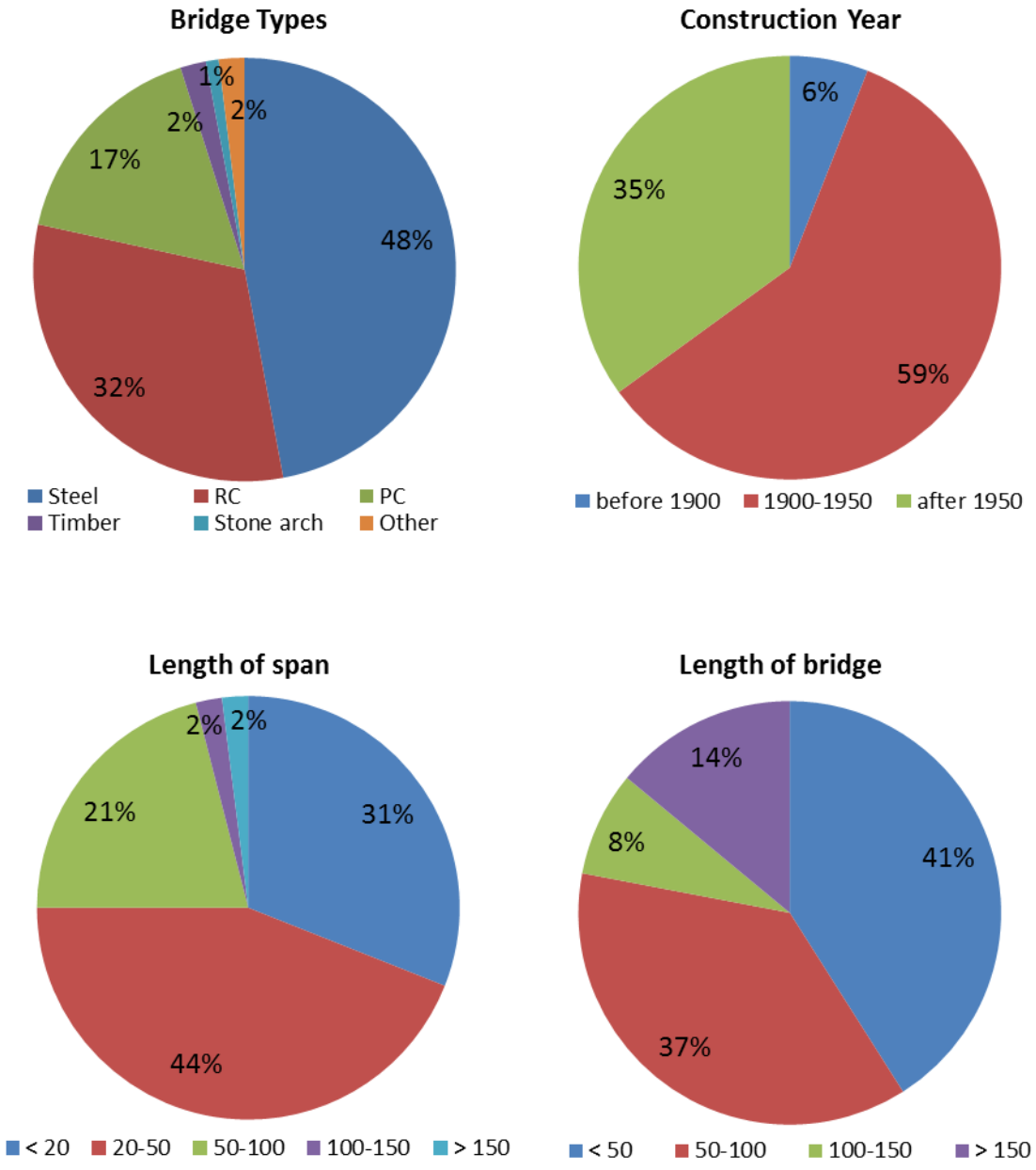

Figure 1.1 Characteristics of railway bridges on main lines in Nebraska and Iowa

Over 60% of railway bridges were constructed before 1950 according to characteristics of railway bridges on main lines in Nebraska and Iowa, shown in figure 1.1, and they require special attention. These statistics are true for entire nation. According to data provided by Union Pacific, summarized in figure 1.1, about 50% of railway bridges are steel structures, about 40% are short bridges with a total length less than 50 ft, and about 75% of railway bridges have span length less than 50 ft.

Railway bridges are very important and must maintain an appropriate level of safety. The current approach to risk is often not rational. Considerable new developments took place in the area of highway bridges with the development of reliability-based design and evaluation codes (AASHTO 2012). The developed methodology can now be applied to railway bridges.

Closure of a railway bridge can cause stoppage of railway traffic and serious logistical problems to detour the trains. Roadway traffic is often much easier to detour than railway traffic due to logistical problems. Moreover, since freight trains constitute the majority of railway traffic, their stoppage can have severe consequences, including impacts on the regional or even national economy. Consequences can include interruption in production due to deficiency or late delivery of raw materials (e.g., coal or iron ore). The cost of interruption in the energy supply, manufacturing process and resumption of production can be very high. Therefore, the consequences of a railway bridge closure can be unacceptably high.

On the other hand, the majority of railway bridges were designed as simply supported spans. Therefore, it is much easier to replace a failed girder or other component in a railway bridge than in a continuous highway bridge. The rehabilitation costs are higher for continuous multi-spans bridges.

An important question facing the owners and administrators of railway bridges is how to assure safety of existing structures under their jurisdiction. The development of a rational ranking system requires consideration of many factors including: identification of critical loads and other parameters that affect safety and durability of railway bridges; development of a statistical load model for rating existing railway bridges; development of accurate and efficient procedures for assessing existing bridges; and development of procedures for predicting the remaining lifetime of existing bridges.

When evaluating bridges, both the primary and secondary components have to be considered. There is a need for efficient methods to evaluate the safety reserve in the railway bridges by identifying the most sensitive parts of the bridge. Different types of bridges have a unique performance function as it applies to their service. Each part of a bridge system influences the bridge safety with a different importance ratio. This approach can be used to optimize the prioritization of repair and reconstruction of railway bridges.

1.2 Objective and Scope of the Research

The objective of this study is to develop a reliability model for railway bridges. It will be demonstrated on two through-plate girder structures. The research involved review and analysis of the major factors that influence structural performance. However, these factors are random in nature; therefore, it is convenient to consider reliability as a measure of performance. The relationship between various conditions and ability to perform the required function (i.e., carry the freight trains) will be established in form of limit state function(s). Using the available data, the statistical parameters will be determined for each factor by Monte Carlo simulations. The reliability as a measure of structural performance will be expressed in terms of a reliability index. Reliability indices will be calculated for selected representative railway bridges and, based on the

results, a target reliability index will be selected. A sensitivity analysis will be performed to establish the relationship between the load and resistance factors and reliability and will be presented in the form of graphs and tables. The results will serve as a basis for the development of general conclusions for through-plate girder railway bridges.

The research work will involve identification of the basic load and resistance parameters, and the development of advanced analytical procedures for modeling structural behavior. The load model utilizes the available results of field measurements, including static and dynamic effects. Structural analysis will be performed using advanced FEM programs. The analysis will be conducted on a representative railway bridge.

The following tasks will be implemented in this report:

- Review of structural reliability models and probabilistic approach in structural engineering.
- Description of the design load model and development of the statistical load model based on the available data.
- Development of the FEM models for through-plate girder railway bridges with open and ballasted deck. Adjusting the results of FEM analysis for further study.
- A fatigue analysis. Development of simulation model of the live load effect for the bridges with calculation of effective stress and number of cycles. Finding the statistical parameters for live load effect and fatigue resistance.
- A reliability analysis. Development of limit state functions for railway bridges. Calculating reliability index for individual components and connections.

1.3 Prior Investigation

The design code for railway bridges, AREMA, is still based on the allowable stress design. The current design load model was first presented in 1894 by Theodore Cooper. Cooper's loading system was based on a standard of E10 which means a pair of 2-8-0 type steam locomotives could pull an infinite number of rail cars. Although, rail transport has changed and steam locomotives were replaced with electric locomotives, the standard did not change it just increased to E80. For many researchers, the Cooper E Loading is recognized as useful tool for the overall design of a bridge in terms of maximum stress for girder design. However, the Cooper E80 Loading is not suitable for fatigue loading. Therefore, in 2011 Dick et al. presented research on the development of a unique loading, which is representative of current loading conditions, for design and rating of a bridge for fatigue.

The load and the resistance model contain many uncertainties. For this reason, any evaluation of the fatigue behavior of bridges is estimation rather than an exact formula. Therefore, probabilistic methods are the most convenient way to provide levels of safety for various design cases.

The theory of structural system reliability has been studied for many years and by many researchers, such as Ang and Tang (1984); Ayyub and McCuen (1997); and Nowak and Collins (200). Structural reliability assessments were first implemented for building code by Galambos and Ravindra (1918) and for highway bridge design code by Nowak and Lind (1979). In the field of railway bridges, the reliability approach is not very popular. In 1997, Tobias et al. presented research on a reliability-based method for fatigue evaluation of railway bridges. Their study involved a large-scale bridge instrumentation program along with the fatigue resistance test database compiled at the University of Illinois at Urbana-Champaign. The fatigue model

includes strengths and loadings described by probability distributions. The probability of failure was calculated by applying a modified version of Miner's damage law and the distribution function for load and resistance function. These studies give a broad view of the potential remaining lives of shorter-span railway bridges subjected to unit train loadings.

More recently, global finite element analyses of a typical riveted railway bridge in England indicated that the fatigue critical details are the inner stringer-to-cross-girder connections (Imam et al. 2005). The stringer to floor beam connections in a through-plate girder riveted railway bridge are commonly constructed with double angle connections and considered as simple shear connections during the design stage. In many cases, a considerable amount of end moment may be developed at the connection because of unintentional connection stiffness. Consequently, the connection can be susceptible to fatigue damage (Fisher et al 1987; Al-Emrani 2005). The fatigue damage is typically associated with cracking in the connection angles or in the rivets connecting the outstanding leg to the floor beam web because of rotational deformation on the top of the connection angles and axial forces in the rivets included by the restrain moment. Other researchers—for instance M. Al-Emrani (2005) and R.K Goel (2006)—also pointed out this issue. The topic was expanded by probabilistic fatigue life estimates for a stringer-to-cross-girder connection of a riveted railway bridges in England (Imam et al. 2008).

1.4 Organization

Chapter 1 of this report presents the introduction, problem statement, objective and scope of the research and the prior investigation in subject area. Chapter 2 reviews the principles of the reliability theory that is considered in this study. Basic definitions of probabilistic theory that are introduced include random variable, limit state functions and a reliability index. The basic information on system behavior with uncorrelated and correlated elements is provided.

Chapter 3 describes the load models used for design railway bridges and the actual load under current operating conditions. The design load includes static and dynamic live load and fatigue load. Loading spectra under current operating condition is present and the statistical parameters of the live load model are developed and summarized in tables and plotted on graphs.

Chapter 4 presents the definition and principles of the finite element method (FEM) along with their application. The description of the detail structures used in this study is illustrated. The FEM models for through-plate girder railway bridges with open and ballasted deck are developed. A verification study of the FEM model is compared with results from field-testing. Results of the FEM analysis with directions for further analysis are presented. Chapter 5 studies fatigue of bridge components and connections. The background theory used for this part of study is presented. The process of calculating load cycles and their magnitude is described. The results of number of cycles and equivalent stresses are presented in tabulated form. The statistical parameters for load and resistance are developed. Chapter 6 presents the reliability theory for fatigue of railway bridges. Ultimate and fatigue limit state functions are considered. The reliability indices are calculated for three cases of load on two representative railway bridges. The results are presented for periods of time from 10 to 100 years. Chapter 7 presents the summary and conclusions of research performed for the scope of this report.

Chapter 2 Structural Reliability Models

2.1 Introduction

Structural reliability is the application of probabilistic principles to an evaluation of acceptable and unacceptable structural performance. Safety can be measured in terms of the probability of uninterrupted operation under a given set of conditions. However, many sources of uncertainty are inherent in structural performance. Overall structural safety depends on uncertainty involved in material strength and properties, applied load on the structure, analysis procedure and methodology used for evaluation and design. The reliability approach can be used successfully in the design and evaluation of a structure.

2.2 Basic Definitions

A random variable is defined as a function that maps events onto intervals on the axis of real numbers (Nowak and Collins 2000). A random variable can be either a continuous random variable or discrete random variable. The variable is continuous if it can assume any value of the positive real axis, and if can assume only some discrete integer values.

For discrete random variables, the probability mass function (PMF) is defined. For continuous random variables, the probability density function (PDF) is defined. The cumulative distribution function (CDF) is defined for both discrete and continuous random variables. The PDF for continuous random variables is the first derivative of the CDF and this relation is formulated as follows:

$$PDF = f_x(x) = \frac{d}{dx} F_x(x) \tag{2.1}$$

and

$$CDF = F_x(x) = \int_{-\infty}^{x} f_x(x) \quad . \tag{2.2}$$

These two formulas apply for any continuous distribution function. Therefore, PDF and CDF can be defined for each type of distribution using statistical parameters. In general, there are many types of distribution functions. The best known and most widely used is the Gaussian distribution, which is also known as the normal distribution (Ang and Tang 1970). Other, very important variables used in structural reliability analysis are as follows: Uniform, Lognormal, Gamma, extreme Type 1, Poisson, Exponential, and Beta.

A very important descriptor of variables is the central tendency measure. The average value is the most commonly used central tendency descriptor (Ayyub and McCuen 1997. For a continuous random variable, the average value or mean value is given:

$$\mu_x = \int_{-\infty}^{+\infty} x \cdot f_x(x) \cdot dx = E(X) \quad . \tag{2.3}$$

The expected value of variable X is commonly denoted by E(X) and is equal to the mean value of the variable. The second parameter is the variance of X, which is defined as the expected value of $(X-\mu_X)^2$ and for continuous random variable it is equal to:

$$\sigma_x{}^2 = \int_{-\infty}^{+\infty} (x - \mu_x)^2 \cdot f_x(x) \cdot dx = E(X^2) - \mu_x{}^2 \quad . \tag{2.4}$$

The standard deviation of X, σ_X, is defined as the positive square root of the variance. The non-dimensional coefficient of variation, V_X, is defined as the standard deviation divided by the mean (this parameter is always taken to be positive). Additional distribution parameters apply for other types of distribution functions.

Normal probability paper is a very good tool for the graphical expression of particular distribution. The construction and use of the normal probability paper is described in textbooks (Benjamin and Cornell 1979; Nowak and Collins 2000). It is a convenient way to present CDF, as it allows for an easy evaluation of the most important statistical parameters as well as a type of distribution function. The horizontal axis is a standard linear scale of the value of the random variable. The vertical axis is the inverse normal probability scale, and it represents the distance from the mean value in terms of standard deviations. The vertical coordinate can also be considered as the probability of exceeding the corresponding value of the variable. For any value of variable (horizontal axis), the vertical coordinate of CDF corresponds to a certain probability of being exceeded. For example, a value of 1 on the vertical scale corresponds to 0.159 probabilities that the value of a variable will be exceeded. More examples of the relationship between a vertical coordinate of CDF and probability of occurrence are presented in table 2.1. The CDF can be used for an efficient interpretation of statistical data as presented in figure 2.1. Any normal CDF plotted on normal probability paper is represented by a straight line and any straight line represents a normal CDF.

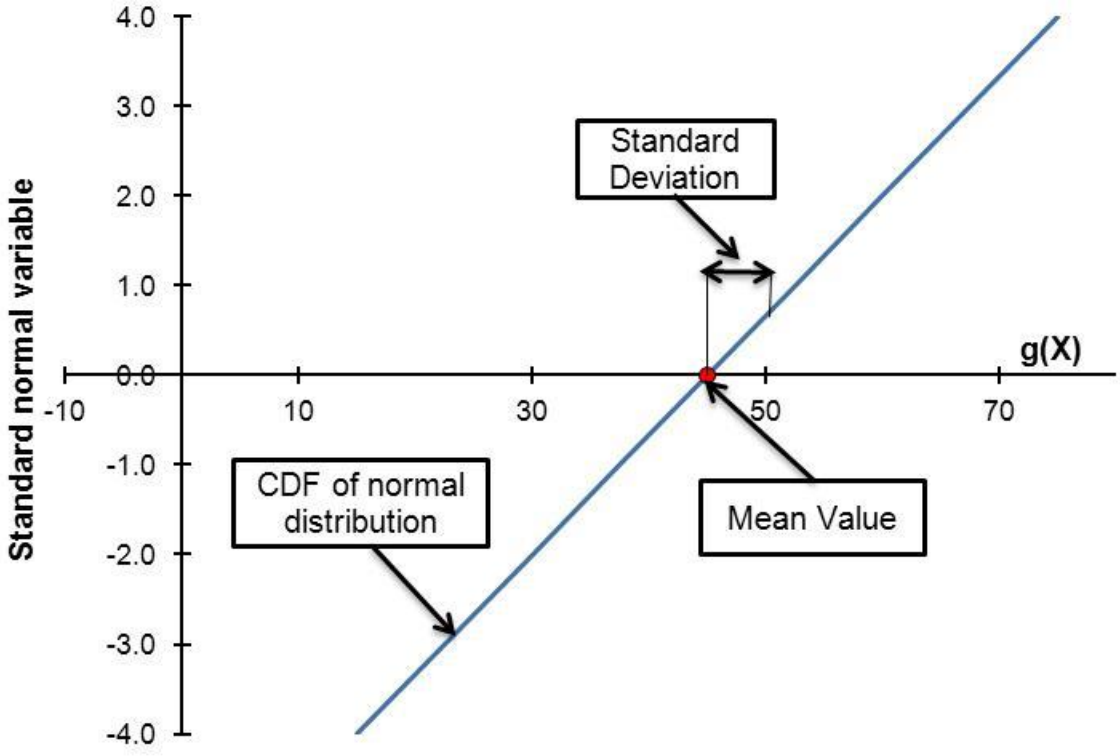

Figure 2.1 Interpretation of a straight-line plot on normal probability paper in terms of the mean and standard deviation of the normal random variable

Table 2.1 Examples of standard normal variable for various values of probability

Standard normal variable	Cumulative probability of occurrence
4.0	0.9999683
3.0	0.99865
2.0	0.9772
1.0	0.841
0.0	0.5
-1.0	0.159
-2.0	0.0228
-3.0	0.00135
-4.0	0.0000317

2.3 Limit State Function

The concept of limit state is used to define failure in the context of structural reliability analyses. Limit state is a boundary between desired and undesired performance of the structure. This boundary is often represented mathematically by a limit state function or performance function in the general form of:

$$g(R,Q) = R - Q \qquad \text{or} \qquad g(R,Q) = \frac{R}{Q} - 1 \tag{2.5}$$

where R is a capacity (or resistance) and Q is a load effect. Setting the border g(R,Q) = 0 between acceptable and unacceptable performance, the limit state function g(R,Q) > 0 represents the safe performance and g(R,Q) < 0 represents failure. Following the definition of the structural reliability it can be defined that:

$$P_f = P\big(g(R,Q) < 0\big) = P\big((R - Q) < 0\big) \tag{2.6}$$

$$P_f = P\big(g(R,Q) < 0\big) = P\left(\frac{R}{Q} < 1\right) \tag{2.7}$$

where P_f is the probability of failure. The variables R, Q and g can be a function of n random variables:

$$g(R,Q) = g(X) = g(X_1, X_2, ..., X_n) \tag{2.8}$$

Structural limit states tend to fall into two major categories: strength and serviceability. Strength limit states are potential modes of structural failure, mostly related to the loss of load-carrying capacity. The strength limit state can be written in a general form of:

$$\text{Required Strength} \leq \text{Provided Strength.} \tag{2.9}$$

The required strength is the internal force that is derived from analysis of the structure being designed. For example, when designing a beam, the required strength may be the maximum moment, M, computed for the beam due to applied load. The nominal strength is the predicted capacity of the beam in bending. It is the maximum moment, M_n, that the beam is capable of supporting; in other words, a function of the stress capacity of the material and the section properties of the member.

Serviceability limit states are those conditions that are related to gradual deterioration, user's comfort, or maintenance costs. The most common serviceability modes of failure include excessive deflection, excessive vibration, and permanent deformation. Serviceability limit states can be written in the general form of:

$$\text{Actual Behavior} \leq \text{Allowable Behavior.} \tag{2.10}$$

Serviceability Limit States tend to be less rigid requirements than strength based limit states since safety of the structure is not in question.

2.4 Reliability Index

Probabilistic methods used in structural design are based on the reliability index. Assuming that the limit state is normally distributed, the reliability index is related to probability of failure as:

$$\beta = -\Phi^{-1}\left(P_f\right) \tag{2.11}$$

where $-\Phi^{-1}$ is the inverse standard normal distribution function (Cornell 1967). In this section, the reliability index is limited to the failure of one component according to one failure mode, or one limit state function.

The simplest method to calculate the reliability index is the First-Order Second-Moment method (Nowak and Collins 2000). This method takes into consideration the linear limit state functions or their linear approximation by using Taylor series. First order means that only the first Taylor derivative is used in calculations and Second-Moment refers to the second moment of the random variable (Der Kiureghian et al. 1987; Ditlevsen and Madsen 1996). First moment is the expected value E(X) and the second moment E(X2) is a measure of the dispersion: in other words, the variance.

For a linear limit state function with uncorrelated random variables X_i the formula is:

$$g\left(X_1, X_2,...,X_n\right) = a_0 + a_1X_1 + a_2X_2 + ... + a_nX_n = a_0 + \sum_{i=1}^{n} a_iX_i \tag{2.12}$$

where the a_i terms (i=0,1,2…,n) are constants. The reliability index for linear function can be calculated as:

$$\beta = \frac{a_0 + \sum_{i=1}^{n} a_i X_i}{\sqrt{\sum_{i=1}^{n} (a_i \sigma_{Xi})^2}} \quad . \tag{2.13}$$

There is no explicit relationship between β and the type of probability distribution of the random variables. If the random variables are all normally distributed and uncorrelated, then this formula is exact. Otherwise, this method provides only an approximate means of relating β to a probability of failure.

For special cases, such as two normal distributed, uncorrelated random variables, R and Q, reliability index is given by:

$$\beta = \frac{\mu_R - \mu_Q}{\sqrt{\sigma_R{}^2 + \sigma_Q{}^2}} \quad . \tag{2.14}$$

In the case where R and Q are both lognormal, uncorrelated random variables, reliability index can be approximated by the following formula (Rosenblueth 1975 and 1981):

$$\beta = \frac{\mu_{\ln R} - \mu_{\ln Q}}{\sqrt{\sigma_{\ln R}{}^2 + \sigma_{\ln Q}{}^2}} = \frac{\ln\left(\frac{\mu_R}{\mu_Q}\right)}{\sqrt{V_R{}^2 + V_Q{}^2}} \quad . \tag{2.15}$$

For a nonlinear limit state function with uncorrelated random variables X_i the approximate formula obtained by linearizing the function using a Taylor series expansion is:

$$g(X_1, X_2,...,X_n) \approx= g\left(x_1^*, x_2^*,..., x_n^*\right)+\sum_{i=1}^{n}(X_i - x_i)\frac{\delta g}{\delta X_i}\bigg|_{evaluated\_at\_\left(x_1^*, x_2^*,..., x_n^*\right)} \quad (2.16)$$

where (x_1*, x_2*,…,x_n*) is the point about which the expansion is performed. One choice for a linearization point is the point corresponding to the mean values of random variables. Thus, Equation 2.16 becomes:

$$g(X_1, X_2,...,X_n) \approx g\left(\mu_{X_1}, \mu_{X_2},..., \mu_{X_n}\right)+\sum_{i=1}^{n}\left(X_i - \mu_{X_i}\right)\frac{\delta g}{\delta X_i}\bigg|_{evaluated\_at\_\left(\mu_{X_1}, \mu_{X_2},..., \mu_{X_n}\right)} \quad (2.17)$$

The reliability index for linear function can be calculated as:

$$\beta = \frac{g\left(\mu_{X_1}, \mu_{X_2},..., \mu_{X_n}\right)}{\sqrt{\sum_{i=1}^{n}\left(a_i\sigma_{Xi}\right)^2}} \qquad \text{where} \qquad a_i = \frac{\delta g}{\delta X_i}\bigg|_{evaluated\_at\_\left(\mu_{X_1}, \mu_{X_2},..., \mu_{X_n}\right)}. \quad (2.18)$$

The implementation of the First-Order Second-Moment (FOSM) method can be performed for normal distributions. The reliability index for distributions other than normal includes considerable level of error (Nowak and Collins 2000; Thoft-Christensen and Murotsu 1982).

2.5 Simulation Methods

Simulation methods are used in cases where the computation of reliability index using simplified methods is too complex or not possible. This is particularly true for complex engineering problems where many random variables are related through a nonlinear equation. In these cases, simulation methods can be very useful to estimate the reliability index without losing accuracy. Moreover, this procedure can be used for linear and nonlinear limit state functions. Monte Carlo simulation provides an efficient way to determine reliability index or probability of failure.

The first step in this procedure is generation of random numbers that are uniformly distributed between 0 and 1. Then, simulated values of the random variables in the limit state equation are generated with proper distribution. These values are then used to simulate the limit state function itself. In the last step, simulated values of limit state function are plotted on normal probability paper. The probability of failure can be found at the location where the plotted data curve intersects a vertical line passing through the origin. β corresponds to the value of the standard normal variable at the intersection point. If the plotted curve does not intersect the vertical axis, the plotted curve can be extrapolated as shown in figure 2.2.

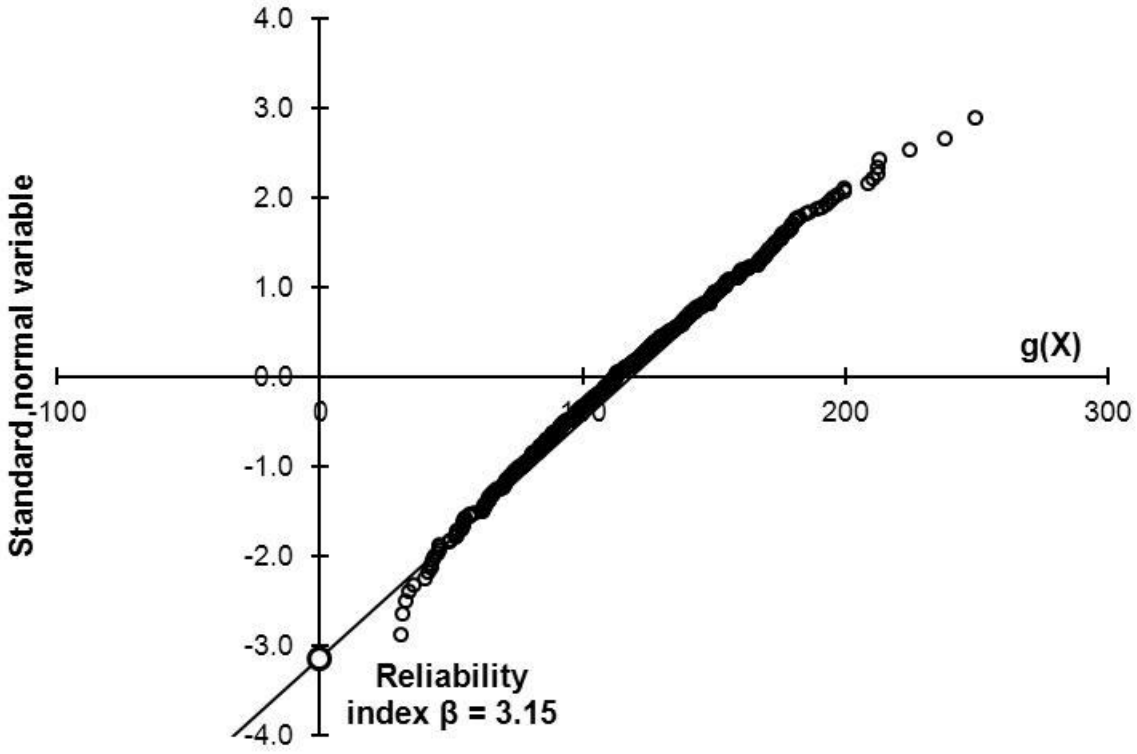

Figure 2.2 Simulated values of the limit state functions generated by Monte Carlo method

Accuracy of the method depends on the number of simulations. The number of simulations may have to be two orders of magnitude larger than the expected probability of failure, or the probability can be assessed using extrapolation of results.

2.6 System Reliability

In the previous sections, the reliability index was limited to the failure of one component according to one limit state function. In general, a component can fail in one of several failure modes. The treatment of the multiple failure modes requires modeling the component behavior as a system. Also, a system can be defined as an assemblage of several components that serves some function or purpose (Ayyub and McCuen 1997).

System analysis requires the recognition and modeling of some system characteristics that include: post-failure behavior of a component; the contribution of a component failure or

failure-mode occurrence to the system's failure; the statistical correlation among failure modes and components' failure; and the definition of failure at the system level. The post-failure behavior of a component is required to determine the remaining contribution of the system response. If a system contains brittle components, they lose their strength completely after failure and can be removed from the structural analysis of a system. In the case of a system built with ductile components, those that fail continue to contribute to the behavior of system and their contribution needs to be considered in the analysis of the system.

The contribution of a component failure or failure-mode occurrence to the system's failure depends on the level of redundancy in the system. Some components can lead to failure; others can weaken the system and remaining components will not result in system failure. The statistical correlation among failure modes and components' failure can have a large effect on the reliability of the system; however, is very hard to assess this correlation.

Bridges are structural system of many components. Therefore, evaluation of an entire bridge should take into account each part of the structure. Various types of bridges are composed of different elements and these elements can have different effects depending on the type of bridge.

In some cases, such as girder bridges, several components must fail simultaneously for an overall structural failure to occur (Moses 1997). However, for some structures like truss bridges one member would cause the entire structure to collapse. The behavioral distinction for these two cases is caused by geometry. In girder bridges elements work alongside in a parallel system, as opposed to truss members, which work as series system or chain system. A system can be characterized not only by its geometry but also by material properties and statistical correlation.

To assess the reliability of a bridge system, the behavior of the entire structure has to be analyzed and the influence of each component within the structure has to be estimated. To analyze system reliability more information is required and other methods are applied.

2.6.1 Series System

A system in a series, also referred as a weakest-link system, can be represented as shown in figure 2.3. In a series system, the failure of one component of the n components can lead to failure of the system. The connectivity of the components is a logical connectivity in terms of the contribution of component failure to the system failure. The logical connectivity can be different than the physical connectivity of the components in the real system (Ayyub and McCuen 1997). An example of the weakest-link system is a statically determinate truss, as shown in figure 2.4 because the failure of a component in the truss results in the failure of the entire system. The physical connectivity of the components in the truss structure is different than logical connectivity in series system; however, it works in this same way.

Figure 2.3 A system of n components in series

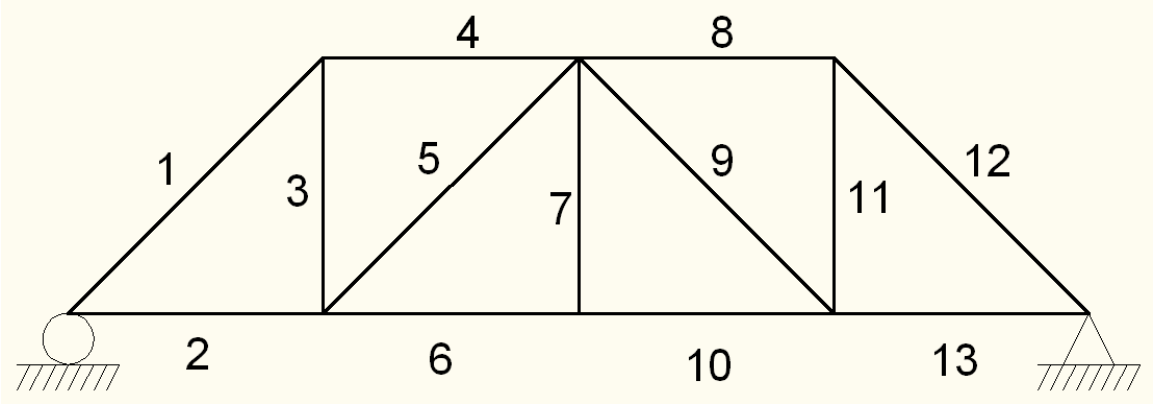

Figure 2.4 A truss structural system

Suppose we have a series system consisting of n elements, and the strength of each element is a random variable. The system is subjected to a deterministic load. Failure of the system implies that the strength is less than the load. In terms of probability, the probability of failure of one element would be a probability that resistance is less than load (as shown in equations 2.6 and 2.7). With the assumption that the strengths of the elements are all statistically independent, we can calculate the probability of failure for system as follows:

$$P_f = 1 - \prod_{i=1}^{n} \left[1 - P_{fi}\right] \quad (2.19)$$

2.6.2 Parallel System

A system in parallel also referred to as a redundant system, can be represented as shown in figure 2.5. In this case, the n components need to fail in order for the system to fail.

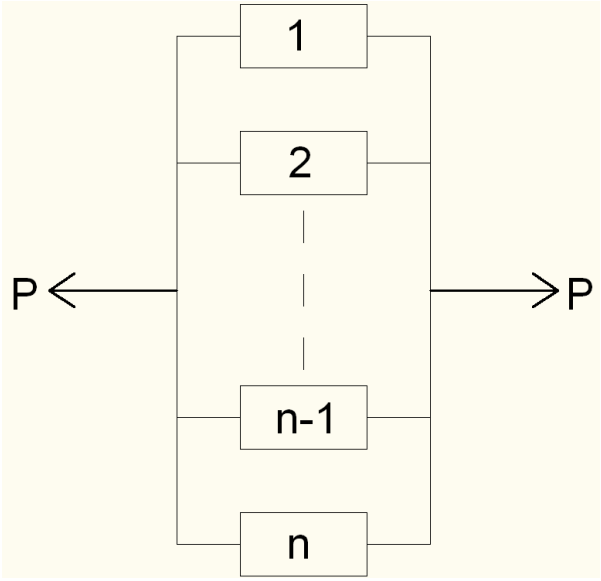

Figure 2.5 A system of n components in parallel

The probability of failure of the system of ductile elements can be determined as the following example indicates. Consider load q acting on the system, in which each element will carry a portion of the total load. Failure of the element will correspond to the event that resistance of the element is less than a portion of the load applied on the element, and the probability of the element can be calculated according to equation 2.6 and 2.7. With this information, the probability of failure of the system can be determined as follows:

$$P_f = \prod_{i=1}^{n} \left[P_{fi} \right] . \tag{2.20}$$

The multiplication of probabilities is allowed because we have assumed that all strengths are independent and because we have neglected any possibility of load redistribution in the system

once one or more elements start to yield. Thus, the failure events of each element is entirely independent (Nowak and Collins 2000).

For a parallel system with brittle elements, if one of the elements fails, then it loses its capacity to carry load. The load must be redistributed to remaining elements. If after the load is redistributed, the system does not fail, the load can be increased until the next element fails. The process of failure and load redistribution is repeated until overall failure of the system occurs.

2.6.3 Hybrid Systems

Many real structures can be considered a hybrid system, which is a combination of series and parallel systems. Figure 2.6 is a diagram of a hybrid system with n components.

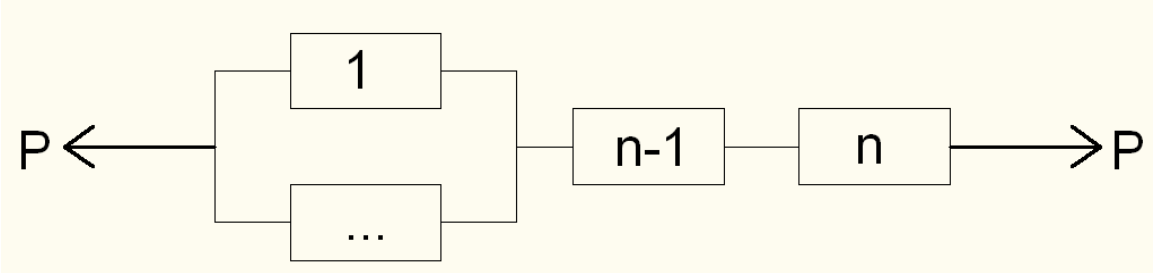

Figure 2.6 A hybrid system of n components

The hybrid system can be analyzed using the technique specified for parallel and series systems. It is convenient to divide the problem into a subsystem and then analyze the subsystems.

2.6.4 Systems with Correlation

Sections 2.6.1, 2.6.2, and 2.6.3 describe the simplest cases where the elements were all independent and uncorrelated; therefore, the procedures were relatively straightforward. In the real structures, some or all elements can be correlated. The exact calculation of probability of failure of the correlated system is typically very difficult and sometimes impossible. For all

systems with positive correlation between pairs of elements, the solution should be within defined boundaries. Positive correlation means that the correlation coefficient is greater or equal to zero.

For a parallel system that contains elements with positive correlation, the limits for probability of failure are defined in equation 2.21. The lower bound corresponds to the case where the elements are all uncorrelated. The probability of failure for this case was defined in equation 2.20. The upper bound is a system with perfectly correlated elements and the reliability of the system for this case is determined by the safest element.

$$\prod_{i=1}^{n} P\left[F_i = 1.0\right] \leq P_f \leq \min_i \left\{P\left[F_i = 1.0\right]\right\} \tag{2.21}$$

For a series system with positive correlation, the probability of failure must satisfy the limits defined in equation 2.22. The lower bound is the probability of failure when all elements are fully correlated. Series system with fully correlated elements will tend to fail if one of the elements fails, so the probability of failure of the system has the largest probability of failure among the constituent elements (Nowak and Collins 2000). The upper bound is the probability of failure when all elements are uncorrelated, as described previously in section 2.6.1.

$$\max_i \left\{P\left[F_i = 1.0\right]\right\} \leq P_f \leq 1 - \prod_{i=1}^{n} \left\{1 - P\left[F_i = 1.0\right]\right\} \tag{2.22}$$

Chapter 3 Load Model

3.1 Introduction

The live load model available in the design code AREMA 2005 is the Cooper E80 load, which is composed of two steam locomotives and relatively smaller uniform trailing weight. Today's freight trains are quite different than this design loading. Over the last decades, trailing rail car weights have increased (Foutch et. al. 1996), and the distributions of axle load have changed. Nowadays, the diesel-electric locomotives have a similar axial load as freight cars.

3.2 Design Live Load

Cooper's loading system is based on a standard of E10, shown in figure 3.1, and this means that a pair of 2-8-0 type steam locomotives is pulling an infinite number of rail cars. Each locomotive was given an axle loading of 10,000 pounds for the driving axles; 5,000 pounds for the leading truck; and 6,500 pounds for the tender trucks. Each trailing rail car was given an axle loading of 1,000 pounds per foot of track.

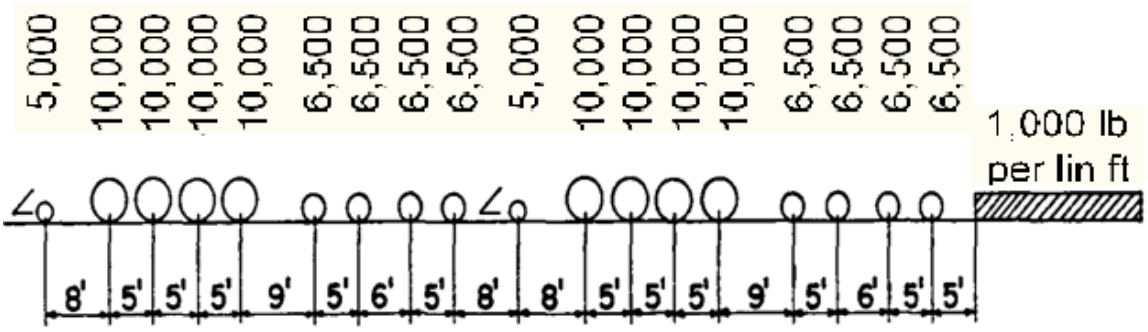

Figure 3.1 Cooper's loading system-standard E10

During the 1880s, railway bridges were built using an equivalent rating of E20. By 1894, when Cooper presented his standard, he recommended a standard of E40, or four times the E10

standard. By 1914, the standard had increased to E60. In the mid-1990s, the American Railway Engineering Association, AREA, was recommending E72 (7.2 times the E10 standard) for concrete structures, and E80 for steel structures (Coopers Loading System, 2012). Since 2005, AREMA recommends E80 for concrete structures and E80 for steel structures. A set of forces with certain spacing characterize Cooper E80 and is present in figure 3.2.

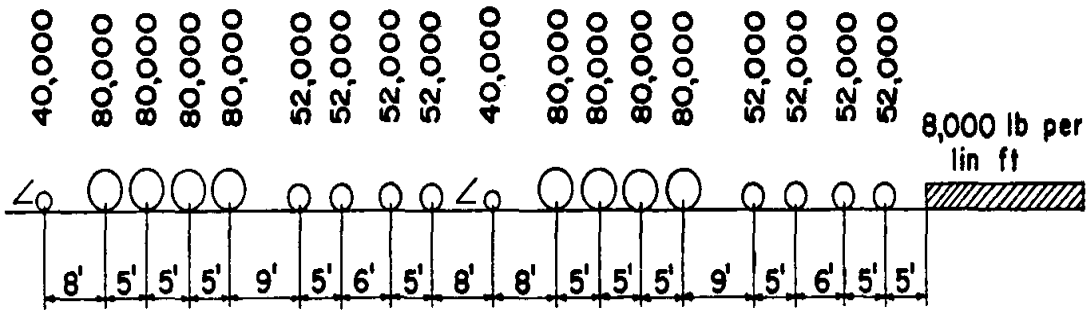

Figure 3.2 Cooper's E80 load

Moreover, AREMA allows use of Alternate Live Load on 4 axles, spaced as shown in figure 3.3 or in whichever order produces the greater stresses.

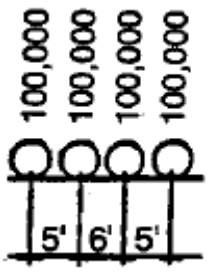

Figure 3.3 Alternate live load on four axles

AREMA does not provide explicit load combinations, but it does incorporate combinations in various design recommendations (Sorgenfrei and Marianos 2000). Table 3.1 outlines load combinations that apply to the steel superstructure design found in various AREMA recommendations (Unsworth 2010).

Table 3.1 Load combinations for steel railway superstructure design

Load Case	Load Combinations	Members	F_L
A1	DL + LL + I + CF	All members	1.00
A2	DL + LLT + I + CF	Truss web members	1.33
B1	DL + LL + I + W + LF + N + CWR	All members, except floor beam hangers and high strength bolts	1.25
B1A	DL + LL + I + W + LF + N + CWR	Floor beam hangers and high strength bolts	1.00
B2	DL + LLT + I + W + LF + N + CWR	Truss web members, except floor beam hangers	1.66
C	(LL + I) range	All members	f_{fat}
D1	SL + N + CF	Members resisting overall instability	1.50
D2	Q	Members resisting overall instability	1.50
E1	DL + EQ	All members	1.50
E2	DL + LL + I + CF + EQ	Members in long bridges only	1.50
F	W or LV	Members loaded by wind only	1.00
G	DF	Cross frame, diaphragms, anchor rods	1.50
H1	DL	Members stressed during lifting or jacking	1.50
H2	DL	Members stressed during erection	1.25
H3	DL + W	Members stressed during erection	1.33

NOTE: **FL** = Allowable stress load factor (multiplier for basic allowable stresses), **DL** = Dead loads (self-weight, superimposed dead loads, erection loads), **LL** = Live load, **I** = Impact (dynamic amplification), **CF** = Centrifugal force on a curved railway bridge, **W** = Wind forces (on live load and bridge), **LF** = Longitudinal forces from equipment (braking and locomotive traction), **N** = Lateral forces from equipment (nosing), **CWR** = Forces from bridge thermal interaction (lateral and longitudinal), **EQ** = Forces from earthquake (combined transverse and longitudinal), **DF** = Lateral forces from out-of-plane bending and from load distribution effects, **LV** = "Notional" lateral vibration load, **LLT** = Live load that creates a total stress increase of 33% over the design stress (computed from load combination A1) in the most highly stressed chord member of the truss, **SL** = Live load on leeward track of 1200 lb/ft without impact, I, **Q** = Derailment load, ***ffat*** = Allowable stress based on member loaded length and fatigue detail category.

3.3 Design Dynamic Load

In addition to static load, trains traversing a railway bridge create dynamic actions in longitudinal, lateral, and vertical directions. The dynamic effect on the railway bridge is a very complex issue because the dynamic effect on the bridge has various sources. Parameters affecting the dynamic behavior of a steel railway bridges are:

- Dynamic characteristics of the live load (mass, vehicle suspension stiffness, natural frequencies, and damping). For passenger vehicles, the train frequency is generally in range 0.9 to 1.2 Hz (circular frequency 6-8 rad/sec). For freight wagons this frequency can raise to 2.5 Hz in loaded and up to 4 Hz in the tare condition (circular frequency 16-25 rad/sec).
- Train speed (a significant parameter).
- Train handling (causing pitching acceleration).
- Dynamic characteristics of bridge (mass, stiffness, natural frequencies, and damping).
- Span length and continuity (increasing impact due to higher natural frequencies of short-span bridges).
- Deck and track geometry irregularities on the bridge (surface roughness) a significant parameter).
- Track geometry irregularities approaching the bridge.
- Rail joints and flat or out-of-round wheel conditions (a significant parameter of particular importance for short spans).
- Bridge supports (alignment and elevation).
- Bridge layout (member arrangement, skewed, and curved).
- Probability of attaining the maximum dynamic effect concurrently with maximum load.

According to AREMA 2007, the impact load due to the sum of vertical effects and rocking effect created by passage of locomotives and trainloads, shall be determined by taking a percentage of the live load and shall be applied vertically at top of each rail. For all freight and passenger railcars and diesel locomotives (without hammer blow), the vertical impact is calculated using the following equations:

For L less than 100 ft

$$I = 40 - \frac{3L^2}{1600} \tag{3.1}$$

and

For L 100 ft and more

$$I = 16 + \frac{600}{L - 30}. \tag{3.2}$$

For steam engines with hammer blow the impact factor is larger. For beam spans, stringers, floor beams, posts of deck truss carrying a load from the floor beam only, and floor beam hangers, the impact factor is calculated as follows:

For L less than 100 ft

$$I = 60 - \frac{L^2}{500} \tag{3.3}$$

and

For L 100 ft and more

$$I = 10 + \frac{1800}{L - 40}. \tag{3.4}$$

For steam locomotives on truss spans the impact factor is calculated using the following equation:

$$I = 15 + \frac{400}{L + 25} \tag{3.5}$$

For truss spans:

where L is a length in feet, center to center of supports for main members.

As a summary of the equations above, the percentage of impact load for various span lengths is presented in table 3.2.

Table 3.2 Impact load factor (% of LL) for steel structures

L, ft	For equipment without hammer blow (freight and passenger cars)	For steam locomotive with hammer blow	
		Beam spans	Trusses
10	40	60	129
20	39	59	104
30	38	58	88
40	37	57	77
50	35	55	68
60	33	53	62
70	31	50	57
80	28	47	53
90	26	44	50
100	25	40	47
120	23	33	43
140	21	28	39
160	21	25	37
180	20	23	35
200	20	21	33
250	19	19	30
300	18	17	27
350	18	16	26
400	18	15	24

These equations and tabulated values are defined for open deck bridges. For ballasted deck bridges, the impact load shall be reduced to 90% of that specified for open deck bridges. Percentage of impact load for various span length is presented in table 3.2.

Additional impact due to rocking effect, RE, is created by the transfer of the load from the wheels on one side of a car or locomotive to the other side from periodic lateral rocking of the equipment. RE shall be calculated from loads applied as a vertical force couple, each being 20% of the wheel load without impact, acting downward on one rail and upward on the other. The couple shall be applied on each track in the direction that will produce the greatest force in the member under consideration. For traffic that is not classified as light rail or commuter rail, the dynamic factor is reduced to 35% of the design value for fatigue analysis (AREMA 2007).

3.4 Fatigue Loading

The AREMA fatigue design criteria include Cooper E Loading and Alternate Live Load, which were described in Chapter 3.2. The Cooper E Loading has limited use since the loading is governed by the uniform load pattern, unlike actual railcar loading. Alternate Live Load represents heavy axle loading on a shorter span and can be more useful in fatigue analysis.

The second source of design load is the Association of America Railroads (AAR) which specifies minimum railcar dimensions for the design of new freight cars. The dimensions for AAR design cars are listed in table 3.3. All three cars have a similar total length which is about 42 ft with some variation of axle spacing.

Table 3.3 Dimensions for AAR railcar configuration (all four-axle cars)

Car Type	S_O, ft	S_T, ft	S_I, ft	L_O, ft	GW, kips	Empty car weight, kip
AAR 1	3.36	5.83	23.58	41.96	286.0	50.0
AAR 2	3.86	5.83	22.54	41.92	286.0	50.0
AAR 3	4.36	5.83	21.50	41.88	286.0	50.0

*L_O – overall length of railroad car measured over the pulling face of the coupler; S_O – Outboard Axle Spacing; S_T – Truck Axle Spacing; S_I – Inboard Axle Spacing

However, the actual loading is different than the design load, which is a crucial factor for fatigue analysis. In predicting maximum fatigue damage it is important to consider trainload with an axle configuration corresponding to current operating conditions. Maximum stresses on the bridge and the number of cycles have an influence on overall performance of the bridge. The Cooper E80 Loading is, therefore, not suitable for fatigue loading. Additionally, the current criteria focus on mid-span effect while fatigue analysis needs to consider all critical location along plate girders as well as secondary elements and connections.

In 2011, Dick et al. presented research on the development of a unique loading for design and rating of a bridge for fatigue. The model was developed based on current loading conditions. Figure 3.4 displays the general dimensions and descriptions of equipment and table 3.4 provides the specific lengths and weight values for the locomotive and cars.

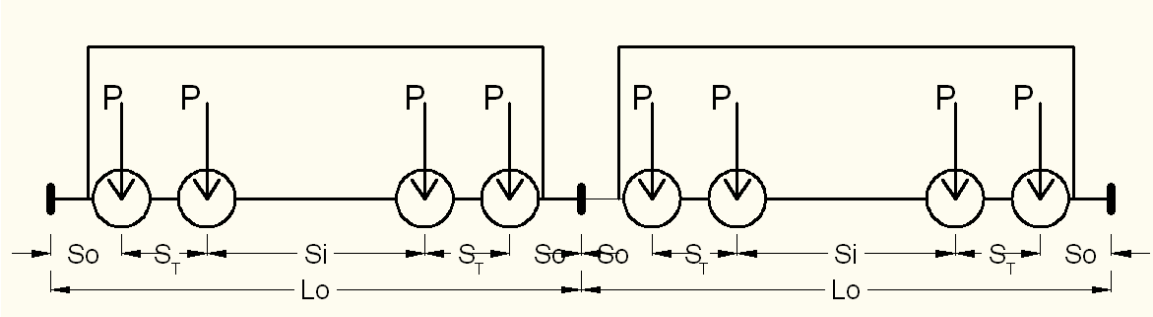

Figure 3.4 Dimensions used for analysis

NOTE:
P – Axle load
L_O – overall length of railroad car measured over the pulling face of the coupler
S_O – Outboard Axle Spacing
S_T – Truck Axle Spacing
S_I – Inboard Axle Spacing

Table 3.4 Dimensions for locomotives and railcars used in fatigue analysis

Car Type	S_O, ft	S_T, ft	S_I, ft	L_O, ft	GW, kip	Empty car weight, kip
6-axles Locomotive	5.95	6.83	34.79	74.0	429.0	429.0
4-axles cars:						
Sand/Cement Hooper	3.36	5.83	23.58	41.96	286.0	50.0
Coal	3.38	5.83	34.67	53.08	286.0	65.0
Long Hopper	3.36	5.83	50.63	69.00	286.0	80.0
TOFC	11.42	5.83	60.17	94.67	286.0	75.0

During the research study conducted by Dick et al., they concluded that fatigue load should have certain characteristic that would allow for general use both for rating and design. Accordingly, it should possess a relatively high magnitude of repetitive moment, should have sufficient overall maximum moment, resemble actual equipment in its configuration, and should have simple dimensions (Dick et al. 2011).

Table 3.5 presents the length and weight for the F80 loading along with F71.5. Using F80 cars in a train allows analysis for both maximum moment and repetitive moment that is experienced during a train passage (Dick et al. 2011).

Table 3.5 Proposed fatigue car dimensions, four-axle cars (Dick et. al. 2011)

Car Type	S_O, ft	S_T, ft	S_I, ft	L_O, ft	GW, kips	Empty car weight, kip
Fatigue F80	3.0	5.0	60.0	76.0	320.0	90.0
Fatigue F71.5	3.0	5.0	60.0	76.0	286.0	90.0

In this study, many possible configurations of trains will be analyzed along with current loading spectra. The trains used in this report are listed in table 3.6 with specific dimensions of cars described earlier. For the mixed train scenarios, the maximum cycle production is developed overall on a bridge by a combination of two loaded cars followed by two empty cars followed by two loaded cars followed by two empty cars and so forth.

Table 3.6 Trains used in this report for fatigue analysis

Train Type	Car Type	Total GW of train, kip
F80	100 railcars	32,000
AAR 1	Three locomotives and 60 railcars	18,447
Coal	Three locomotives and 150 railcars	44,187
Long Hopper	Three locomotives and 60 railcars	18,447
TOFC	Three locomotives and 100 railcars	29,887
Mixed F80	100 railcars	20,500
Mixed AAR 1	Three locomotives and 60 railcars	11,367
Mixed Coal	Three locomotives and 150 railcars	27,612
Mixed Long Hopper	Three locomotives and 60 railcars	12,267
Mixed TOFC	Three locomotives and 100 railcars	19,337

In addition to the idealized model of trains listed in table 3.5, the statistical train was considered. The statistical train contains 200 pieces of railroad equipment which includes 62% of coal hoppers; 21.5% of mixed freights, 8% of four axle intermodals, 4% of auto-racks, 3% of 6-axle locomotives, and 1.5% of 4-axle locomotives. The simulated train is described in greater detail in section 3.6.

3.5 Railcars and Locomotives Used in the Current Rail Transport System

The current loading spectra, to which railroad bridges are subjected, are significant for bridge evaluation. Not only type of load and magnitude are important, but also statistical parameters like mean value, standard deviation, expected maximum load, and probability of occurrence. The probabilistic characteristics of maximum live load depends on the temporal variation of the load, the duration of the sustained load, the design lifetime, and statistics of the involved random variables (Chalk and Corotis 1980).

The general layout of railroad equipment has been in existence for almost the entire 200 years since the railroad was invented. During the passage of time many changes occurred in the size, weight, and design of cars and locomotives. The breakthrough happened when steam locomotives were replaced by diesel locomotives in 1940s. Until that time, steam locomotives represented the heaviest load of the entire train. Innovations were made in car design to increase the capacity of freight cars and safety of passenger cars.

The main categories of locomotives are often subdivided in their usage in rail transport operations by passenger locomotives and freight locomotives. The majority of locomotives are built with two- or three-axle trucks. The overall dimension, spacing between axles, and gross weight vary between different manufacturers. Typical diesel electric locomotives are four-axles with total weight of 120-140 tons and total length up to 60 ft, or six-axles with total weight of 160-210 tons and total length up to 80 ft. Passengers train equipment is designed for moving people and for hauling express shipments and mail. The term passenger car can also be associated with a sleeping, baggage, or dining car. The total length of the car is usually 85 ft with a weight of 50 to 110 tons. Most of the cars are four-axles.

Freight train equipment has been developed to transport every type of commodity imaginable. There are, however, nine basic types of railcars used in international trade. They are:

boxcar, refrigerated boxcar (reefer), flatcar, tanker, container carrier, gondola, hopper, center partition railcar, auto transporter.

From their inception, boxcars have been the most common type of freight cars and are used worldwide. Boxcars come in 50, 60, and 86-foot lengths with load capacities ranging from 70 to 105 tons. Boxcars are designed to carry many types of shipments such as paper products, canned goods, and bulky freight. Different railcar manufacturers worldwide produce a variety of models designed for specific applications, capacity and dimensions. Reefers (refrigerated) boxcars are designed to carry perishable freight at specific temperatures. Common commodities transported in reefer boxcars include vegetables, fruit, orange and other juices, milk, meat, and poultry. Although the reefers are designed for different purposes, the dimension and capacity is similar to the boxcars.

Flat cars are designed to transport any shipment that must be loaded from the side or the top. Standard cargo for platform trailers include: heavy construction equipment, farm tools, lumber, plywood, steel products, pipes and rebars. Length, capacity, and weight depend on railcar manufacturer, railcar model, and rail system requirements. Tankers are used to carry bulk liquids. Common commodities transported in tankers include refined gasoline, heating oil, alcohol, industrial chemicals, acids, clay slurry, corn syrup and other. Container carriers are designed to carry international standard 20', 40', 45', 48', and 53' ocean freight containers in various stacking combinations.

Two types of gondolas are used for the shipments of the freight. Mill gondolas are extremely sturdy railcars designed to transport iron and steel scrap, steel ingots, coiled steel, sheet steel, pipes, and other steel products. Aggregate gondolas are designed to transport industrial minerals, crushed rock and gravel. Both have standard lengths ranging from 48' to 66'.

The purpose of hoppers is to transport free flowing dry bulk commodities like grains, industrial minerals, plastic pellets, crushed rock, gravel, and sand. Hopper cars can be covered or uncovered depending on the shipment material. Center partition railcars (also called center beam flatcars) are designed to transport lumber, plywood, building materials and other packaged products. Auto carriers are designed to transport automobiles from and to automobile manufacturing plants, ocean import/export facilities, and distribution centers. Rail auto carriers are the most efficient way to transport large numbers of automobiles long distances by land. Different railcar manufacturers worldwide produce a variety of models designed for different container and stacking configurations. Tables 3.7, 3.8, and 3.9 present some types of railcars with typical dimensions and capacities.

Table 3.7 Examples of dimensions and capacity for various freight cars

	Exterior Length	**Truck centers**	**Freight Capacity, tons**
50' Standard Box	55' 5"	40’ 10”	65-90
50' Hi-roof Box	58' 4"	46’ 8”	90
60' Standard Box	67' 11"	46’ 3”	90
60' Hi-roof Box	67' 7"	-	90
86' Auto Box	93' 6"	66’ 0”	95
Small Coal Hopper	49’ 8”	36’ 2”	90
Jumbo Coal Hopper	55’-65’	-	90-100
52’ Gondola	56' 11"	43’ 4”	65-90
65’ Gondola	71' 3"	57’ 2”	90-100
Flat car	93' 10"	68’ 0”	105
Tanker	90' 6"	66’ 0”	102.5
Container Carrier	76' 0"	61’ 6”	30,000 gal.
Center Partition	80' 6"	60’ 0”	105
Auto Transporter	145' 4"	64’ 0”	50

Table 3.8 Examples of weight and axle load for various freight cars

	Empty Car, kips	Gross Car Weights, kips	Axle Loads, kips
50' Standard Box	71	200-286	50 – 72
50' Hi-roof Box	74	286	72
60' Standard Box	79.3	286	72
60' Hi-roof Box	79	286	72
86' Auto Box	95	315	79
Small Coal Hopper	61.8	263	66
Jumbo Coal Hopper	-	263-286	66-72
52’ Gondola	65.5	286	72
65’ Gondola	75.0	263-286	66 – 72
Flat car	60	286	72
Tanker	60	286	72
Container Carrier	65.7	263	66
Center Partition	61	286	72
Auto Transporter	148	260	65

Table 3.9 Examples of weight and axle load for different locomotives

	Exterior Length	Truck centers	Gross Weights, kips	Axle Loads, kips
4-axle GP 20D	56' 02"	40’ 00”	240	60.0
4-axle GP 60	59’ 02”	43’ 09”	270	67.5
6-axle SD-70MAC	74’ 00”	60’ 02”	415	69.2
6-axle SD-90MAC	80’ 02”	68’ 00”	425	70.8

3.6 Loading Spectra under Current Operating Conditions

The loading spectra to which railway bridges are currently being subjected is more essential for an evaluation of the bridge rather than the design load model. One of the extensive measurements of loading spectra was taken in 1996 by D. Tobias, D. Foutch, and J. Choros. They recorded load from 508 trains at the five typical riveted steel bridges located in Illinois, Virginia and Tennessee. The collected data included the speed of each train, the distance between each axle, and dynamic wheel loads. The measured axle spacing was compared to known rail car dimensions to determine general car types. Table 3.10 presents specific freight types identified in three general types: unit commodity, intermodal, and mixed freight.

Table 3.10 Database of recorded freight types

Freight type	Number of cars in data-base	Total load of cars, ton
Unit commodity		
Coal hopper	21,161	2,543,882
Ballast hopper	390	48,934
Potash hopper	77	9,550
Subtotal	**21,628**	**2,602,366**
Intermodal		
Four-axle intermodal	2,604	170,422
Autorack	1,236	102,151
Five-pack intermodal	450	83,783
Two-axle intermodal	279	9,214
Subtotal	**4,569**	**365,570**
Mixed freight		
Four-axle mixed freight	**7,489**	**492,632**
Locomotive		
Six-axle locomotive	1,050	196,579
Four-axle locomotive	406	51,843
Subtotal	**1,456**	**248,422**
Total	**35,142**	**3,708,990**

The basic statistic for car loading is presented in figure 3.5. About 60% of railroad equipment currently used are coal hoppers; mixed freights are about 20%, four axle intermodal are 7.5%, auto-racks are 3.5%, and 9% includes locomotives and other type of cars.

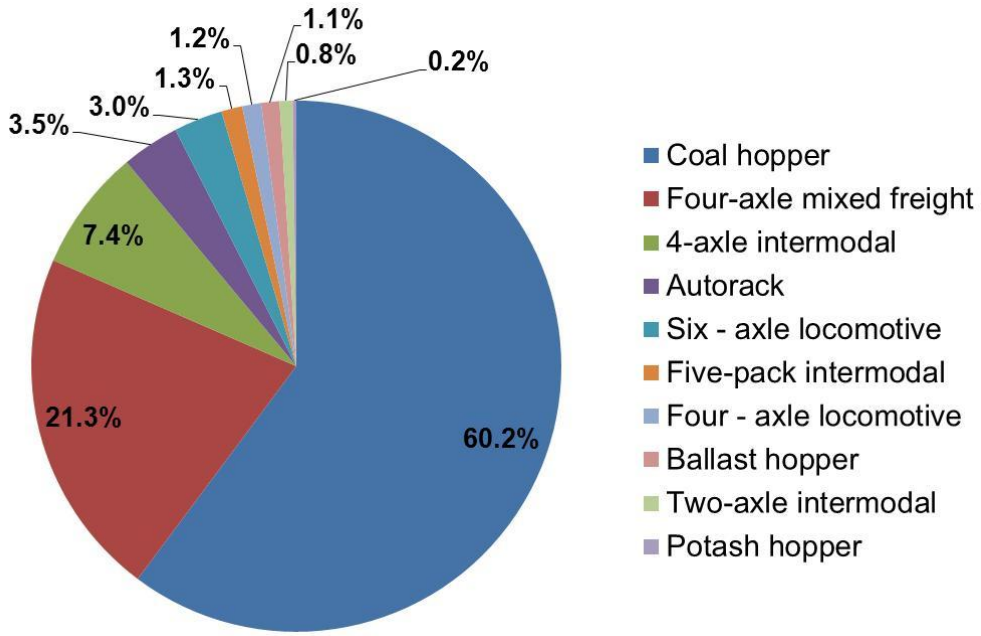

Figure 3.5 Basic statistics for car loading

Collected data were analyzed and five probability distribution functions were chosen as the best fit to the test measurements. The determination of a reasonably well fitted distribution using various statistical tests helps to give a clearer picture of the actual probability of loading (Tobias et. al 1996). Tables 3.11 and 3.12 present the results for car and axle load with the best fit distribution and value of standard deviation. Table 3.13 presents maximum car load and maximum axle load for each measured freight type. Additional analyses on the fitted distributions were performed to determine the loads that 5% and 1% of each population exceed and the results are presented in Foutch et al. (1996).

Table 3.11 Basic fit probabilities and basic statistic for car loadings

Freight type	Best fit distribution	Average car load, kip	Standard deviation, kip
Coal hopper	Weibull	265.50	20.01
Coal hopper 91 t	Normal	254.71	17.76
Coal hopper 100 t	Normal	281.69	9.67
Ballast hopper	Log normal	276.96	8.32
Potash hopper	Log normal	273.82	6.52
Four-axle intermodal	Normal	142.53	33.95
Auto-rack	Gamma	182.77	15.74
Five-pack intermodal	Beta	410.95	133.76
Two-axle intermodal	Beta	73.29	21.36
Four-axle mixed freight	Bimodal normal	80.03; 238.75	20.46; 40.69
Six-axle locomotive	Gamma	413.20	22.03
Four-axle locomotive	Gamma	282.14	19.33

Table 3.12 Basic fit probability and basic statistic for axle loadings

Freight type	Best fit distribution	Average axle load, kip	Standard deviation, kip
Coal hopper	Log normal	66.32	6.07
Coal hopper 91 t	Log normal	63.62	5.40
Coal hopper 100 t	Gamma	70.37	4.95
Ballast hopper	Normal	69.24	4.27
Potash hopper	Log normal	68.34	5.17
Four-axle intermodal	Normal	35.97	9.89
Autorack	Normal	45.64	4.72
Five-pack intermodal	Gamma	34.17	14.39
Two-axle intermodal	Normal	36.42	11.24
Four-axle mixed freight	Bimodal normal	20.23 ; 60.25	5.85 ; 10.12
Six-axle locomotive	Log normal	68.79	6.07
Four-axle locomotive	Log normal	70.37	6.74

Table 3.13 Maximum car and axle loadings

Freight type	Number of axles	Maximum car load, kip	Maximum axle load, kip
Coal hopper	4	336.99	109.03
Coal hopper 91 t	4	339.01	109.03
Coal hopper 100 t	4	339.01	105.88
Ballast hopper	4	305.07	106.56
Potash hopper	4	301.02	95.09
Four-axle intermodal	4	238.07	67.89
Autorack	4	263.03	71.04
Five-pack intermodal	12	845.96	91.05
Two-axle intermodal	2	127.92	67.89
Four-axle mixed freight	4	328.90	95.09
Six-axle locomotive	6	484.91	95.99
Four-axle locomotive	4	361.94	102.96

The load model for reliability analysis for railway bridge systems is based on the load spectra presented by Tobias et al. (1996) and summarized in this subsection. However, collected data include dynamic effect which is subjected to span type and length and many other parameters. Tested bridges were diversified: open deck double plate girder, ballasted deck double plate girder, warren though truss, and through-double plate girder. Also span length varied from 40 ft to 156 ft.

3.7 Maximum Moment of Simply Supported Beams Subjected to Current Railroad Equipment

Based on the large variety of railroad equipment used currently by railroads, theoretical equipment was modeled. This hypothetical train contains two 6-axle locomotives at the beginning, two 4-axle locomotives at the end and twenty railcars with different dimensions and axle forces between locomotives. The locomotives and cars were chosen with maximum capacity and axle spacing was picked to represent the real equipment. Table 3.14 presents the axle load

and spacing between axles used for analyses. This table contains ten common types of railcars. To build an idealized train model, each railcar was used twice. In the results, the train contains 104 moving forces that pass the bridge.

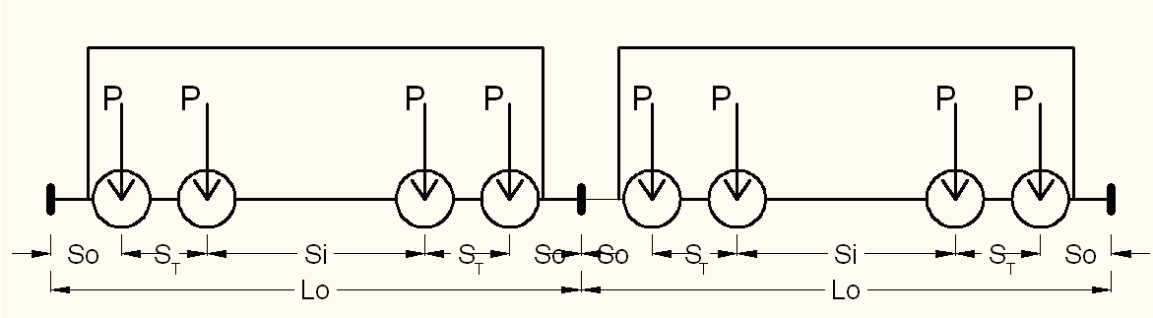

Figure 3.6 Dimensions used for analysis

NOTE:
P – Axle load
L_O – overall length of railroad car measured over the pulling face of the coupler
S_O – Outboard Axle Spacing
S_T – Truck Axle Spacing
S_I – Inboard Axle Spacing

Table 3.14 Idealized train dimensions and axle load

Car Type	P, kips	S_O, ft	S_T, ft	S_I, ft	L_O, ft
6-axle locomotive	69.0	6.0	7.0	34.0	74.0
4-axle locomotive	67.5	8.0	9.0	34.0	59.0
Boxcar	72.0	4.5	5.0	31.0	50.0
Boxcar	72.0	5.5	5.0	39.0	60.0
Boxcar	79.0	6.5	5.5	61.0	85.0
65’ Gondola	72.0	5.5	5.5	43.0	65.0
Container Carrier	66.0	6.0	5.5	52.0	75.0
Center Partition	72.0	6.0	6.0	56.0	80.0
Flatcar	72.0	11.0	6.0	60.0	94.0
Tanker	72.0	5.0	5.0	35.0	55.0
Tanker	72.0	6.0	5.5	47.0	70.0
Auto transporter	65.0	4.5	5.5	60.0	145.5

Ten span lengths were considered from 10 ft up to 100 ft. For each span, moment versus time was plotted and figures 3.7 through 3.10 are the examples of these histograms. There is a significant difference between the shape of the moment for very short span, 10 ft, and longer

span 100 ft. For the shorter span each group of axles create one cycle of the moment from zero to zero. Also, the moment cycles approach zero when the distance between axles is more than the span length. For longer spans, there are no zero moments during a train passing the bridge and the numbers of cycles are smaller.

Maximum moment, moment at mid span, and moment at quarter point were calculated due to passing the idealized train and the results are summarized in table 3.14. The maximum moment was calculated for 100 points on the bridge under a moving set of forces with step of 0.01 ft. The results show that the idealized train, which represents current operating load, produces maximum moments 20% to 40% less than E-80 or the alternative load from AREMA.

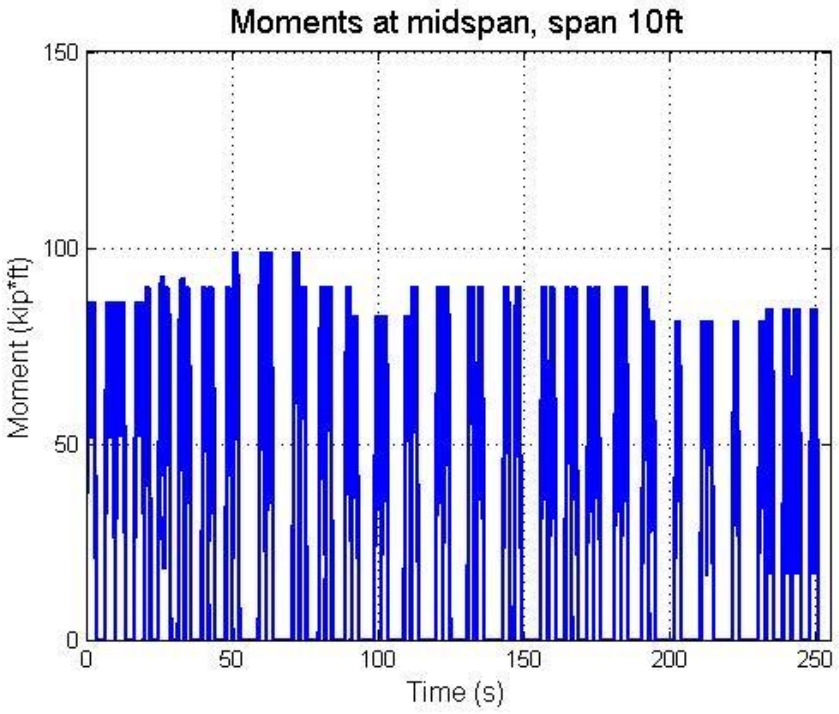

Figure 3.7 Moment at mid span for 10 ft span length

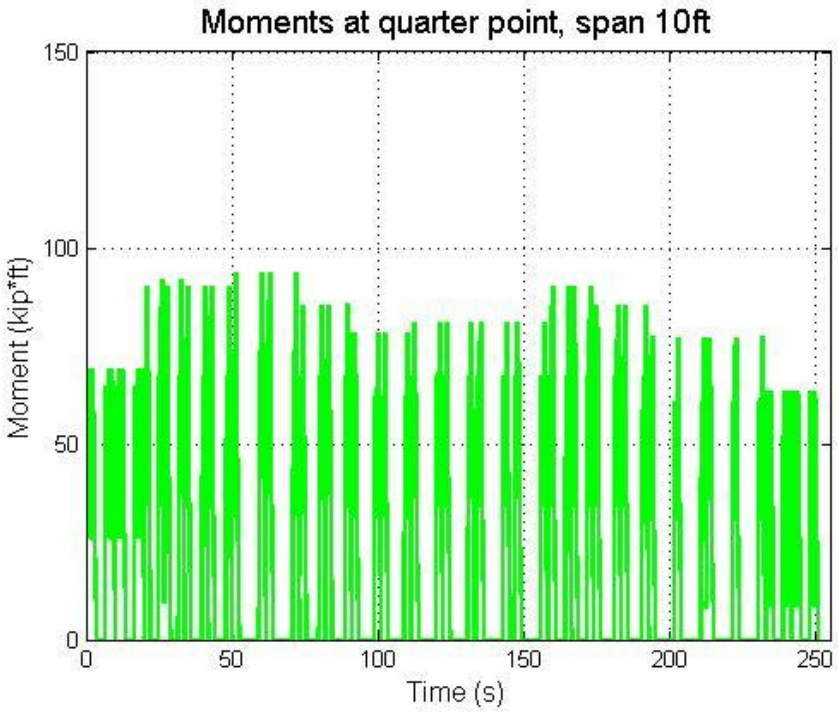

Figure 3.8 Moment at quarter point for 10 ft span length

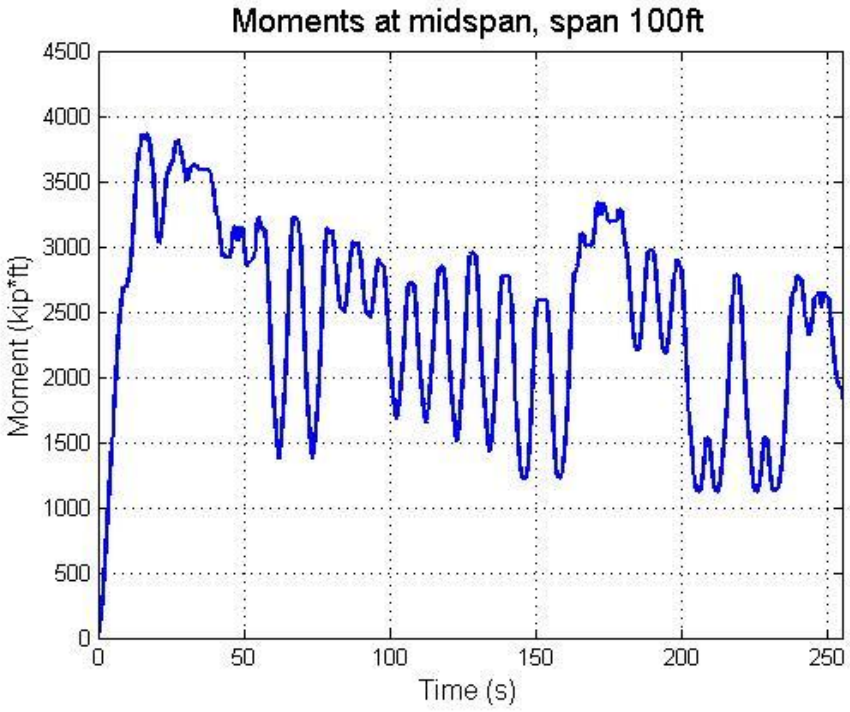

Figure 3.9 Moment at mid span for 100 ft span length

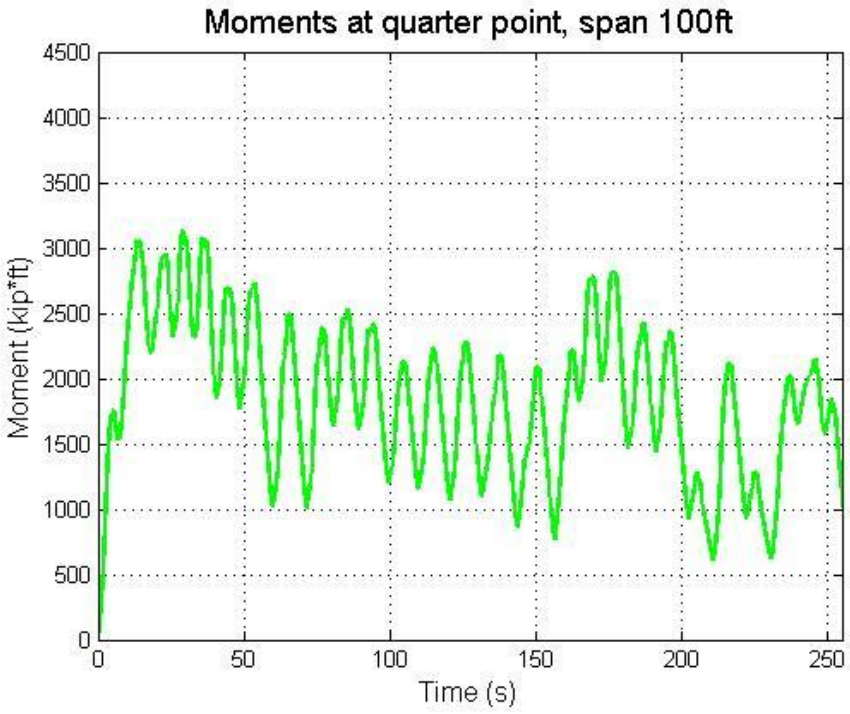

Figure 3.10 Moment at quarter point for 100 ft span length

Table 3.15 Moments for various span lengths

Span Length, ft	E-80 or Alt.		Idealized train		
	Max. Moment	Moment at ¼ Point	Max. Moment	Moment at Mid Span	Moment at ¼ Point
10	140.63	125.0	**103.85**	98.70	93.85
20	475.0	362.5	**295.44**	293.04	241.95
32	1064.06	800.0	**678.66**	656.04	525.73
40	1461.25	1100.0	**964.05**	946.04	743.23
50	1959.00	1481.05	**1364.76**	1363.5	1057.6
60	2597.80	2010.0	**1803.37**	1802.3	1414.6
70	3415.00	2608.2	**2303.49**	2277.0	1802.7
80	4318.90	3298.0	**2817.70**	2794.5	2190.8
90	5339.10	4158.0	**3332.46**	3312.0	2583.3
100	6446.30	5060.5	**3912.34**	3863.9	3136.7

Figure 3.11 shows the moment envelopes for various span lengths. The maximum moment is always close to the mid span, and the red marks on the graph represent the position for maximum bending moment for each span.

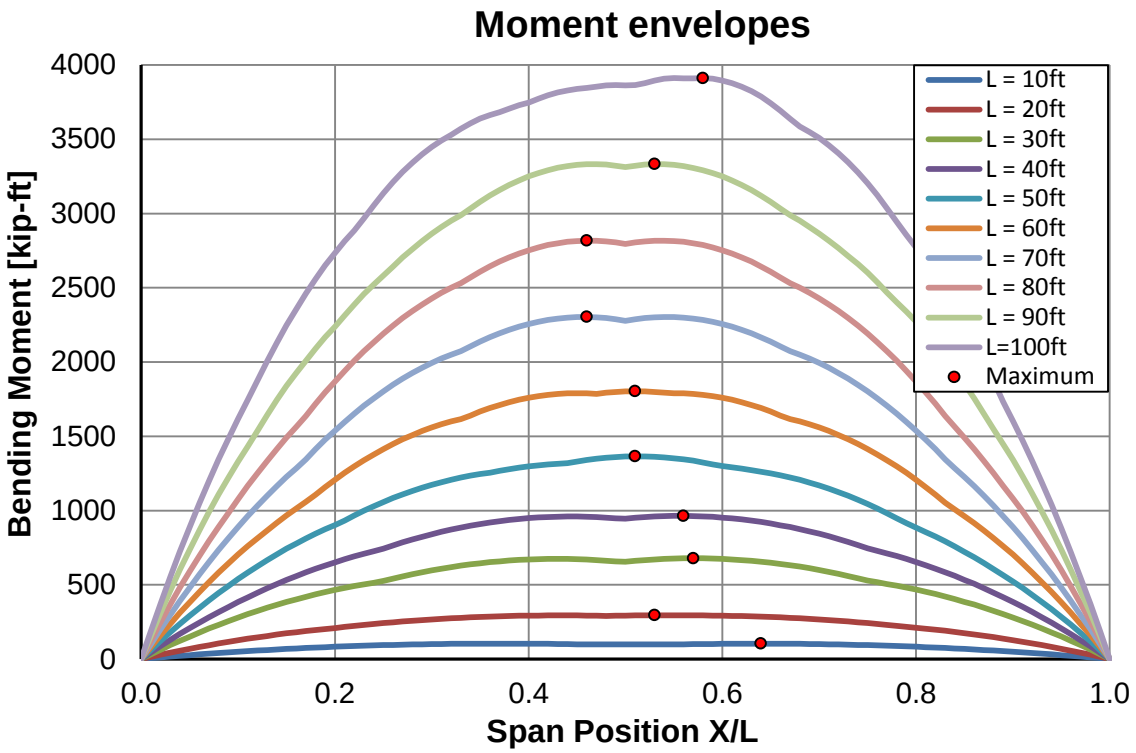

Figure 3.11 Moment envelopes for various span lengths

3.8 Initial Results of Simulations

The Monte Carlo method is a special technique used to generate some variable numerically to establish the probability distributions of the important parameters. In this study the applied load-forces are simulated using Monte Carlo method to estimate mean value and coefficient of variation of bending moment. Statistics for axle loading are taken from Tobias et al. The maximum moment on different span length is calculated and compared to the design moment from AREMA. The CDF of results are plotted on the normal probability paper.

In complete simulation, Model I was generated 450 times, Model II was 225, Model III was 9300, Model IV was 3225, Model V was 1200, and Model VI was 600. Entire train contains 15,000 pieces of railroad equipment with 62% coal hopper; 21.5% mixed freights, 8% of four

axle intermodal, 4% auto-racks, 3% of 6-axle locomotives and 1.5% of 4-axle locomotives. The percentage of equipment corresponds to statistics for car loading from Tobias et al. Cargo cars were modeled as empty, loaded, and fully loaded. The graphics in table 3.15 presents models used in simulation. Dimension of cars were picked as a constant. Axle forces were simulated as a variable with the parameters given in table 3.16.

Table 3.16 Load simulation models

Load simulation – Model I

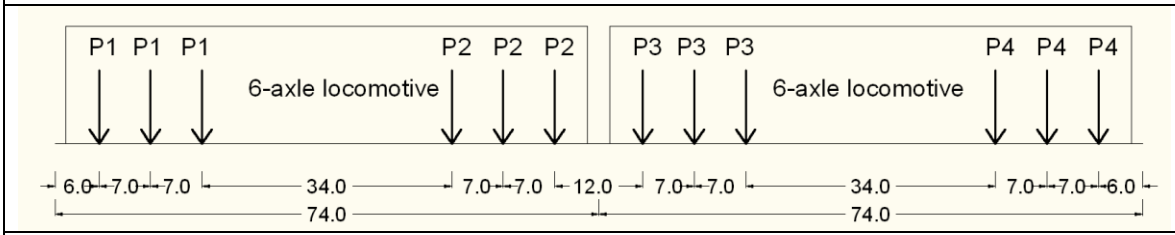

Load simulation – Model II

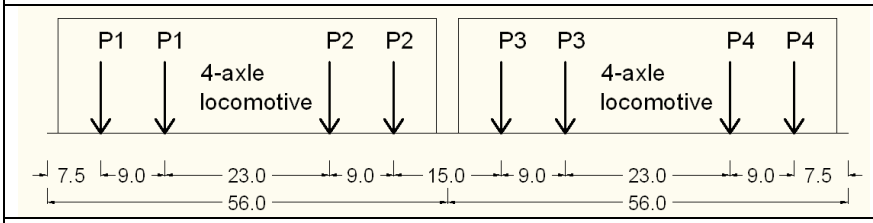

Load simulation – Model III

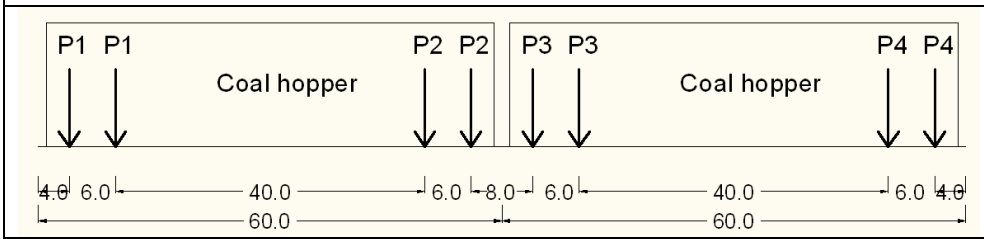

Load simulation – Model IV

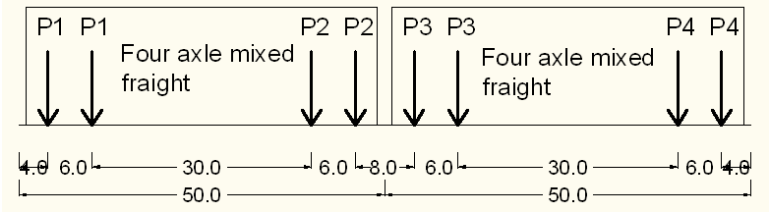

Load simulation – Model V

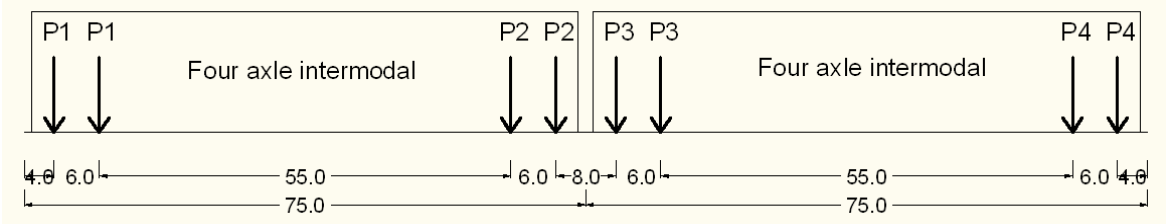

Load simulation – Model VI

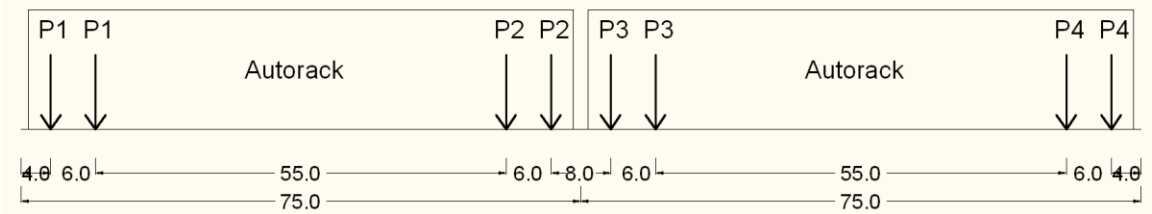

Table 3.17 Statistical parameters of axle load used in the simulation

	Distribution	Mean	Standard deviation	Coefficient of Variation	Additional parameters
Model I	Lognormal	68.79	6.07	0.09	σ_{lnX} = 0.09; μ_{lnX} = 4.23
Model II	Lognormal	70.37	6.74	0.10	σ_{lnX} = 0.10; μ_{lnX} = 4.25
Model III	Lognormal	66.32	6.07	0.09	σ_{lnX} = 0.09; μ_{lnX} = 4.19
	Gamma	70.37	4.95	0.07	λ=2.872; k=202.1
Model IV	Normal	60.25	10.12	0.17	-
Model V	Normal	35.97	9.89	0.27	-
Model VI	Normal	45.64	4.72	0.10	-

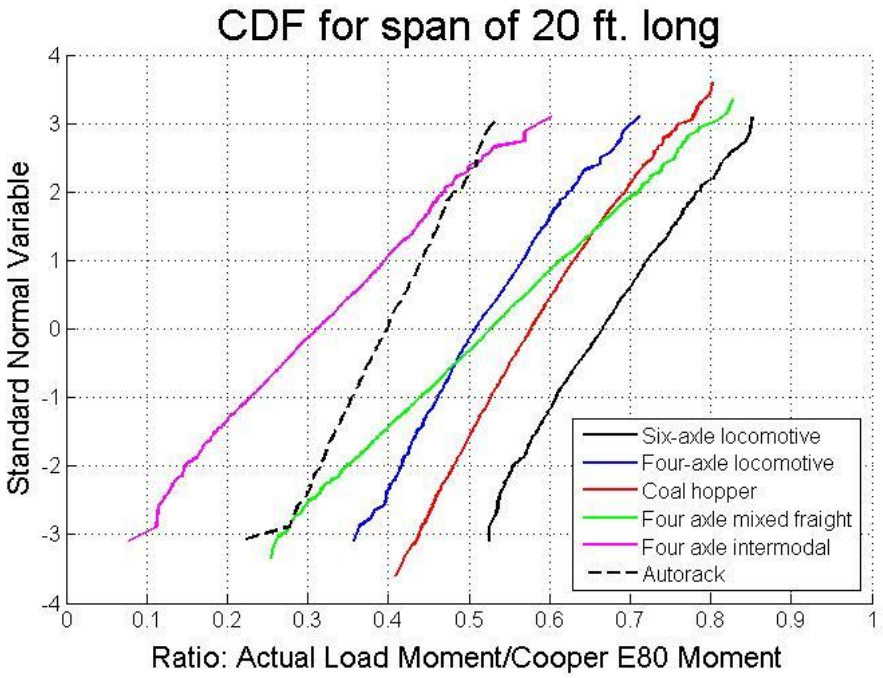

Figure 3.12 CDF of ratio of actual load moment to Cooper E80 Moment for 20 ft span, each type of car plotted separately

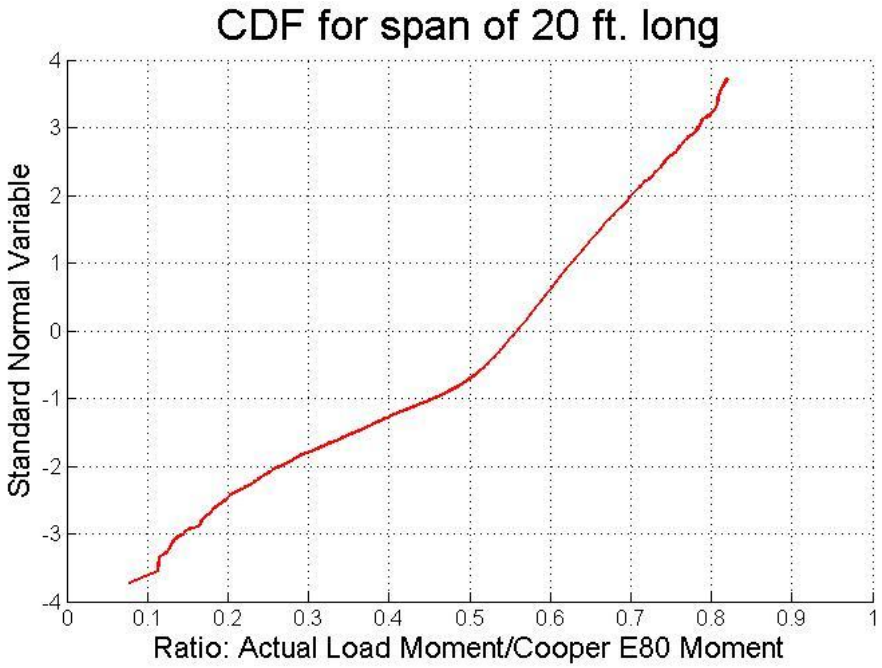

Figure 3.13 CDF of ratio of actual load moment to Cooper E80 Moment for 20 ft span, all cars plotted together (using appropriate proportion)

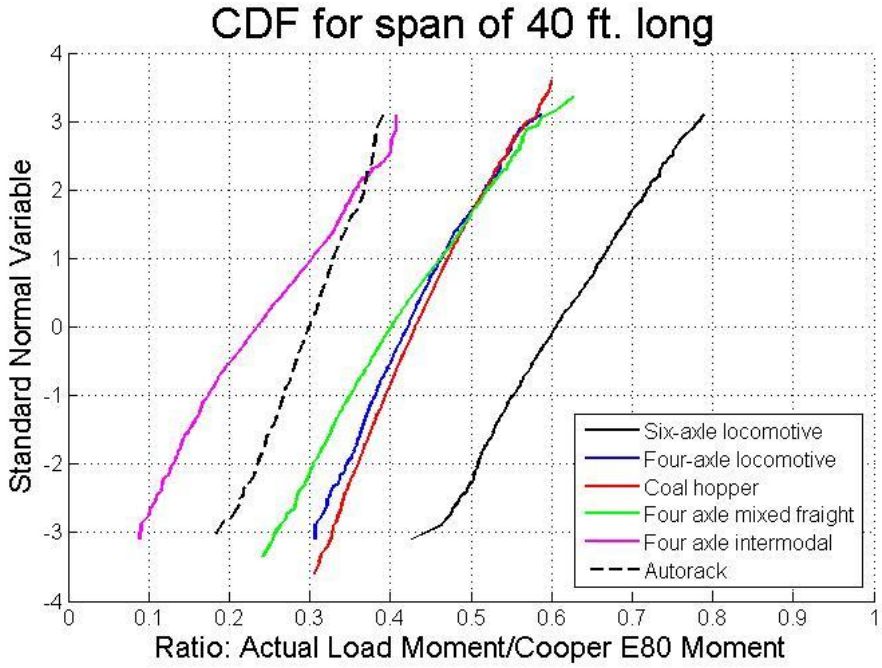

Figure 3.14 CDF of ratio of actual load moment to Cooper E80 Moment for 40 ft span, each type of car plotted separately

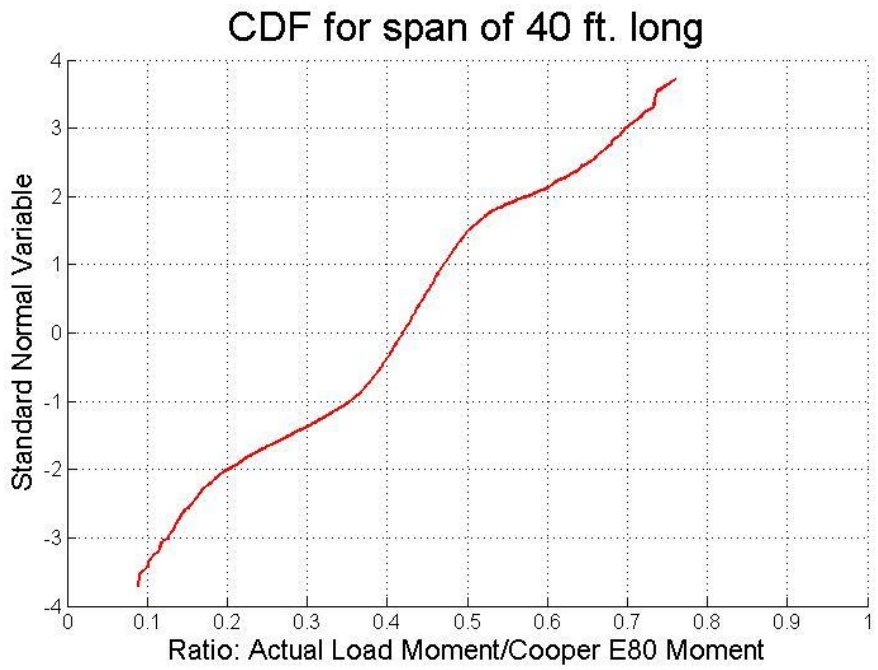

Figure 3.15 CDF of ratio of actual load moment to Cooper E80 Moment for 40 ft span, all cars plotted together (using appropriate proportion)

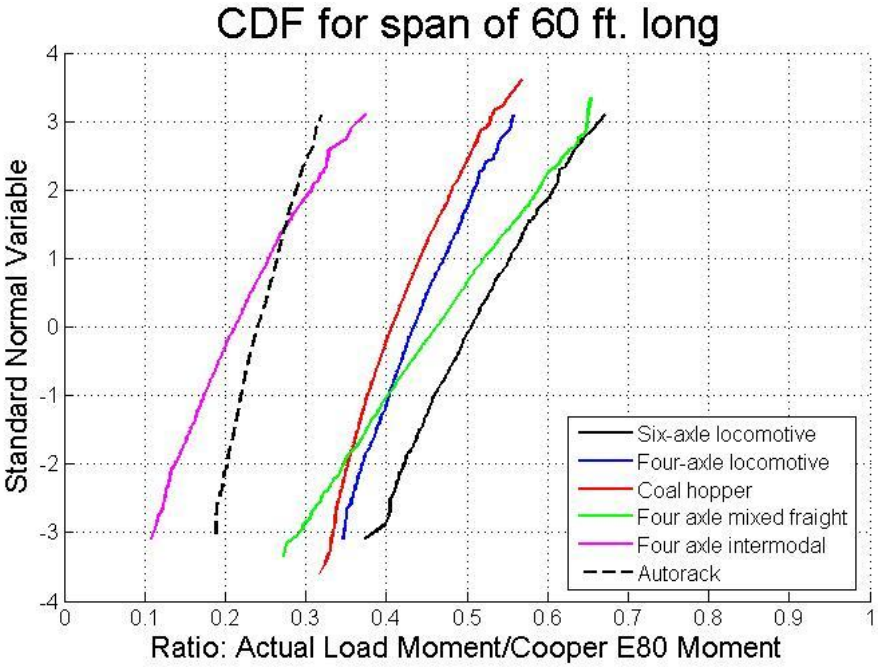

Figure 3.16 CDF of ratio of actual load moment to Cooper E80 Moment for 60 ft span, each type of car plotted separately

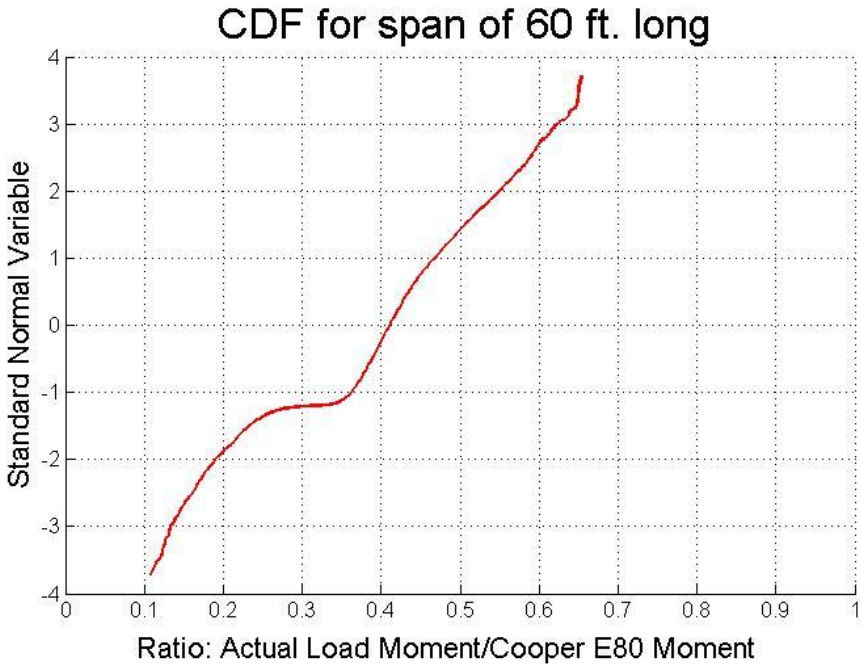

Figure 3.17 CDF of ratio of actual load moment to Cooper E80 moment for 60 ft span, all cars plotted together (using appropriate proportion)

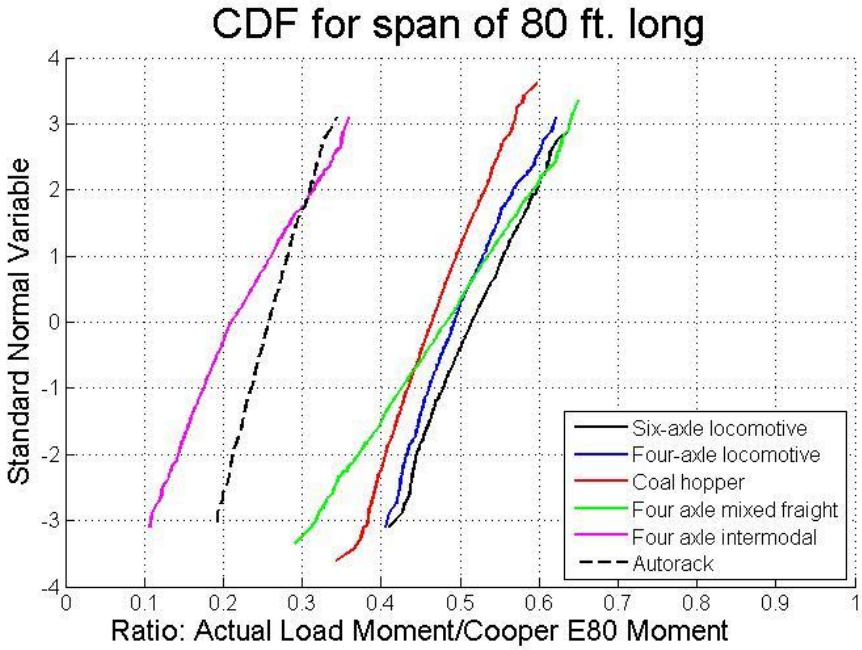

Figure 3.18 CDF of ratio of actual load moment to Cooper E80 Moment for 80 ft span, each type of car plotted separately

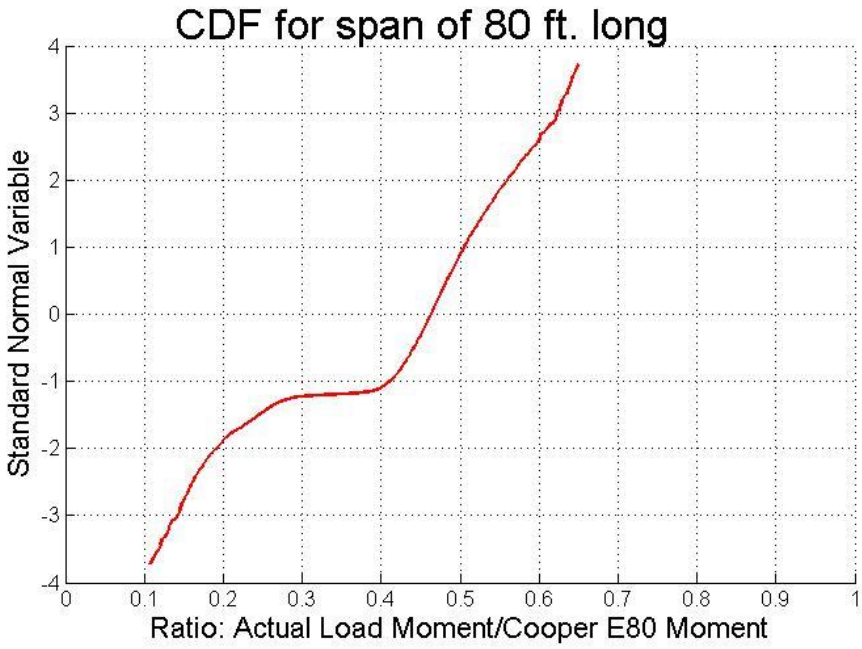

Figure 3.19 CDF of ratio of actual load moment to Cooper E80 moment for 80 ft span, all cars plotted together (using appropriate proportion)

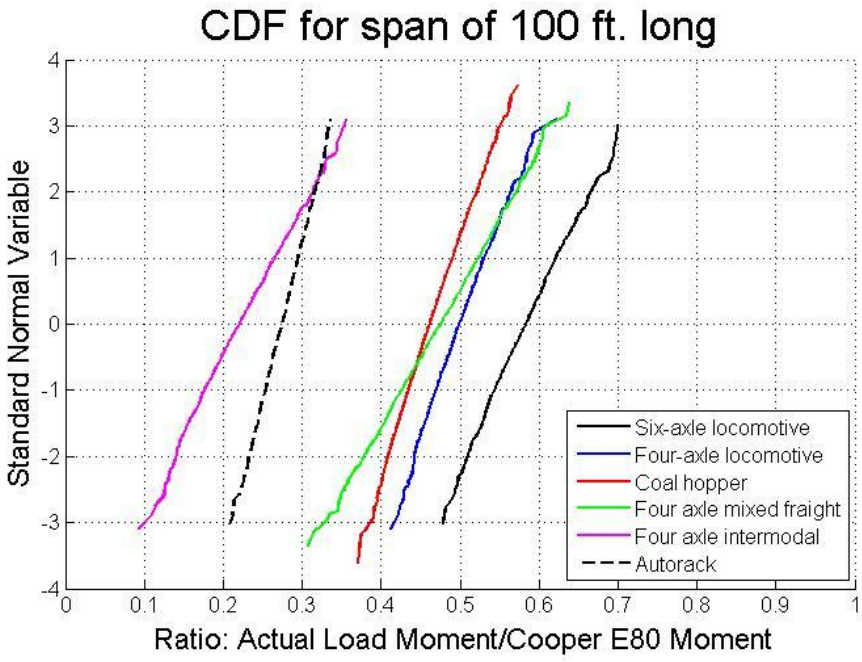

Figure 3.20 CDF of ratio of actual load moment to Cooper E80 moment for 100 ft span, each type of car plotted separately

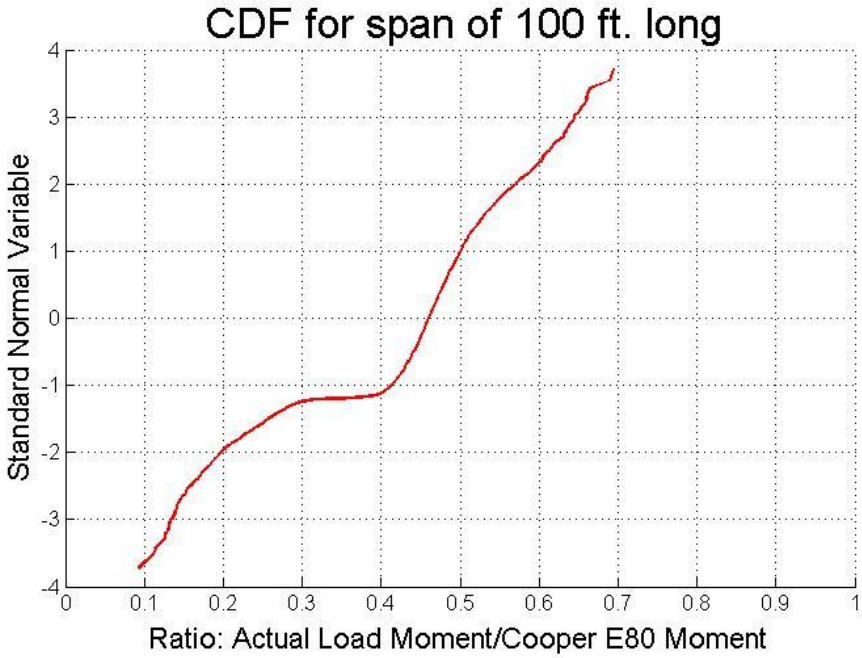

Figure 3.21 CDF of ratio of actual load moment to Cooper E80 moment for 100 ft span, all cars plotted together (using appropriate proportion)

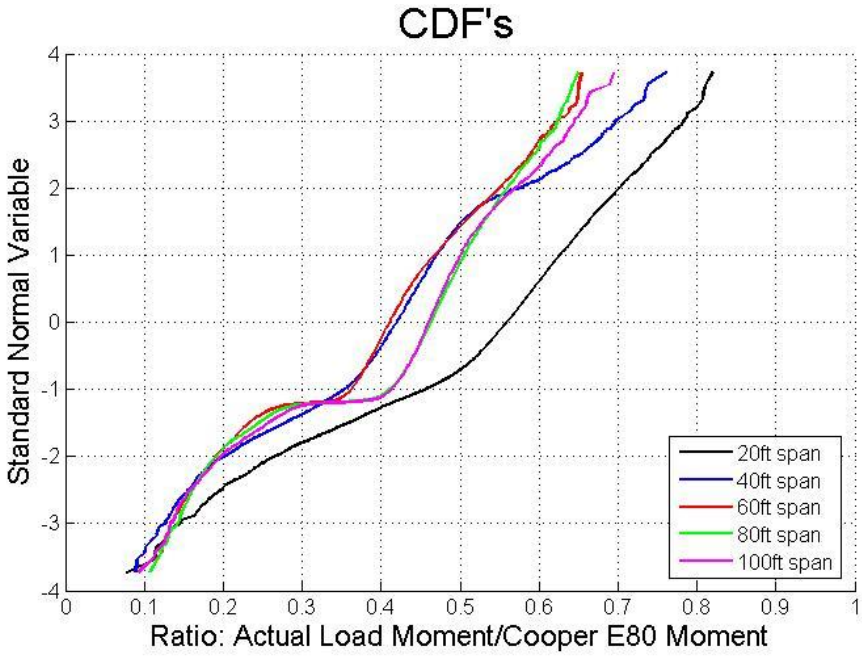

Figure 3.22 CDF of ratio of actual load moment to Cooper E80 moment for different span lengths

Table 3.18 Statistical parameters of bending moment for various span lengths

Span length	Mean	COV	Mean + 1.5 σ
20 ft	0.56	0.12	0.66
40 ft	0.42	0.12	0.50
60 ft	0.42	0.12	0.50
80 ft	0.46	0.10	0.53
100 ft	0.46	0.10	0.53

Chapter 4 Structural Analysis

4.1 Overview

The Finite Element Method (FEM) was used to investigate the behavior and performance characteristic of the bridge structure. FEM is a numerical technique for finding approximate solutions of partial differential equations as well as integral equations. "The solution approach is based either on eliminating the differential equation completely through steady state problems, or rendering the PDE into an approximating system of ordinary differential equations, which are then numerically integrated using standard techniques such as Euler's method, Runge-Kutta, and so forth" (Finite element method 2012).

Widely used structural analysis software is based on the FEM approach. In this study, three dimensional element models were developed by using the FEM software called ABAQUS/CEA. This software provides a simple, consistent interface for creating, submitting, monitoring, and evaluating results from ABAQUS/Standard and ABAQUS/Explicit simulations. ABAQUS/Standard is a general-purpose FEA that uses a traditional implicit integration scheme. ABAQUS/Explicit is a special purpose FEA that employs an explicit integration scheme to solve highly nonlinear systems with many complex contacts under transient loads (en.wikipedia.org).

ABAQUS/Standard provides both linear and nonlinear response options. The program is truly integrated, so linear analysis is always considered as linear perturbation analysis. The nonlinear procedures in ABAQUS/Standard offer two additional approaches: direct user control of increment size and automatic control approach. Automatic control approach is usually more efficient because the user cannot predict the response ahead of time. In ABAQUS/Explicit the time incrementation is controlled by the stability limit of the central difference operator. Hence, the time incrementation scheme is fully automatic and requires no user intervention.

In this study, structural analytical calculations are implemented by ABAQUS/Standard FEM software. Standard static simulations as well as steady-state dynamic simulations were performed. Inelastic behavior of materials was included and elastic-plastic properties of steel, wood, and gravel were defined based on the available models in ABAQUS. Very complex models were created for two through-plate girder riveted railway bridges: a 32 ft span open deck and a 64 ft span ballasted deck. Models were built from plate girders, floor beams, stringers, cover plates, rails, rail ties, wood decks, gravel, connection angles, and rivets.

4.2 Introduction to Finite Element Method

ABAQUS/Standard generally uses Newton's method as a numerical technique for solving nonlinear equilibrium equations (ABAQUS Analysis User's Manual). The advantage of Newton's method as compared to alternate methods, such as modified Newton or quasi-Newton methods is primarily the rate of convergence of the results. However, Newton's method is not good for large finite element codes for two reasons. First of all, it is difficult to formulate a complete Jacobian matrix and, second, formulating and solving the Jacobian for each iteration is time consuming. In the modified Newton method, the Jacobian is recalculated only occasionally. Therefore this method can be used for mildly nonlinear problems involving softening behavior, but is not recommended for strictly nonlinear cases.

All nonlinear solutions are based on obtaining the solution by numerical methods when it is not possible to find an analytic solution. The iteration continues until a numerical solution gives a very close approximation to the true solution. During the process, series of increments are created with iterations to obtain equilibrium within each of the increments. Hence, the increment size controls the efficiency and speed of calculations. Increments that are too large require more iterations and, in some cases, the program does not manage to find a solution at all.

ABAQUS provides both “automatic” time step choice and direct user control for all classes of problems (ABAQUS Analysis User’s Manual). For nonlinear problems, automatic schemes in ABAQUS provide a reliable approach.

4.2.1 Finite Element

ABAQUS has a wide range of elements available. Each element is characterized by family, degree of freedom, number of nodes, formulation, and integration. Figure 4.1 shows the element families most commonly used in a stress analysis. One of the major distinctions between different element families is the geometry type that each family assumes.

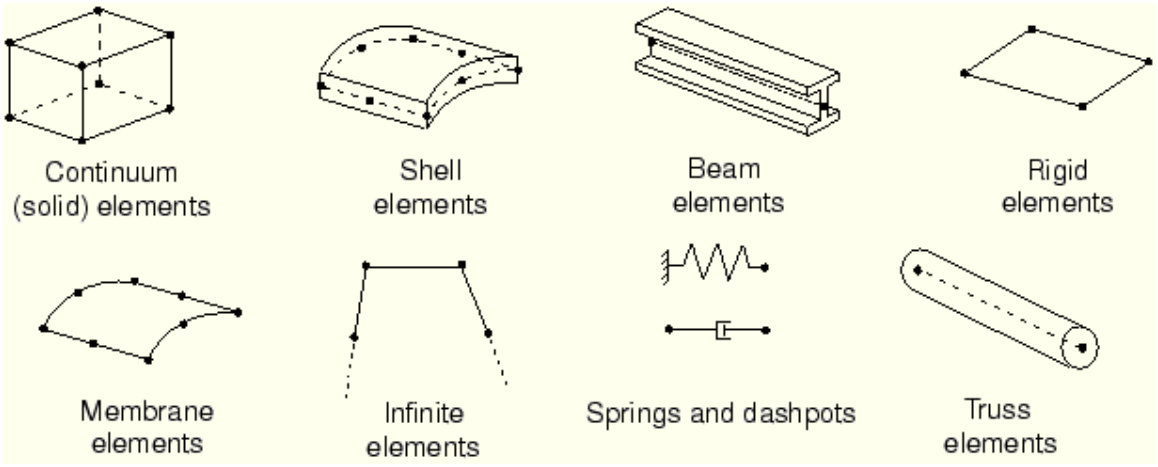

Figure 4.1 Commonly used element families (ABAQUS Analysis User’s Manual)

The degrees of freedom (DOF) are the fundamental variables calculated during the analysis. For a stress/displacement simulation, the degrees of freedom are the translations at each node. Some element families, such as the beam and shell families, have rotational degrees of freedom as well. The basic DOF are presented in figure 4.2. Additional DOF include, among others, warping in open-section beam elements and temperature for continuum elements or temperature at the first point through the thickness of beams and shells.

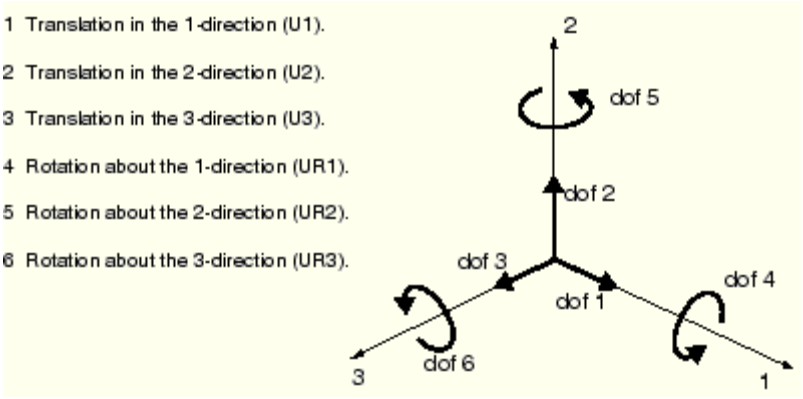

Figure 4.2 Displacement and rotational degrees of freedom (ABAQUS Analysis User's Manual)

Displacements, rotations, temperatures, and the other degrees of freedom mentioned in the previous section are calculated only at the nodes of the element. At any other point in the element, the displacements are obtained by interpolating from the nodal displacements. Usually the interpolation order is determined by the number of nodes used in the element. Elements that have nodes only at their corners, such as the 8-node brick, use linear interpolation in each direction and are often called linear elements or first-order elements. Elements with mid-side nodes, such as the 20-node brick, use quadratic interpolation and are often called quadratic elements or second-order elements. Modified triangular or tetrahedral elements with mid-side nodes, such as the 10-node tetrahedron, use a modified second-order interpolation and are often called modified or modified second-order elements. A selection of elements is presented in figure 4.3.

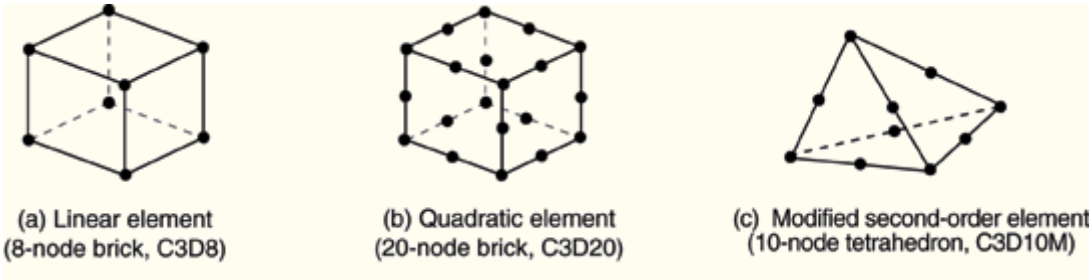

Figure 4.3 Linear brick, quadratic brick, and modified tetrahedral elements (ABAQUS Analysis User's Manual)

An element's formulation refers to the mathematical theory used to define the element's behavior. In the absence of adaptive meshing, all of the stress/displacement elements in ABAQUS are based on the Lagrangian or material description of behavior. That is, the material associated with an element remains associated with the element throughout the analysis, and material cannot flow across element boundaries. In the alternative Eulerian or spatial description, elements are fixed in space as the material flows through them. Eulerian methods are used commonly in fluid mechanics simulations.

ABAQUS uses numerical techniques to integrate various quantities over the volume of each element. Using Gaussian quadrature for most elements, ABAQUS evaluates the material response at each integration point in each element. Some continuum elements in ABAQUS can use full or reduced-integration; a choice that can have a significant effect on the accuracy of the element for a given problem.

In this study, shell elements with 6 degrees of freedom per node were used to model stringers, floor beam, plate girders, connection angles, and cover plates. Continuum elements, along with an 8-node brick, were used to model rails, rail ties, wood deck and gravel.

4.2.2 Connections and Constraints

In ABAQUS, many types of kinematic constrains can be defined. Two surfaces can be tied together using surface-based tie constraints. In this type of connection each node on the first, or slave, surface has the same values for its degrees of freedom as the point on the second, or master, surface to which it is closest. A surface-based tie constraint can be used to make the translational and rotational motion, as well as all other active degrees of freedom, equal for a pair of surfaces. The offset distances between the surfaces' elements can be defined in the constraints or can be taken as a default; the simulation takes the initial thickness and offset of shell elements underlying the surface into account. The surface-to-surface formulation generally avoids stress noise at tied interfaces. Only a few surface restrictions apply to the surface-to-surface formulation.

ABAQUS can use one of two approaches to generate the coefficients: the "surface-to-surface" approach or the "node-to-surface" approach. The true "surface-to-surface" approach optimizes the stress accuracy for a given surface pairing. The improved stress accuracy with the surface-to-surface approach is realized only if neither surface of the tie pairing is node-based. The surface-to-surface method for establishing the tie coefficients involves a more complex algorithm than the node-to-node method because it generally uses more master nodes per constraint.

In this study the "surface-to-surface" approach in tie constrains were used to create a riveted connection. Also, as a general mechanical constraint, the displacement and rotation were assigned for boundary conditions on both ends of the plate girders.

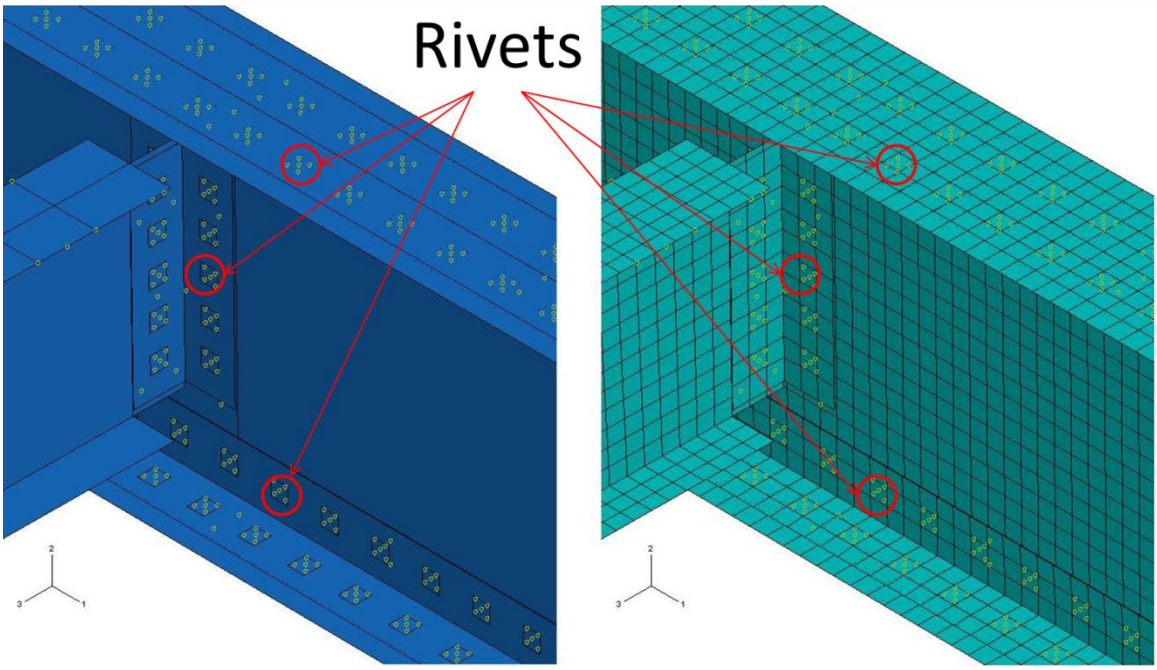

Figure 4.4 The riveted connection model used in the analysis

Two types of load were assigned to the problem: dead load (DL) and live load (LL). The dead load is characterized by self-weight and live load is created by the train passing the bridge. Both loads were created as general static load. For self-weight, ABAQUS has an option of gravity load for the whole model with a parameter of acceleration due to gravity and direction of action (but, first all materials used in the analysis must be assigned a density). The train passing the bridge can be simulated using static load with the steady-state dynamic approach. To create moving load in ABAQUS/Standard the time variant can be defined by various amplitudes. The position of the train is a function of time. First, the position of a train at any specified time should be predicted, and then adequate amplitude must be defined.

Consider a set of two forces moving through the simply supported beam. If the beam is 4 ft long, the distance between forces is 1 ft. For each 0.1 second the tandem is moving 1 ft forward, then four locations of the beam can be considered. Instead of dividing the task into

four subtasks this can be modeled in one by defining four amplitudes. In this approach, the bridge response varies with time, because the load changes its position. This allows for analysis under moving load but no dynamic effect is considered—hence, the name steady-state dynamic.

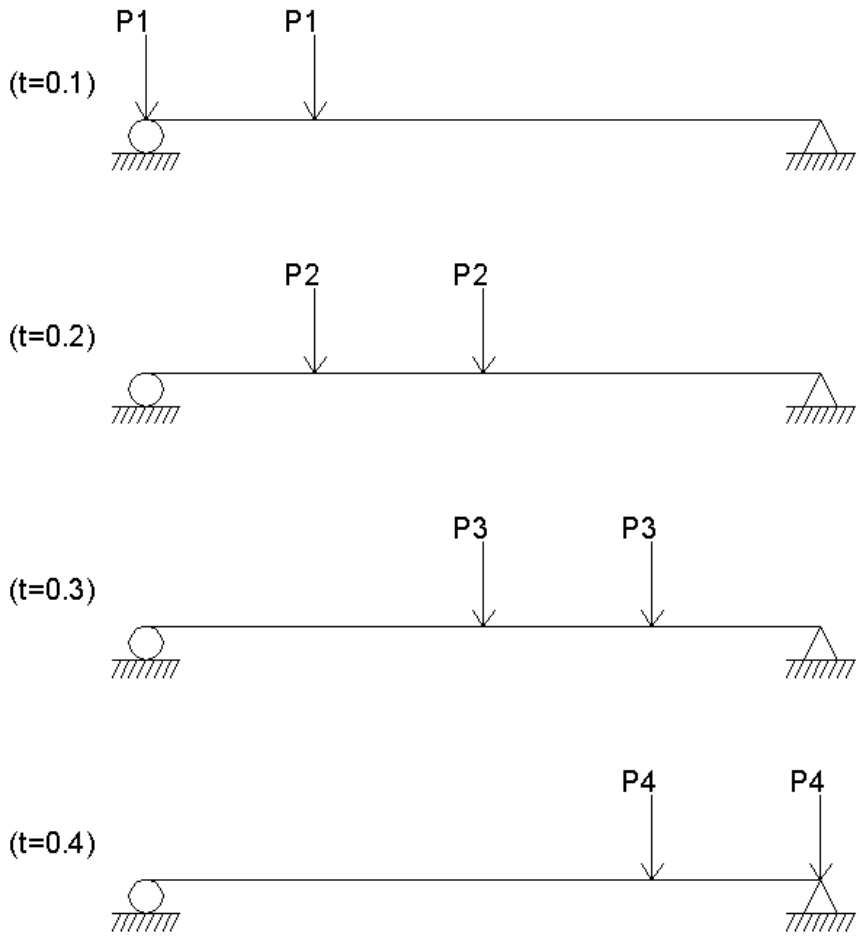

Figure 4.5 Set up of tandem on the beam at different times

In this study the bridge response is calculated under an adjustable load on the bridge at a distance of one foot.

4.2.3 Material Models

The constitutive library provided in ABAQUS contains a range of linear and nonlinear material models for all categories of materials. It include simple models such as isotropic, linear

elastic without temperature dependence as well as a very sophisticated material models which include much more detail of the material's response under failure. For a routine design of the component, which is not in any critical situation, the simple model is sufficient. However, if the component is subjected to a severe overload, it is important to determine how it might deform under that load and whether it has sufficient ductility to withstand the overload without catastrophic failure. From a numerical viewpoint, the implementation of a constitutive model involves the integration of the state of the material at an integration point over a time increment during a nonlinear analysis. In the inelastic response models that are provided in ABAQUS, the elastic and inelastic responses are distinguished by separating the deformation into recoverable (elastic) and non-recoverable (inelastic) parts.

In this study three types of materials were modeled: structural steel, wood, and gravel (only for ballasted deck bridge). With the assumption that wood parts and gravel elements that are not subjected to any critical situation do not cause failure of the bridge, the simple model was sufficient. Therefore, isotropic, linear elastic without temperature dependence models were used, and the general properties were assigned as it concerns density, Young's Modulus, and Poisson's Ratio. This approach allowed for proper computation of self-weight and adequate load distribution in a complex model. However, main parts of the bridge made of structural steel should be carefully investigated. That is why more sophisticated material models were defined for structural steel. Therefore, steel was modeled as nonlinear elastic-plastic material. In ABAQUS a few models define plastic behavior. One of which is user-defined data, where the yield stress is defined as a function of plastic strain. Figure 4.6 shows a typical tensile stress-strain curve with characteristic points for standard steel. The characteristic points are

proportional limit, yield point, ultimate stress, and failure point. Bellow, the proportional limit stress-strain relation is linear and referred to as the Young's Modulus.

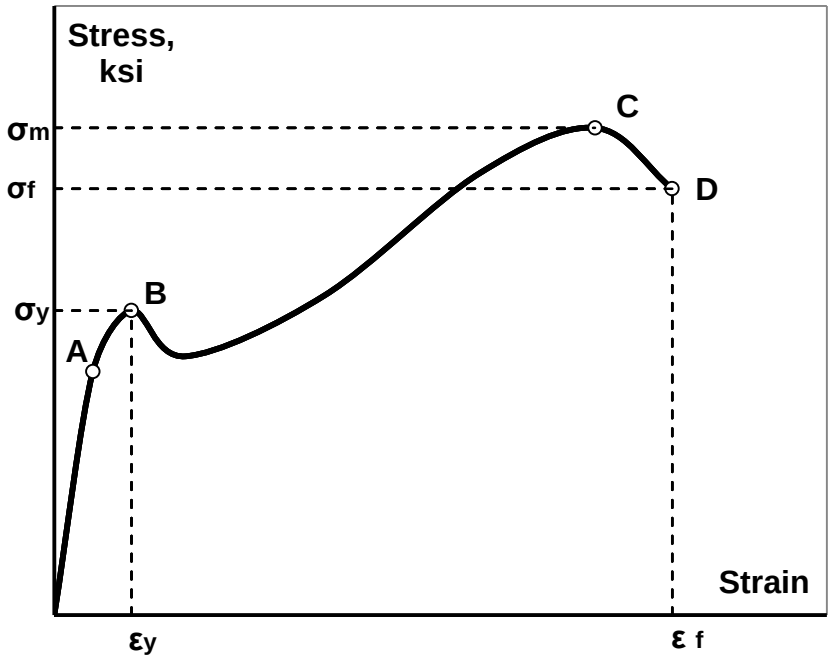

Figure 4.6 Tensile stress-strain curve for steel (a = elastic limit, b = upper yield stress, c = ultimate stress, d = breaking stress)

Yield stress is the maximum stress for which the material shows an elastic behavior, and it means that the deformations are reversible. Figure 4.7 shows the stress-strain path for elastic material under loading and unloading.

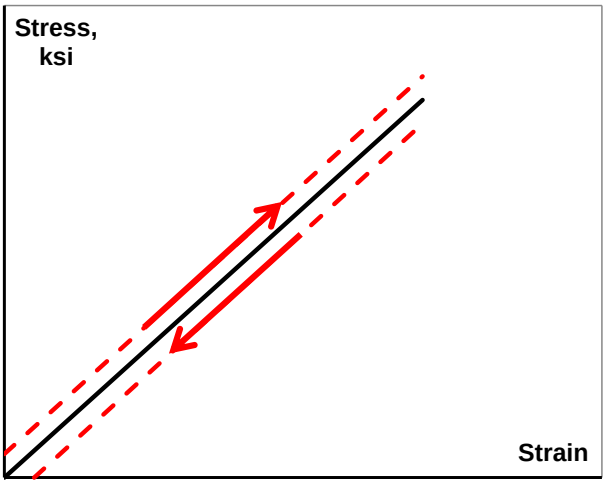

Figure 4.7 Elastic behavior

When the yield point is reached and the load continues to grow, then plastic deformation occurs. Plastic deformation is not reversible, so after releasing the load strain it does not return to 0. For plastic behavior the stress-strain path is presented in figure 4.8. The left side of figure 4.8 demonstrates that after the first loading and completed unloading the deformation is maintained, while the right side shows that a new loading takes place and the previous unloading path.

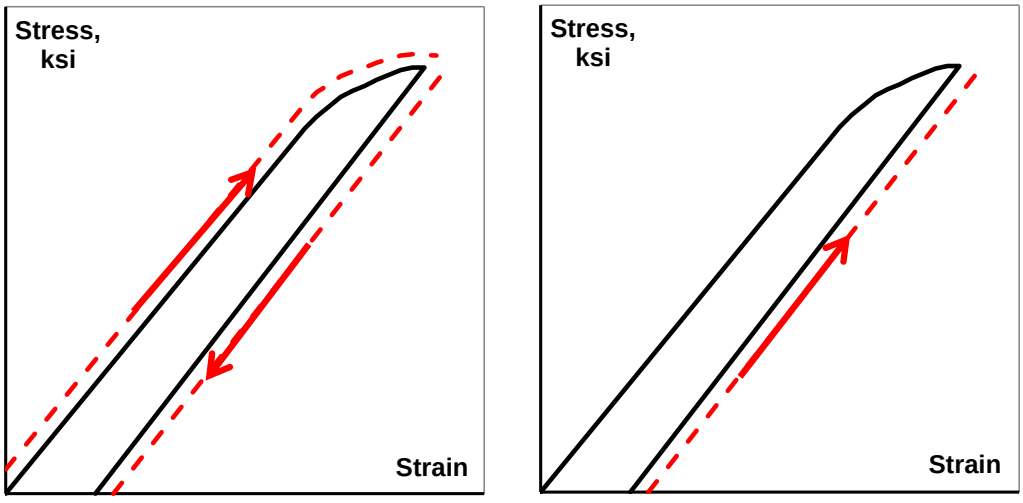

Figure 4.8 Plastic behavior

In addition to tensile stress-strain relation, other characteristics of steel are important. When a material is stretched in one direction, it usually tends to shrink in the other two directions perpendicular to the direction of stretching. The Poisson's ratio is a ratio of transverse and longitudinal strain.

4.3 Bridge Description

4.3.1 Bridge #1

Bridge #1 is a through-plate girder, riveted, open deck railway bridge, designed according to AREA and built in 1894. The structure is located on the main railway line connecting Bangkok to the north and northeast of Thailand (Chotickai and Kanchanalai 2010). The overall inspection shows that the structure is in good condition with minor loss of sections due to corrosion. The bridge has a one simply supported span which is 32 ft 9 in. (10 m) long with the floor system presented in the graphic in figure 4.9. The main structural components include two main plate girders and a floor system of floor-beams and stringers. The girders are spaced transversely at 10 ft 2 in. (3.1 m) from center to center, the floor beams are spaced 10 ft 11 in. (3.33 m) in the longitudinal direction, and the stringers are spaced transversely at 4 ft 11 in. (1.6 m).

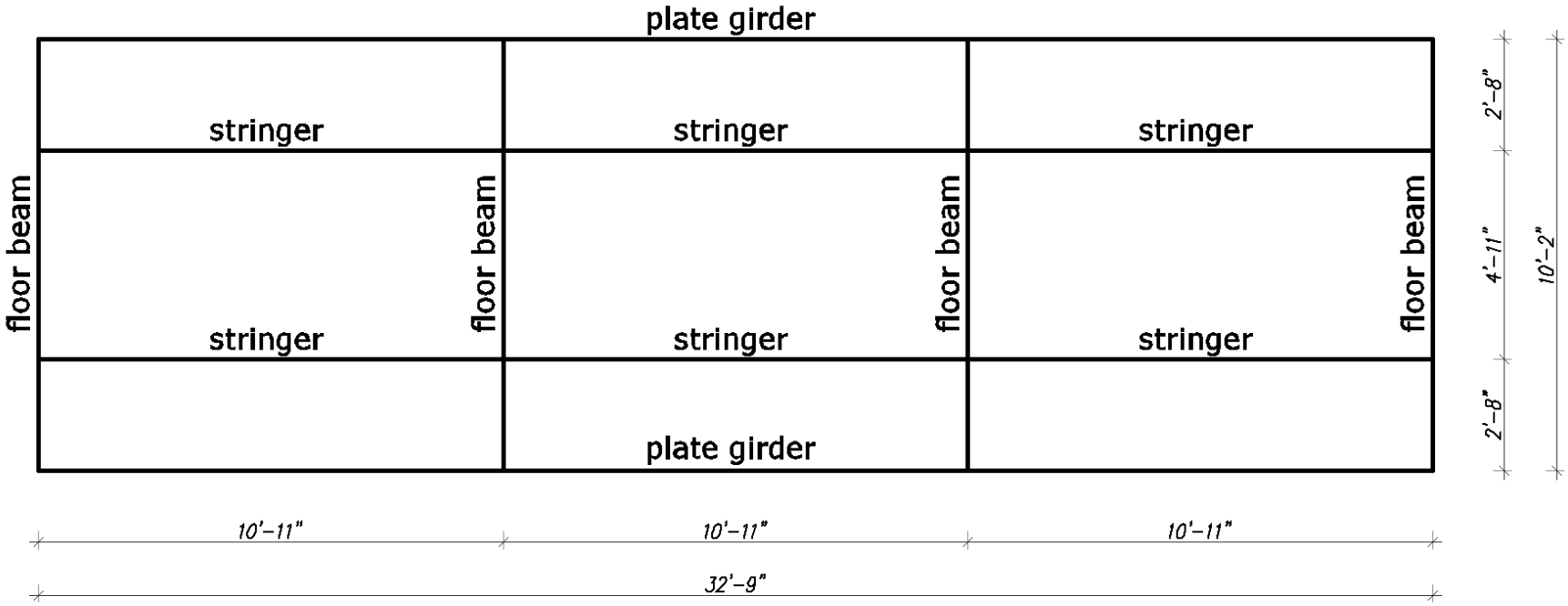

Figure 4.9 Floor system of bridge #1

The main girders are built up from a web plate of 3 ft 6 in. (1.06 m) total depth, 9.85 in. by 0.4 in. (250 x 10 mm) upper and lower cover plates, structural L shapes and vertical web stiffeners in about 3 ft 3 in. (1 m) intervals. Track systems (rails and rails tie) are lying directly on stringers, which are supported by floor beams. The floor beams are also built up sections that contain 24 in. x 0.4 in. (610 x 10 mm) web plates, 9.85 in. x 0.4 in. (250 x 10 mm) upper and lower cover plates and double angles. The stringers are rolled I beams with a 1 ft 4 in. by 0.5 in. (410 x 12 mm) web and 6 in. by 0.8 in. (150 x 20 mm) flanges. The stringers contain upper cover plates that are 6 ft by 0.4 in. (150 x 10 mm).

All connections between members within the structure are made using rivets with a nominal diameter of 0.8 in. (20 mm). The stringer-to-floor beam connection is made using double angles riveted to stringer and floor-beam webs. This type of connection is intended to be a simple shear connection that does not transmit the moment. The components and connections of the bridge are presented in the graphics in figures 4.10 and 4.11. Elements such as rails and rail ties were not specified; therefore, 136-lb. AREMA rails and timber ties were assumed. Rail ties are spaced 17.5 in. (44.45 cm) center to center and are 5.5 in. (14.0 cm) high, 6.5 in. (16.5 cm) wide and 7.5 ft (2.3 m) long. Rail specification is presented in APPENDIX A. The steel of superstructure and rails has an elastic modulus of 29000 ksi (200GPa) and yield stress of 30 ksi (207 MPa).

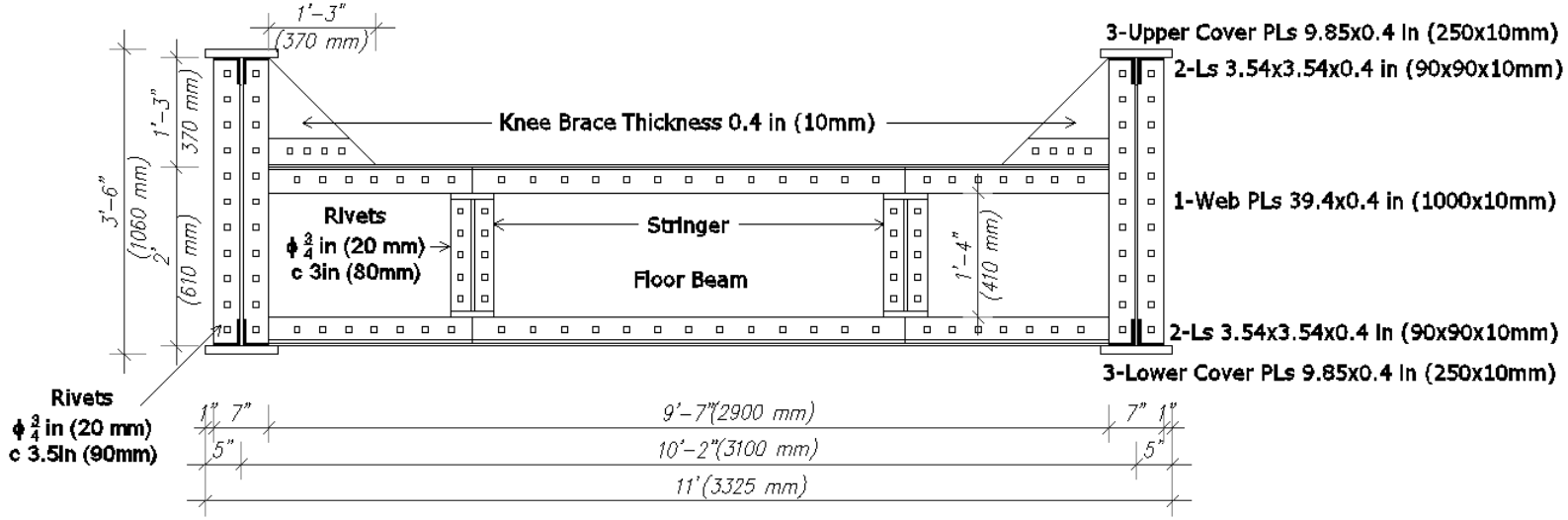

Figure 4.10 The floor beam of bridge #1

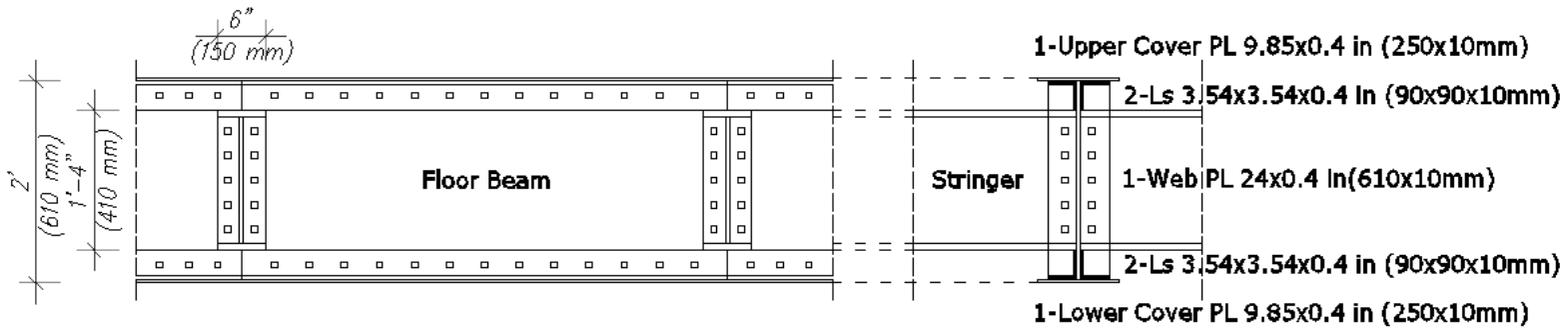

Figure 4.11 The stringer-to-floor-beam connections of bridge #1

4.3.2 Bridge #2

Bridge #2 is a through-plate girder, riveted, ballasted deck Railway Bridge. The bridge was constructed in 1898 and is located in New Mexico. The bridge has three simply supported spans which are 64 ft (19.5 m) long with the floor system presented in the graphic in figure 4.12. The main structural components include two main plate girders and floor system of five floor-beams and sixteen stringers. The girders are spaced transversely at 16 ft 1 in. (4.9 m) from center to center, the floor beams are spaced at 15 ft 8 in. (4.8 m) in the longitudinal direction and the stringers are spaced transversely with 2 ft 9 in. (2.75 m) from exterior stringers to the interior stringer and 2 ft 2 in. (0.66 m) between internal stringers. Only one span of the bridge was considered in the analysis.

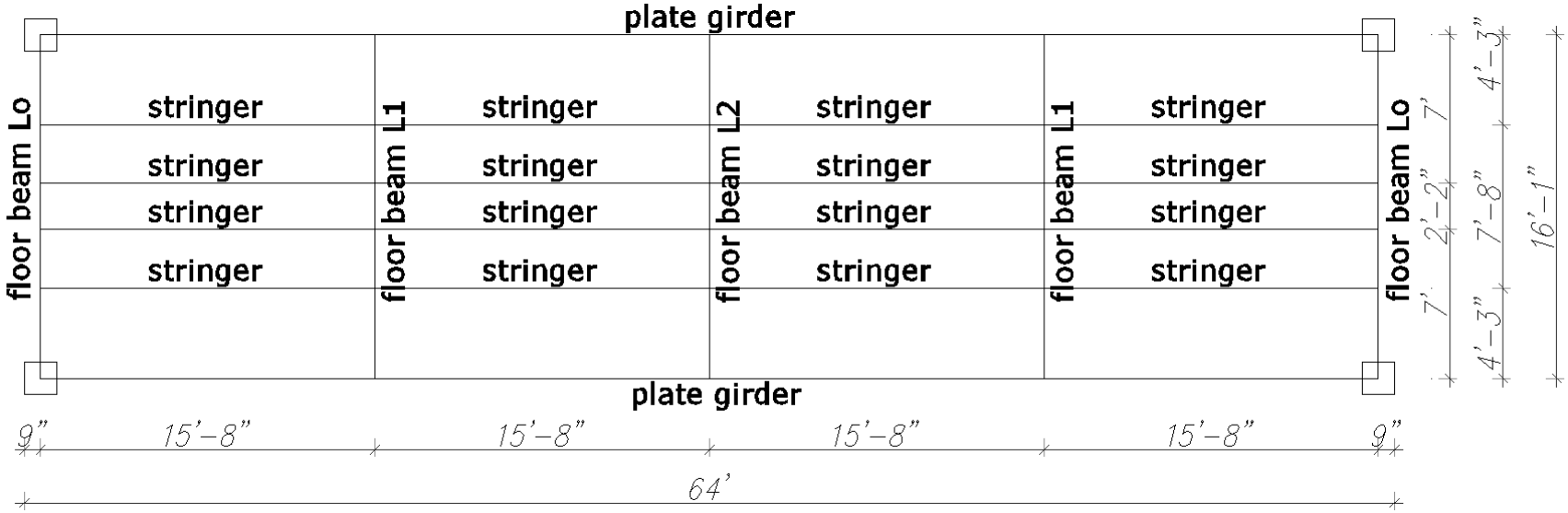

Figure 4.12 The floor beam of bridge #2

The main girders are built up from 3/8 in. (9.5 mm) web plates of 6 ft 1 in. (1.85 m) total depth, 14 in. (356 mm) upper and lower cover plates, 6 in. x 6 in. x 3/8 in. (152.4 mm x 152.4 mm x 9.5 mm) structural L shapes and vertical web stiffeners in about 7 ft (2.1 m) intervals. The girder profile is presented in the figure 4.13. At mid-span, three upper cover plates and three lower cover plates are used. Description of total thicknesses of girder sections is presented in table 4.1.

Table 4.1 Trains used in this study

	Total thickness	
	Top Cover plates	Bottom Cover plates
Section 1	0.625	0.00
Section 2	0.625	0.625
Section 3	1.125	1.125
Section 4	1.625	1.625

The floor-beams are also built up sections containing 42.25 in. x 0.375 in. (1073 x 9.5 mm) web plates and structural L shapes. External floor-beams L0 contain 6 in. x 6 in. x 9/16 in. (152.4 mm x 152.4 mm x 14.3 mm) double angles, while internal floor beams L1 and L2 contain 6 in. x 6 in. x 3/4 in. (152.4 mm x 152.4 mm x 19 mm) double angles. At the connection with the plate girder, floor-beams provide knee bracing by extending web plates up to the top of the girders. The floor-beam profile is presented in figure 4.14.

The stringers are rolled S20x75 beams with 20 in. by 0.635 in. (508 x 16 mm) web and 6.39 in. by 0.795 in. (162 x 20 mm) flanges. All connections between members within the structure are made using rivets with a nominal diameter of 0.875 in. (22 mm). The stringer-to-floor beam connection is made using double angles riveted to stringer and floor-beam webs. The components and connections of the bridge are presented in the graphics of figures 4.13 and 4.14.

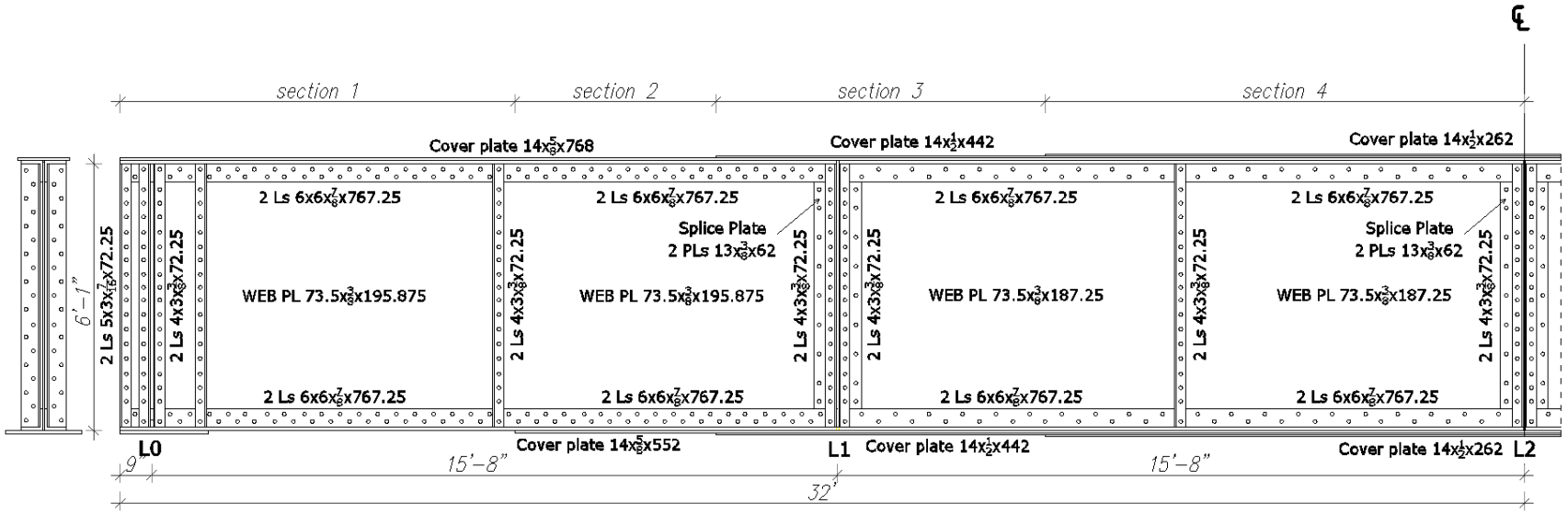

Figure 4.13 The girder profile of bridge #2

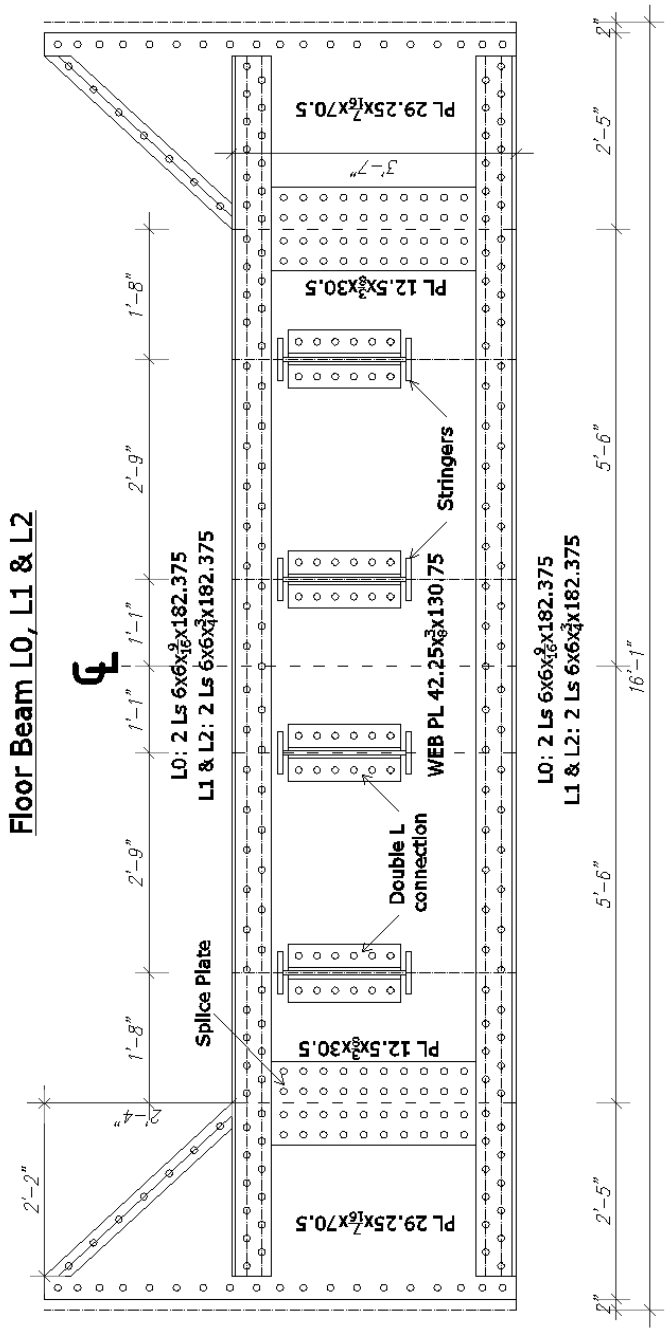

Figure 4.14 The floor-beam profile of bridge #2

Track systems (rails and rails tie) are lying directly on wood deck made from 6 in. by 8 in. by 14 ft (152.4 mm x 203.2 mm x 4.3 m) treated timbers placed on the top flange of the stringers. The 0.5 in. (12.7 mm) apron plates are fastened over floor beams. Timber ballast curbs

are attached along the edges of the deck. The crushed stone ballast cover timber deck at the height of 6 in.

Rail ties are spaced 19 in. (44.45 cm) from center to center, are 6 in. (152.4 mm) high, 8 in. (203.2 mm) wide and 8 ft (2.4 m) long. Track gauge is a standard gauge of 4.71 ft (1.435 m) and weight of 136 lb/yd. (67.5 kg/m). The specification of AREMA Rail at 136 lb is presented in APPENDIX A. The steel of superstructure and rails has an elastic modulus of 29000 ksi (200GPa), a yield stress of 30 ksi (207 MPa), and an ultimate stress of 50 ksi (345 MPa).

4.4 Verification Study of Bridge #1

The FEM analysis was used to investigate behavior and performance characteristics of the bridge's structural components. A three dimensional model of the bridge was developed using shell elements with a 6 degree of freedom per node to model stringers, floor beam, plate girders, connection angles, cover plates, and continuum elements, while using an 8-node brick to model rails and rail ties. The "surface-to-surface" approach in tie constraints were used to create double angle riveted connections between members. As a general mechanical constraint, displacement and rotation were assigned for boundary conditions on both ends of the plate girders to create a simple support.

It is important to realize that the accuracy of analytical procedures depends on the accuracy of the input data; namely, boundary conditions, load and load distribution parameters, material properties, degree of redundancy and load sharing, contribution of nonstructural members, and other factors. It is a common practice to make conservative assumptions to account for uncertainties in quantification of these parameters in the analysis. As such, there is often a need for either a more detailed analysis and/or experimental verification of analytical assumptions using field testing procedures. This report does not cover any field measurements.

The bridge was, however, analyzed by Chotickai and Kanchanalai and the results of their field measurements were published in the TRB Journal (2010). Therefore, results from field testing were used to verify the FEM model.

The strain or stress history caused by a train crossing the structure is commonly used to characterize structural performance. The calibration train consists of a six-axle locomotive and four-axle passenger car with the axle configuration shown in the graphic figure 4.15.

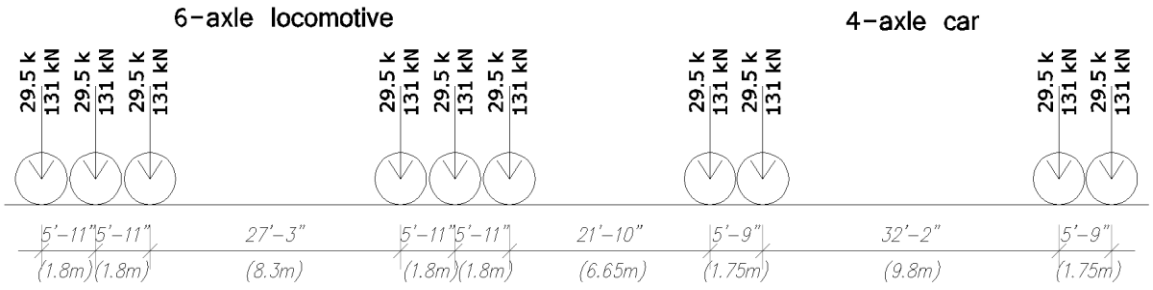

Figure 4.15 Axle configuration of the calibration train

Figures 4.16 to 4.18 present a comparison of the field measurement and the predicted values from the FEM analysis. Figure 4.16 shows response at the bottom flange at the center of the exterior stringer. Figure 4.17 shows response at the bottom flange of the floor-beam at the connection to the stringer. Figure 4.18 shows response at the bottom flange of the plate girder at the connection to floor-beam.

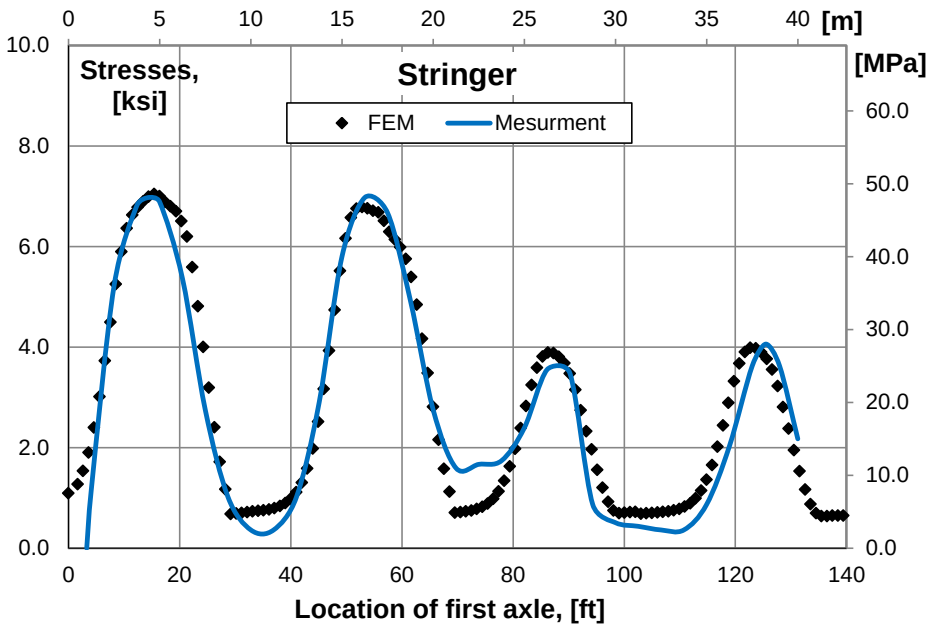

Figure 4.16 Measured and analytical stress response, center of exterior stinge
r

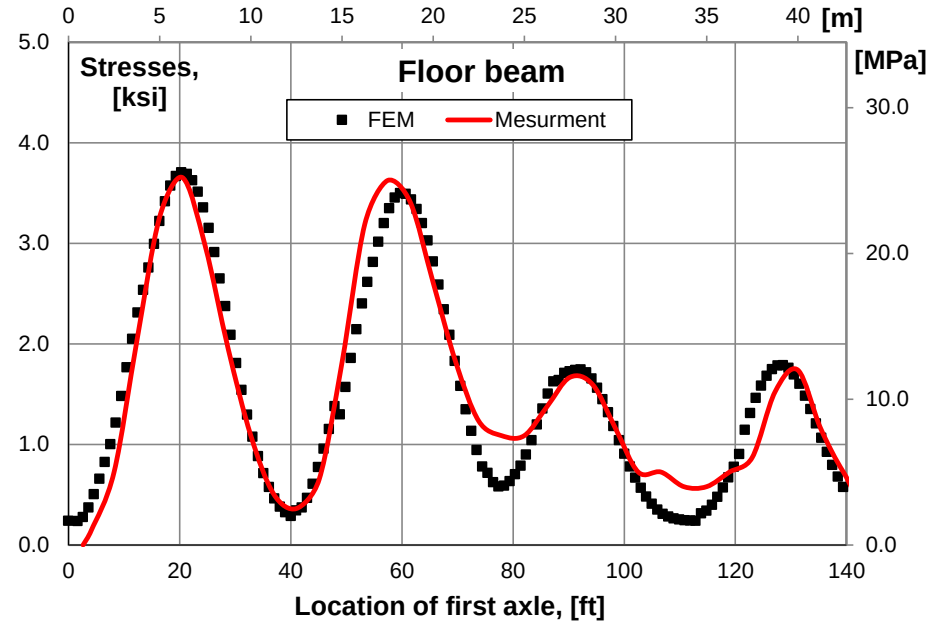

Figure 4.17 Measured and analytical stress response, interior floor beam at the connection with the stringer

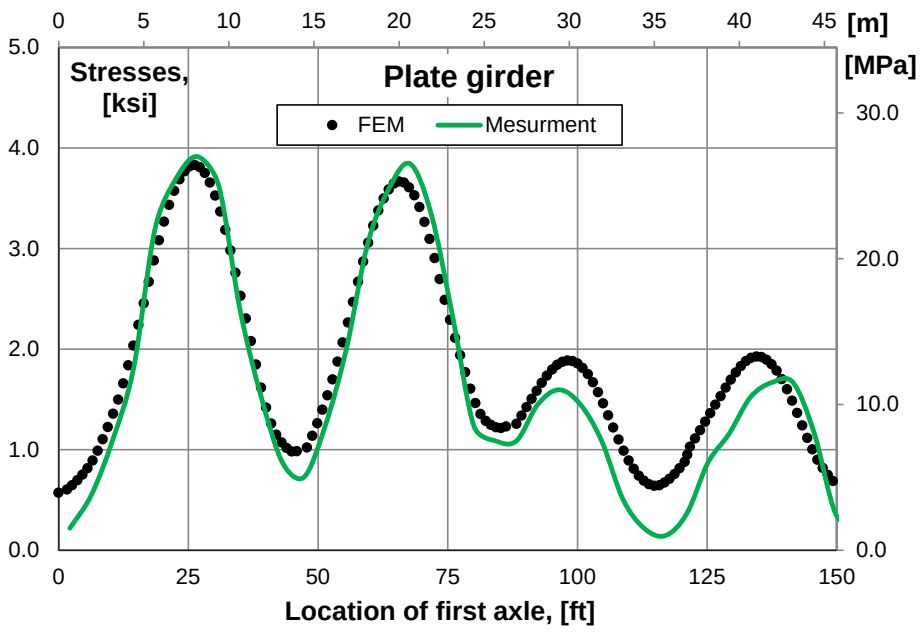

Figure 4.18 Measured and analytical stress response, plate girder at the connection with the interior floor beam

The maximum stresses were caused by a group of axles spaced closely and the valleys in the stress history were due to the wide spacing between inboard axles. The maximum measured stresses were 7.15 ksi (49.3 MPa), 3.76 ksi (25.9 MPa), and 3.96 ksi (27.3 MPa) for stringer, floor beam, and plate girder, respectively (Chotickai and Kanchanalai 2010). The FEM model provided the maximum stress response of 7.05 ksi (48.6 MPa), 3.7 ksi (25.5 MPa), and 3.8 ksi (26.4 MPa) for stringer, floor beam, and plate girder, respectively. The largest difference between measured peak stresses and the maximum stresses from FEM analysis was approximately 3%. However, the prediction of stresses was more accurate under the load from the locomotive then under the passenger car. To summarize, stresses obtained from FEM analysis provide a relatively good estimate of the structural response as compared to field measurements. Thus, the introduced FEM modeling can be used to further analysis.

4.5 Results of Structural Analysis of the Bridge #1

The FEM model developed and described in the previous section was used to investigate behavior and performance of the bridge structural components under design load. According to AREMA, two design live loads can be used: Cooper E80 or Alternative Live Load on four-axles as described in Chapter 3.2. The selection of the load shall be such as will produce the greatest stresses in the members. Using a simple calculation, the location of the axle load that causes the maximum interaction was found and is presented in the illustration in figure 4.19 for Alternative Live Load and in the illustration in figure 4.20 for Cooper E80.

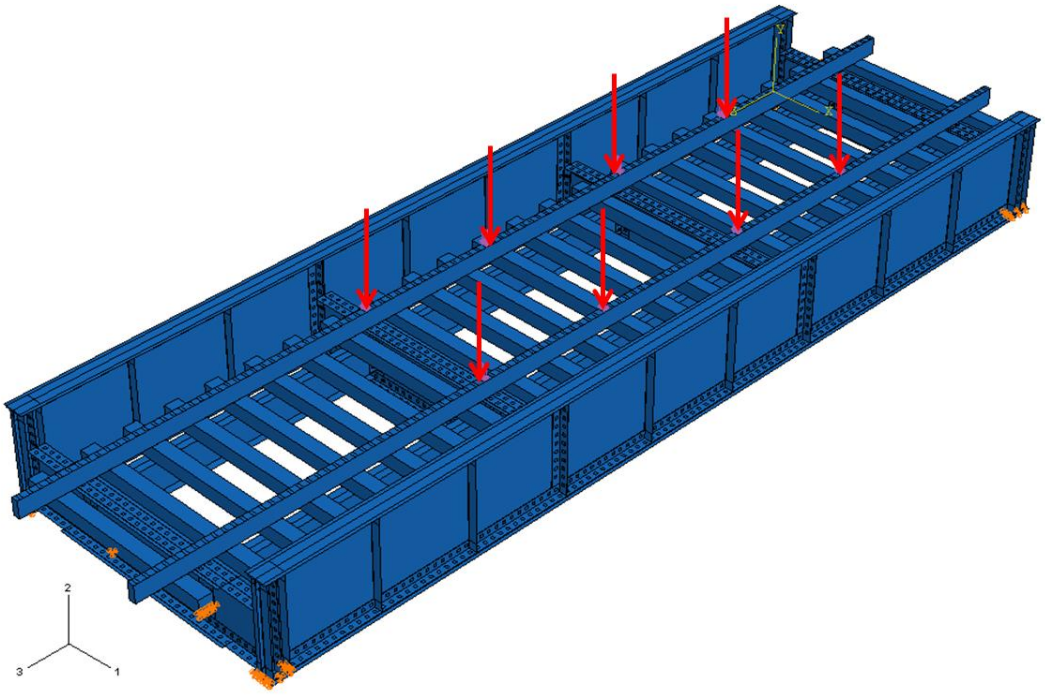

Figure 4.19 Alternative live load applied on bridge #1

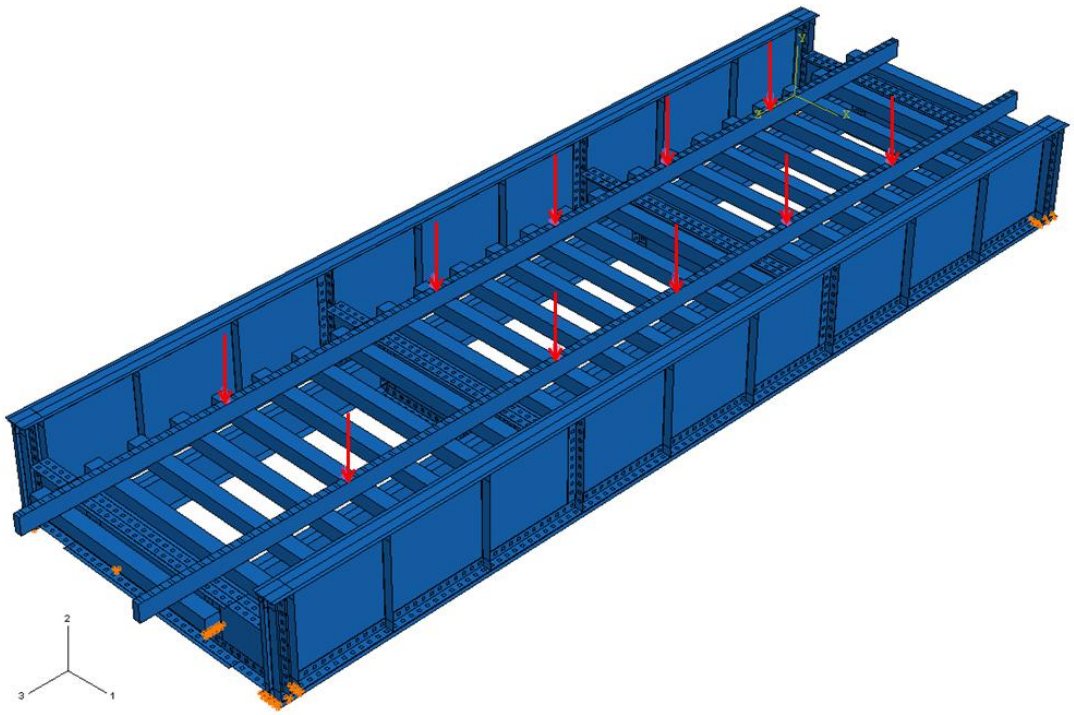

Figure 4.20 Cooper E80 applied on bridge #1

Besides live load, the bridge carries dead load, self-weight of the bridge, and dynamic load. According to AREMA, dynamic load due to the passage of locomotives and train loads shall be determined by taking a percentage of the live load. The formulas for calculation of the dynamic impact factor are presented in section 3.3. The dynamic factors for members in the Bridge #1 are presented in table 4.2.

Table 4.2 Dynamic impact factors for bridge #1

Member type	Dynamic impact	Rocking effect	Design impact	Impact for fatigue analysis
Stringer L = 10'-11"	39.8 %	20 %	59.80 %	20.9 %
Floor beam L = 10'-2"	39.8 %	9.84 %	49.64 %	17.4 %
Plate girder L = 32'-9"	38.0 %	9.84 %	47.84 %	16.7 %

During the FEM analysis the concentrated loads presented in figures 4.19 and 4.20 were gradually increasing from 0 to 350 kips for Alternative Live Load and from 0 to 280 kips for Cooper E loading.

4.5.1 Stresses Due to Applied Load

Two cases of load were considered: Cooper E80 and Alternate Live Load on four axles. Figure 4.21 presents stresses due to Alternate Live Load for main bridge elements: interior stringer, interior floor beam, and plate girder. Under this same level of load, the stringer achieves the highest stress. For Alternate Live Load, 100 kips per axle, the stringer reaches 16.76 ksi (115.6 MPa), the floor beam reaches 12.61 ksi (87.0 MPa), and plate girder reaches 13.95 ksi (96.2 MPa). The stresses due to dead load, static live load, dynamic load and total load are listed in table 4.3. The maximum response under design load was 27.22 ksi (187.7 MPa) in the stringer and was still below nominal yield stress of 30 ksi (207 MPa).

Table 4.3 Stresses due to design load, alternate live load, 100 kip, bridge #1

Member type	Dead Load, ksi (MPa)	Static load, ksi (MPa)	Dynamic portion, ksi (MPa)	Total, ksi (MPa)
Interior Stringer	0.44 (3.0)	16.76 (115.6)	10.02 (69.1)	27.22 (187.7)
Interior Floor beam	0.26 (1.8)	12.61(87.0)	6.26 (43.2)	19.13 (131.9)
Plate girder	0.60 (4.1)	13.95 (96.2)	6.67 (46.0)	21.22 (146.3)

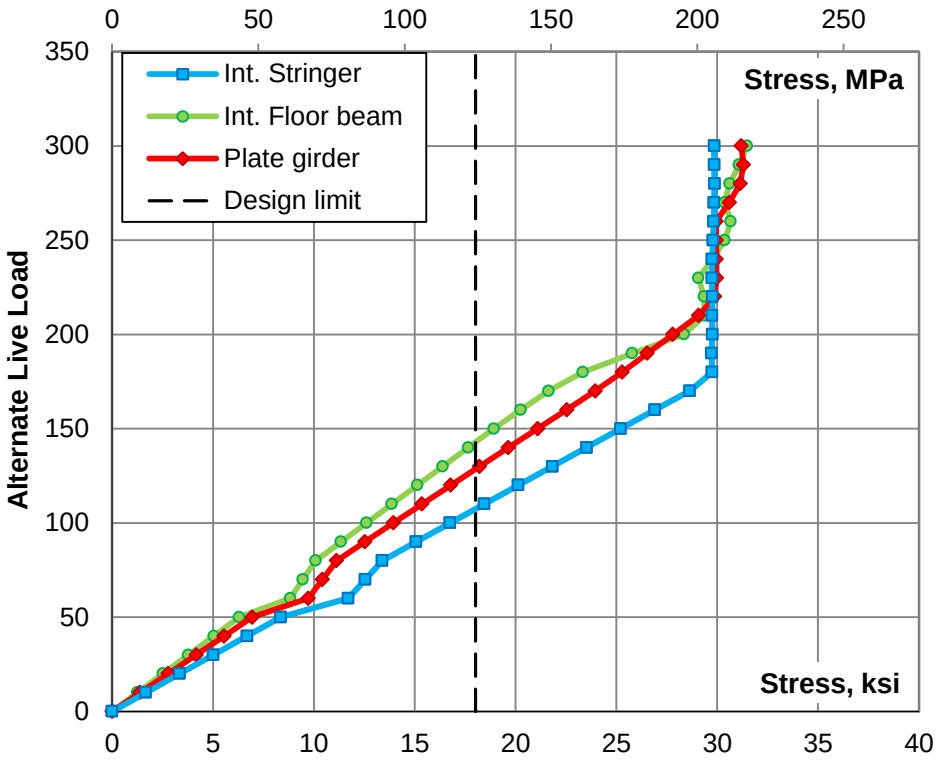

Figure 4.21 Stresses due to gradually increased alternate live load, bridge #1

Figure 4.22 presents stresses due to Cooper E Loading for these same bridge elements: interior stringer, interior floor beam, and plate girder. The behavior of members under applied load was comparable to Alternative Live Load; however, the stresses were much lower. For Cooper E80 the stringer reaches 13.72 ksi (94.6 MPa), the floor beam 10.71 ksi (73.8 MPa), and the plate girder 11.90 ksi (82.0 MPa). Additional results are listed in table 4.4. The assumption that for shorter bridges Alternative Live Load governs was confirmed.

Table 4.4 Stresses due to design load, Cooper E80 loading, bridge #1

Member type	Dead Load, ksi (MPa)	Static load, ksi (MPa)	Dynamic portion, ksi (MPa)	Total, ksi (MPa)
Interior Stringer	0.44 (3.0)	13.72 (94.6)	8.20 (56.6)	22.36 (154.1)
Interior Floor beam	0.26 (1.8)	10.71(73.8)	5.31 (36.6)	16.28 (112.2)
Plate girder	0.60 (4.1)	11.90 (82.0)	5.69 (39.2)	18.18 (125.3)

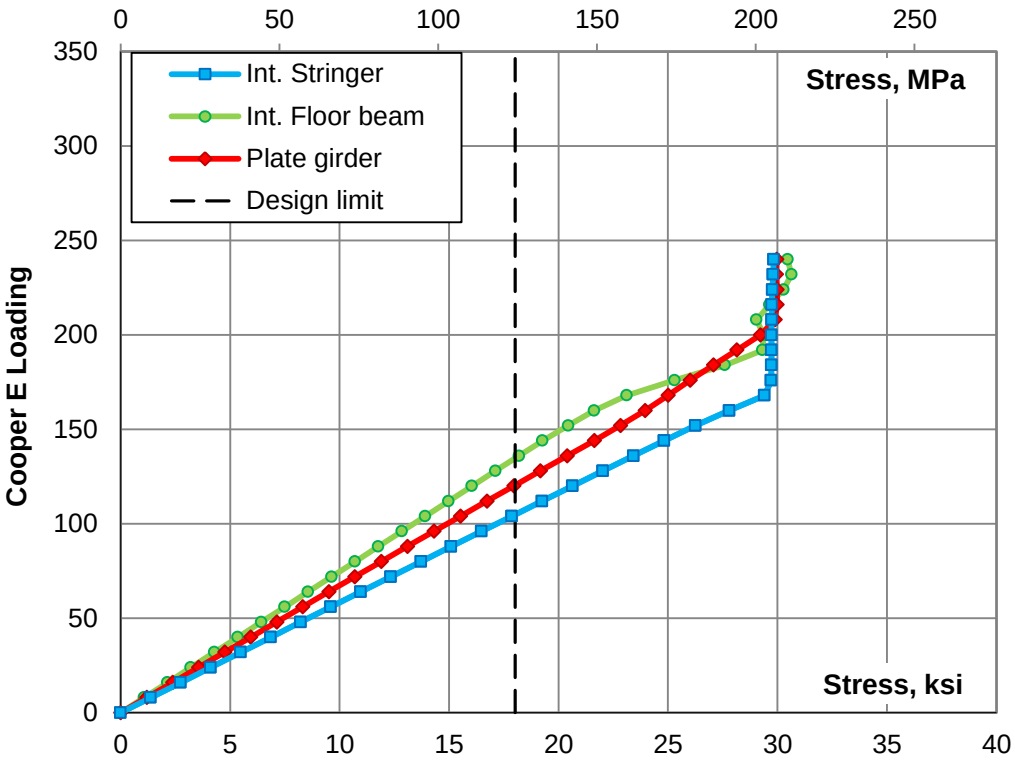

Figure 4.22 Stresses due to gradually increased Cooper E loading, bridge #1

The stress to displacement relationship presented in figure 4.23 shows similarity between the Cooper E Loading and Alternate Live Load. In both cases, the character of graphs corresponds to the stress-strain relation for steel with yield strength of 30 ksi (207 MPa). This proves that the material model has been defined appropriately and the results can be considered as correct.

Figure 4.24 presents the relationship between plastic strain and applied load. The gradually increased load produced plastic strain when the axial forces were close to 180 kip. It is more than design load and it means that the bridge elements remain in the elastic zone.

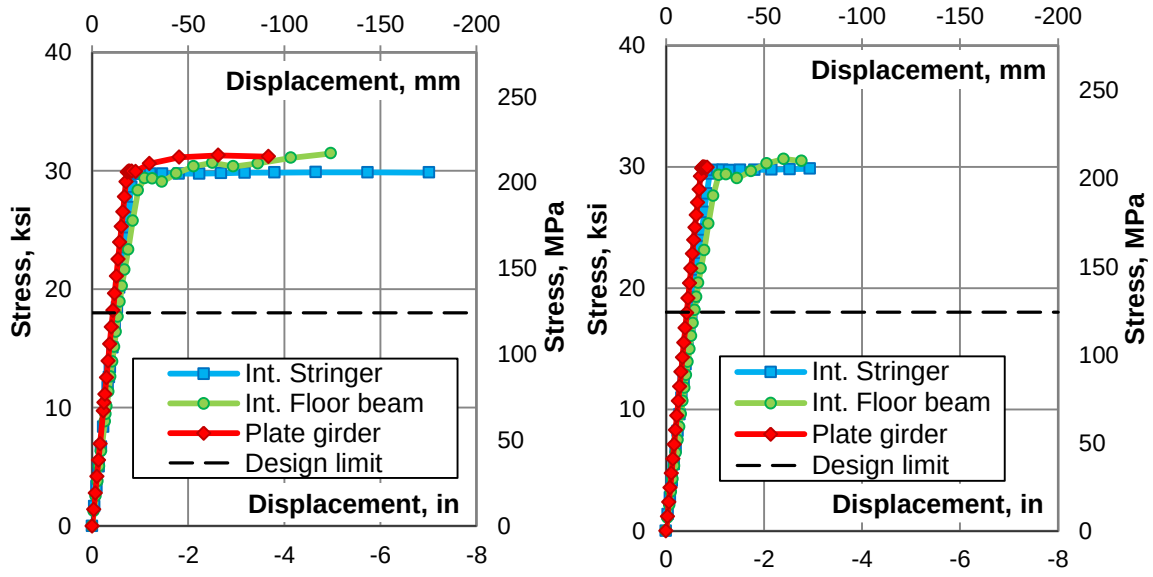

Figure 4.23 The stress to displacement relation for alternate live load (left side) and Cooper E loading (right side), bridge #1

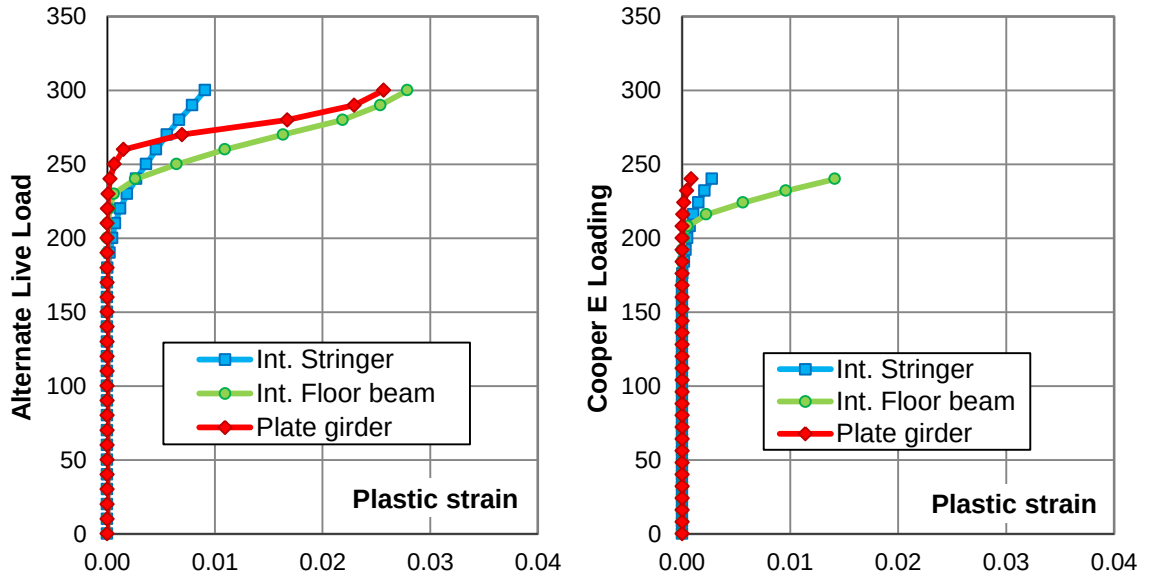

Figure 4.24 Plastic strain due to gradually increased load; alternate live load on left side and Cooper E loading on right side, bridge #1

4.5.2 Displacement and Deflection Due to Design Load

Displacement in the critical points in a stringer, a floor beam, and a plate girder were analyzed under Alternate Live Load on four axles and Cooper E80. Figure 4.25 presents

displacement under a gradually increased Alternate Live Load whereas figure 4.26 presents displacement under a gradually increased Cooper E Loading.

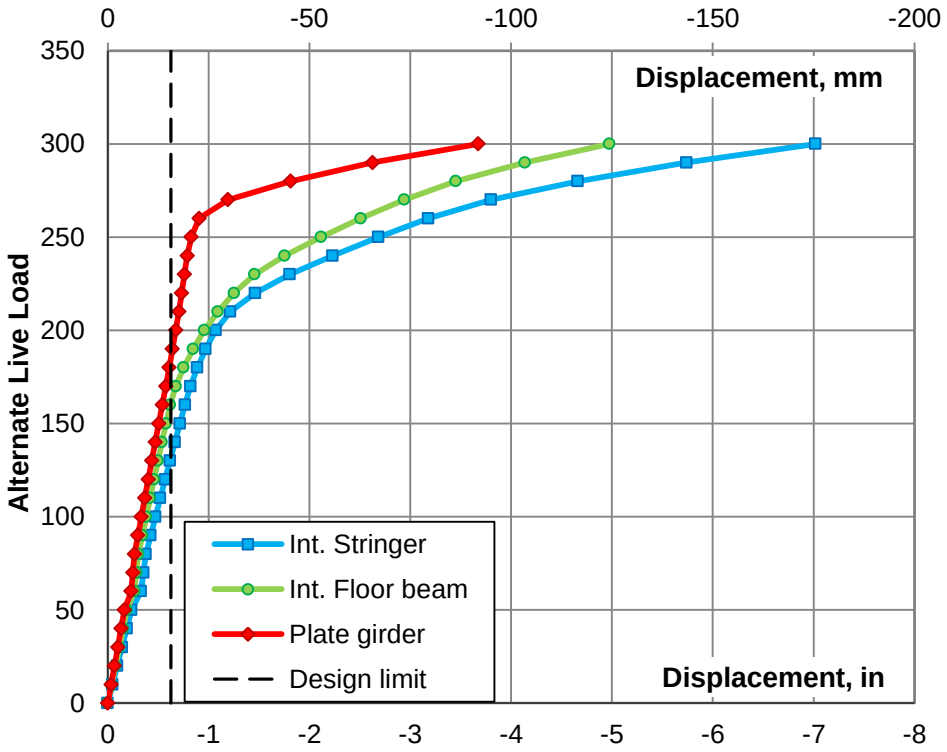

Figure 4.25 Displacement due to gradually increased alternate live load, bridge #1

Table 4.5 Displacement due to design load, alternate live load, 100 kip, bridge #1

Member type	Dead Load, in (mm)	Static load, in (mm)	Dynamic portion, in (mm)	Total, in (mm)
Interior Stringer	0.019 (0.48)	0.473 (12.01)	0.283 (7.18)	0.775 (19.68)
Interior Floor beam	0.018 (0.45)	0.381 (9.67)	0.189 (4.80)	0.588 (14.92)
Plate girder	0.016 (0.40)	0.333 (8.46)	0.159 (4.05)	0.508 (12.91)

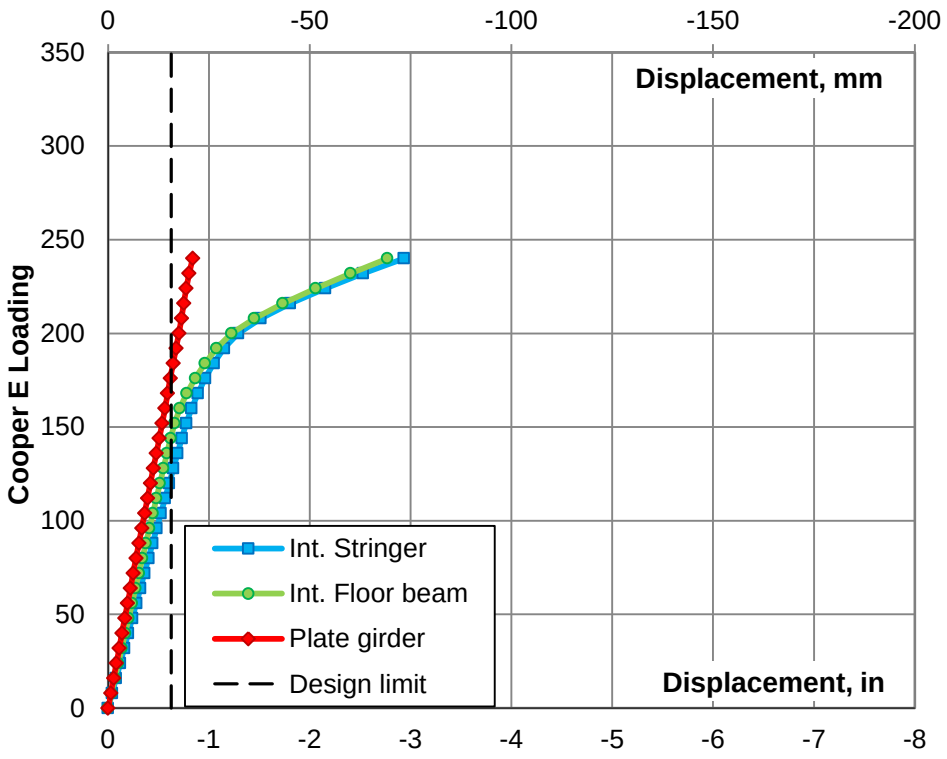

Figure 4.26 Displacement due to gradually increased Cooper E loading, bridge #1

Table 4.6 Displacement due to design load, Cooper E 80 loading, bridge #1

Member type	Dead Load, in (mm)	Static load, in (mm)	Dynamic portion, in (mm)	Total, in (mm)
Interior Stringer	0.019 (0.48)	0.401 (10.19)	0.240 (6.10)	0.660 (16.77)
Interior Floor beam	0.018 (0.45)	0.340 (8.64)	0.169 (4.29)	0.526 (13.37)
Plate girder	0.016 (0.40)	0.278 (7.06)	0.133 (3.38)	0.427 (10.84)

Displacement under Alternate Live Load is slightly higher than for Cooper E loading. In both cases, the stringer and the floor beam demonstrate bigger displacement than the plate girder under this same level of load. This is affected by absolute and relative displacement. In the floor system of the bridge when the main element moves the other elements move with it; therefore, the deflection needs to be calculated as a relative displacement between the plate girder and the floor system.

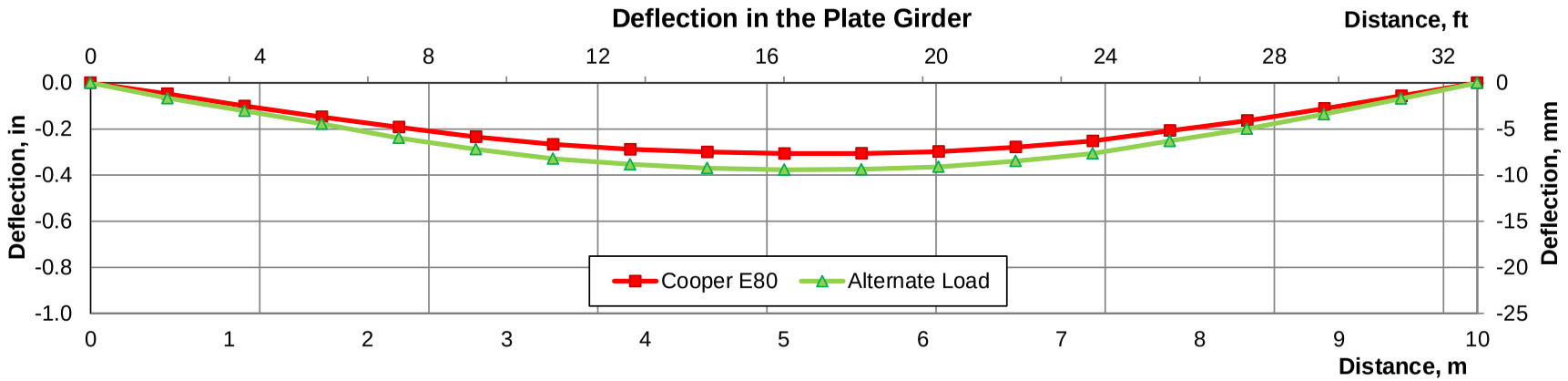

Figure 4.27 Deflection due to live load in the plate girder, bridge #1

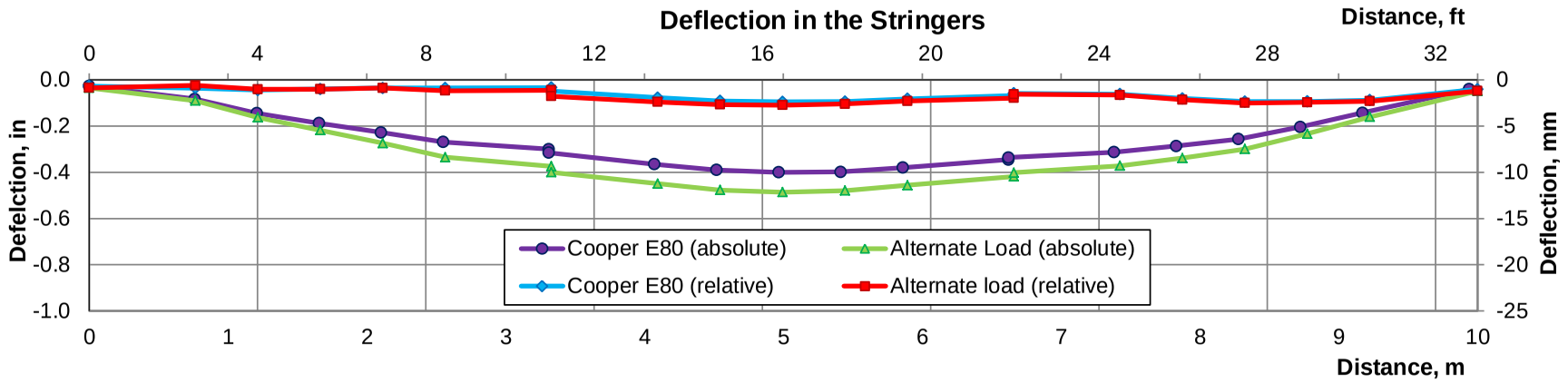

Figure 4.28 Deflection due to live load in the stringer, bridge #1

Deflection in the plate girder corresponds to the vertical displacement, and it is presented in by the line graphs plotted in figure 4.27. Deflection in the stringer is presented in the line graphs plotted in figure 4.28 and includes relative and absolute displacement. The absolute deflection corresponds to the vertical displacement whereas relative deflection is a difference in the displacement of the plate girder and the stringer.

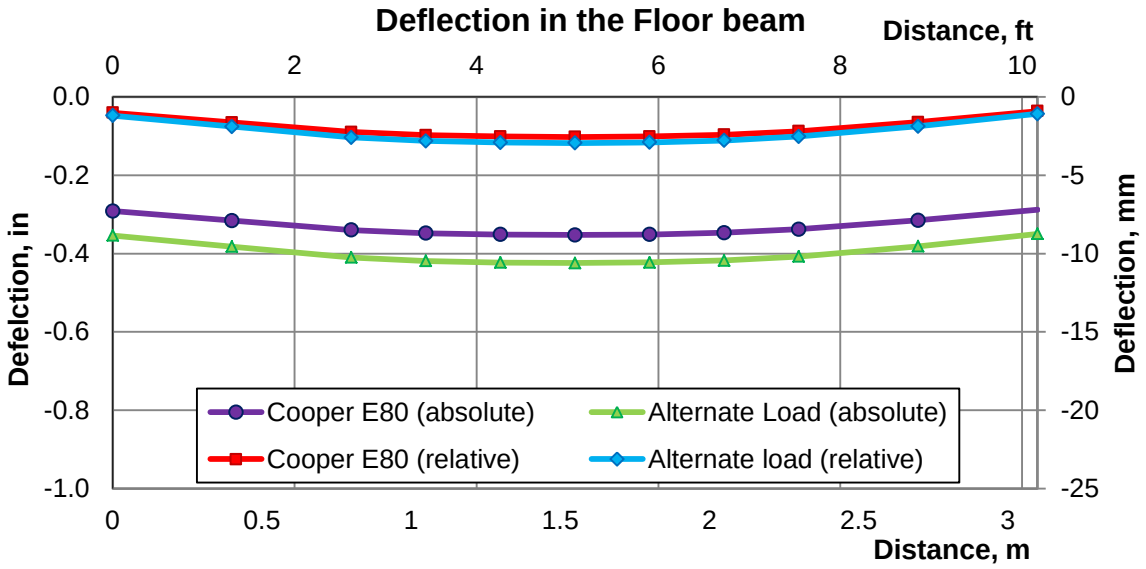

Figure 4.29 Deflection due to live load in the floor beam, bridge #1

Figure 4.29 contains absolute and relative deflection in the floor beam due to design live load. Absolute deflection in the floor beam is the total vertical displacement and relative deflection is a difference in the displacement of the plate girder and the floor beam. The maximum relative deflections for structural members due to Alternate Live Load are presented in table 4.7 and for Cooper E80 in table 4.8.

The deflection limit for railway bridges is L/640; therefore, the deflection limit for a span length of 32 ft 9 in. (10 m) is 0.6 in. (15.6 mm). For both load cases, the actual deflection is less than the deflection limit.

Table 4.7 Relative deflection due to design load, alternate live load, 100 kip, bridge #1

Member type	Dead Load, in (mm)	Static load, in (mm)	Dynamic portion, in (mm)	Total, in (mm)
Interior Stringer	0.003 (0.08)	0.140 (3.55)	0.084 (2.12)	0.227 (5.76)
Interior Floor beam	0.002 (0.05)	0.048 (1.21)	0.024 (0.60)	0.073 (1.86)
Plate girder	0.016 (0.40)	0.333 (8.46)	0.159 (4.05)	0.508 (12.91)

Table 4.8 Relative deflection due to design load, Cooper E 80 loading, bridge #1

Member type	Dead Load, in (mm)	Static load, in (mm)	Dynamic portion, in (mm)	Total, in (mm)
Interior Stringer	0.003 (0.08)	0.123 (3.14)	0.074 (1.88)	0.200 (5.09)
Interior Floor beam	0.002 (0.05)	0.062 (1.58)	0.031 (0.78)	0.095 (2.41)
Plate girder	0.016 (0.40)	0.278 (7.06)	0.133 (3.38)	0.427 (10.84)

4.5.3 Stringer to Floor Beam Connections

The stringer-to-floor-beam connections in a through-plate girder riveted railway bridge are commonly constructed with double angle connections and considered as simple shear connections during the design stage. In many cases, a considerable amount of end moment may be developed at the connection because of unintentional connection stiffness. Consequently, the connection can be susceptible to fatigue damage (Fisher et al. 1987; Al-Emrani 2005); therefore, during FEM analysis the stresses were checked in the double angle connections. Figures 4.30 and 4.31 present a detailed rendering of the double angle connection in Bridge #1 before and after applied load, respectively.

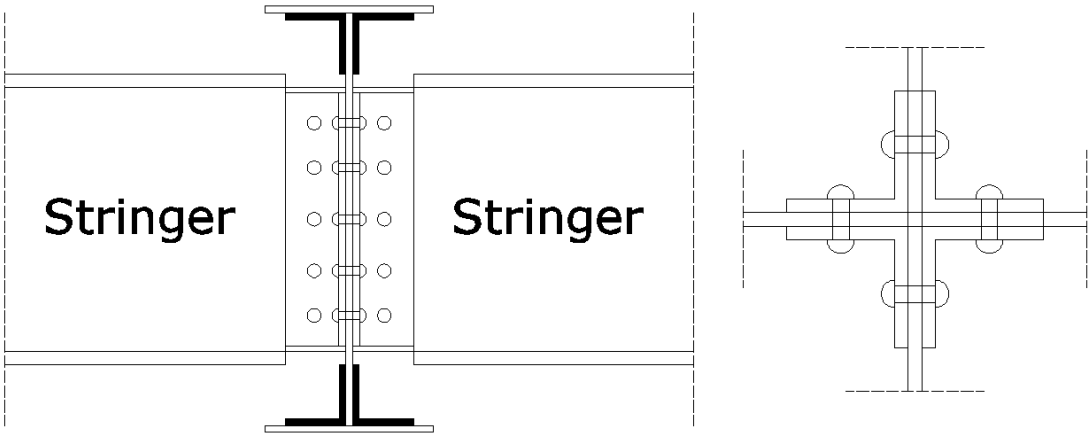

Figure 4.30 Detail of double angle connection in bridge #1

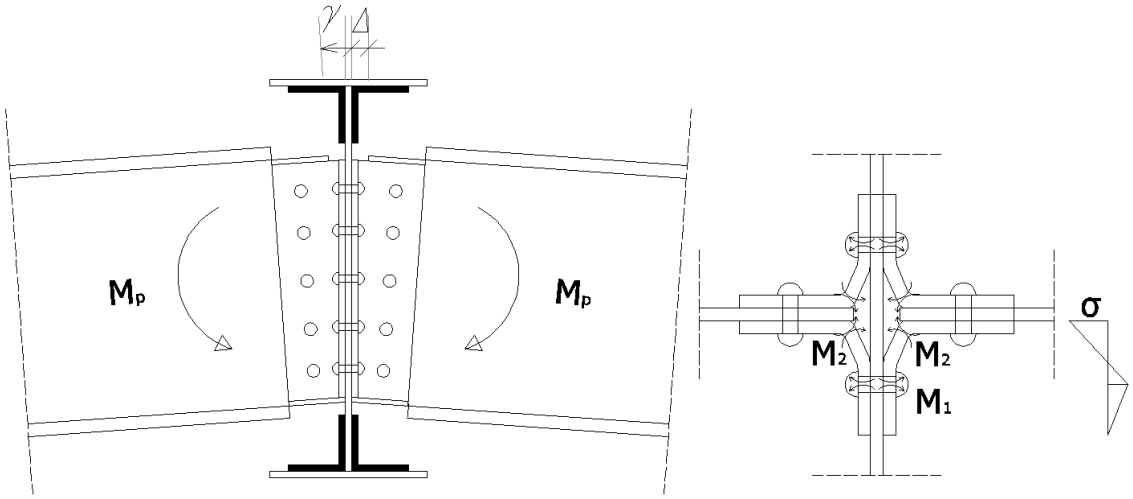

Figure 4.31 Distortion of outstanding legs of connection angles due to applied load, bridge #1

Figures 4.32 and 4.33 present stresses due to gradually increased load. The connections concentrate stresses in different directions and, for this reason; the results are presented for von Mises stress. Based on the von Mises theory, the equivalent tensile stress is a scalar stress value that can be computed from the stress tensor.

$$\sigma^2 = 0.5 \cdot \left[(\sigma_{11} - \sigma_{22})^2 + (\sigma_{22} - \sigma_{33})^2 + (\sigma_{11} - \sigma_{33})^2 + 6(\sigma_{12}{}^2 + \sigma_{13}{}^2 + \sigma_{23}{}^2) \right] \qquad (4.1)$$

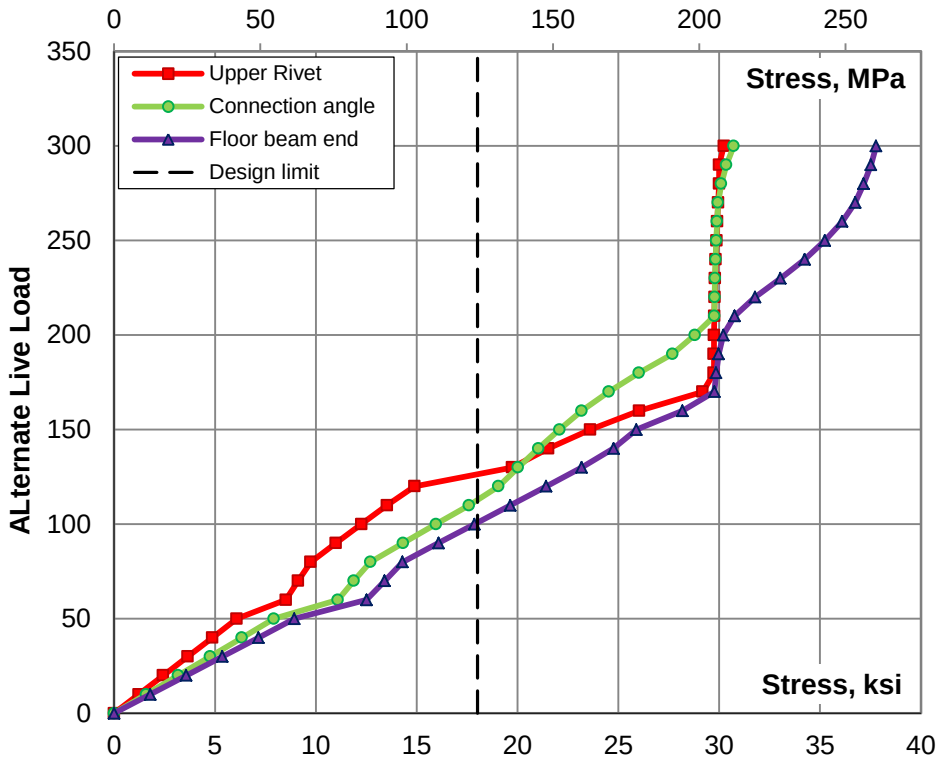

Figure 4.32 Stresses due to gradually increased alternate live load, bridge #1

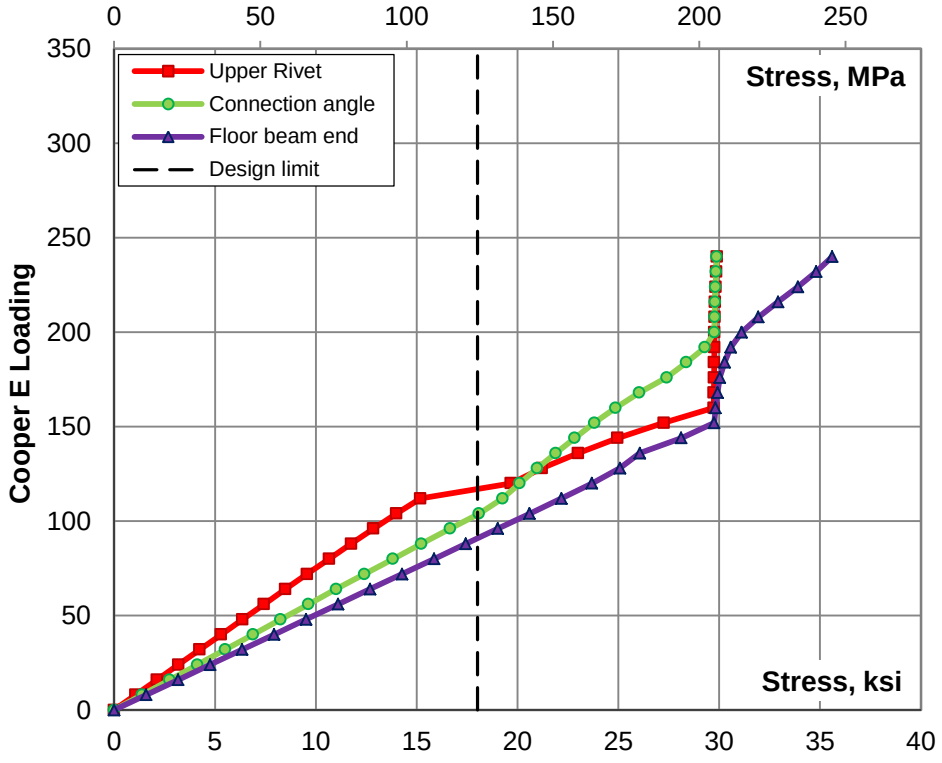

Figure 4.33 Stresses due to gradually increased Cooper E Loading, bridge #1

The analysis shows that the connection between stringer and floor beam acquires a certain degree of rotational stiffness and develops stresses due to bending moment. Also, the connections between the floor beam and plate girder reach high stress and plastic deformation.

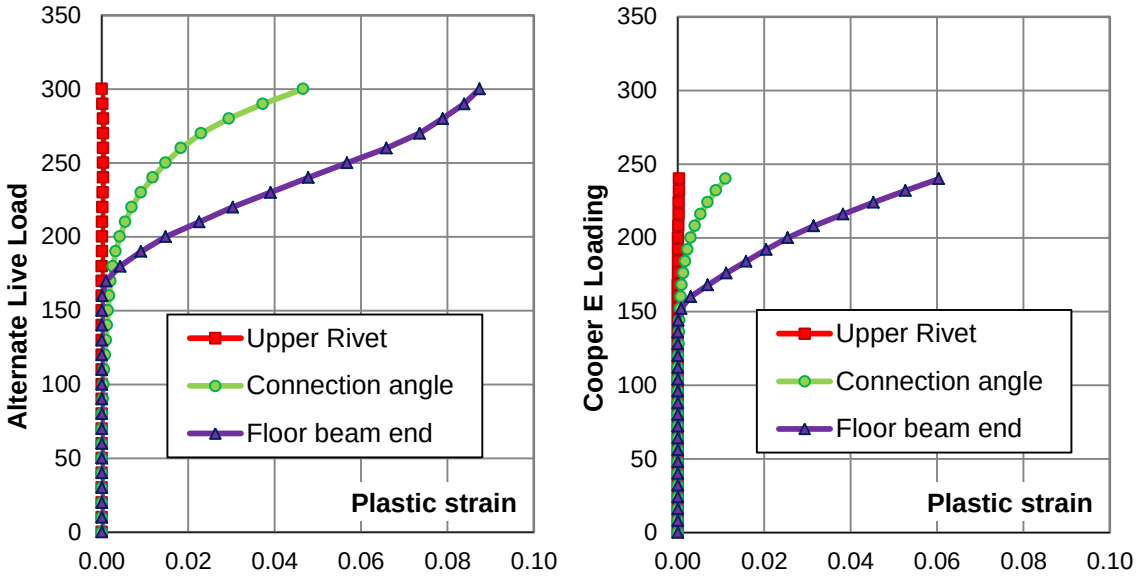

Figure 4.34 Plastic strain due to gradually increased load; alternate live load on left side and Cooper E loading on right side, bridge #1

Figure 4.34 presents the relationship between plastic strain and applied load. The gradually increased load produced plastic strain when the axial forces were close to 150 kip. The connection developed plastic deformation much faster than the main elements on the bridge. The connections are more critical than the primary members and need to be considered in fatigue analysis. Also, additional calculations were made using ROBOT Structural Analysis for a continuous beam with and without pin connections (APPENDIX B). The stringers in the FEM model behave as a partially continuous three spans beam with negative moment at the interior floor beams.

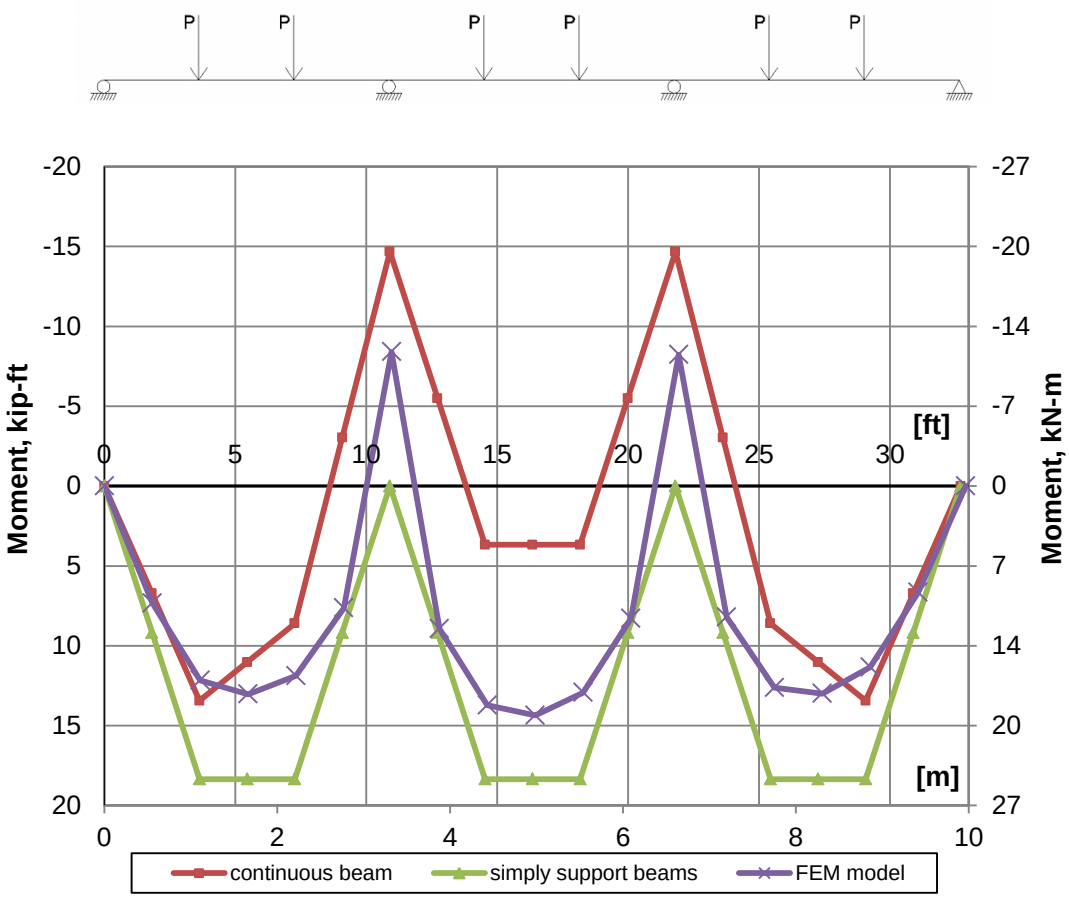

Figure 4.35 Moment diagram for continuous beam, simply supported beams and fem model, bridge #1

The results presented in figure 4.35 show that the double angle connections in the FEM model were capable of developing 60% of the corresponding moment of the fully continuous beam, and this finding has been proved by other researchers (Al-Emrani 2006; Charles et al. 2001; Goel R.K. 2006; Krajewski 2009).

4.5.4 Influence Lines

The FEM analysis of bridge #1 showed that the most critical points of the bridge remain in elastic stage under the design load. It is expected that the loading spectra under current

operating conditions do not exceed the design load, which was developed in section 3.8. Therefore, for further analysis of fatigue evaluation, the principal of super position can be applied. For that purpose, an influence line for each member of the bridge was developed. The influence lines for selected members and locations are given in figures 4.36 through 4.39.

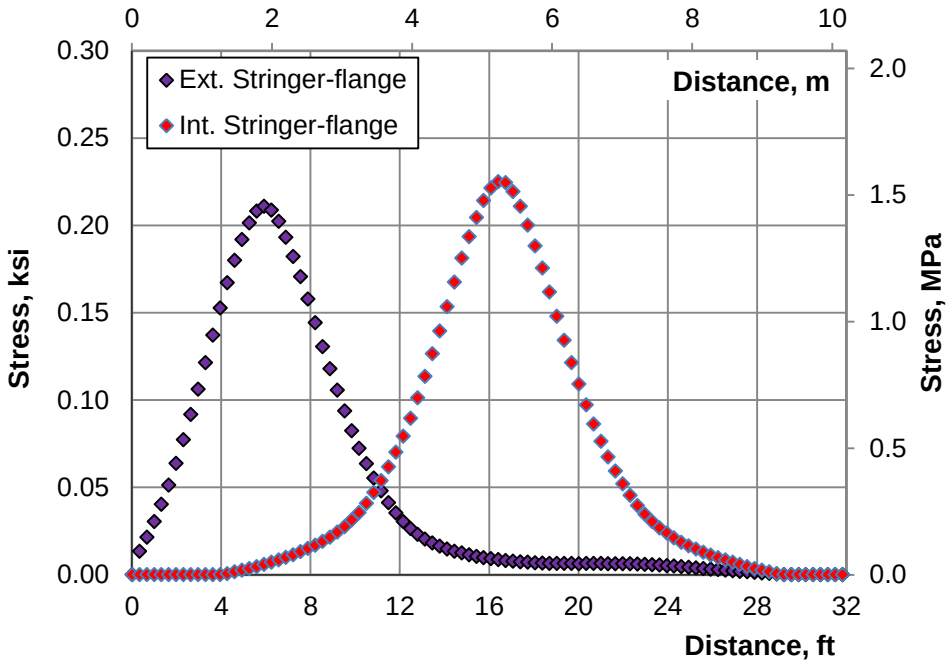

Figure 4.36 Influence lines for bridge #1 at mid-span location of exterior and interior stringer, bridge #1

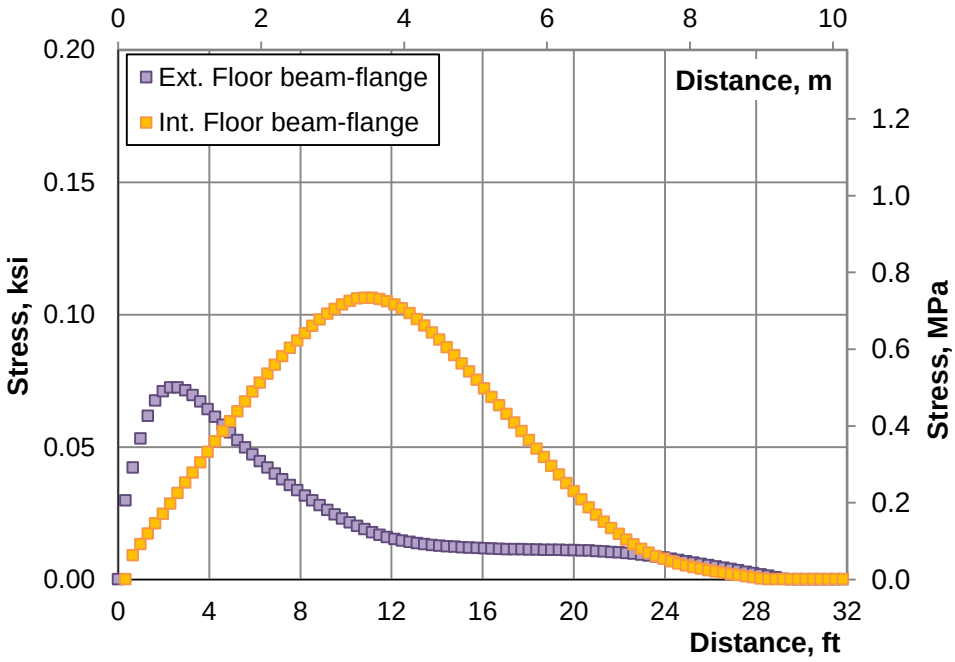

Figure 4.37 Influence lines for bridge #1 at mid-span location of exterior and interior floor beam, bridge #1

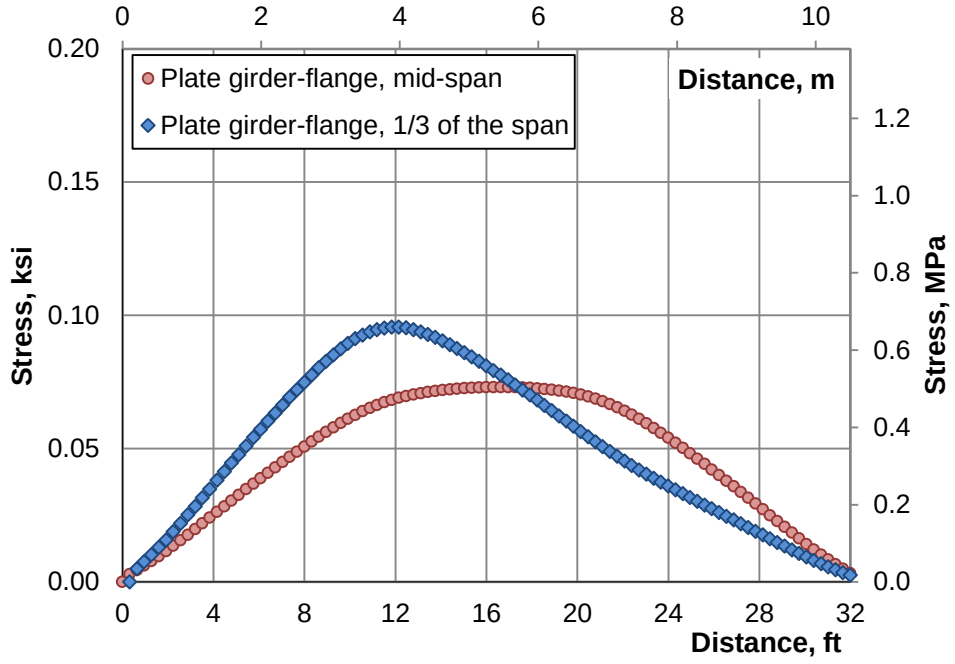

Figure 4.38 Influence lines for bridge #1 at center and 1/3 of the span of the plate girder, bridge #1

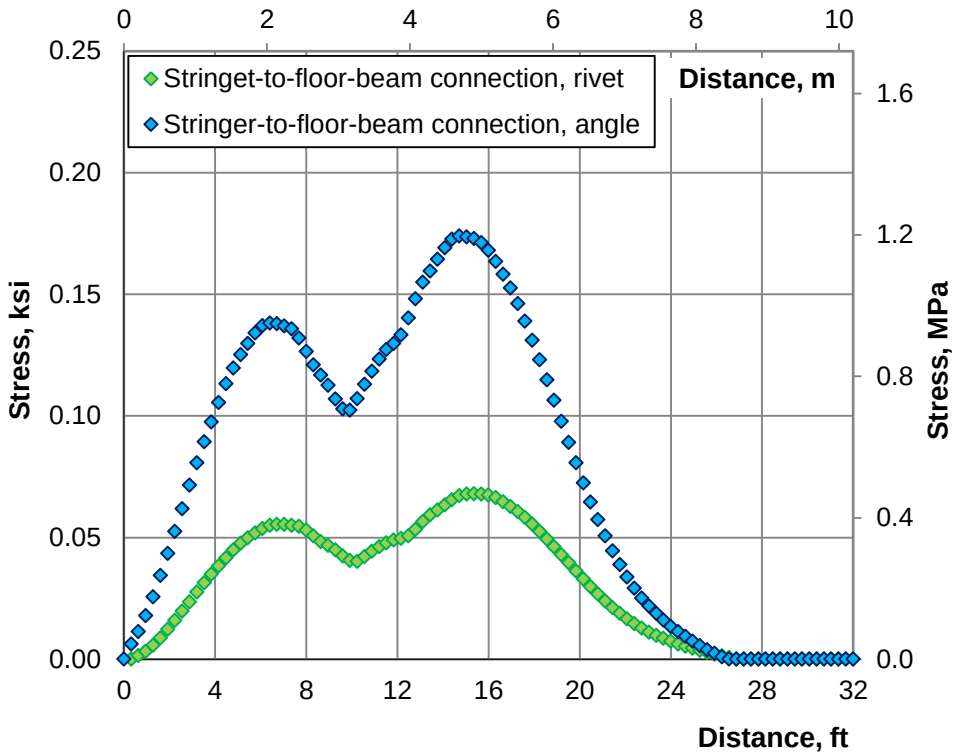

Figure 4.39 Influence lines for bridge #1 at stringer-to-floor-beam connection for the rivet and the angle, bridge #1

4.6 Results of Structural Analysis of the Bridge #2

The FEM model developed and described in the previous section was used to investigate behavior and performance of the bridge structural components under design load. Two design live loads were considered: Cooper E80 and Alternative Live Load on four-axles, as described in Chapter 3.2. Four critical locations on the bridge have been chosen: the center of the exterior and interior stringer, the interior floor beam, and plate girder. Using a simple analysis, the location of axle load which produce greatest stresses in the members has been found and is presented on figure 4.40 for Alternative Live Load and on figure 4.41 for Cooper E80.

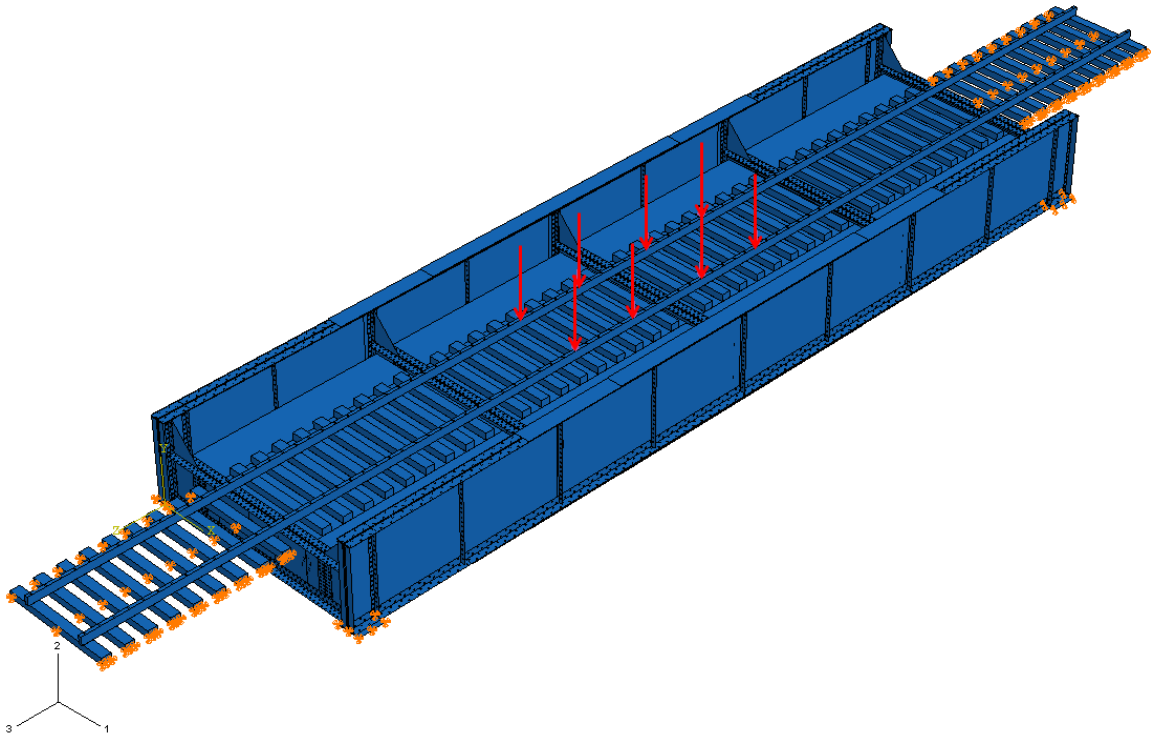

Figure 4.40 Alternative live load applied on bridge #2

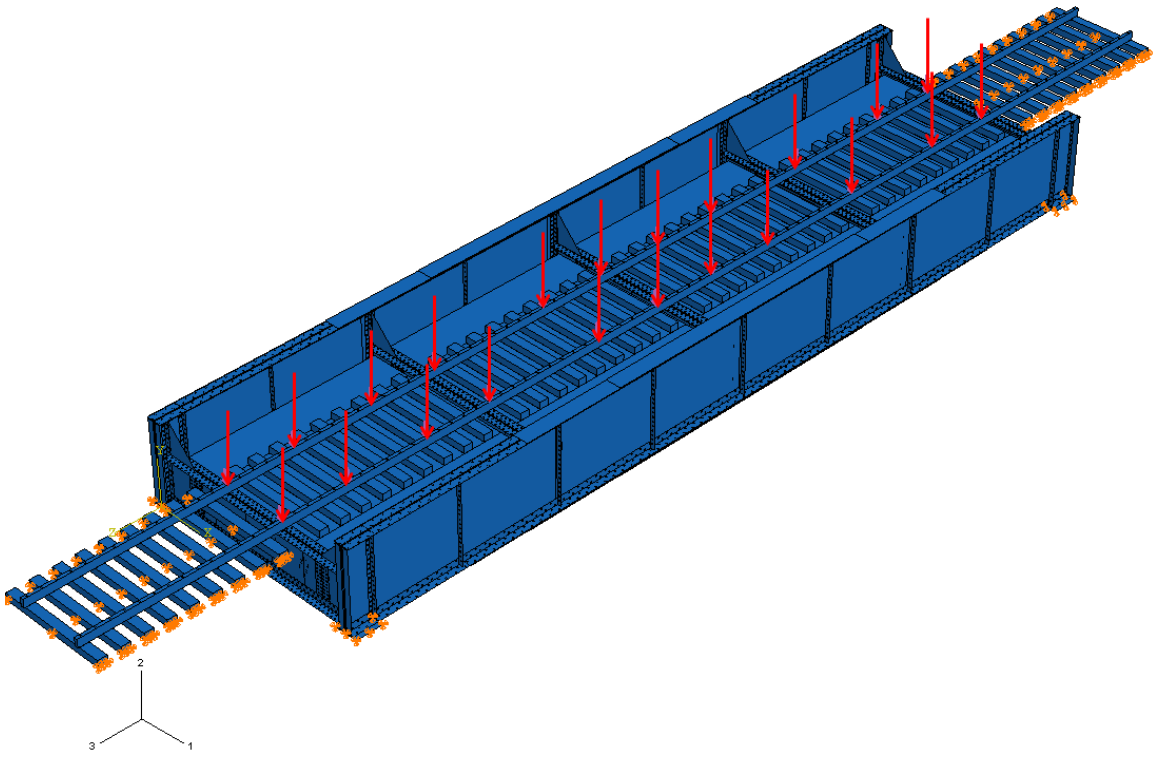

Figure 4.41 Cooper E80 applied on bridge #2

Besides live load, the bridge carries dead load, self-weight of the bridge, and dynamic load. According to AREMA, dynamic load due to the passage of locomotives and train loads shall be determined by taking a percentage of the live load. The formulas for calculation of dynamic impact factor are presented in section 3.3. The dynamic factors for members in Bridge #2 are presented in table 4.9.

Table 4.9 Dynamic impact factors for bridge #2

	Dynamic impact	Rocking effect	Design impact	Impact for fatigue analysis
Stringer exterior L = 15'-8"	39.5 %	7.6%	47.1 %	17.4 %
Stringer interior L = 15'-8"	39.5 %	19.1 %	58.6 %	21.7 %
Floor beam L = 16'-1"	39.5 %	6.2 %	45.7 %	16.9 %
Plate girder L = 64'-0"	32.3 %	6.2 %	38.5 %	14.2 %

During the FEM analysis, the concentrated loads presented in figures 4.40 and 4.41 were gradually increasing from 0 to 380 kips for Alternative Live Load and from 0 to 260 kips for Cooper E loading.

4.6.1 Stresses Due to Applied Load

Two cases of load were considered: Cooper E80 and Alternate Live Load on four-axles. Figure 4.42 presents stresses due to Alternate Live Load for the following main bridge elements: exterior stringer, interior stringer, interior floor beam, and plate girder. Under this same level of load, the interior floor beam achieves the highest stress. For Alternate Live Load, 100 kips per axle, the interior stringer reaches 8.71 ksi (60.0 MPa), the exterior stringer is 8.23 ksi (56.7 MPa), the floor beam is 10.27 ksi (70.8 MPa), and the plate girder is 8.48 ksi (58.4 MPa). The

stresses due to dead load, static live load, dynamic load and total load are listed in table 4.10. The maximum response under design load was 15.65 ksi (107.9 MPa) in the interior floor beam and was below the nominal yield stress of 30ksi (207 MPa) and below the allowable stress of 18 ksi (124 MPa).

Table 4.10 Stresses due to design load, alternate live load, 100 kip, bridge #2

Member type	Dead Load, ksi (MPa)	Static load, ksi (MPa)	Dynamic portion, ksi (MPa)	Total, ksi (MPa)
Interior Stringer	0.82 (5.65)	8.71 (60.0)	5.10 (35.2)	14.63 (100.9)
Exterior Stringer	1.00 (6.88)	8.23 (56.7)	3.87 (26.7)	13.10 (90.3)
Interior Floor beam	0.69 (4.74)	10.27 (70.8)	4.69 (32.3)	15.65 (107.9)
Plate girder	1.57 (10.9)	8.48 (58.4)	3.26 (22.5)	13.31 (91.8)

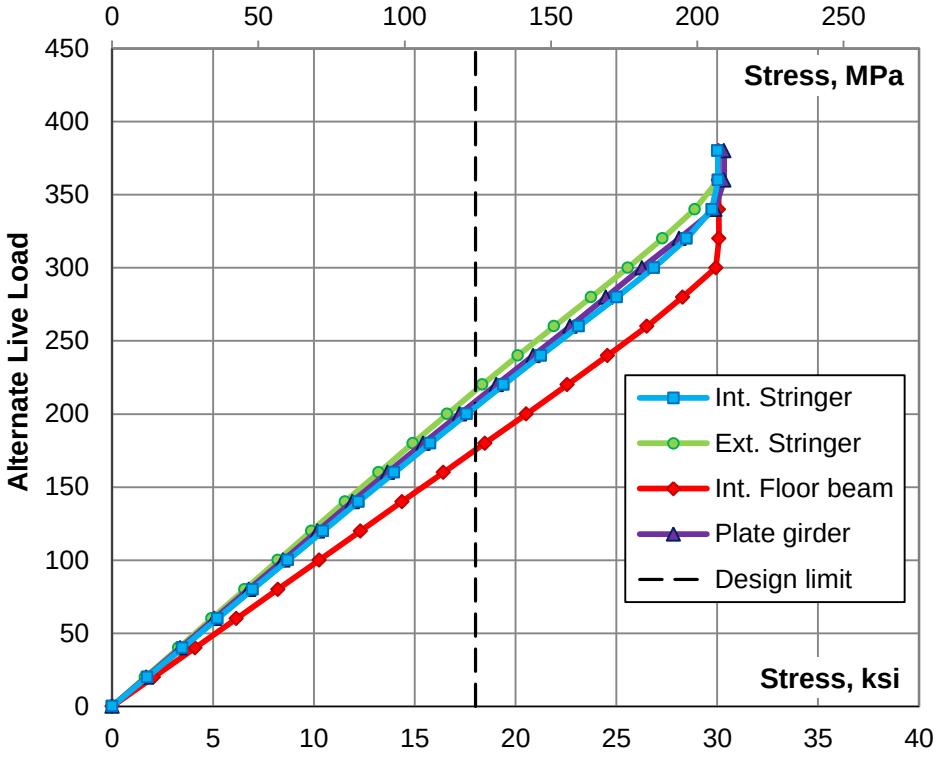

Figure 4.42 Stresses due to gradually increased alternate live load, bridge #2

Figure 4.43 presents stresses due to Cooper E Loading for these same bridge elements: exterior and interior stringers, interior floor beam, and plate girder. Behavior of members under applied load was comparable to Alternative Live Load; however, the stresses were slightly lower. For Cooper E80, the stringer reaches 13.43 ksi (92.6 MPa), the floor beam is 13.50 ksi (93.1 MPa), and the plate girder is 13.64 ksi (94.1 MPa). Remaining results are listed in table 4.11. While the Alternative Live Load governs for stringers and floor beams, Cooper E 80 produced bigger stress for the plate girder. According to AREMA, for span length above 50 ft Cooper E80 caused bigger bending moment on the simply supported beam. As a result, the plate girder achieved slightly higher stress.

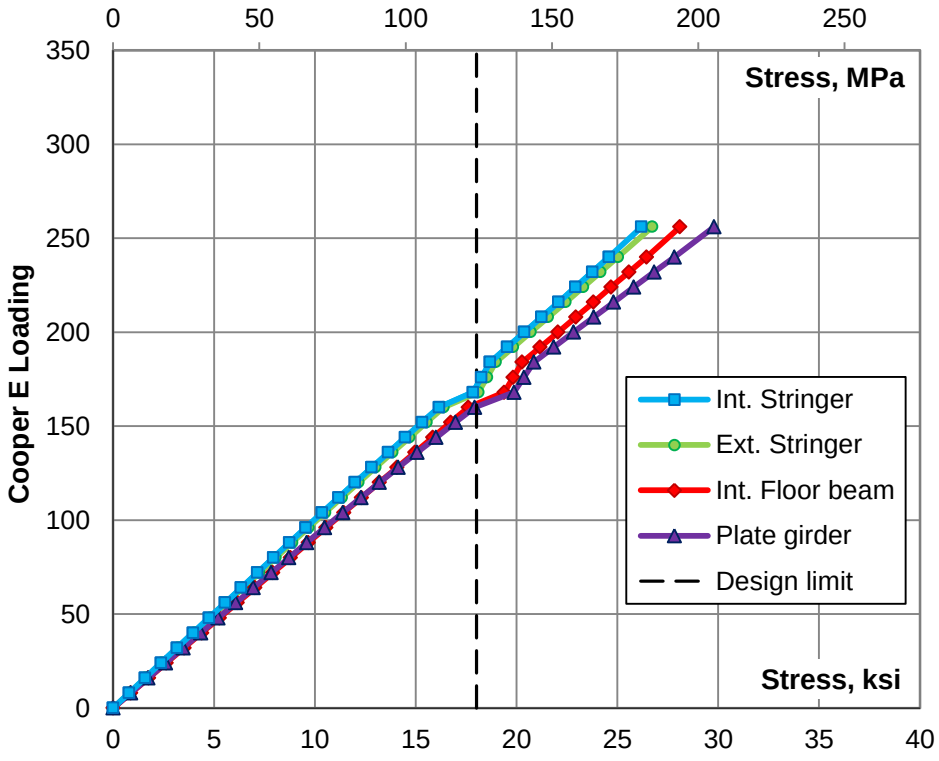

Figure 4.43 Stresses due to gradually increased Cooper E loading, bridge #2

Table 4.11 Stresses due to design load, Cooper E80 loading, bridge #2

Member type	Dead Load, ksi (MPa)	Static load, ksi (MPa)	Dynamic portion, ksi (MPa)	Total, ksi (MPa)
Interior Stringer	0.82 (5.65)	7.95 (54.8)	4.66 (32.1)	13.43 (92.6)
Exterior Stringer	1.00 (6.88)	8.07 (55.6)	3.80 (26.2)	12.87 (88.7)
Interior Floor beam	0.69 (4.74)	8.79 (60.6)	4.02 (27.7)	13.50 (93.1)
Plate girder	1.57 (10.9)	8.72 (60.1)	3.36 (23.1)	13.64 (94.1)

The stress to displacement relationship presented in figure 4.44 shows similarity for Cooper E Loading and Alternate Live Load. For Cooper E Loading the stresses in main members did not reach yield stress because applied load was smaller. The process of gradually increased load slowed down when the load reached 150 kips for main axle. The analysis shows that the plastic deformations were developed in the connections and this was a reason for very slow progress.

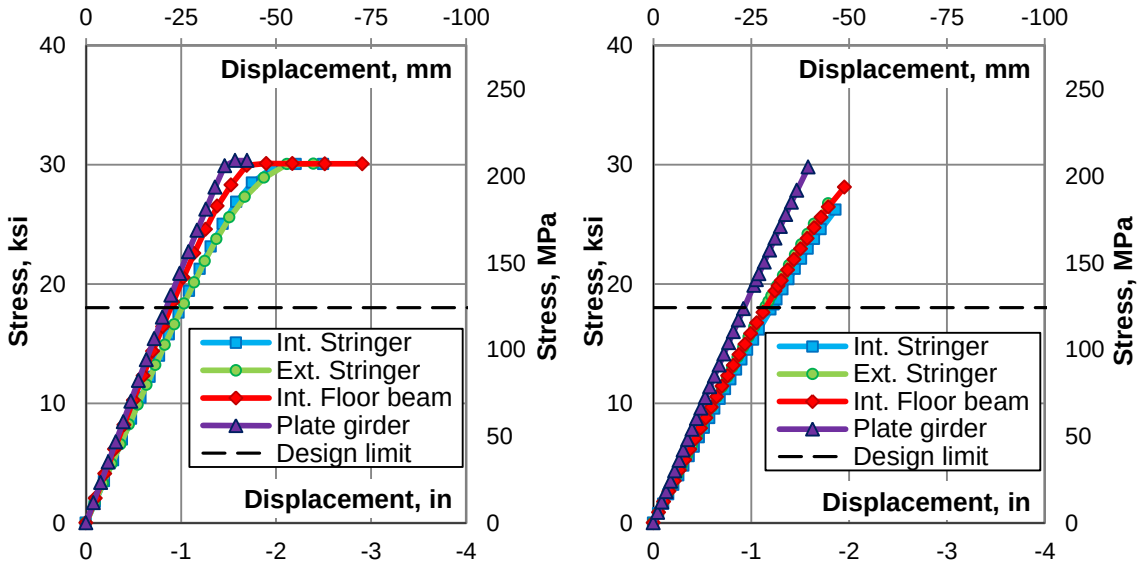

Figure 4.44 The stress to displacement relation for alternate live load (left side) and Cooper E loading (right side), bridge #2

4.6.2 Displacement and Deflection Due to Design Load

Displacement in the critical points in a stringer, a floor beam, and a plate girder were analyzed under Alternate Live Load on four-axles and Cooper E80. Figure 4.45 presents displacement under a gradually increased Alternate Live Load whereas figure 4.46 presents displacement under a gradually increased Cooper E Loading.

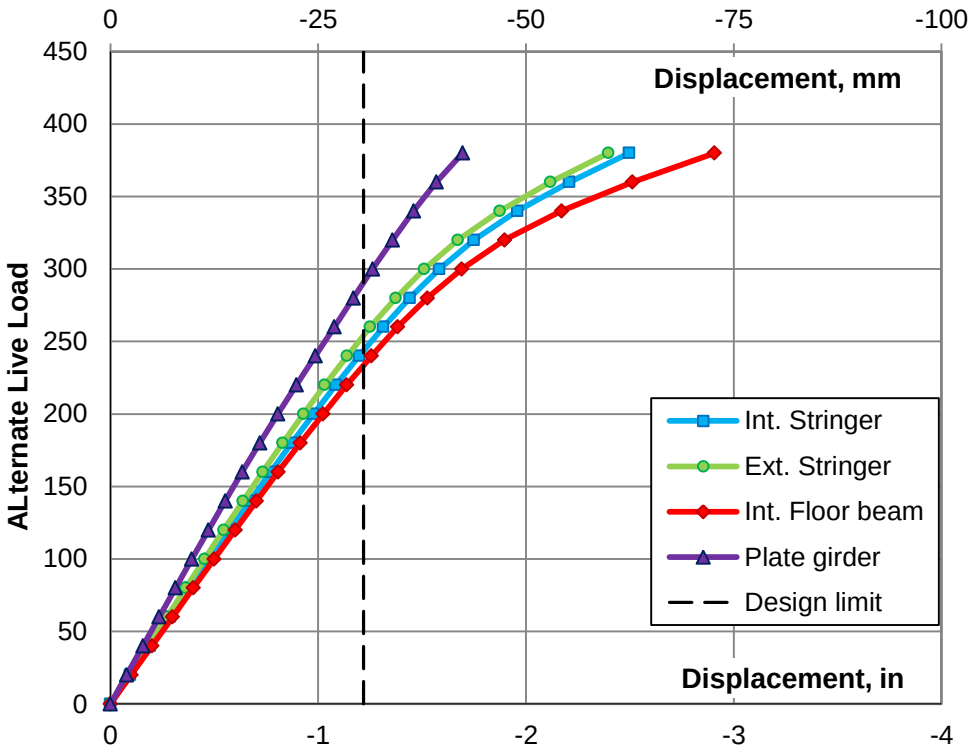

Figure 4.45 Displacement due to gradually increased alternate live load, bridge #2

Table 4.12 Displacement due to design load, alternate live load, 100 kip, bridge #2

Member type	Dead Load, in (mm)	Static load, in (mm)	Dynamic portion, in (mm)	Total, in (mm)
Interior Stringer	0.089 (2.26)	0.478 (12.12)	0.285 (7.25)	0.852 (21.64)
Exterior Stringer	0.090 (2.29)	0.453 (11.51)	0.225 (5.72)	0.769 (19.52)
Interior Floor beam	0.097 (2.47)	0.499 (12.68)	0.248 (6.29)	0.844 (21.44)
Plate girder	0.086 (2.19)	0.392 (9.95)	0.187 (4.76)	0.665 (16.90)

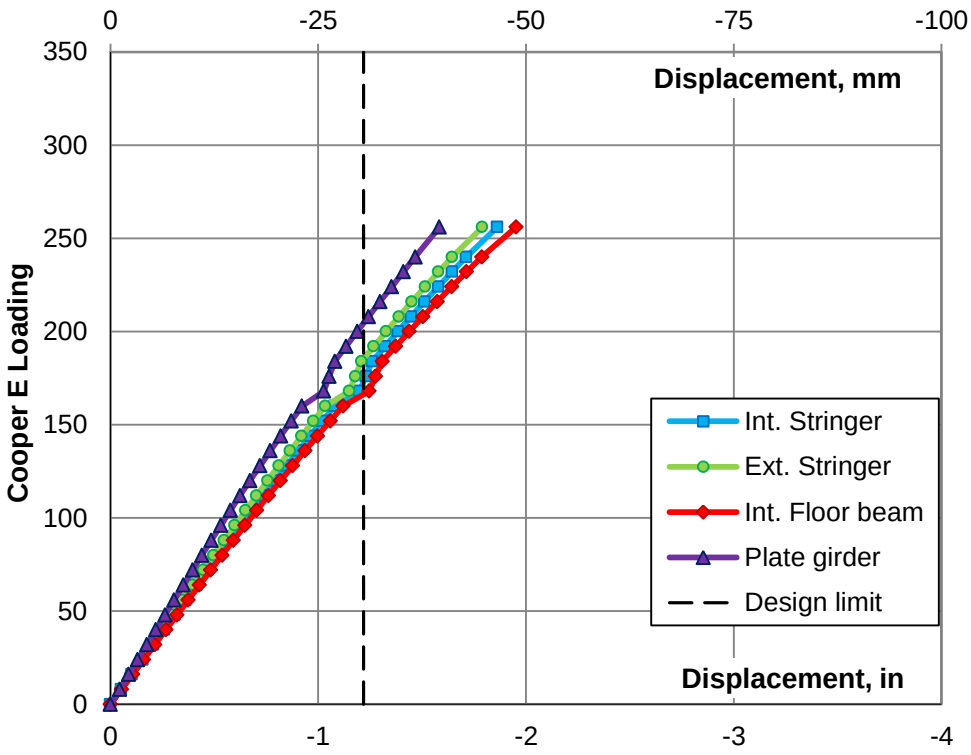

Figure 4.46 Displacement due to gradually increased Cooper E loading, bridge #2

Table 4.13 Displacement due to design load, Cooper E80 loading, bridge #2

Member type	Dead Load, in (mm)	Static load, in (mm)	Dynamic portion, in (mm)	Total, in (mm)
Interior Stringer	0.089 (2.26)	0.519 (13.19)	0.310 (7.88)	0.919 (23.34)
Exterior Stringer	0.090 (2.29)	0.497 (12.62)	0.247 (6.26)	0.833 (21.17)
Interior Floor beam	0.097 (2.47)	0.537 (13.64)	0.267 (6.77)	0.901 (22.89)
Plate girder	0.086 (2.19)	0.440 (11.18)	0.211 (5.35)	0.737 (18.72)

Displacement under Cooper E loading is slightly higher than for Alternate Live Load. In both cases, the stringers and the floor beam demonstrate bigger displacement than the plate girder under this same level of load. This is affected by absolute and relative displacement. In a floor system of the bridge when the main element moves the other elements move with it. Therefore, the deflection needs to be calculated as a relative displacement between the plate girder and the floor system.

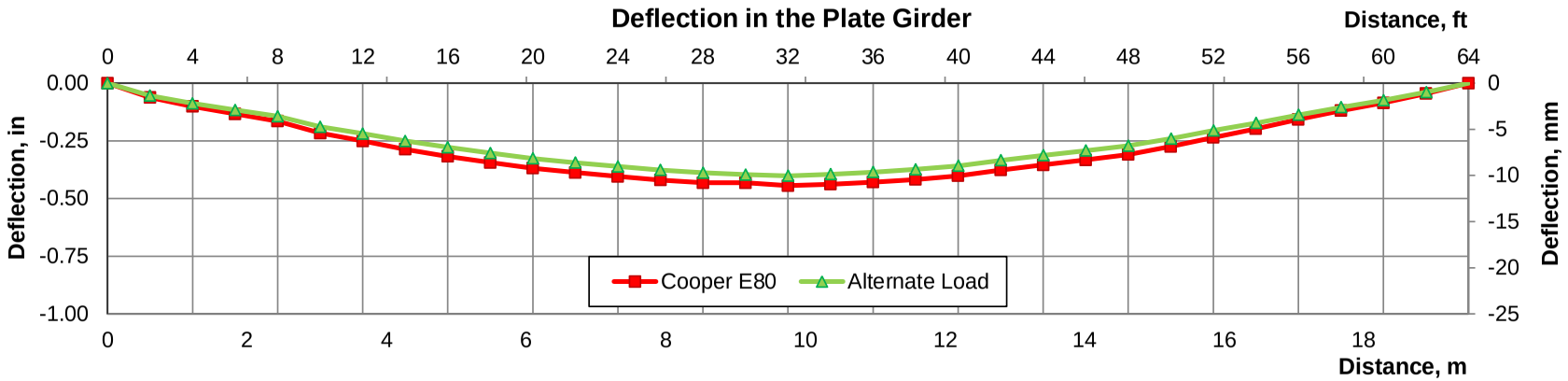

Figure 4.47 Deflection due to live load in the plate girder, bridge #2

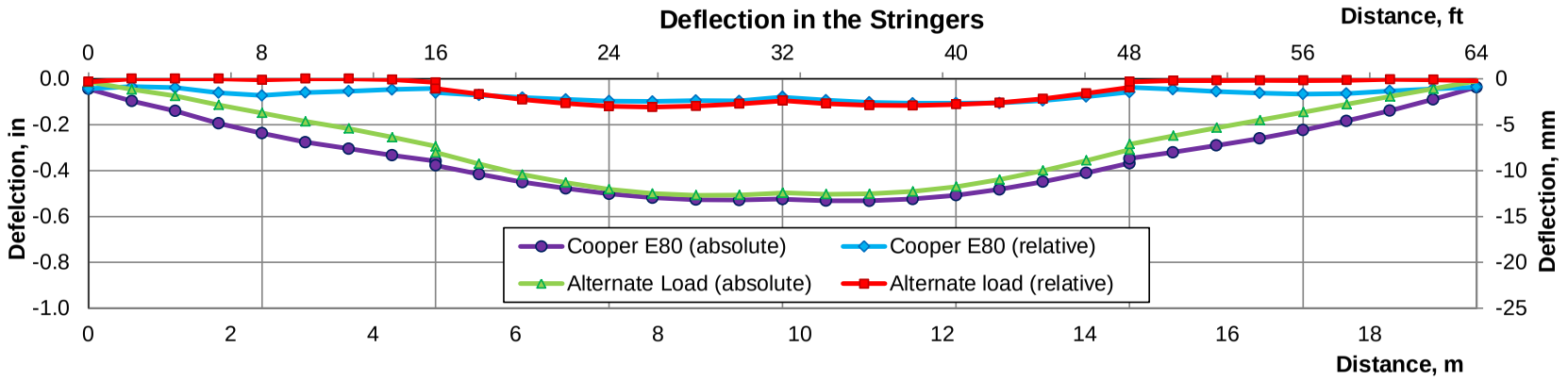

Figure 4.48 Deflection due to live load in the stringer, bridge #2

Deflection in the plate girder corresponds to the vertical displacement as presented in the dotted line graph in figure 4.47. Deflection in the stringers is present in the dotted line graph in figure 4.48 and includes relative and absolute displacement. The absolute deflection corresponds to vertical displacement whereas relative deflection is a difference between the displacement of the plate girder and the stringer.

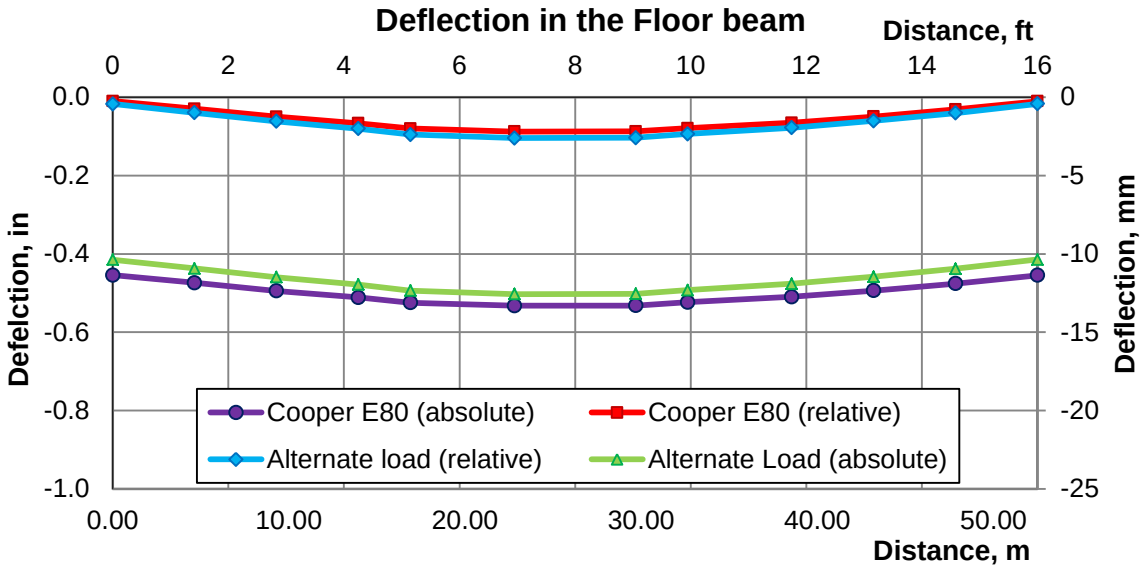

Figure 4.49 Deflection due to live load in the floor beam, bridge #2

Figure 4.49 contains absolute and relative deflection in the floor beam due to design live load. Absolute deflection in the floor beam is the total vertical displacement while relative deflection is a difference between the displacement of the plate girder and the floor beam. The maximum relative deflections for structural members due to Alternate Live Load are presented in table 4.14 and for Cooper E80 in table 4.15.

Table 4.14 Relative deflection due to design load, alternate live load, 100 kip, bridge #2

Member type	Dead Load, in (mm)	Static load, in (mm)	Dynamic portion, in (mm)	Total, in (mm)
Interior Stringer	0.003 (0.08)	0.085 (2.17)	0.051 (1.30)	0.139 (3.55)
Exterior Stringer	0.004 (0.11)	0.061 (1.56)	0.031 (0.78)	0.096 (2.44)
Interior Floor beam	0.011 (0.28)	0.107 (2.73)	0.053 (1.35)	0.172 (4.37)
Plate girder	0.086 (2.19)	0.392 (9.95)	0.187 (4.76)	0.665 (16.90)

Table 4.15 Relative deflection due to design load, Cooper E80 loading, bridge #2

Member type	Dead Load, in (mm)	Static load, in (mm)	Dynamic portion, in (mm)	Total, in (mm)
Interior Stringer	0.003 (0.08)	0.079 (2.00)	0.047 (1.20)	0.129 (3.27)
Exterior Stringer	0.004 (0.11)	0.056 (1.43)	0.028 (0.71)	0.088 (2.25)
Interior Floor beam	0.011 (0.28)	0.097 (2.46)	0.048 (1.22)	0.156 (3.96)
Plate girder	0.086 (2.19)	0.440 (11.2)	0.211 (5.35)	0.737 (18.7)

The deflection limit for railway bridges is L/640; therefore, the deflection limit for a span length of 64 ft (19.5 m) is 1.2 in. (30.5 mm). For both cases of load, the actual deflection does not exceed deflection limit.

4.6.3 Stringer to Floor Beam Connections

The stringer-to-floor-beam connections in the Bridge #2 are constructed with double angle connections. As mentioned before, these types of connections are considered as simple shear connections during the design stage. However, a considerable amount of end moment is developed at the connection because of unintentional connection stiffness. Since the connections can be susceptible to fatigue damage, during FEM analysis the stresses were considered in the angles and rivets of those connections. The graphics presented in figures 4.50 and 4.51 present the detail of a double angle connection in Bridge #2 before and after applied load, respectively.

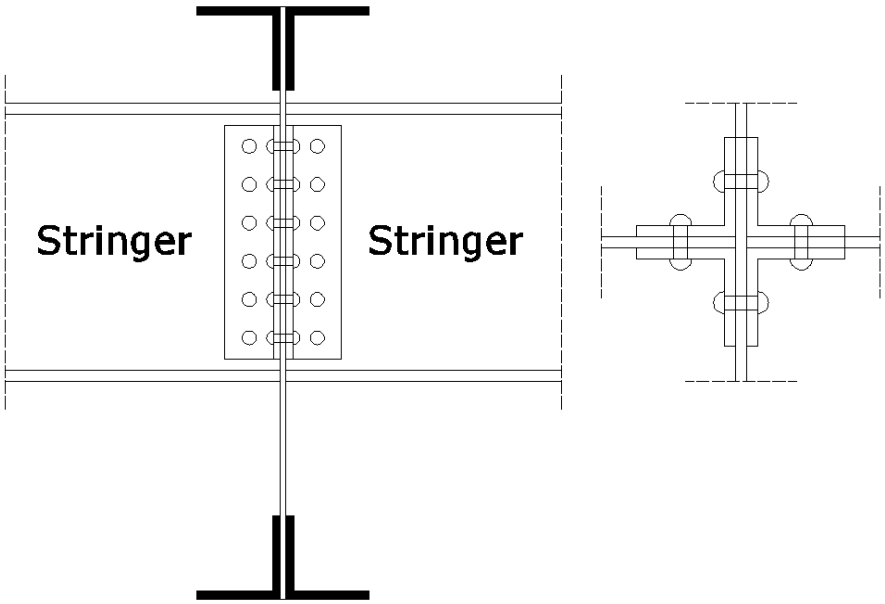

Figure 4.50 Detail of double angle connection in bridge #2

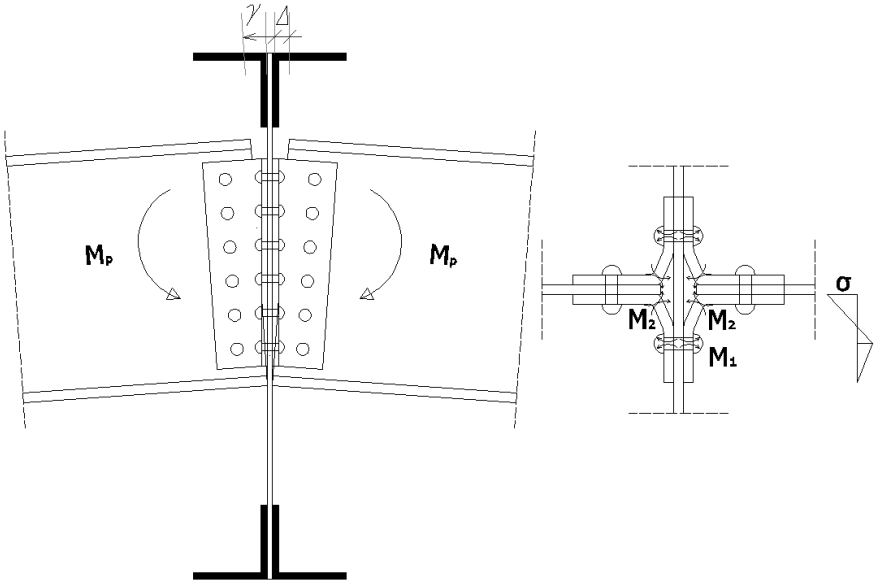

Figure 4.51 Distortion of outstanding legs of connection angles due to applied load, bridge #2

Figures 4.52 and 4.53 present stresses due to a gradually increased load on Bridge #2. Because the connections concentrate stresses in different directions, the results are presented for

von Mises stress. Based on the von Mises theory, the equivalent tensile stress is a scalar stress value that can be computed from the stress tensor (see equation 4.1).

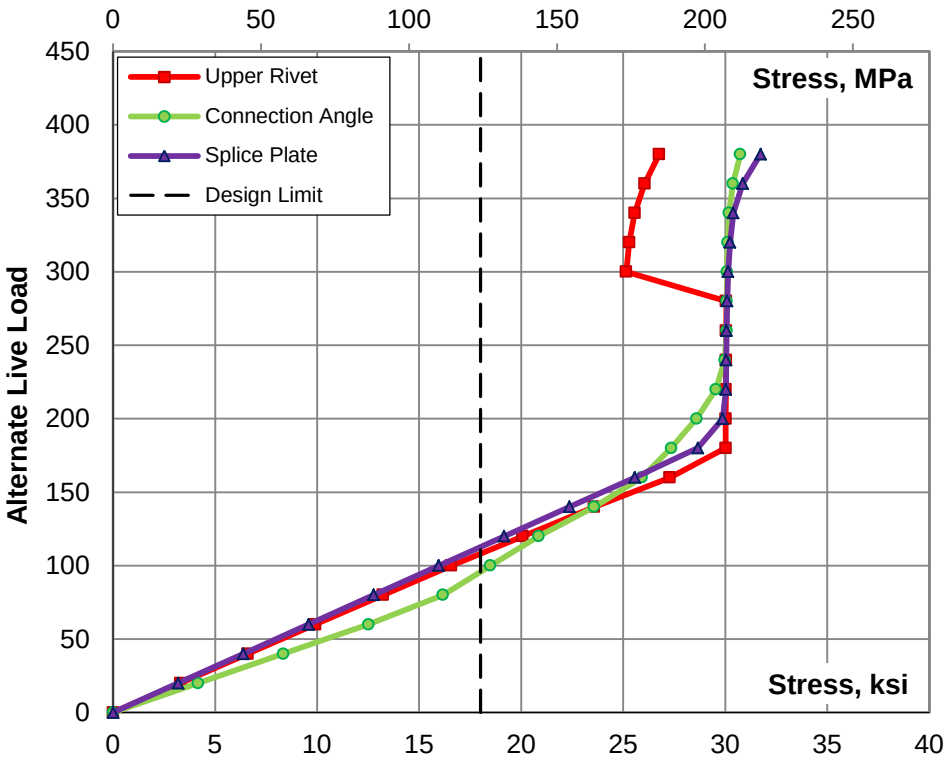

Figure 4.52 Stresses due to gradually increased alternate live load, bridge #2

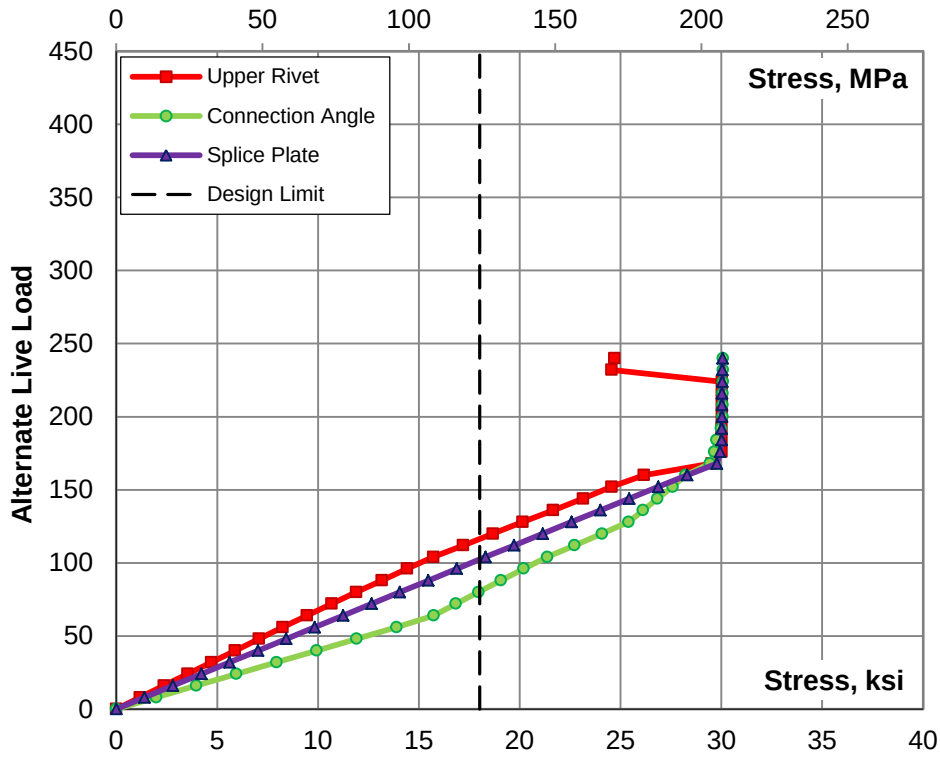

Figure 4.53 Stresses due to gradually increased Cooper E loading, bridge #2

The analysis shows that the connection between stringer and floor beam acquires a certain degree of rotational stiffness and develops stresses due to bending moment. Also, the connections between floor beam and plate girder reach high stress and plastic deformation close to the splice plates.

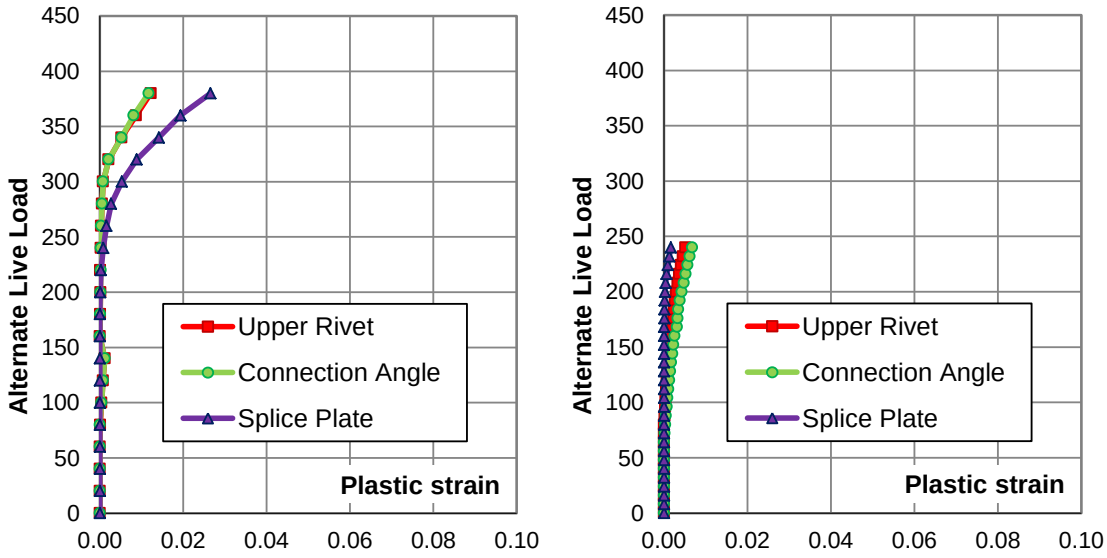

Figure 4.54 Plastic strain due to gradually increased load; alternate live load on left side and Cooper E loading on right side, bridge #2

Figure 4.54 presents the relationship between plastic strain and applied load. The gradually increased load produced plastic strain when the axial forces were close to 100 kip in Cooper E Loading and 150 kip in Alternate Load. The connection developed plastic deformation much faster than the main elements on the bridge. Therefore, the connections are more critical than the primary members and need to be considered in fatigue analysis. Also, additional calculations were made using ROBOT Structural Analysis for a continuous beam with and without pin connections (APPENDIX B). The stringers in the FEM model behave as partially continuous for a four spans beam with negative moment at the interior floor beams.

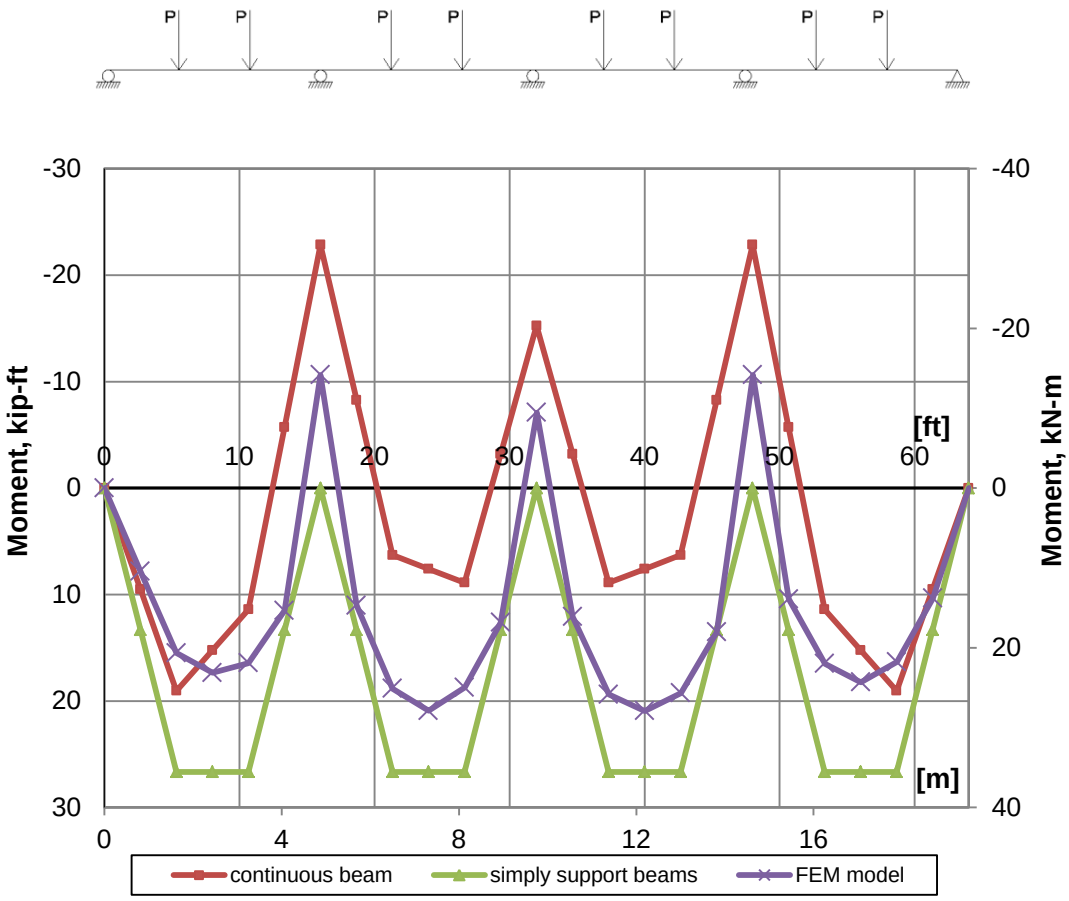

Figure 4.55 Moment diagram for continuous beam, simply supported beams and fem model, bridge #2

The results presented in figure 4.55 show that the double angle connections in the FEM model for Bridge #2 were capable of developing up to 60% of the corresponding moment of a fully continuous beam, and this finding was also proven by other researchers (Al-Emrani 2006; Charles et al. 2001; Goel R.K. 2006; Krajewski 2009).

4.6.4 Influence Lines

FEM analysis of bridge #2 showed that most critical points of the bridge remain in elastic stage under the design load. It is expected that the loading spectra under current operating conditions do not exceed the design load, which was developed in section 3.8. Therefore, for

further analysis of fatigue evaluation, the principal of super position can be applied. For that purpose, an influence line for each member of the bridge was developed. The influence lines for selected members and locations are given in the charts showing in figures 4.56 through 4.59.

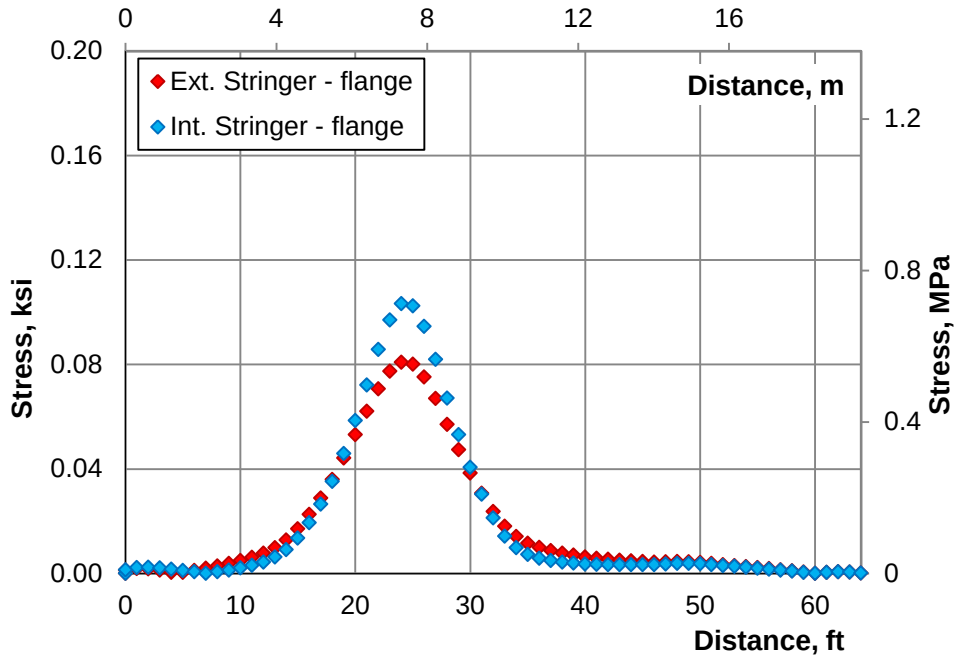

Figure 4.56 Influence lines for bridge #2 at mid-span location of exterior and interior stringer

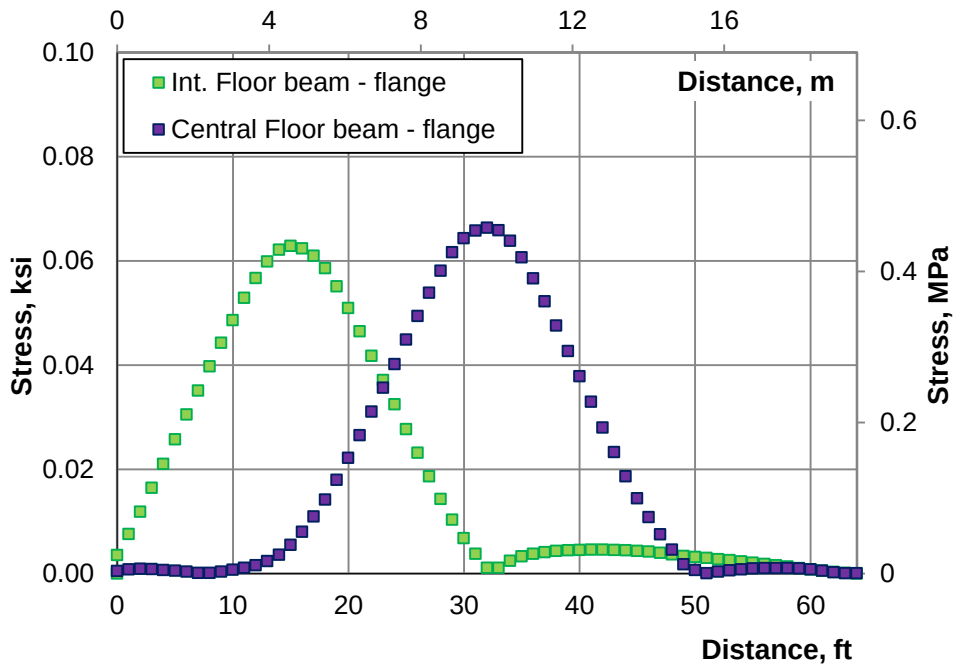

Figure 4.57 Influence lines for bridge #2 at mid-span location of central and interior floor beam

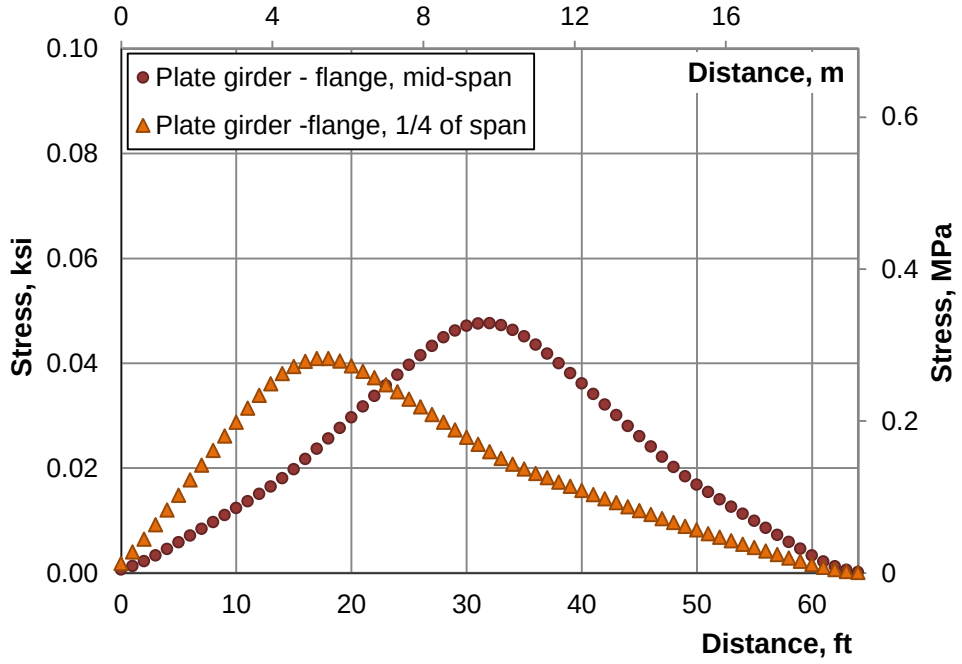

Figure 4.58 Influence lines for bridge #2 at center and 1/4 of the span of the plate girder

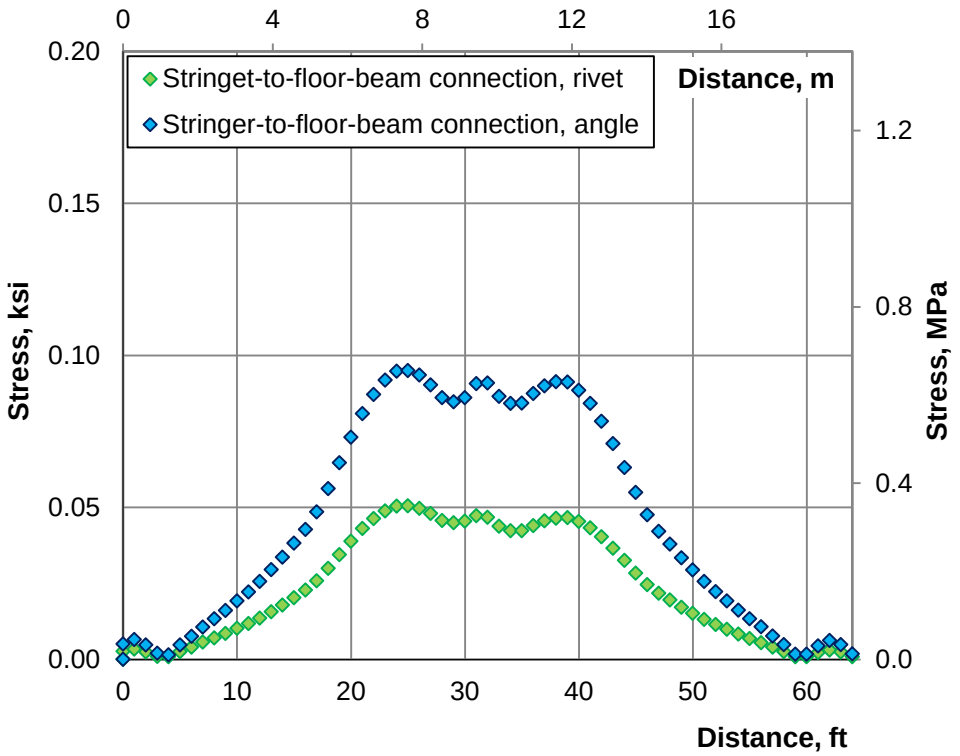

Figure 4.59 Influence lines for bridge #2 at stringer-to-floor-beam connection for the rivet and the angle

Chapter 5 Fatigue Analysis

5.1 Overview

Many railroad bridges in the US are over 100 years old and are classified as fracture-critical. The term fracture-critical indicates that failure of a single component may result in complete collapse of the structure, such as the one experienced by the I-35 W Bridge. Components and connection need to be analyzed for possible damage caused by fatigue. Railway bridges are exposed to repetitive high stress due to the live load and constant, relatively low stress due to dead load. Repeated application of live load may lead to failure even when the stress level is lower than for the allowable stresses. Fatigue analysis, whether for design or rating of steel railway girders, needs to account for the possibility of a high number of fatigue cycles (Dick, Otter, and Connor 2011). The basic approach for estimating the remaining fatigue life of a structure element is to use S-N curves, which present the number of cycles to failure as a function of the constant stress amplitude. The other approach uses methods that apply fracture mechanics theory.

In a fracture mechanics approach, the problem can be considered in terms of crack initiation and crack propagation. From a practical standpoint, crack initiation is very difficult to predict; therefore, in the analysis, the crack flow size is often assumed. The initial crack size needs to be estimated accurately because this assumption affects the number of cycles to failure. A method to investigate crack propagation must take into account the geometry of the detail, the magnitude of the stress range, and material parameters.

Load and resistance parameters are random variables; consequently, structural performance can be measured in terms of reliability (Nowak and Szerszen 1998). In the 1990s, reliability models were developed for highway bridges and are currently used in AASHTO

LRFD. Fatigue load requires a special approach because it contains two parameters: magnitude and number of cycles. Fatigue resistance and material strength both need to be considered in relation to the load. Considerable effort was exerted derivations of S-N curves for various categories of details for steel structures by many researchers (Fisher et al. in 1970, 1974, 1987). The distribution of the number of cycles to failure can be approximated as normal with the coefficient of variation decreasing for decreasing stress level (Nowak and Szerszen 1998).

The current design provisions of Fatigue Limit States are divided to Fatigue Limit State I related to infinite fatigue life and Fatigue Limit State II related to finite fatigue life. The fatigue load in infinite fatigue life reflects the load levels with the maximum stress range less than the constant amplitude fatigue limit. The fatigue load in finite fatigue life is intended to reflect a load level found to be representative of the effective stress range of the load population with respect to the induced number of load cycles and their cumulative damage effects on the bridge components (AASHTO).

5.2 Introduction

An accurate estimation of reaming fatigue life of a structural component is very important in prioritizing bridge rehabilitation and replacement. However, existing procedure to evaluate the fatigue behavior of bridges are estimation rather than the exact formulas because the load and the resistance model contain many uncertainties. Therefore, probabilistic methods are the most convenient way to provide levels of safety for various design cases. In design and evaluation procedures, the main parameter is stress range. The background for reliability-based fatigue design and evaluation of bridges was formulated by Moses et al. (1987). The evaluation method includes the procedure to calculate the remaining mean life and the remaining safe life of a detail. The difference between the remaining mean life and the remaining safe life is in the

degree of safety. It was found that the reliability index for fatigue evaluations is relatively low because the associated safety reserve is in terms of the remaining life rather than a strength failure used in design procedures for the ultimate limit states. Therefore, for the evaluation of existing highway bridges the target $\beta_T = 1.35$ for redundant and $\beta_T = 1.75$ for nonredundant members, according to AASHTO Guide Specifications for Fatigue Evaluation of Existing Steel Bridges (1990).

It was observed, that laboratory specimens tested with a constant-amplitude stress range have a scatter number of cycles. In the real structures subjected to variable-amplitude stress range, the degree of scatter is expected to be even larger. Hence, the fatigue life can only be assured in terms of probability. The fatigue reliability and some criteria for fatigue resistant design are presented by Ang (1977). According to his research, the reliability analysis is based on the following basic assumptions:

- all fatigue properties of material are characterized by S-N curves
- failure caused by fatigue is defined by the necessary S-N relationship
- cumulative damage is based on Miner's linear rule, assumed to hold for random fatigue load.

The fatigue resistance design can be expressed in the form of the root-mean-square stress-range. For the required mean life, the allowable stress-range used in the design can be obtained from the constant-amplitude loading, directly from the S-N curve. For a random or variable loading, the corresponding allowable design stress-range can be given as the expected value of the stress-range (Nowak and Szerszen 1998).

5.3 Rain-Flow Counting Method

Railway bridges are subjected to variable-amplitude stress ranges during their service live load. Based on the available fatigue load models described in Chapter 3 and influence lines developed in Chapter 4, stress histories can be determined. The stress histories caused by statistic load are irregular with variable frequencies and amplitudes. Also, theoretical fatigue load models give varied stress ranges for bridge components and connections.

Many different counting procedures are available and can be used, but only two provide accurate results: rain-flow counting and range pair (Dowelling 1982). For variable stress history, the rain-flow cycle counting is a method recommended by ASTM. This method was presented by Matsuishi and Endo in 1968. This method counts the number of fully reversal cycles as well as half cycles and their range amplitude for a given load time history. A fully reversal cycle is when a cycle range goes up to its peak and back to the starting position. A half cycle goes only in one direction, from the "valley" to the "peak" or from the "peak" to the "valley" (Rakoczy 2011). The method can be described by the following steps:

- Step 1: The stress history is reduced to local maxima, peaks, and minima or turning points and valleys, as seen in the line graphs in figure 5.1.

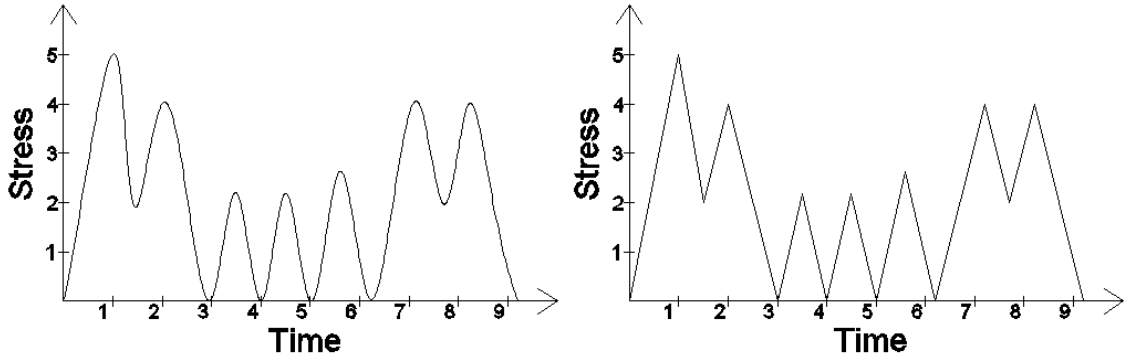

Figure 5.1 Original stress history and stress history reduced to turning points

- Step 2: After the new stress history is reduced to turning points it is plotted and rotated 90 degrees clockwise.
- Step 3: Imagine that the time history is a template for a rigid sheet (pagoda roof). Each turning point is imagined as a source of water that "drips" down the pagoda. The graphic in figure 5.2 shows the visualization of this.

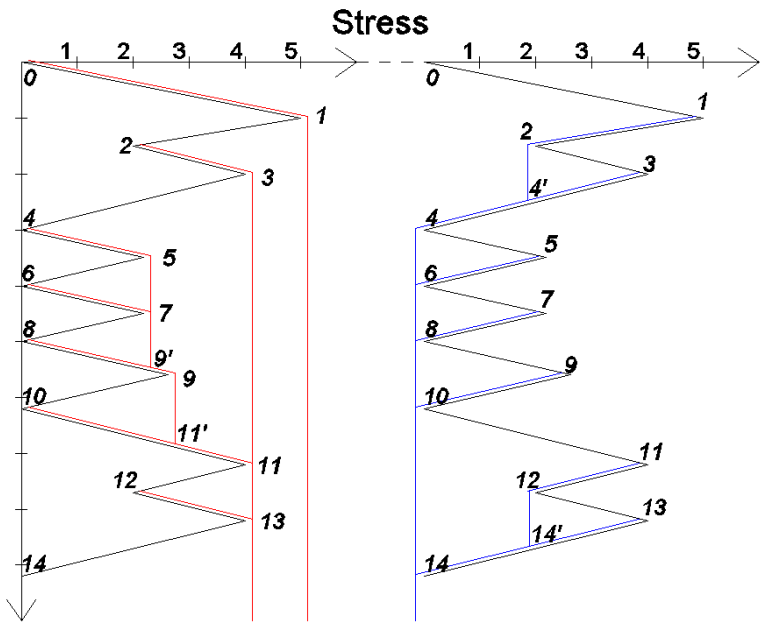

Figure 5.2 Rain-flow counting diagram

- Step 4: Count the numbers of half-cycles. The magnitude of one half-cycle is the horizontal coordinate which flows before it reaches the end of the time history, or collides with the “flow” from above
- Step 5: Repeat step 4 for compressive.

Table 5.1 Half cycles

Positive direction		Negative direction	
Range	Amplitude	Range	Amplitude
0-1-end	5	1-2-4-end	5
2-3-end	2	3-4’	2
4-5-9-11-end	4	5-6	2
6-7	2	7-8	2
8-9’	2	9-10	3
10-11’	3	11-12-14	4
12-13-end	2	13-14’	2

- Step 6: Tension and compression half cycles of the same magnitude are paired to make full cycles, as shown in table 5.2.

Table 5.2 Load cycles after rain-flow counting

Amplitude	Number of cycles
2	4
3	1
4	1
5	1

5.4 Miner’s Rule

When the number of cycles of stress range is determined, Miner’s rule may be applied. Generally, Miner’s law is proposed to find the relationship between variable-amplitude fatigue behavior and constant-amplitude behavior. According to the Palmgren-Miner’s rule, fatigue damage due to a variable-amplitude loading is expressed by the equation shown in 5.1.

$$D = \sum_i \frac{n_i}{N_i} \tag{5.1}$$

Where D is the accumulated damage; n_i is the number of cycles at ith stress range magnitude; and N_i is the corresponding N value from S-N curve at ith stress range magnitude (Miner 1945). Theoretical failure occurs when the sum of the incremental damage equals or exceeds 1. In practice, a value of D less than unity indicates failure. Therefore, to be more conservative it is recommended to use D as lognormal distributed with a mean value equal to 0.9 (Imam et al 2008). The coefficient of variation of D was found to be reasonable at the level of 30% (Wirsching 1995).

Miner's rule can be rearranged to develop an equivalent constant amplitude cycling loading. The equivalent constant stress produces the same fatigue damage as a variable amplitude load for the same number of cycles (Schilling et al. 1977). This theory is based on the exponential model of stress range life relationship presented in equation 5.2 (Fisher, 1977)

$$N = AS^{-n} \tag{5.2}$$

where N is number of cycles to failure, S is the nominal stress range, A is a constant for a given detail and n is the slope constant. After short derivation and assumption that the number of cycles at ith stress range magnitude n_i, is a product of the probability of occurrence of cycle with amplitude S_i and the total number of cycles N_T, the equivalent stress range is:

$$\sum_i \frac{n_i}{AS_i^{-n}} = 1$$

$$n_i = p_i N_T = p_i A S_e^{-n}$$

$$\sum_i \frac{p_i A S_e^{-n}}{AS_i^{-n}} = \sum_i \frac{p_i S_e^{-n}}{S_i^{-n}} = \sum_i \frac{p_i S_i^n}{S_e^n} = 1 \qquad (5.3)$$

$$S_e^n = \sum_i p_i S_i^n$$

$$S_e = \sqrt[n]{\sum_i p_i S_i^n}$$

where S_e is the equivalent stress for a constant amplitude. The exponent n for most structural details is 3 and, therefore, the final equation for equivalent stress is referred as a Root Mean Cube (RMC) of the stress distribution equation 5.4.

$$S_e = \sqrt[3]{\sum_i p_i S_i^3} = \sqrt[3]{\sum_i \frac{n_i}{N_T} S_i^3} \qquad (5.4)$$

5.5 S-N Curve

The S-N curves define the number of cycles to failure that a particular detail is able to withstand under corresponding constant amplitude stress range. Each S-N curve represents a category of details. The design specifications present seven S-N curves for seven categories of weld details, defined as the detail categories A, B, B', C, D, E, and E' (shown in the line graph of fig. 5.3). The S-N curves are based on a lower bound to a large number of full-scale fatigue test data with a 97.5% survival limit. Therefore, a detail optimally designed with these S-N curves and actually exposed to the stress ranges assumed in design has a 2.5% probability of cracking during the specified lifetime (O'Connell 2001).

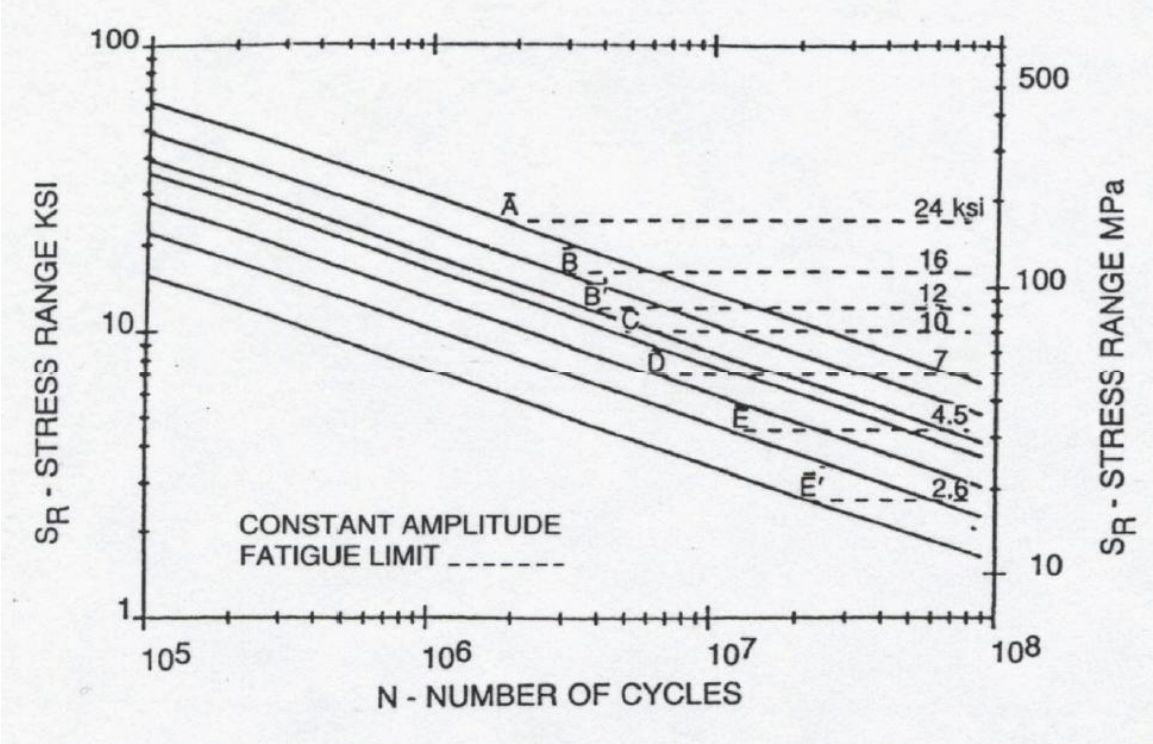

Figure 5.3 Design S-N curves from AREMA code

S-N fatigue data created in laboratory do not always represent actual conditions and often contain a considerable amount of scatter, even when carefully machined standard specimens out of the same lot of material are used. The statistical parameters are developed based on the available fatigue data.

The through-plate girder contains mainly two categories of details. These are the riveted connections, such as riveted cover plates, and double angle connections which are category D and plain section, or cleaned surface which are category A. Therefore, the S-N plots and CDF's are presented only for the A and D categories. For the remaining details, the S-N plots and CDF's are presented in Appendix C.

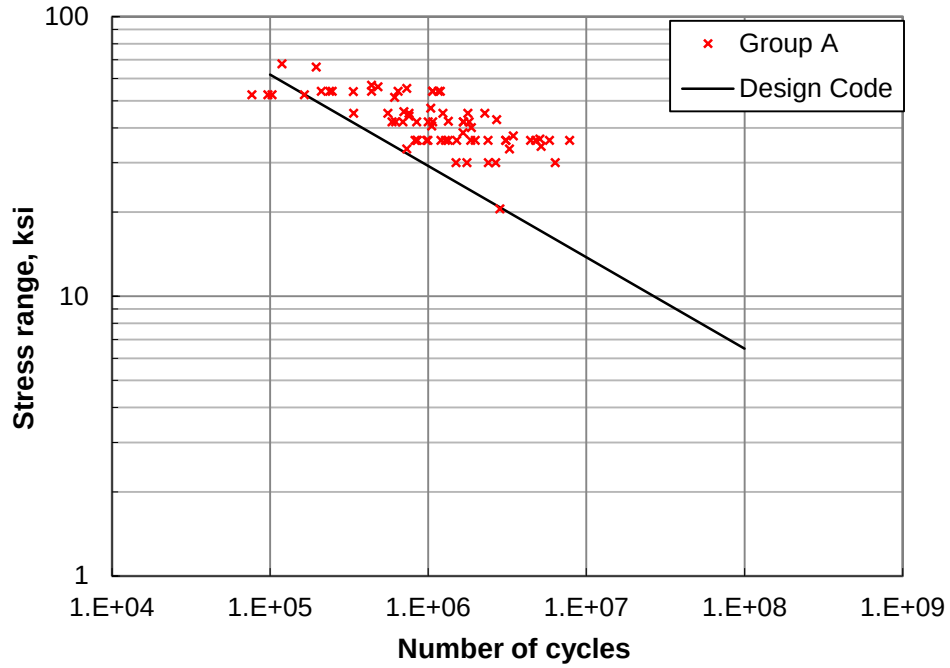

Figure 5.4 S-N data for category A

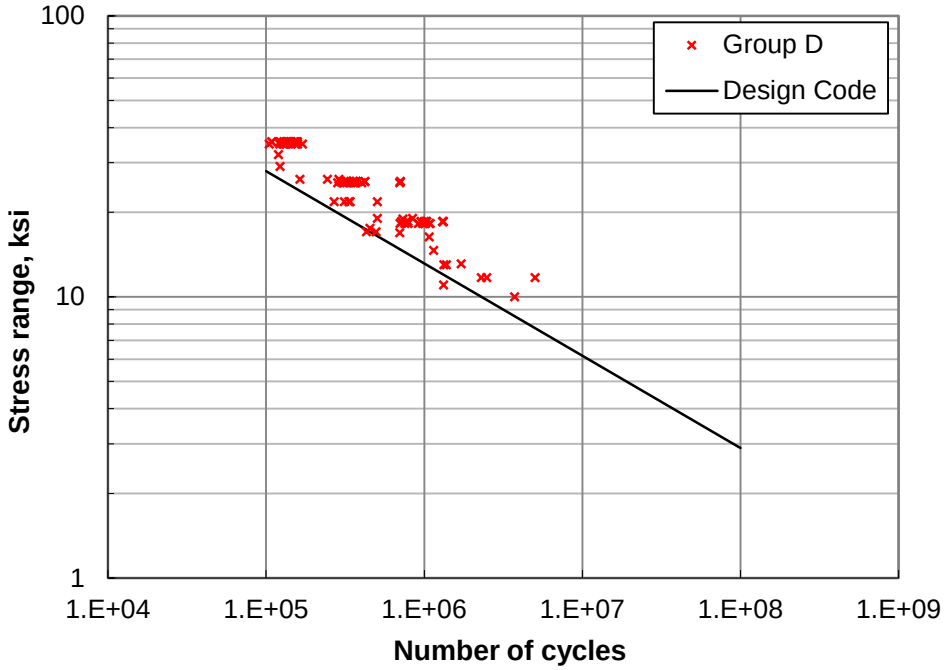

Figure 5.5 S-N data for category D

The points plotted in the scatter in figures 5.4 and 5.5 present results of the laboratory specimens tested with a constant-amplitude stress range. It is obvious that the S-N data have a scatter number of cycles under this same stress range. In this situation, fatigue resistance should be presented in terms of probability. The fatigue resistance design can be expressed in the form of the cube root of the number of cycles times the stress to the third power, $(S^3N)^{(1/3)}$. Therefore, the cumulative distribution function (CDF) of the fatigue resistance, $(S^3N)^{(1/3)}$, are plotted on the normal probability paper for each category of details, as seen in figure 5.6. The construction and use of the normal probability paper was described previously in the Chapter 2.2 and can be also found in textbooks on probability, such as that by Nowak and Collins (2000). The shape of the CDF is an indication of the type of distribution, and if the resulting CDF's are close to straight lines, they can be considered as normal random variables.

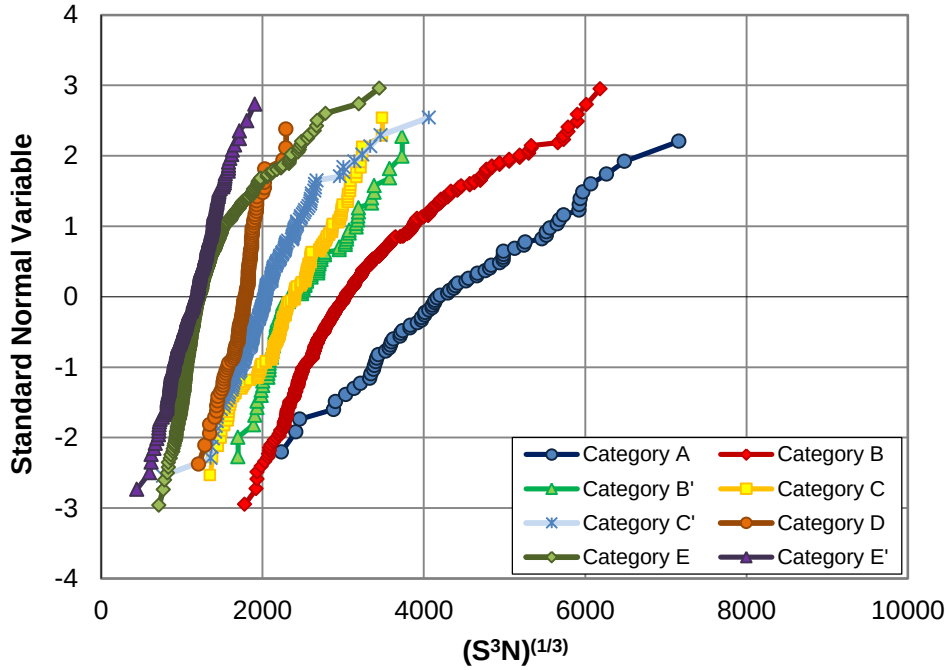

Figure 5.6 CDF of fatigue resistance for each category of details

In addition, the statistical parameters are determined by fitting a straight line to the lower tail of the CDF. The most important parameters are the mean value, standard deviation, and the coefficient of variation. Figure 5.7 and 5.8 present the CDF of fatigue resistance for Category A and D, respectively. For the remaining details, the CDF's are presented in Appendix D. The statistical parameters determined by fitting the lower tail with straight lines are summarized in table 5.3.

Table 5.3 The statistical parameters of the fatigue resistance

Category	A	B	B'	C	C'	D	E	E'
Mean value, μ	4205	2980	2280	2430	2050	1810	1200	1150
Standard deviation, σ	835	425	250	480	370	250	140	240
Coefficient of variation, V	20%	14%	11%	20%	18%	14%	12%	21%

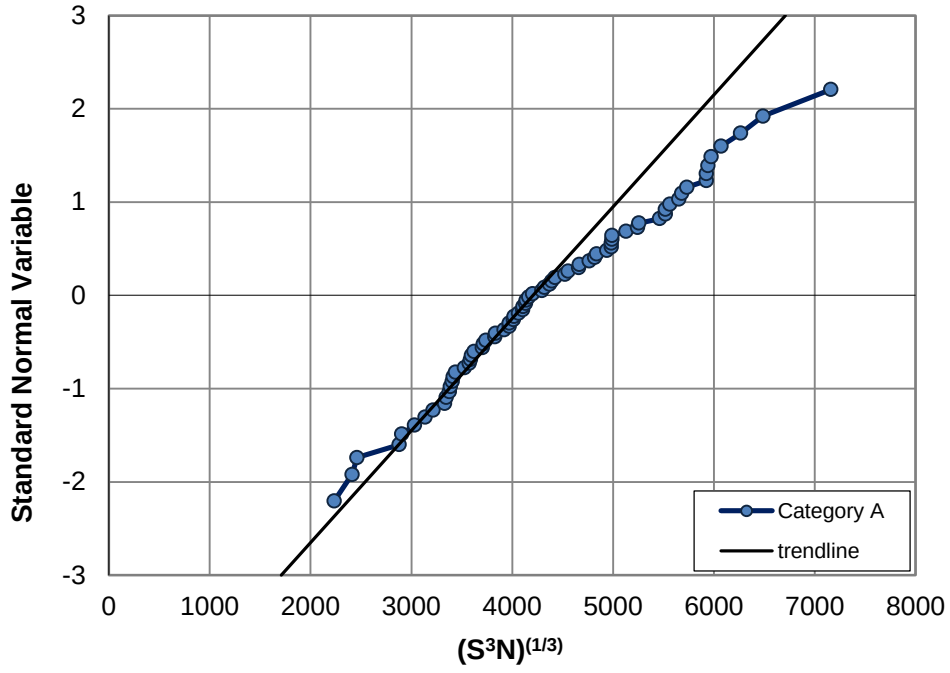

Figure 5.7 CDF of fatigue resistance for category A

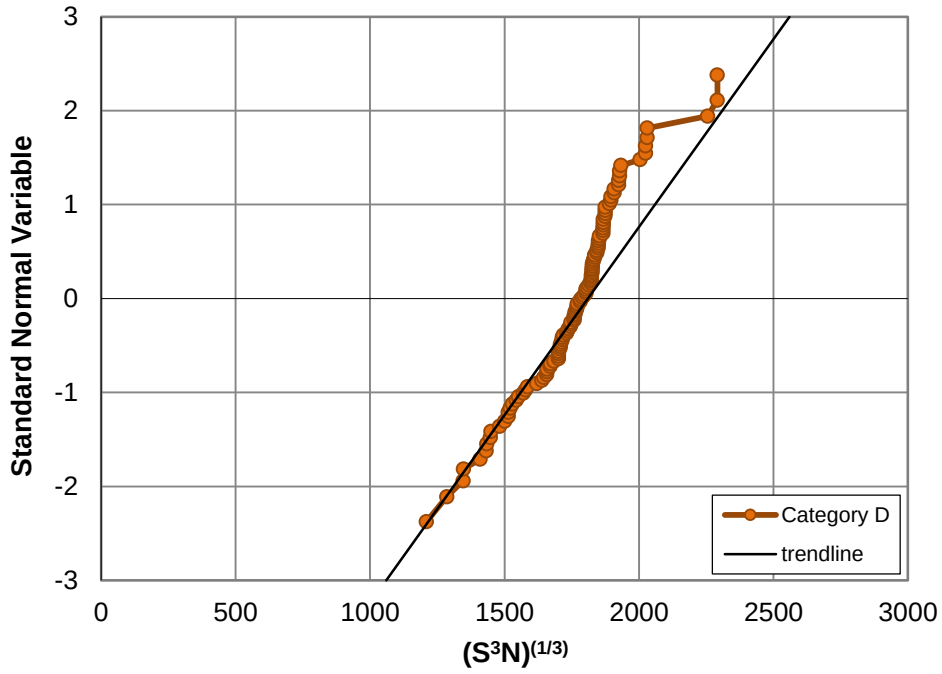

Figure 5.8 CDF of fatigue resistance for category D

5.6 Results of Fatigue Analysis

The response spectra for each component of the bridge were obtained under the statistical load model described in Chapter 3.6 and using developed algorithm in Mat Lab software. The scheme for the algorithm was based on the research of Tobias et al. (1997). It includes train simulation and calculation of stress history. Then the equivalent stress was calculated from stress cycles obtained using rain-flow counting. To obtain a number of cycles and effective stress range for each component Mat Lab was used along with the code written by Przemyslaw Rakoczy (2011). The whole algorithm is as follows:

- Step 1: Operation conditions are specified based on the location and conditions for an individual bridge. In this step the type of freight and million gross metric tons MGMT are categorized.

- Step 2: Specify statistics for types of equipment including occurrence rates and distribution type for each type of locomotive and rail cars. Based on this information, the overall configuration may be determined. The number of rail cars chosen for a train is 200 and is constant.
- Step 3: Car Loading Spectra is assigned for the axle load of particular car or locomotive. It was found that the variation in the axle load is mostly between the first and second truck. There is a minimum variation between axle loads in this same truck. Therefore, two axle forces were simulated and repeated for one truck rather than simulating four different axle forces for one car. In this step, the axle load is simulated in accordance with the distribution and statistical parameters.
- Step 4: Car Dimensions and axle spacing are picked to represent real equipment. Details about the dimensions used in analysis are described in Chapter 3.7.
- Step 5: Impact load was assumed as an increase factor of a live load as prescribed by the AREMA code. The dynamic load is very complex issue because dynamic effect on the bridge has various sources. In this study there is not more realistic value for a dynamic load of considered bridges than the values found in the code.
- Step 6: Influence lines are derived based on the advanced FEM structural analysis. For each bridge the critical places of fatigue can be determined. In through-plate railway girder bridge the critical points due to fatigue are in the floor system. The short components and the connections seem to have the highest value of number of cycles and equivalent stress. In this study, eight critical points were considered: mid-span and quarter point of the plate girder, center of the interior floor beam, the central floor beam,

the interior stringer and the exterior stringer along with the angle and the upper rivet in the single-to-floor-beam connections.

- Step 7: Stress History: The train is run over the bridge and the response versus distance is generated.
- Step 8: Rain-flow algorithm is used for counting the number of fully reversible cycles as well as half cycles and their range amplitude for an obtained stress history.
- Step 9: Miner's rule is applied when the number of cycles of stress range is determined. In this step the number of cycles, equivalent stress, and accumulated damage are calculated. The accumulated damage is presented in the form of the cube root of the number of cycles times the stress to the third power, $(S^3N)^{(1/3)}$.
- Step 10: The simulation is repeated 5000 times and the cumulative distribution function (CDF) of the accumulated damage, $(S^3N)^{(1/3)}$, are plotted on the normal probability paper for each component of the bridge. Then, the statistical parameters of load are derived.

The calculation was performed for both bridges. Two types of load were used: light passenger trains for Bridge #1 and heavy freight trains for Bridge #2. The load model presented in the Chapter 3 is focused only on freight trains; therefore, for passenger trains the dimensions and axle loading were used from the other researchers (S. Dick 2002; Piya and Torkul 2010). It warrants mentioning that the light passenger train has a gross weight 50% less compared to the heavy freight train with the same number of cars. The results of the analysis are presented in the figures 5.9 through 5.12 for Bridge #1 and figures 5.13 through 5.16 for Bridge #2.

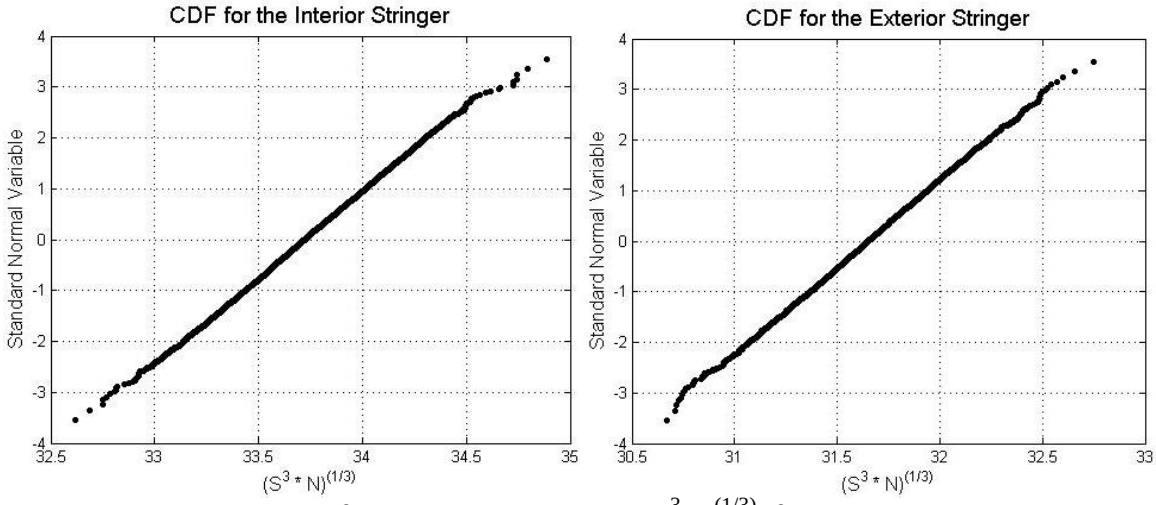

Figure 5.9 CDF of accumulated damage, $(S^3N)^{(1/3)}$, for stingers, bridge #1

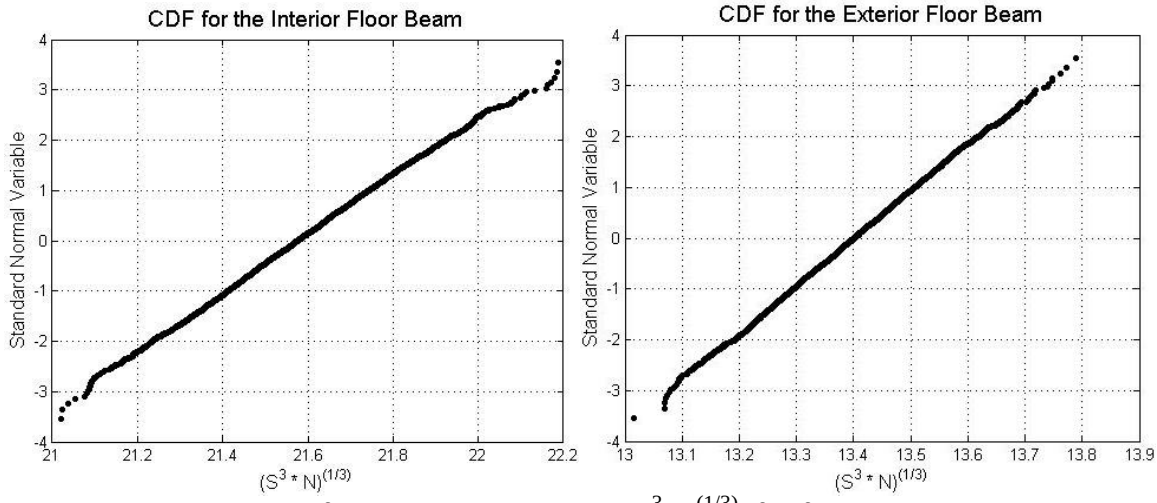

Figure 5.10 CDF of accumulated damage, $(S^3N)^{(1/3)}$, for floor beams, bridge #1

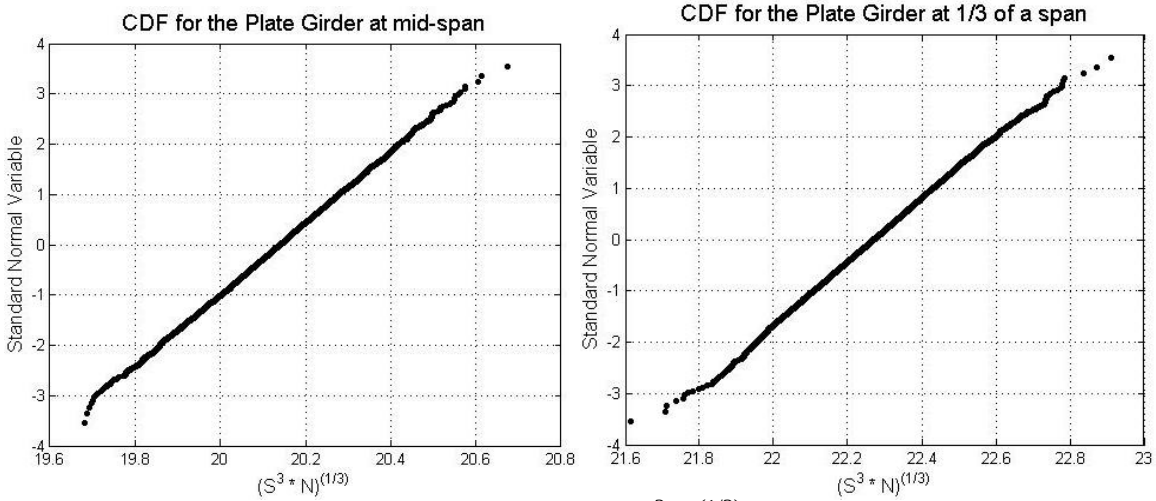

Figure 5.11 CDF of accumulated damage, $(S^3N)^{(1/3)}$, for plate girder, bridge #1

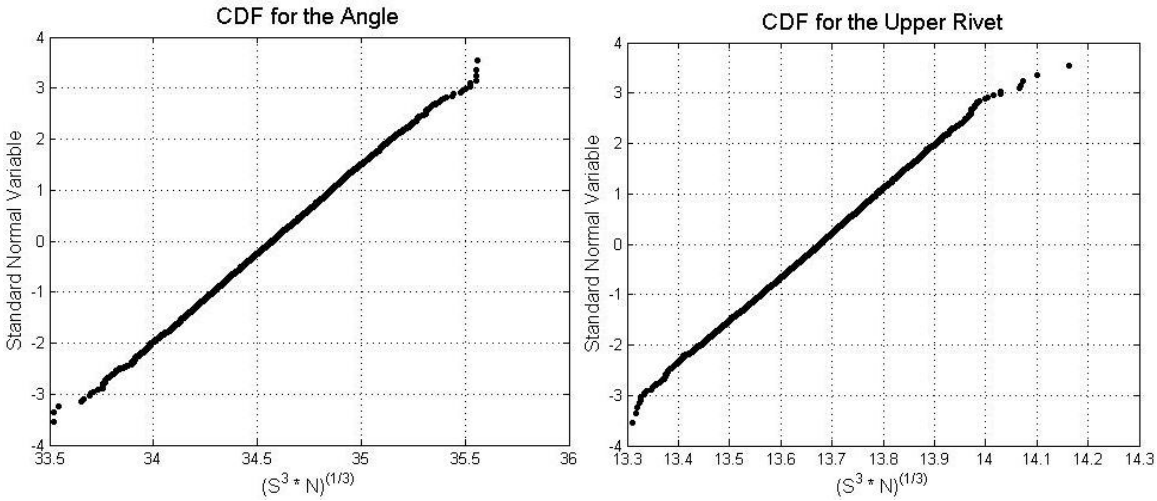

Figure 5.12 CDF of accumulated damage, $(S^3N)^{(1/3)}$, for stringer-to-floor-beam connections, bridge #1

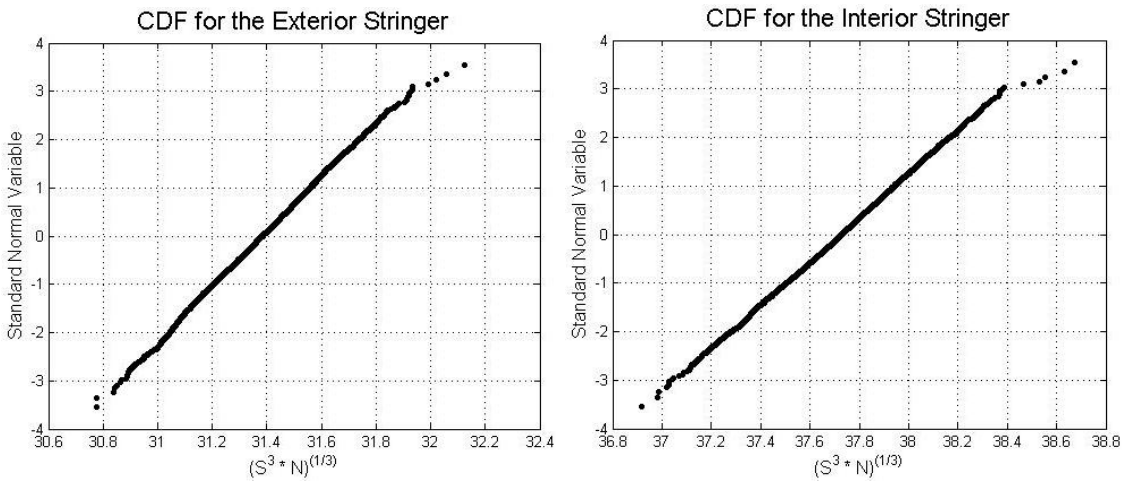

Figure 5.13 CDF of accumulated damage, $(S^3N)^{(1/3)}$, for stingers, bridge #2

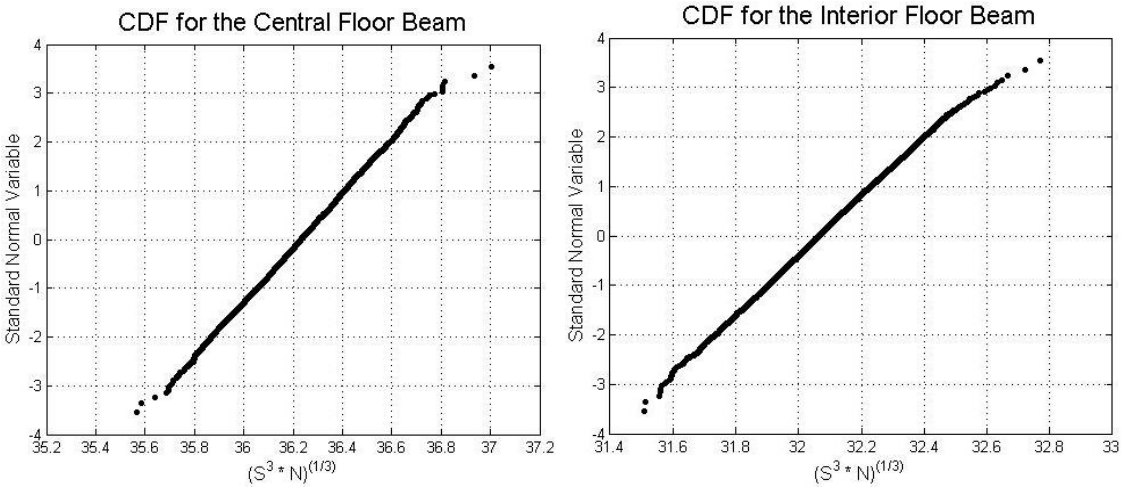

Figure 5.14 CDF of accumulated damage, $(S^3N)^{(1/3)}$, for floor beams, bridge #2

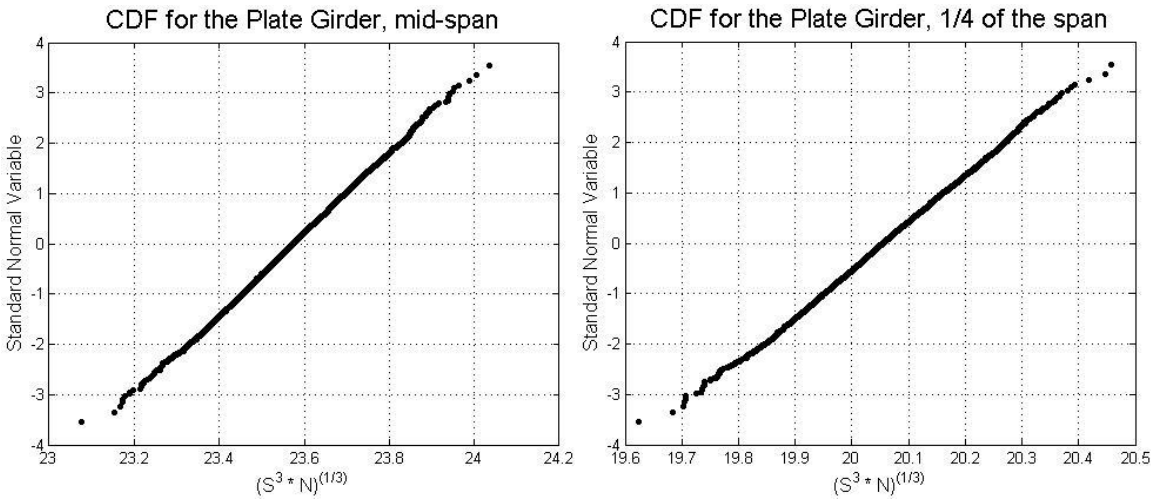

Figure 5.15 CDF of accumulated damage, $(S^3N)^{(1/3)}$, for plate girder, bridge #2

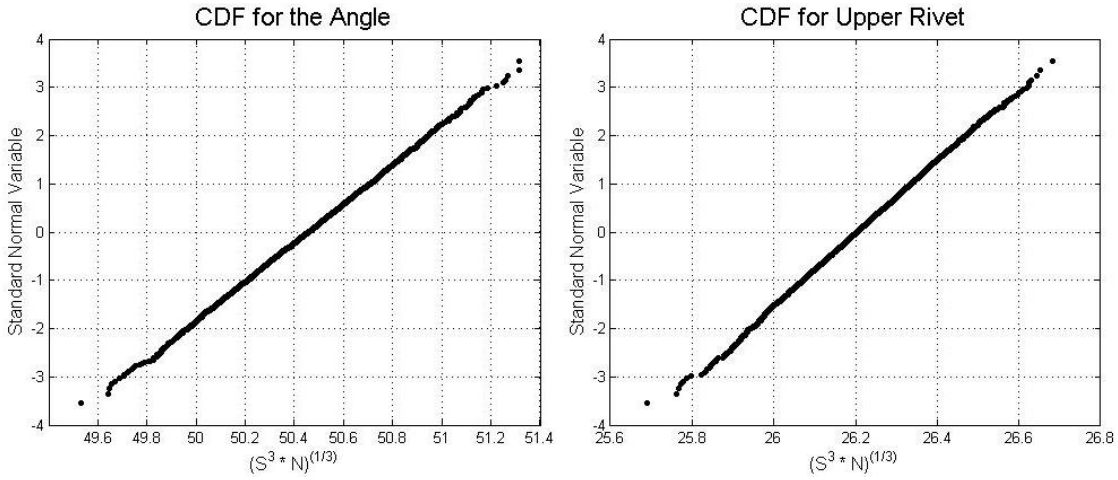

Figure 5.16 CDF of accumulated damage, $(S^3N)^{(1/3)}$, for stringer-to-floor-beam connections, bridge #2

The results of fatigue analysis presented on the normal probability paper indicate that the accumulated damage for each component and connection is close to the straight line. If the curve is close to a straight line, then the variable can be considered as a normal random variable. Therefore, the statistical parameters are determined directly from the graph and they are presented in the tables 5.4 and 5.5.

Table 5.4 The statistical parameters of the fatigue load for bridge #1

Member	# of cycles per train		Equivalent stress		$(S^3N)^{(1/3)}$	
	Mean, μ	CoV, V	Mean, μ	CoV, V	Mean, μ	CoV, V
Interior Stringer	764	0.003	3.69	0.008	33.72	0.0084
Exterior Stringer	718	0.004	3.53	0.009	31.65	0.0089
Interior Floor Beam	370	0.008	3.01	0.008	21.58	0.0076
Exterior Floor Beam	807	0.004	1.44	0.008	13.40	0.0079
Plate girder, center	316	0.006	2.96	0.007	20.14	0.0069
Plate girder, 1/3 L	316	0.003	3.27	0.007	22.27	0.0073
Connection-Angle	593	0.013	4.12	0.009	34.57	0.0082
Connection-Rivet	481	0.010	1.75	0.009	13.68	0.0084

Table 5.5 The statistical parameters of the fatigue load for bridge #2

Member	# of cycles per train		Equivalent stress		$(S^3N)^{(1/3)}$	
	Mean, μ	CoV, V	Mean, μ	CoV, V	Mean, μ	CoV, V
Interior Stringer	391	0.013	5.16	0.006	37.73	0.0084
Exterior Stringer	331	0.012	4.54	0.007	31.38	0.0089
Interior Floor Beam	213	0.005	5.37	0.005	32.07	0.0076
Central Floor Beam	209	0.000	6.11	0.005	36.23	0.0079
Plate girder, center	201	0.000	4.03	0.005	23.57	0.0069
Plate girder, 1/4 L	203	0.000	3.41	0.005	20.05	0.0073
Connection-Angle	414	0.019	6.77	0.007	50.46	0.0082
Connection-Rivet	255	0.012	4.13	0.006	26.20	0.0084

The analysis was also performed for idealized fatigue loads model described in Chapter 3.4. Results are summarized in tables 5.6 through 5.13. Each of these models was generated many times to get a total of gross weight equal to 1 MGMT.

Table 5.6 Number of cycles and equivalent stress for interior and exterior stringers, Bridge #1

Bridge #1	**Interior Stringer**			**Exterior Stringer**		
Type of load	Number of cycles	S_{eq}	$(S^3N)^{(1/3)}$	Number of cycles	S_{eq}	$(S^3N)^{(1/3)}$
F80	14000	14.69	354.05	14000	12.88	310.36
AAR 1	15300	10.61	263.30	30479	7.78	242.93
Coal	15664	11.74	293.69	15766	10.15	254.57
Long Hopper	15664	11.67	291.95	15907	10.07	253.26
TOFC	15664	11.49	287.41	23309	9.52	271.86
Mixed F80	13768	14.05	336.78	19231	11.16	298.92
Mixed AAR 1	16750	10.42	266.59	31924	7.69	243.92
Mixed Coal	16063	11.32	285.63	19226	9.41	251.99
Mixed Long Hopper	18260	10.63	279.97	21365	8.88	246.47
Mixed TOFC	26991	9.17	275.12	30350	8.17	254.78

Table 5.7 Number of cycles and equivalent stress for interior and exterior floor beams, Bridge #1

Bridge #1	**Interior Floor Beam**			**Exterior Floor Beam**		
Type of load	Number of cycles	S_{eq}	$(S^3N)^{(1/3)}$	Number of cycles	S_{eq}	$(S^3N)^{(1/3)}$
F80	7070	10.64	204.25	28000	3.51	106.58
AAR 1	15664	6.44	161.16	31329	2.81	88.59
Coal	15664	6.67	166.82	31329	2.97	93.74
Long Hopper	15664	6.62	165.75	31329	2.96	93.44
TOFC	15589	6.38	159.48	31329	2.86	90.22
Mixed F80	11036	8.33	185.43	43707	2.85	100.39
Mixed AAR 1	16750	6.03	154.21	50842	2.33	86.20
Mixed Coal	16063	6.26	157.87	50135	2.42	89.35
Mixed Long Hopper	15521	6.22	155.03	47112	2.44	87.97
Mixed TOFC	24095	5.20	150.15	48421	2.35	85.72

Table 5.8 Number of cycles and equivalent stress for plate girder at mid-span and 1/3 of a span, Bridge #1

Bridge #1	**Plate Girder, mid-span**			**Plate Girder, 1/3 of a span**		
Type of load	Number of cycles	S_{eq}	$(S^3N)^{(1/3)}$	Number of cycles	S_{eq}	$(S^3N)^{(1/3)}$
F80	7070	10.00	191.99	7070	11.05	212.13
AAR 1	8379	6.16	125.12	8500	7.20	146.86
Coal	8060	8.27	165.86	8111	9.02	181.27
Long Hopper	8379	8.09	164.35	8500	8.81	179.76
TOFC	15589	4.33	108.16	15664	5.37	134.38
Mixed F80	11036	7.42	165.22	11036	8.37	186.35
Mixed AAR 1	13597	5.27	125.83	13794	6.02	144.28
Mixed Coal	12899	6.18	144.96	12980	6.92	162.57
Mixed Long Hopper	12600	6.15	143.18	12782	6.84	160.03
Mixed TOFC	24095	3.84	111.03	24211	4.66	134.73

Table 5.9 Number of cycles and equivalent stress for angle and upper rivet in stringer-to-floor-beam connection, Bridge #1

Bridge #1	**Stringer-to-floor-beam connection**					
	Angle			**Upper Rivet**		
Type of load	Number of cycles	S_{eq}	$(S^3N)^{(1/3)}$	Number of cycles	S_{eq}	$(S^3N)^{(1/3)}$
F80	14000	11.39	274.44	14000	4.48	108.06
AAR 1	16393	8.03	204.11	15907	3.20	80.46
Coal	15968	9.19	231.54	15766	3.64	91.17
Long Hopper	16393	9.05	229.84	15907	3.60	90.50
TOFC	16114	6.93	174.92	15814	2.74	68.72
Mixed F80	13768	9.91	237.58	13768	3.90	93.53
Mixed AAR 1	20889	6.94	191.06	20100	2.77	75.33
Mixed Coal	19551	7.64	205.85	19226	3.03	81.06
Mixed Long Hopper	22095	7.27	204.08	18626	3.03	80.36
Mixed TOFC	24906	5.89	172.01	24442	2.33	67.57

Table 5.10 Number of cycles and equivalent stress for interior and exterior stringers, Bridge #2

Bridge #2	**Interior Stringer**			**Exterior Stringer**		
Type of load	Number of cycles	S_{eq}	$(S^3N)^{(1/3)}$	Number of cycles	S_{eq}	$(S^3N)^{(1/3)}$
F80	14000	7.66	184.54	7070	8.24	158.13
AAR 1	15300	5.58	138.58	15300	4.35	107.98
Coal	15512	5.81	144.78	15512	4.84	120.73
Long Hopper	15300	6.08	150.86	15300	5.23	129.80
TOFC	15439	6.58	163.94	15439	5.12	127.60
Mixed F80	13768	7.50	179.83	11036	6.71	149.39
Mixed AAR 1	16159	5.72	144.57	16159	4.53	114.57
Mixed Coal	15819	5.88	147.55	15819	4.81	120.80
Mixed Long Hopper	17713	5.70	148.49	14974	5.04	124.34
Mixed TOFC	23863	5.37	154.65	23863	4.26	122.66

Table 5.11 Number of cycles and equivalent stress for interior and central floor beams, Bridge #2

Bridge #2	**Interior Floor Beam**			**Central Floor Beam**		
Type of load	Number of cycles	S_{eq}	$(S^3N)^{(1/3)}$	Number of cycles	S_{eq}	$(S^3N)^{(1/3)}$
F80	7210	8.63	166.66	7070	9.30	178.43
AAR 1	15786	4.44	111.38	8014	5.69	113.88
Coal	8111	6.67	133.96	7908	7.38	147.10
Long Hopper	8500	6.78	138.31	8014	7.57	151.45
TOFC	30579	3.51	109.62	15439	4.38	109.17
Mixed F80	13768	6.11	146.52	11036	7.03	156.59
Mixed AAR 1	19509	4.25	114.54	13006	4.99	117.30
Mixed Coal	12980	5.28	124.07	12655	5.72	133.32
Mixed Long Hopper	15156	5.01	123.92	12052	5.87	134.69
Mixed TOFC	32783	3.37	107.78	23863	3.86	111.05

Table 5.12 Number of cycles and equivalent stress for plate girder at mid-span and ¼ of a span, bridge #2

Bridge #2	**Plate Girder, mid-span**			**Plate Girder, 1/4 of a span**		
Type of load	Number of cycles	S_{eq}	$(S^3N)^{(1/3)}$	Number of cycles	S_{eq}	$(S^3N)^{(1/3)}$
F80	7070	7.35	141.08	7070	6.26	120.11
AAR 1	7650	2.42	47.74	7771	2.58	51.05
Coal	7807	4.04	80.15	7807	3.40	67.36
Long Hopper	7771	5.80	114.83	7771	4.94	97.87
TOFC	15215	3.29	81.59	15290	3.25	80.66
Mixed F80	11036	5.48	122.00	11036	4.66	103.67
Mixed AAR 1	12415	3.62	83.89	9656	3.67	78.11
Mixed Coal	12493	3.86	89.56	12493	3.29	76.41
Mixed Long Hopper	11687	4.52	102.52	11687	3.84	87.25
Mixed TOFC	14943	3.34	82.16	20735	2.76	75.78

Table 5.13 Number of cycles and equivalent stress for angle and upper rivet in stringer-to-floor-beam connection, bridge #2

Bridge #2	**Stringer-to-floor-beam connection**					
	Angle			**Upper Rivet**		
Type of load	Number of cycles	S_{eq}	$(S^3N)^{(1/3)}$	Number of cycles	S_{eq}	$(S^3N)^{(1/3)}$
F80	14350	11.11	269.91	14280	5.79	140.55
AAR 1	38614	3.14	106.07	22707	1.95	55.14
Coal	31430	5.58	175.98	8111	4.55	91.42
Long Hopper	24286	7.93	229.63	15786	4.76	119.47
TOFC	31554	4.89	154.38	30804	2.59	81.33
Mixed F80	27645	7.60	229.84	19450	4.45	119.54
Mixed AAR 1	41777	4.82	167.37	27589	2.88	87.03
Mixed Coal	44294	5.02	177.60	18983	3.46	92.30
Mixed Long Hopper	30677	6.41	200.53	20817	3.79	104.28
Mixed TOFC	39965	4.43	151.55	33014	2.48	79.67

Chapter 6 Reliability Analysis

6.1 Overview

The previous chapters show that the load and the resistance model contain many uncertainties. For that reason, evaluation of bridge performance needs to be analyzed by using probabilistic methods. There are several procedures of reliability analysis available for the structural performance in ultimate limit state. Some of them were described in Chapter 2; however, fatigue evaluation in terms of reliability is not well developed. Therefore, a special reliability analysis procedure for fatigue has been developed for this research.

6.2 Reliability Analysis for Ultimate Limit State

Formulation of the limit state function requires a definition of failure since the limit state function represents a boundary between desired and undesired performance of a structure. The format of the limit state function was presented previously in Chapter 2.3. For considered bridges, the maximum stresses were calculated under the statistical load model representing current operating conditions. During the analysis, 5000 unit trains were generated and the bridge response was calculated. Similar to accumulated damage, the statistical parameters were read directly from the CDF plotted on the normal probability paper.

Resistance of a structural component, R, is a function of material properties and dimensions. R is a random variable due to various categories of uncertainties. It is convenient to consider R as a product of three factors:

$$R = R_n \cdot M \cdot F \cdot P \tag{6.1}$$

where:

- Rn- Nominal (design) value of resistance,

- M-Materials factor representing material properties, in particular, strength and modulus of elasticity,
- F-Fabrication factor representing dimensions and geometry of the component, including cross-section area, moment of inertia, and section modulus,
- P-Professional factor representing the approximations involved in the structural analysis and idealized stress/strain distribution models. The professional factor P is defined as the ratio of the test capacity to analytically predict capacity.

The statistical parameters for M, F and P were considered by various researchers and the results were summarized by Ellingwood et al. based on material test data available in the 1970s. For material properties, the bias factor is $\lambda_M = 1.05$ and the coefficient of variation, $V_M = 0.10$; while for dimensions and geometry of the component $\lambda_F = 1.0$ and $V_F = 0.05$; and for professional factor, $\lambda_P = 1.02$ and $V_P = 0.06$. Based on this information, the cumulative distribution function (CDF) of resistance was obtained by generating one million values of R for each considered design case. This served as a basis to calculate the mean of R, μ_R, standard deviation, σ_R, bias factor, λ_R, and coefficient of variation, V_R. The example of this calculation is presented in APPENDIX G. The statistical parameters of load and resistance along with calculation of reliability index are listed in table 5.14 for Bridge #1 and 5.15 for Bridge #2.

Table 6.1 Statistical parameters and reliability index for ultimate limit state for components in bridge #1

Member type	Load			Resistance				Beta
	mean	CoV	stdv	nominal	CoV	bias	stdv	
Interior Stringer	7.34	0.032	0.234	30	0.12	1.1	3.96	**6.5**
Interior Floor beam	5.04	0.025	0.127	30	0.11	1.1	3.63	**7.7**
Plate girder	5.48	0.024	0.132	30	0.11	1.1	3.63	**7.6**

Table 6.2 Statistical parameters and reliability index for ultimate limit state for components in bridge #2

Member type	Load			Resistance				Beta
	mean	CoV	stdv	nominal	CoV	bias	stdv	
Interior Stringer	8.49	0.025	0.216	30	0.13	1.1	4.29	**5.7**
Exterior Stringer	7.21	0.024	0.173	30	0.13	1.1	4.29	**6.0**
Interior Floor beam	8.04	0.021	0.165	30	0.11	1.1	3.63	**6.9**
Plate girder	7.12	0.027	0.190	30	0.11	1.1	3.63	**7.1**

6.3 Reliability Analysis for Fatigue Limit State

The limit state function for fatigue in through-plate girder railway bridges can be expressed in terms of the damage ratio, as seen in equation 6.2.

$$D = \frac{\sqrt[3]{\sum_i {S_{Qi}}^3 \cdot N_{Qi}}}{\sqrt[3]{\sum_i {S_{Ri}}^3 \cdot N_{Ri}}} = 1 \qquad (6.2)$$

If we replace the nominator by a Q and denominator by R we can obtain the simple limit state function presented in the Chapter 2.3, as seen in equation 6.3.

$$g(Q,R)=\frac{\sqrt[3]{\sum_i {S_{Qi}}^3 \cdot N_{Qi}}}{\sqrt[3]{\sum_i {S_{Ri}}^3 \cdot N_{Ri}}}=\frac{Q}{R}=1 \qquad (6.3)$$

Since the statistical parameters of load and resistance were developed in the Chapter 5, the reliability index can be calculated using a simple formula. Both variables, Q and R, demonstrated characteristics of normal distribution. Therefore, the basic statistical parameters which are required for reliability analysis are mean value, μ, standard deviation, σ, and coefficient of variation, V. For special cases, such as a case of two normal distributed, uncorrelated random variables, R and Q, reliability index is given by equation 2.14 as described in Chapter 2.

To calculate reliability index we must specify fatigue category and total load on the bridge. The through-plate girder contains mainly two categories of details: the riveted connections, such as riveted cover plates, and the double angle connection. Therefore, for Interior and Exterior Stringers, the Category A will be used, while for Floor Beams, Plate Girders and Stringer-to-Floor-Beam Connections Category D will be used. The statistical parameters of all Categories are presented in the table 5.3. Whereas the load on the railway bridges is defined in terms of million gross metric tons per year, the statistical parameters for the accumulated damage were developed based on the average unit train which contains 200 cars. To find a gross weight of 1 MGMT, the multiplication of unit train were used. Since a simulation was done for 5000 trains, the total gross weight was about 50 MGMT. Therefore, it was possible to distinguish different ranges of load of 1 MGMT, 5 MGMT, and 10 MGMT, and obtain the statistical parameters. The summary of statistical parameters for both bridges is presented in tables 5.16 and 5.17.

Table 6.3 Statistical parameters of the accumulated damage, $(S^3N)^{(1/3)}$, for unit train and GW equal 1, 5, and 10 MGMT, Bridge #1

Member	Mean value of $(S^3N)^{(1/3)}$				CoV, V
	Unit train	1 MGMT	5 MGMT	10 MGMT	
Interior Stringer	33.72	191.04	326.68	411.59	0.0084
Exterior Stringer	31.65	179.37	306.72	386.44	0.0089
Interior Floor Beam	21.58	122.30	209.13	263.49	0.0076
Exterior Floor Beam	13.40	75.97	129.90	163.66	0.0079
Plate girder, center	20.14	114.13	195.15	245.88	0.0069
Plate girder, 1/3 L	22.27	126.19	215.79	271.88	0.0073
Connection-Angle	34.57	196.01	335.17	422.29	0.0082
Connection-Rivet	13.68	77.50	132.52	166.96	0.0084

Table 6.4 Statistical parameters of the accumulated damage, $(S^3N)^{(1/3)}$, for unit train and GW equal 1, 5, and 10 MGMT, Bridge #2

Member	Mean value of $(S^3N)^{(1/3)}$				CoV, V
	Unit train	1 MGMT	5 MGMT	10 MGMT	
Interior Stringer	37.73	175.16	299.51	377.36	0.0059
Exterior Stringer	31.38	145.71	249.17	313.93	0.0057
Interior Floor Beam	32.07	148.82	254.48	320.63	0.0050
Exterior Floor Beam	36.23	168.19	287.60	362.35	0.0049
Plate girder, center	23.57	109.44	187.13	235.78	0.0051
Plate girder, 1/3 L	20.05	93.06	159.14	200.50	0.0052
Connection-Angle	50.46	234.18	400.44	504.52	0.0049
Connection-Rivet	26.20	121.61	207.95	262.00	0.0050

Then the reliability indices were calculated for various components and connections of through-plate girder bridges. Three cases of load were considered: 1, 5, and 10 MGMT per year. The reliability indices were calculated for the period from 10 to 100 years. The results are presented in the plotted points in the graphs in figures 6.1 to 6.3 for Bridge #1 and on figures 6.4 to 6.6 for Bridge #2. The results shows that Bridge #1 is able to carry a load equal 1 MGMT per year with very high betas. This means that the components and connections have very small probability of occurrence damage due to fatigue in these periods of time. Reliability index $\beta = 4$ corresponds to 0.001% of probability of failure, P_f, $\beta = 3$ corresponds to $P_f = 0.1\%$, $\beta = 2$ corresponds to $P_f = 2.0\%$ of probability of failure, $\beta = 1$ corresponds to $P_f = 15.0\%$, and $\beta = 0$ corresponds to $P_f = 50.0\%$. For 5 MGMT per year, Bridge # 1 still has a high probability that will not have a damage caused by fatigue; whereas, for the last of the case, in which the load is 10 MGMT per year, the connection reached a beta below zero. The negative beta means that the probability of failure is higher than 50.0%. In each considered cases of load, the lowest betas were achieved for the angle in the Stringer-to-Floor-Beam connection. This analysis confirms that the weakest link in the bridge system is the connections.

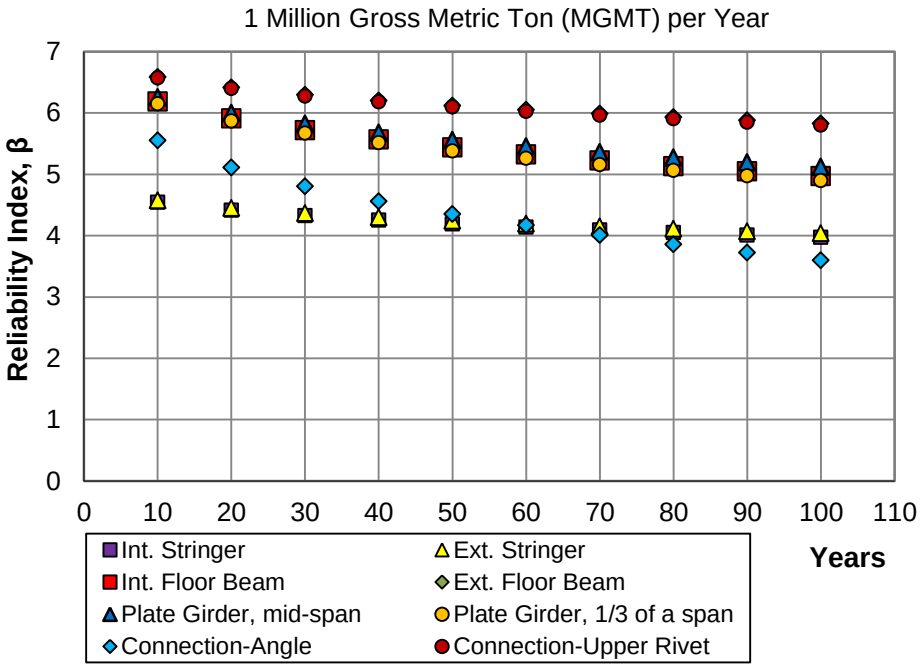

Figure 6.1 Reliability index vs. time in years for Bridge #1 subjected to 1 MGMT per year

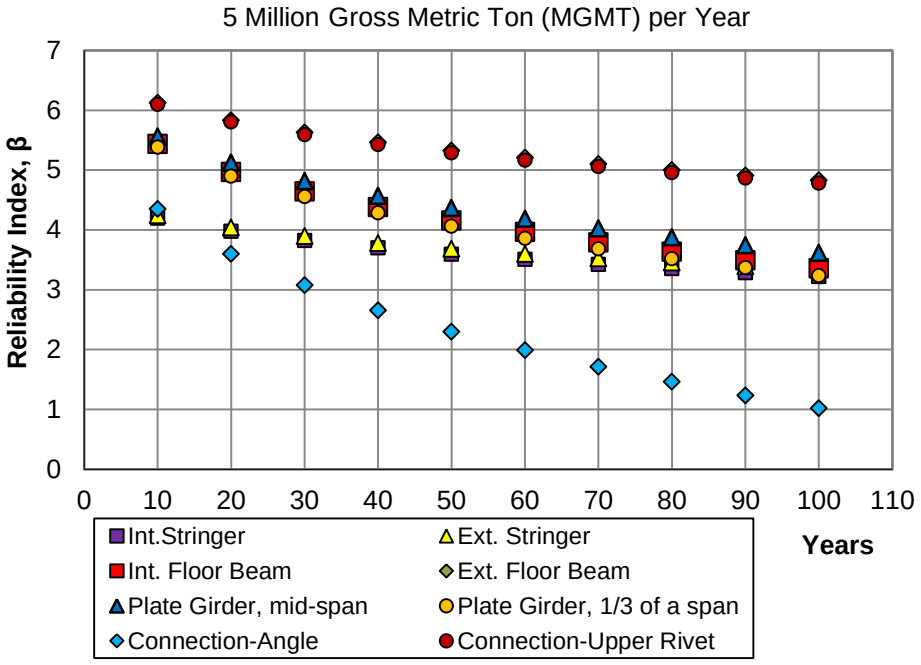

Figure 6.2 Reliability index vs. time in years for Bridge #1 subjected to 5 MGMT per year

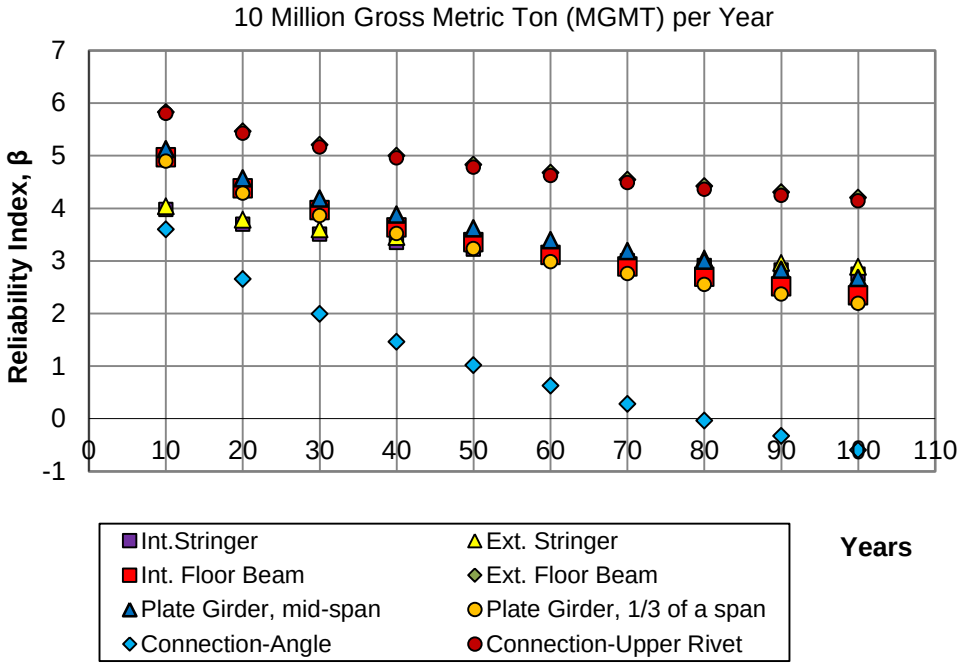

Figure 6.3 Reliability index vs. time in years for Bridge #1 subjected to 10 MGMT per year

The results for Bridge #2 show that the bridge is able to carry a load equal 1 MGMT per year with betas close and higher than 3.0. This means that the highest probability of occurrence damage due to fatigue in these periods of time is about 0.1%. For 100 year period and 5 MGMT per year, Bridge #2 will reach negative betas in the connection angle. The remaining components still have quite high betas, close and above 2.0. In the last case where the load is equal to 10 MGMT per year, the connection reaches the beta below zero for a period of 50 years. This is a very serious case because in the long term it may cause a failure of the entire bridge. This same as for Bridge #1, in each considered cases of load, the lowest beta were achieved for the angle in the Stringer-to-Floor-Beam connection.

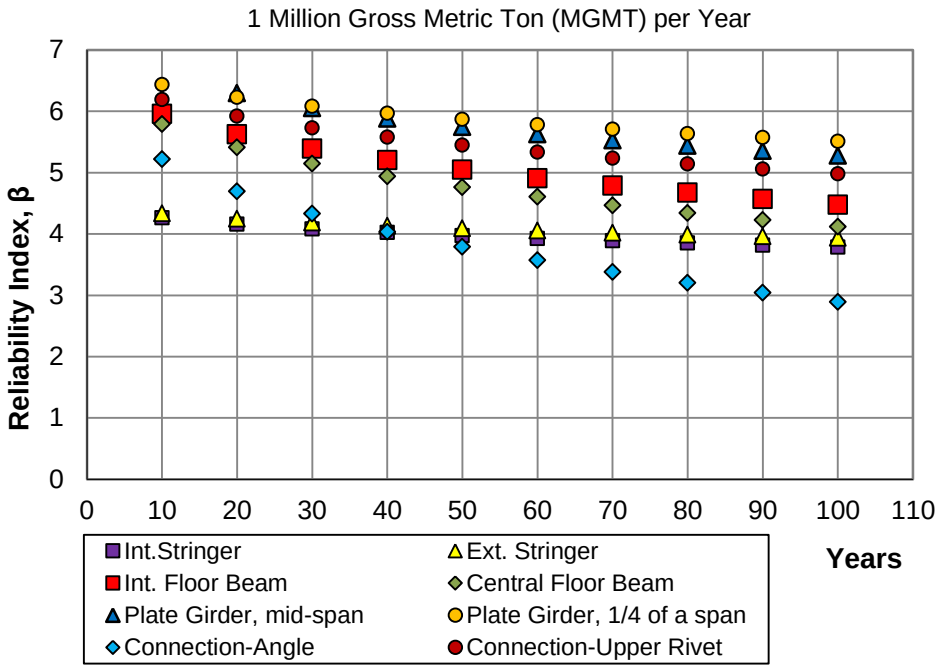

Figure 6.4 Reliability index vs. time in years for Bridge #2 subjected to 1 MGMT per year

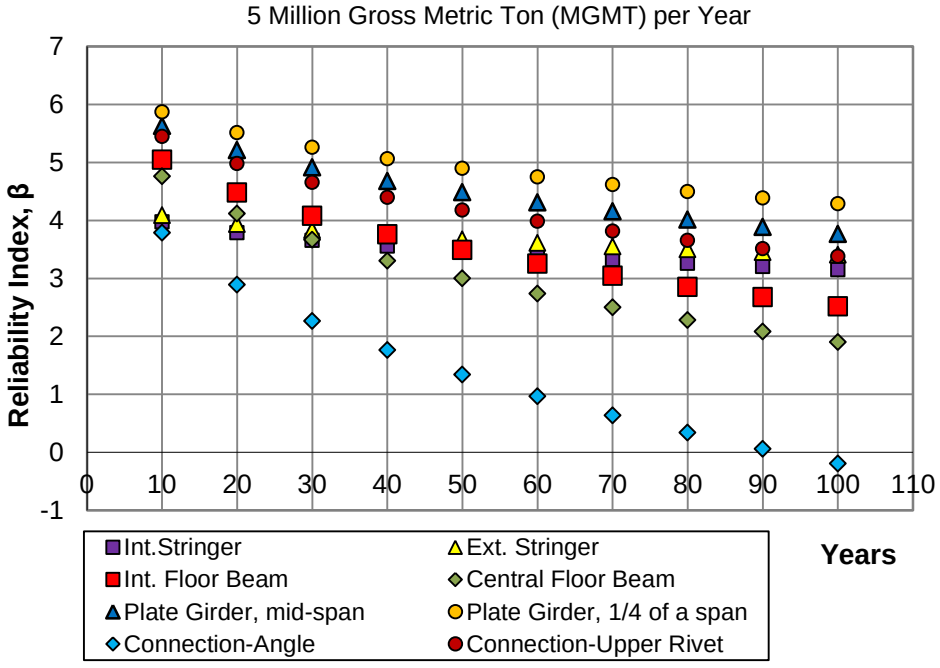

Figure 6.5 Reliability index vs. time in years for Bridge #2 subjected to 5 MGMT per year

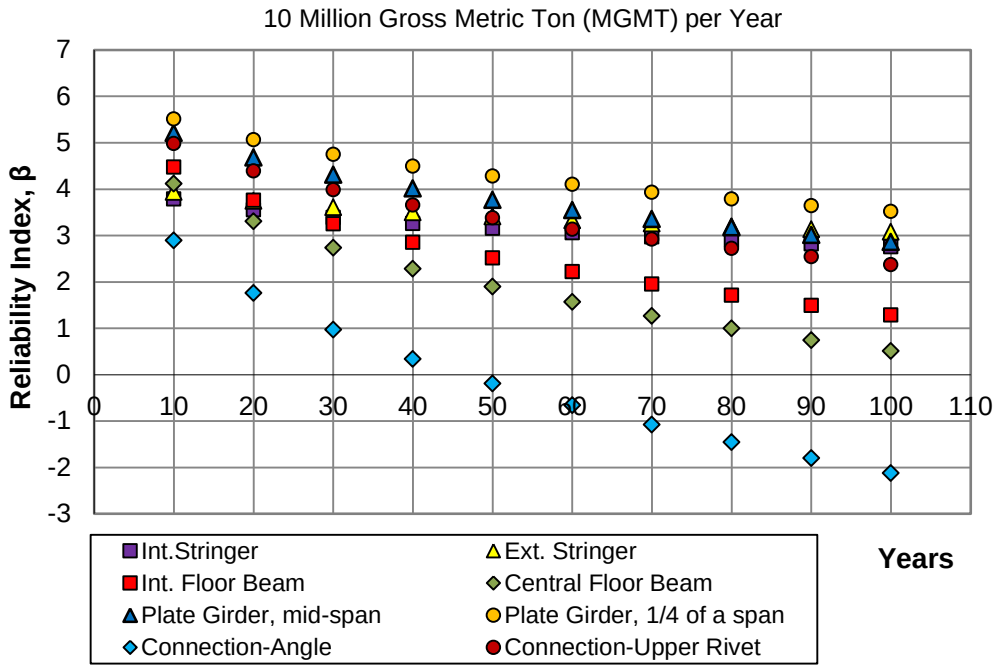

Figure 6.6 Reliability index vs. time in years for Bridge #2 subjected to 10 MGMT per year

In the next step of the reliability analysis, calculations of predicted years of service were carried out. The reliability indices were fixed and were equal 0, 0.5, 1.0, 1.35 and 1.75. Recently, many researchers use $\beta = 0$ in the fatigue analysis of railway bridges (Tobias et al. 1997; Imam 2005; Imam 2008). Even if the reliability index for fatigue evaluations can be relatively low, $\beta = 0$ is too low. For the evaluation of existing highway bridges, the target beta is $\beta_T = 1.35$ for redundant and $\beta_T = 1.75$ for non-redundant members according to AASHTO Guide Specifications for Fatigue Evaluation of Existing Steel Bridges (1990). Therefore, the reliability index for railway bridges also should be retained higher than 0. The results of this analysis are shown in the plotted points on the charts in figures 6.7 to 6.9 for Bridge #1 and in the figures 6.10 to 6.12 for Bridge #2.

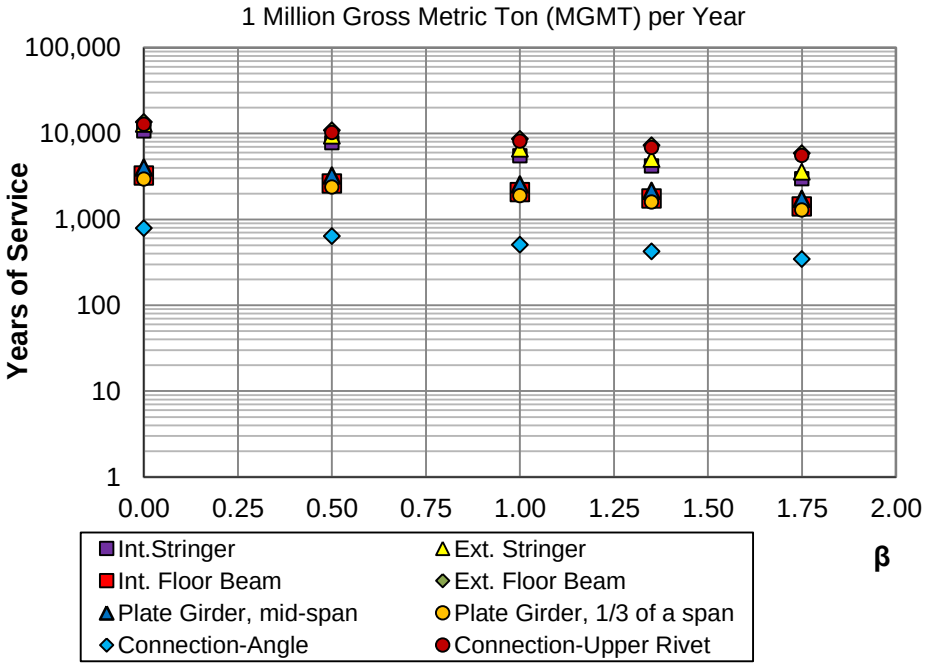

Figure 6.7 Predicted years of service for Bridge #1 subjected to 1 MGMT per year

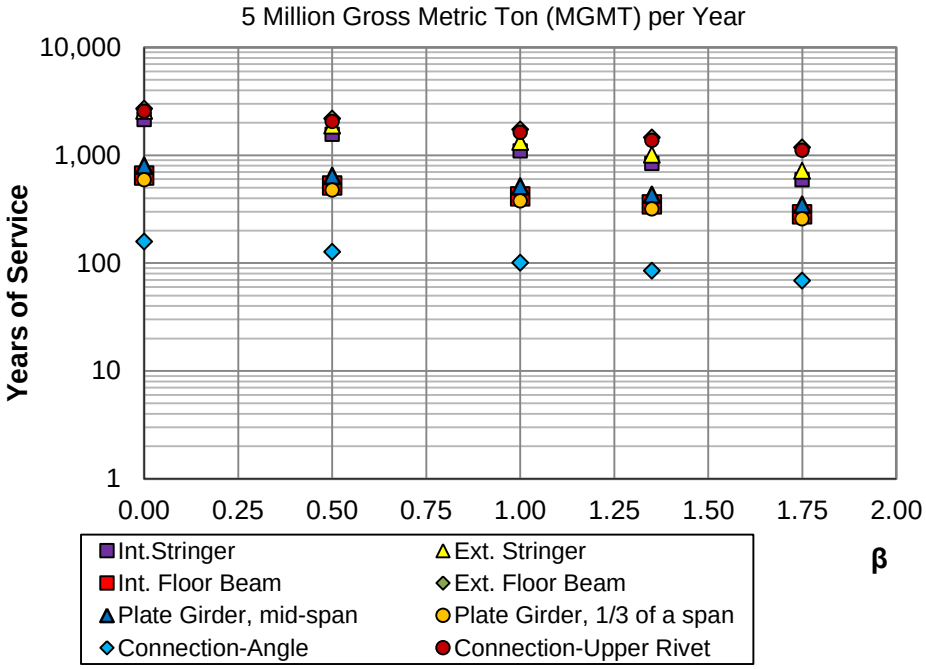

Figure 6.8 Predicted years of service for Bridge #1 subjected to 5 MGMT per year

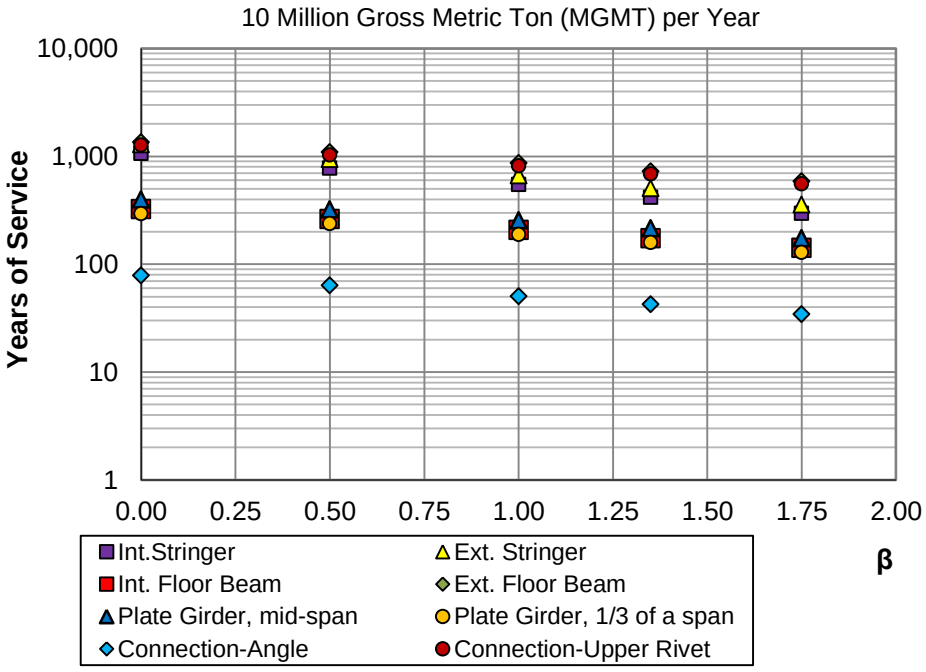

Figure 6.9 Predicted years of service for Bridge #1 subjected to 10 MGMT per year

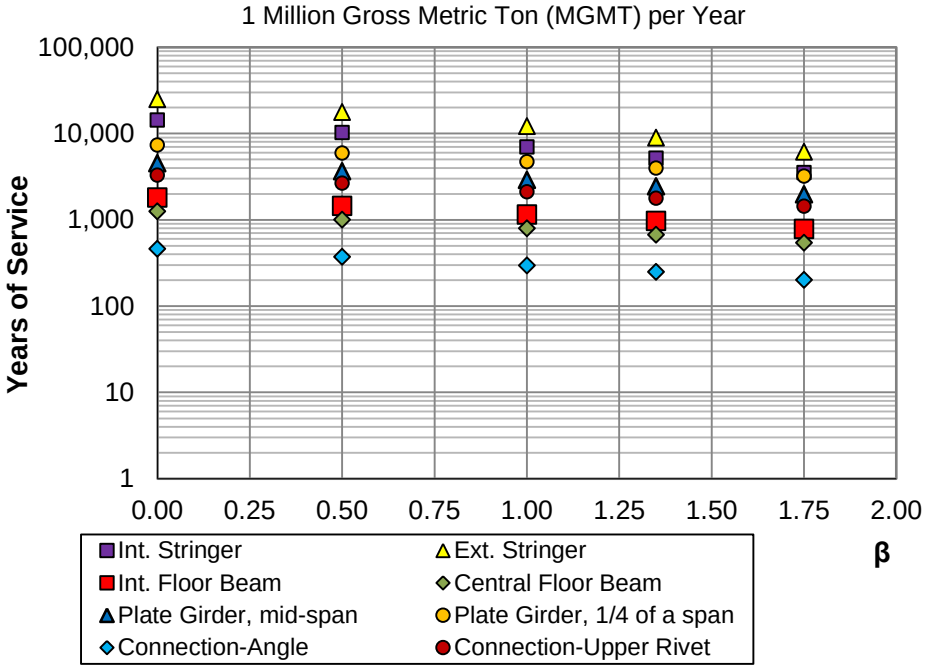

Figure 6.10 Predicted years of service for Bridge #2 subjected to 1 MGMT per year

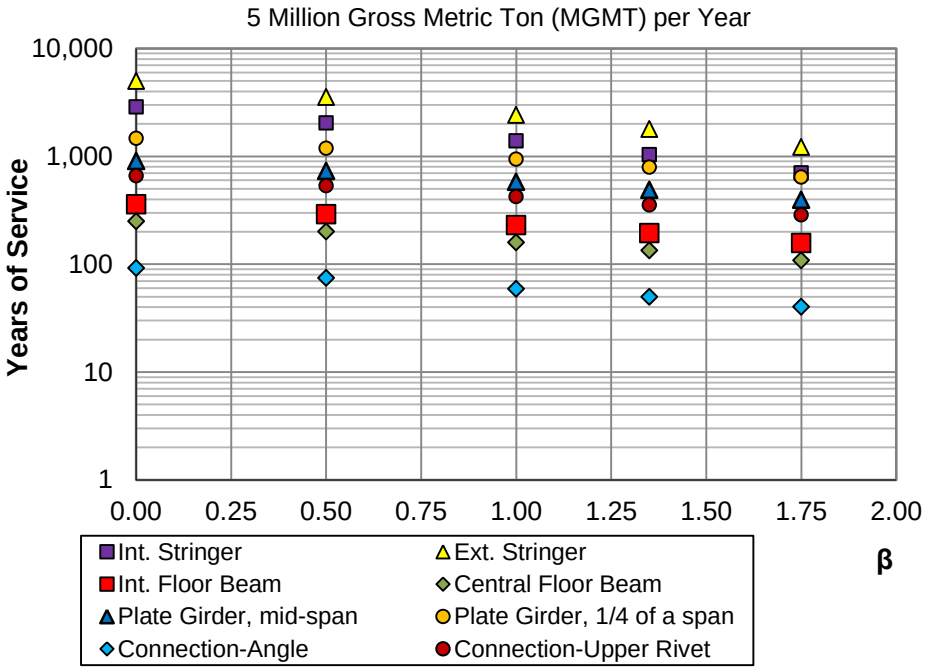

Figure 6.11 Predicted years of service for Bridge #2 subjected to 5 MGMT per year

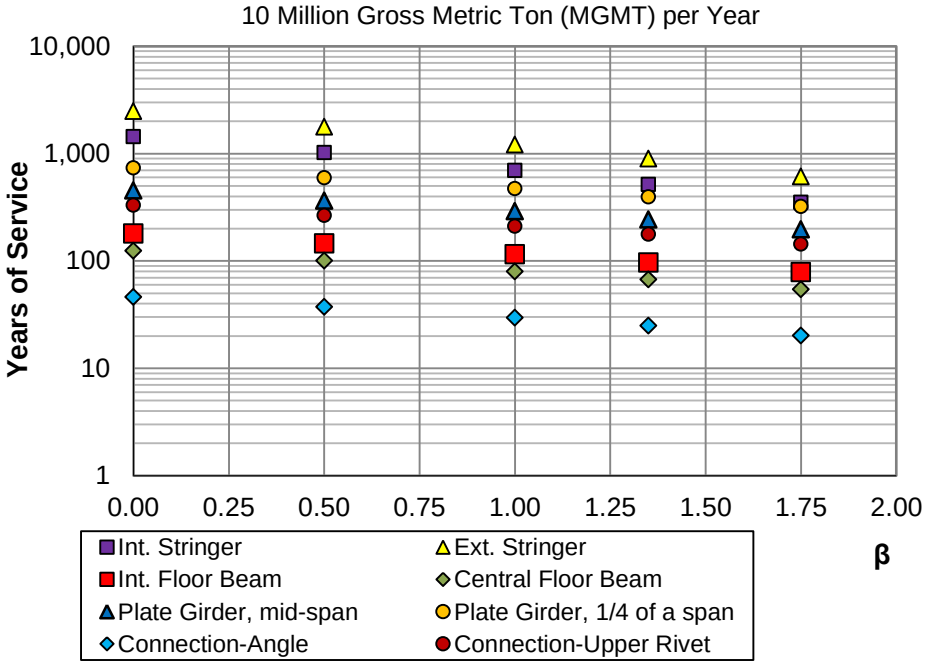

Figure 6.12 Predicted years of service for Bridge #2 subjected to 10 MGMT per year

Chapter 7 Summary and Conclusions

7.1 Summary

This report provides a reliability approach for evaluation and design of railway bridges. The research contains review and analysis of the major factors that influence structural performance. These factors are random in nature; therefore, it is suitable to consider probability as a measure of bridge performance.

The statistical parameters were developed for load, based on the statics provided in the literature. The significant achievement in this study was the development of a simulation model of the live load effect for the bridges. The unit train was built and generated 5000 times for investigation of distribution and statistical parameters. The statistical parameters were developed for maximum bending moments in the girder bridges with a range of span length from 20 ft to 100 ft.

Two representative railway bridges were analyzed in detail. A nonlinear finite element analysis of a typical through-plate girder railway bridge was carried out. The analysis has demonstrated that the maximum stresses are concentrated in the mid-span of the stringers, floor beams and plate girders. The most fatigue-critical component was shown to be stringer-to-floor beam connections. The FEM analysis has identified the partial fixity of those connections. For various components and connections of these bridges, the stress histories were generated and rain-flow algorithms along with Miner's rule were applied. The accumulated damage was presented in the modified form of Palmgren-Miner damage law, $(S^3N)^{(1/3)}$. The accumulated damage was plotted on the normal probability paper for each considerate case and the statistical parameters of load were obtained.

The fatigue life of structure elements was estimated based on the S-N curves, which present the number of cycles to failure as a function of the constant stress amplitude. The S-N

fatigue data, created in a laboratory, contains a considerable amount of scatter, even when standard specimens made from the same material are used. The statistical parameters for fatigue resistance were developed based on the available fatigue data for all categories of details. It was confirmed that the S-N data have various numbers of cycles under this same stress range. The fatigue resistance was expressed by modified form of Palmgren-Miner damage law, $(S^3N)^{(1/3)}$, and plotted on the normal probability paper. Then, the statistical parameters were determined by fitting a straight line to the lower tail of the CDF.

In the reliability analysis, both loading and strength were treated as random variables. The loading side was classified through the gross weight of train traffic per year. The response of the bridge components and connection were simulated using influence lines developed in the FEM and algorithm written in the Mat Lab. Both limit state functions were considered: ultimate and fatigue limit state. The ultimate limit state carries maximum stresses in the mid-span of the main girders and floor systems due to bending moment. The probability of failure for fatigue was calculated by using damage ratio as a limit state function and the distribution of load and resistance. The fatigue was considered in eight critical places on the bridge: mid-span of interior and exterior stringers, mid-span of interior and exterior floor beams, the plate girder in center and quarter of the span, angle and rivet in the stinger-to-floor-beam connections. Total damage in the components and the connections were calculated under the statistical load model for freight and passenger trains. This study give a broad view of the potential remaining fatigue lives of typical railway bridges subjected to unit train loadings.

7.2 Conclusions

The major contribution of this research is the development of the system reliability models for railway bridges. The research involved the development of load and resistance models for new and existing structures, including statistical parameters and type of cumulative distribution

function. Various limit states were considered and it turned out that fatigue limit state governs, especially for older bridges.

The approach is demonstrated on two through plate girder bridges, which work as a series system where the failure of one component can lead to failure of the entire system. The sensitivity analysis pointed out that the connections are the weakest link in the structural system. Therefore, to ensure a safe performance of the bridge, it is recommended to perform periodical inspections with a special attention paid to the connections. In particular, if fatigue damage is observed in a connection angle or in rivets, then the damaged parts have to be replaced.

The currently acceptable reliability index for fatigue in older bridges is 0. However, for the design of new bridges it is recommended to increase the reliability index to 1.5.

The main conclusions from this research include:

A. The reliability approach is the reasonable way to evaluate performance of the railway bridges due to high degree of uncertainty in the fatigue strength of riveted details and loading conditions.

B. Calculation of the maximum bending moment for the girder bridges with a range of span length from 20 ft to 100 ft shows that design load causes a positive moment, which is higher by 40%-50%, than the bending moment due to actual train. This is because the current design load model is based on the heavy steam locomotive with infinite uniform load. The variation of the ratio between maximum bending moment due to current load and Cooper E80 is 10% to 12%.

C. The FEM analysis shows that the connection between stringer and floor beam acquires a certain degree of rotational stiffness and develops stresses due to bending moment. The stringer-to-floor-beam are commonly constructed with double angle connections and considered as simple shear connections during the design stage. Therefore, the

connection is susceptible to fatigue damage. The fatigue damage in stringer to floor beam connections is typically associated with cracking in the connection angles or in the rivets connecting the outstanding leg to the floor beam web because of rotational deformation on the top of the connection angles and axial forces in the rivets due to the restrained moment.

D. The statistical parameters for fatigue resistance confirm that there is a high variation in the number of cycles to failure under these same constant amplitudes. The coefficient of variation for fatigue resistance is 10% to 30% depending on the category of detail. The S-N data presented in the modified form of Palmgren-Miner damage law, $(S^3N)^{(1/3)}$, and plotted on the normal probability paper is very close to the straight line and can be considered as a variable with normal distribution.

E. Fatigue load analysis proves that for shorter components the number of cycles is higher than for longer components. Also the shorter components are more sensitive to the maximum axle load rather than the maximum gross weight of rail car.

F. Fatigue load presented in the modified form of Palmgren-Miner damage law, $(S^3N)^{(1/3)}$, show only little variation about 0.5% to 1.0%. This is because equivalent stress, obtained for a simulated unit train, reduces variable amplitude to constant amplitude and as a result differences disappear. However, this is true only for considering one type of trains (passenger or freight).

G. Reliability index depends on fatigue category and applied load. During service of the bridge the accumulated fatigue damage is increasing in time at different rates, depends on tonnage per year and train type. All these factors must be specified in order to obtain accurate results of reliability analysis.

H. The reliability analysis for the fatigue limit state was presented for various time periods and through three cases of operating conditions. In each of the considered cases of load, the lowest betas were achieved for the angle in the stringer-to-floor-beam connection. This study has confirmed that riveted bridges are not likely to develop fatigue cracks in the primary members because the cyclic loads do not result in stress range levels that exceed the estimate fatigue limit for riveted members (Category D). However, the weakest link in the bridge system is the connection.

I. The fatigue damage was calculated for various fatigue load models. The closest to real conditions is the fatigue load model, F80, presented by Dick et al in 2011. This model gives fair results with about 10% reserves. It is suitable for fatigue evaluation of the bridges under freight trains.

J. The reliability analysis of ultimate limit state for the main components show that reliability indices are very high, above 5.0, and it should not be a concern. This is because the design load for short bridges is overestimated compared to the current conditions.

K. Further research is needed to consider the effect of corrosion on structural performance and prediction of remaining life.

References

AASHTO LRFD Bridge Design Specifications, American Association of State Highway and Transportation Officials, Washington D.C., 2012.

AASHTO, Guide Specifications for Fatigue Evaluation of Existing Steel Bridges, American Association of State Highway and Transportation Officials, 1990.

ABAQUS Analysis User's Manual.

Al-Emrani, M., "Fatigue Performance of Stringer-to-Floor-Beam connections in Riveted Railway Bridges", Journal of Bridge Engineering, Vol. 10, No. 2, pp. 179-185, 2005.

American Railway Engineering and Maintenance of Way Association (AREMA), Manual for Railway Engineering, Chapter 15, Washington, D.C., 2005.

Ang, A. H-S., Bases for Reliability Approach to Structural Fatigue, Proceedings, ICOSSAR'77, Munich, Germany, 1970.

Ang, A. H-S., and Tang W. H., "Probability Concepts in Engineering, Emphasis on Application to Civil Engineering and Environmental Engineering", John Wiley & Sons Inc., USA, 2007.

Ayyub, B. M., and McCuen, R. H., "Probability, Statistics and Reliability for Engineers, CRC Press, New York, 1997.

Chalk, P. L., and Corotis R. B., "Probability models for Design Live Loads." Journal of the Structural Division (ASCE) 106, no.10, pp. 2017-2033, 1980.

Chotickai, P., and Kanchanalai, T., "Field Testing and Performance Evaluation of a Through-Plate Girder Railway Bridge", TRB, No 2172, Transportation Research Board of the National Academies, Washington, D.C., 2010, pp.132-141.

Coopers Loading System, Wikipedia, the free encyclopedia, en.wikipedia.org, 2012.

Daumueller, A. N., Jauregui, D. V., and Roach, D. P., “Development of a Structural Health Monitoring System for the Life Assessment of Critical Transportation Infrastructure”, Sandia Report, SAND2012-0886, February, 2012.

Dick, S. M., “Bending Moment Approximation Analysis for Use in Fatigue Life Evaluation of Steel Railway Girder Bridges”, Ph.D. Report, University of Kansas, Lawrence, Kansas, 2002.

Dick, S. M., Otter, D. E., and Connor, R. J., “Comparison of Railcar and Bridge Design Loadings for Development of a Railroad Bridge Fatigue Loading”, AREMA 2011 Annual Conference, Minneapolis, MN, September 20, 2011.

Downing, S. D., Socie, D. F. "Simple rain-flow counting algorithms", International Journal of Fatigue, Volume 4, Issue 1, January, 31-40, 1982.

Finite element method, Wikipedia, the free encyclopedia, en.wikipedia.org, 2012.

Fisher, J.W., Frank, K.H., Hirt, M.A. and McNamee, B.M., National Cooperative Highway Research Program Report 102-Effect of Weldments on the Fatigue Strength of Steel Beams, Highway Research Board, 1970.

Fisher, J.W., et al. (1974), Fatigue Strength of Steel Beams with Welded Stiffeners and Attachments, Report 147, Transportation Research Board, National Council, Washington, DC, 1974.

Fisher, J. W., "Bridge Fatigue Guide – Design and Details", AISC Manual, Chicago 1977

Fisher, J. W., Yen, B. T., Wang, D., and Mann J. E., “NCHRP Report 302: Fatigue and Fracture Evaluation for Rating Riveted Bridges”, TRB, National Research Council, Washington D.C., pp. 25-35, 1987.

Foutch, D. A., Tobias, D. H., and Choros, J., "Bridge loads under current operating conditions." Struct. Res. Ser. Rep., Department of Civil Engineering, University of Illinois at Urbana-Champaign, Urbana, IL, Manual for railway engineering. American Railway Engineering Association, Washington, D.C., 1996.

Galambos, T. V., and Ravindra, M. K., "Load and Resistance Factor Design", Journal of Structural Division, ASCE, ST9, Proc. Paper 14008, 1978.

Goerl, R. K., "Study of Behavior of Stringer to Floor Beam Connection in Riveted Railway Open Web Girder Bridges", Journal of IPWE, April, 2006.

O'Connell, H. M., Dexter R. J., and Bergson P. M., "Fatigue Evaluation of the Deck Truss of Bridge 9340", Minnesota Department of Transportation, MN/RC-2001-10.

Imam, B., Righiniotis, T. D., and Chryssanthopoulos, M.K., "Connection Fixity Effects on Stress Histories in Riveted Rail Bridges" Proceedings of the 2nd International Conference on Bridge Maintenance, Safety and Management: Kyoto, 2004.

Imam, B., Righiniotis, T. D., and Chryssanthopoulos, M.K., "Remaining Fatigue Life Estimates for Riveted Railway Bridges", Proceedings of the 5th International Conference on Bridge Management, Thomas Telford, UK, 2005.

Imam, B., Righiniotis, T. D., and Chryssanthopoulos, M. K., Bell, B., "Probabilistic Fatigue Life Estimates for Riveted Railway Bridges", Proceedings of the 3rd International Conference of Bridge Maintenance, Safety and Management, 2008.

Krajewski, J., "Repair of Fatigue Damaged Stringer to Floor-Beam Connections", ODOT Bridge Design Conference, Oregon 2009.

Miner, M. A., "Cumulative Damage in Fatigue", J. Appl. Mech. 12, 1945.

Moses, F., “Problems and prospects of reliability-based optimization,” Engineering Structures, Vol. 19, No. 4, pp. 293-301, 1997.

Nowak, A.S. and Collins, K.R., “Reliability of Structures”, McGraw Hill, New York, 2000.

Nowak, A. S. and Lind, N. D., “Practical Bridge Code Calibration”, Journal of Structural Division, ASCE, pp. 2497-2510, December 1979.

Nowak, A.S., “Calibration of LRFD Bridge Design Code”, NCHRP Report 368, Transportation Research Board, Washington, D.C., 1999.

Nowak, A.S. and Szerszen, M. M., “Assessment, Inspection and Monitoring of Steel Bridge Components for Fatigue Effects”, Progress Report 1998.

Rakoczy, P., “WIM Based Load Models for Bridge Serviceability Limit States”, Report Thesis, UNL, 2011.

Roeder, C. W., MacRae, G. A., Kalogiros, A. Y., Leland, A., “Fatigue Cracking of Riveted, Coped, Stringer-to-Floor-Beam Connections”, Washington State University Research Report WA-RD 494.1, March 2001.

Rosenbueth, E., "Point Estimates for Probability Moments", Proceedings of the Nature Academy of Science, Vol. 72 (No. 10), 1975.

Rosenbueth, E. "Two Point Estimate in Probabilities", Applied Mathematical Modeling Journal, 1981.

Sawicki, M. and Bien, J., “Condition rating and maintenance for railway bridges in Poland”, Journal of the Transportation Research Board, 1995, pp 32-37.

Schilling, C. G., Klippstein, K. H., Barsom, J. M. and Blake, G. T., ”Fatigue of Welded Steel Bridge Members under Variable Amplitude Loading", NCHRP Report 188, Transportation Research Board, 1977.

Sorgenfrei, D. F. and Marianos, W. N., “Railroad bridges”, Bridge Engineering Handbook, Chen, W. F. and Duan, L. (Eds), CRC Press, Boca Raton, FL, 2000.

Thoft-Christensen, P., and Baker, M.J., “Structural Reliability Theory and Its Applications”, Springer-Verlag, New York, New York, 1982.

Tobias D. H., Foutch D. A., and Choros J., “Loading Spectra for Railway Bridges under Current Operating Conditions”, Journal of Bridge Engineering (ASCE), pp. 127-134, 1996.

Tobias, D. H., and Foutch, D.A., “Reliability-Based Method for Fatigue Evaluation of Railway Bridges”, Journal of Bridge Engineering 2(2), pp.53-60, 1997.

Unsworth, J. F., “Design of Modern Steel Railway Bridges”, CRC Press, Boca Raton, FL, 2010.

Wirsching, P. H., “Probabilistic Fatigue Analysis”, Probabilistic Structural Mechanics Handbook, C. Sundararajan, Ed., Chapman and Hall, New York, NY, USA, 1995.

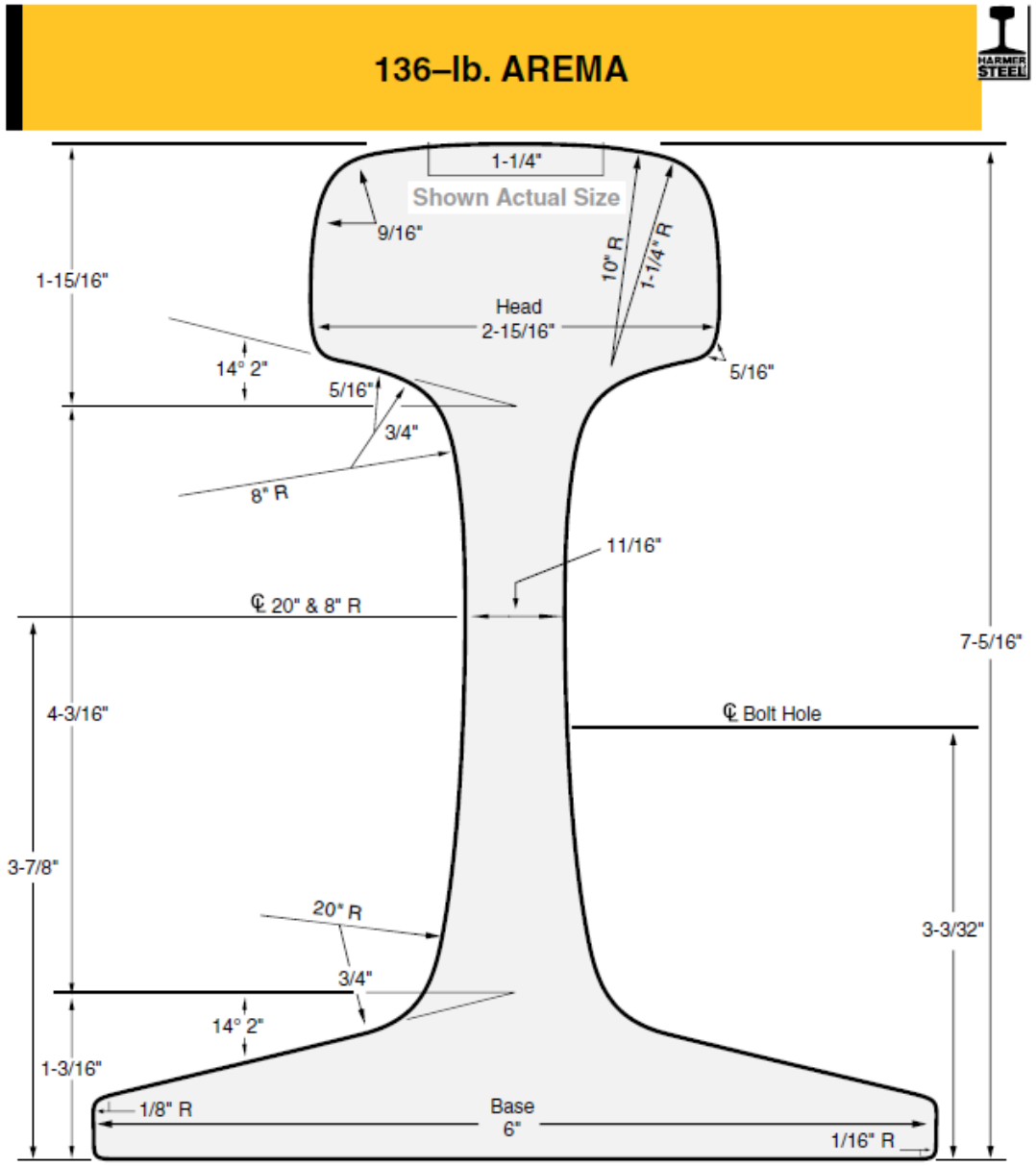

Rail Type:	136 RE
Section Number:	13625
Nominal Weight:	136 lbs/yd
Standard Length:	39', 80'
Standard Drilling:	3-1/2" X 6" or 3-1/2" X 6" X 6" with 1-1/4" dia. holes
Joint Bar Length:	24" or 36"
Joint Bar Weight:	**4-Hole bars:** 70 lbs/pr **with hardware:** 79 lbs/pr **6-Hole bars:** 117 lbs/pr **with hardware:** 130 lbs/pr
Track Bolt:	1" X 6"

Area in^2: 13.32
Section Modulus in^3:
Head: 23.78
Base: 28.3
Moment of Inertia in^4: 93.7

BOLT SIZE MAY VARY DEPENDING ON BAR MANUFACTURE & TYPE OF WASHER USED.

www.HarmerSteel.com sales@harmersteel.com © 2010 (503) 286-3691 FAX (503) 286-2097

I – 20

Figure A.1 Rail dimensions and section properties (www.HarmerSteel.com)

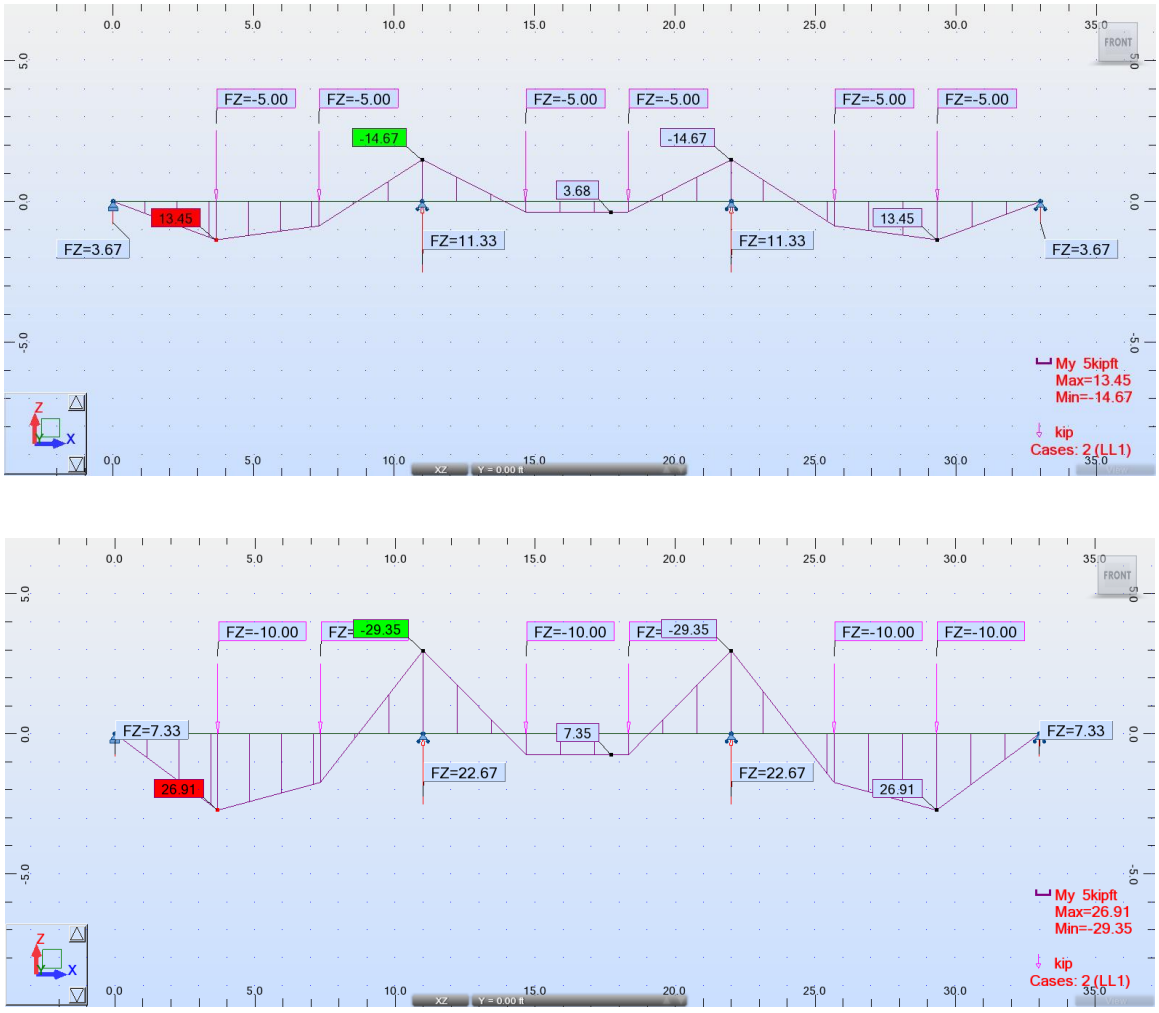

Figure B.1 The three-span continuous beam

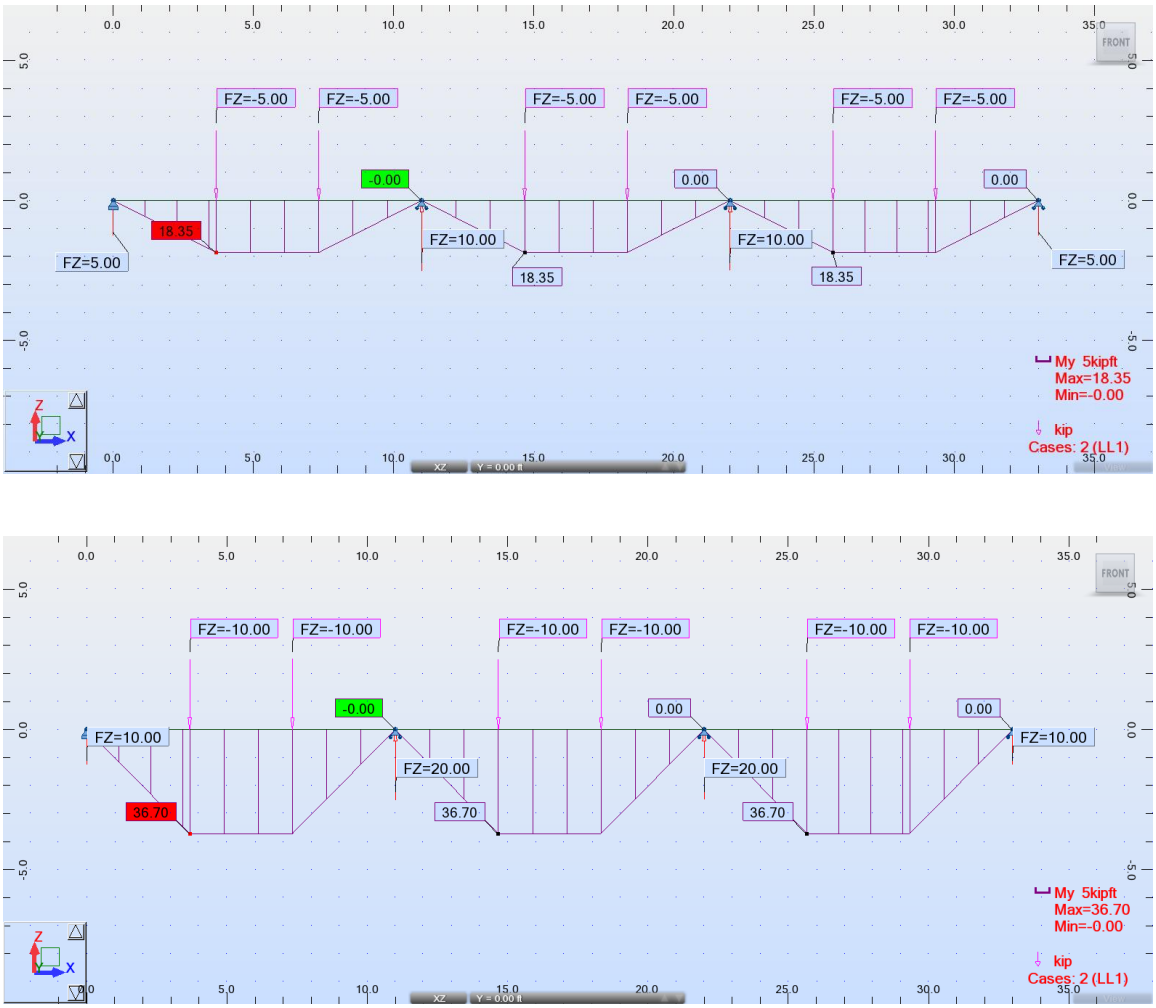

Figure B.2 Three single beams

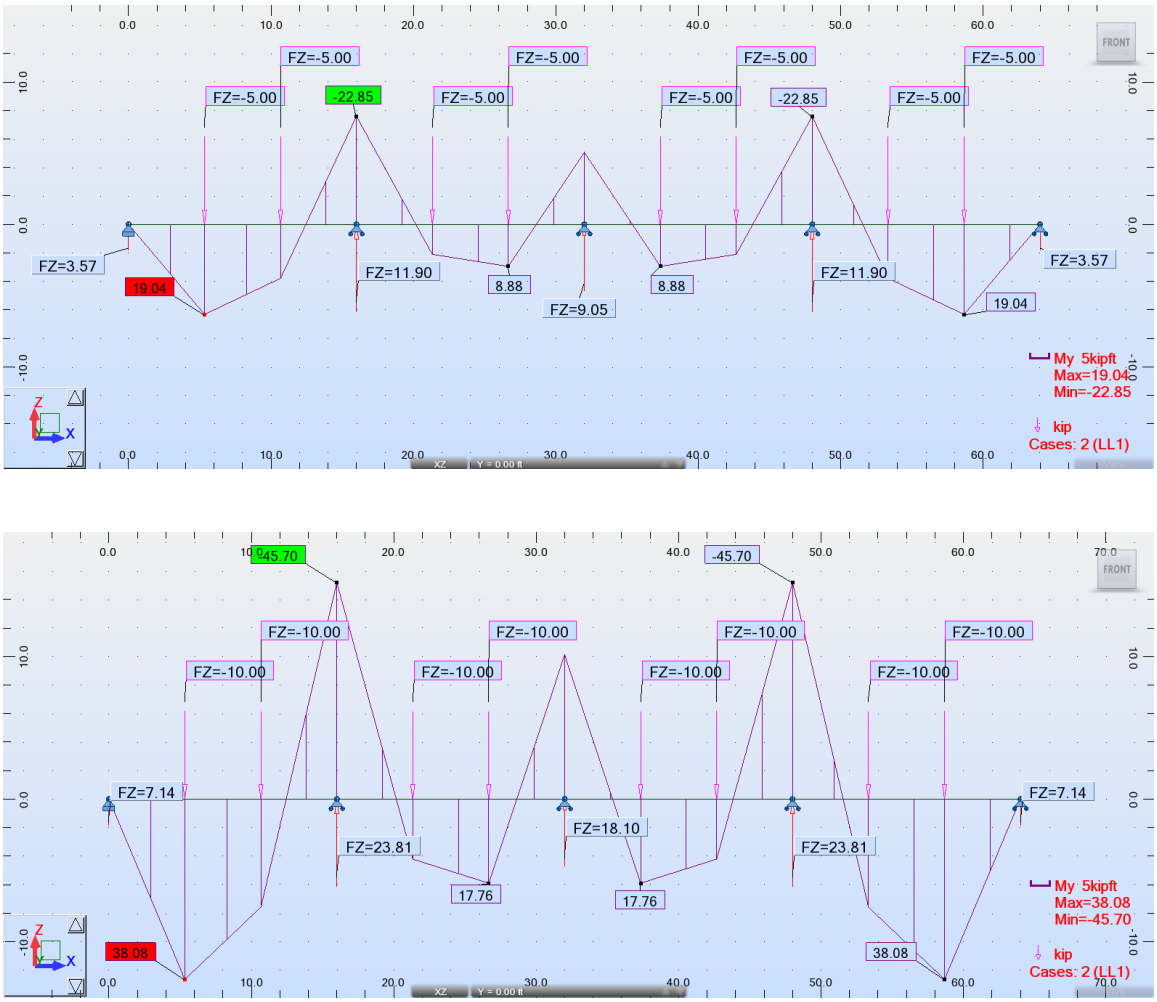

Figure B.3 The four-span continuous beam

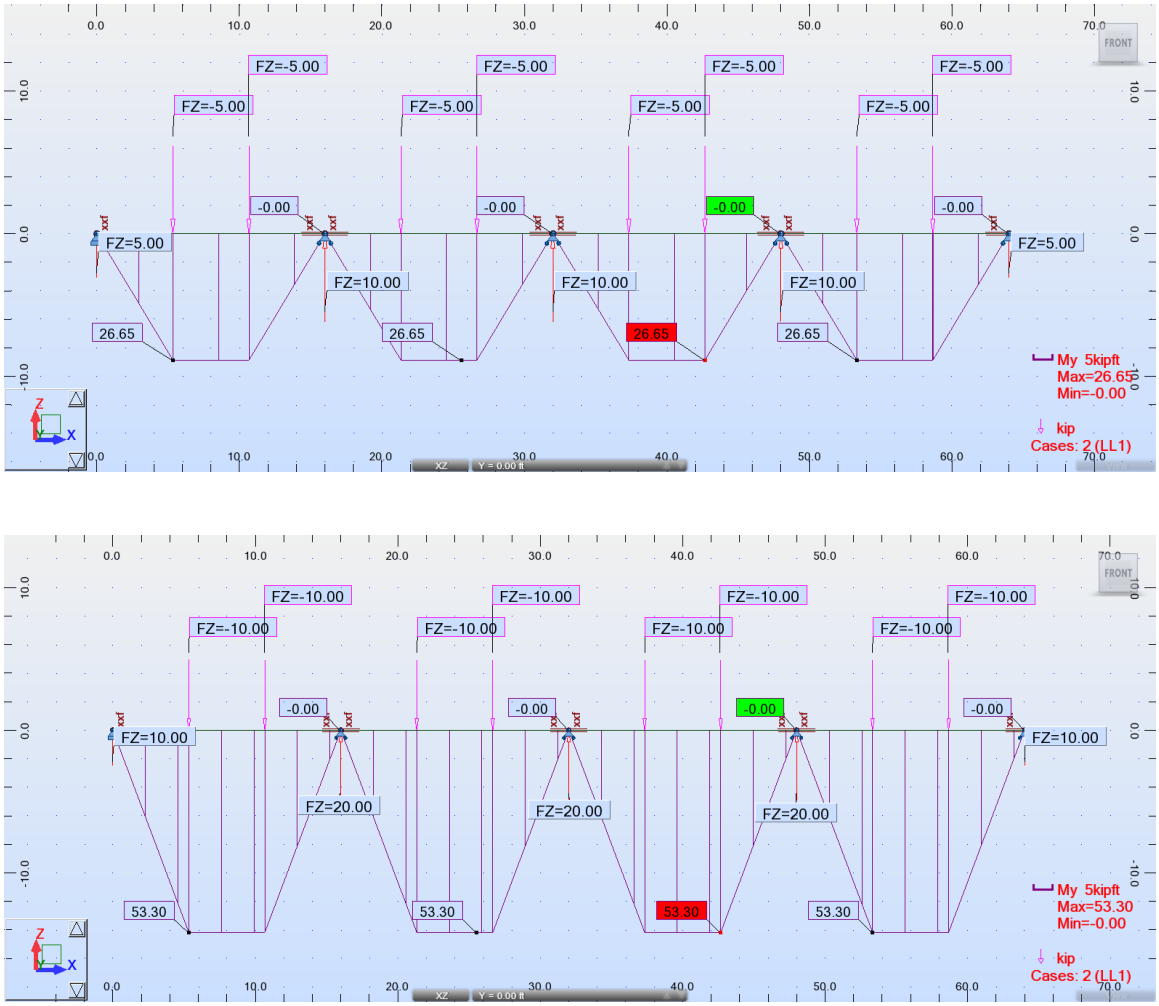

Figure B.4 Four single beams

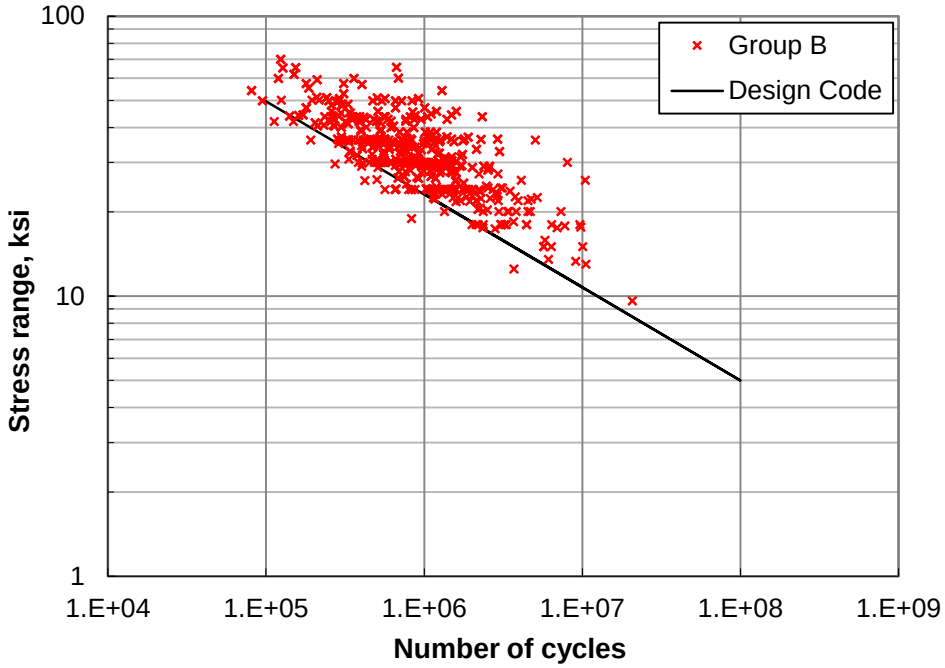

Figure C.1 S-N Data for Category B

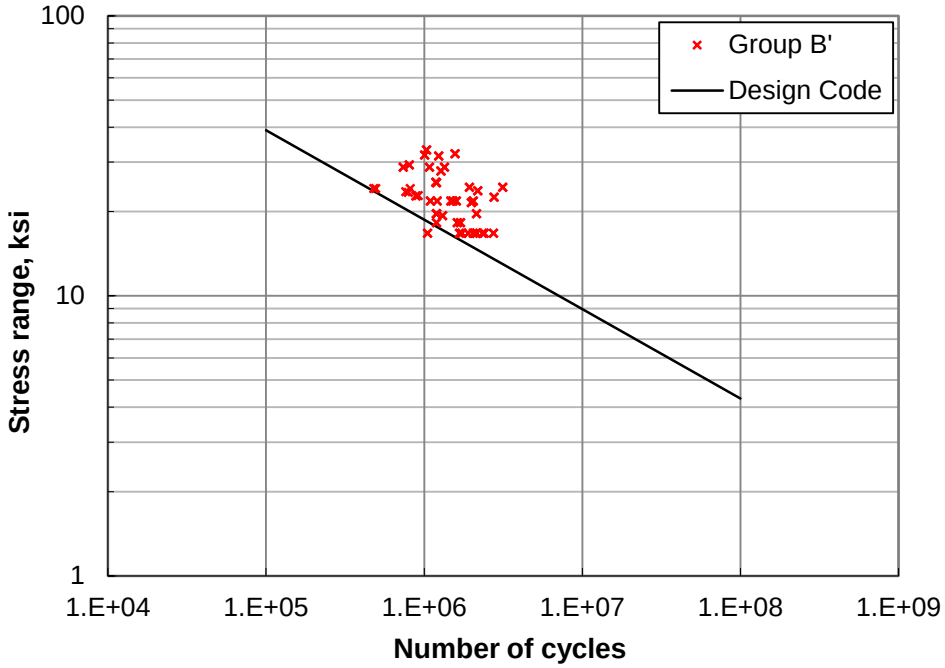

Figure C.2 S-N Data for Category B’

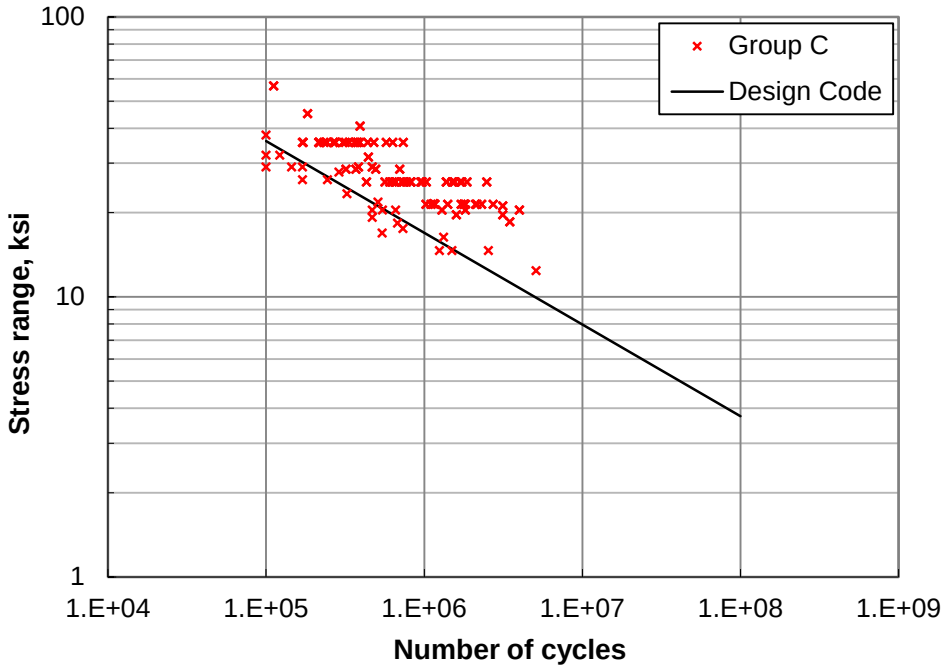

Figure C.3 S-N Data for Category C

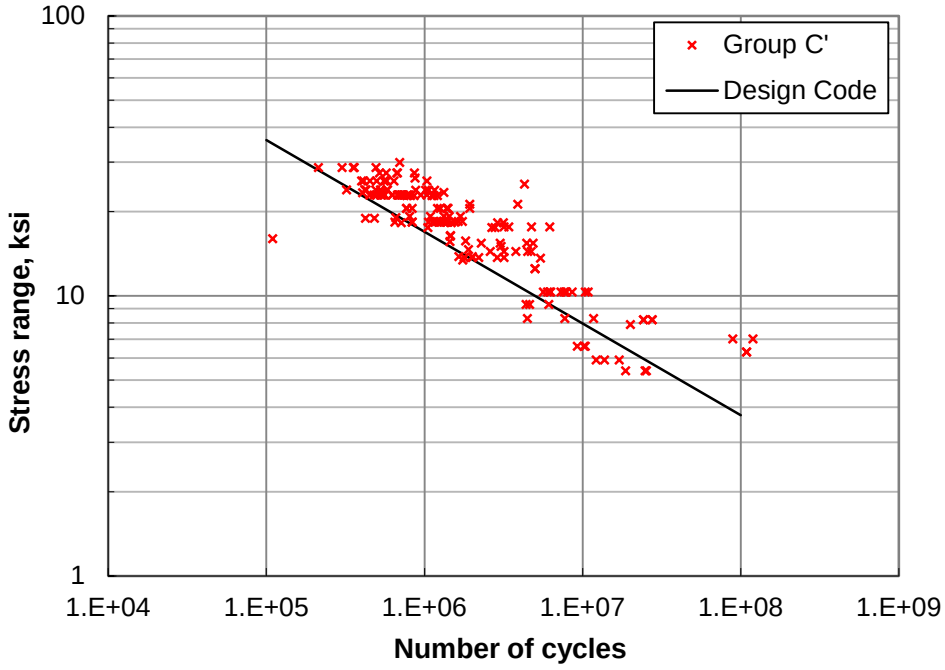

Figure C.4 S-N Data for Category C'

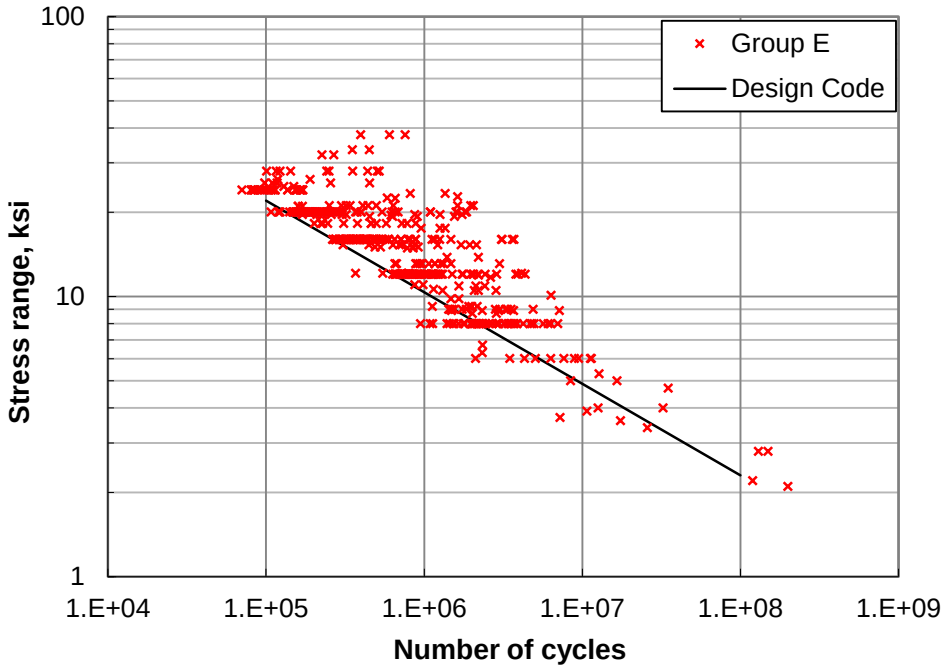

Figure C.5 S-N Data for Category E

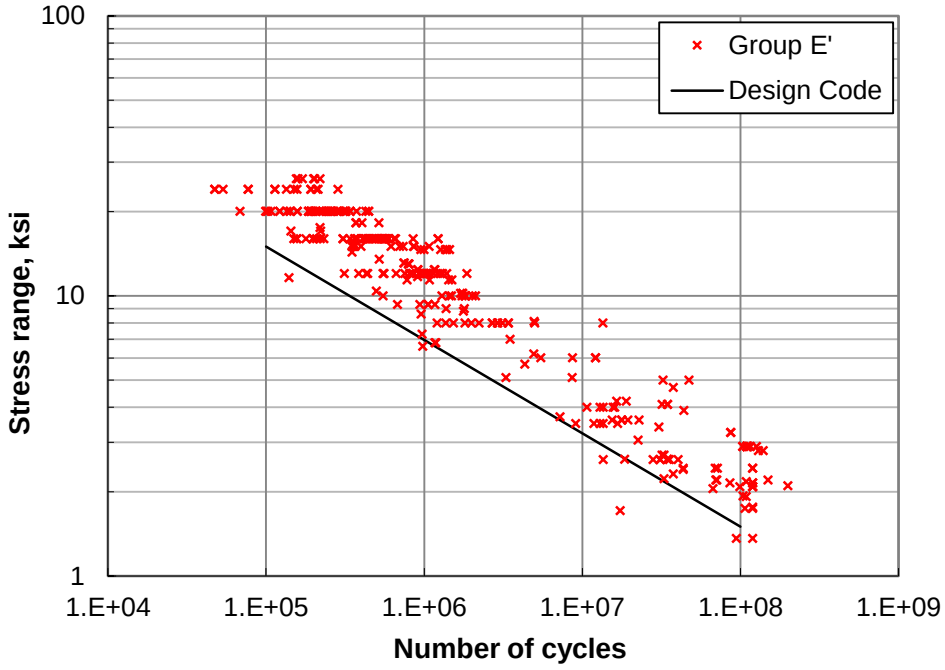

Figure C.6 S-N Data for Category E'

Appendix D CDFs for Fatigue Resistance

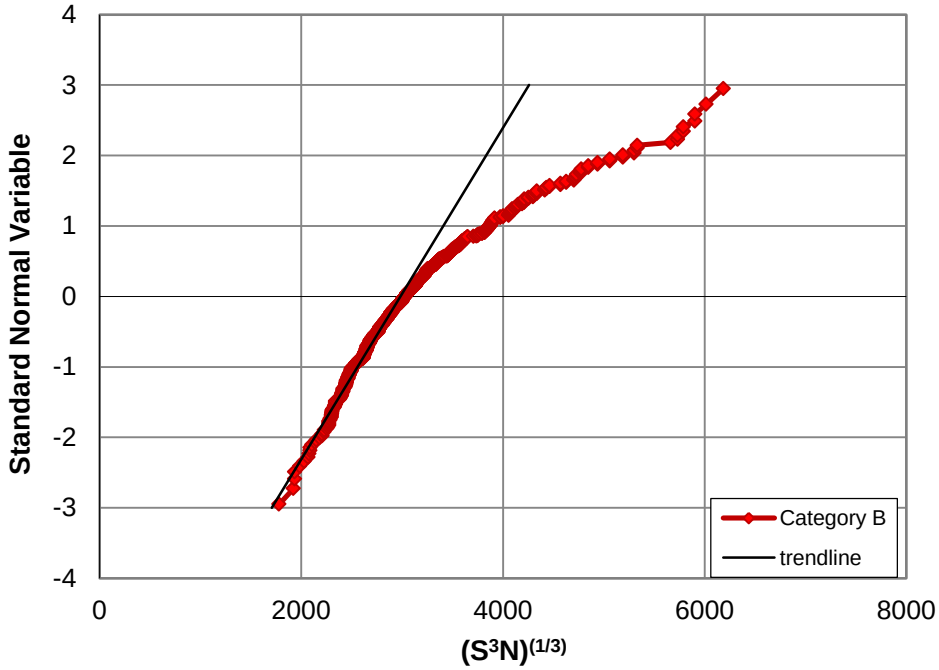

Figure D.1 CDF of fatigue resistance for Category B

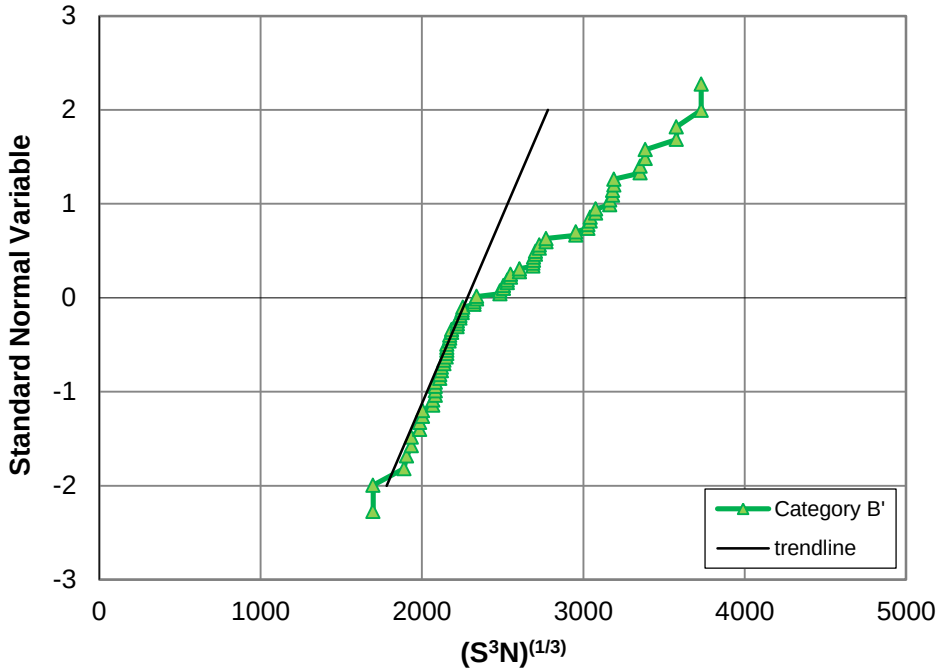

Figure D.2 CDF of fatigue resistance for Category B'

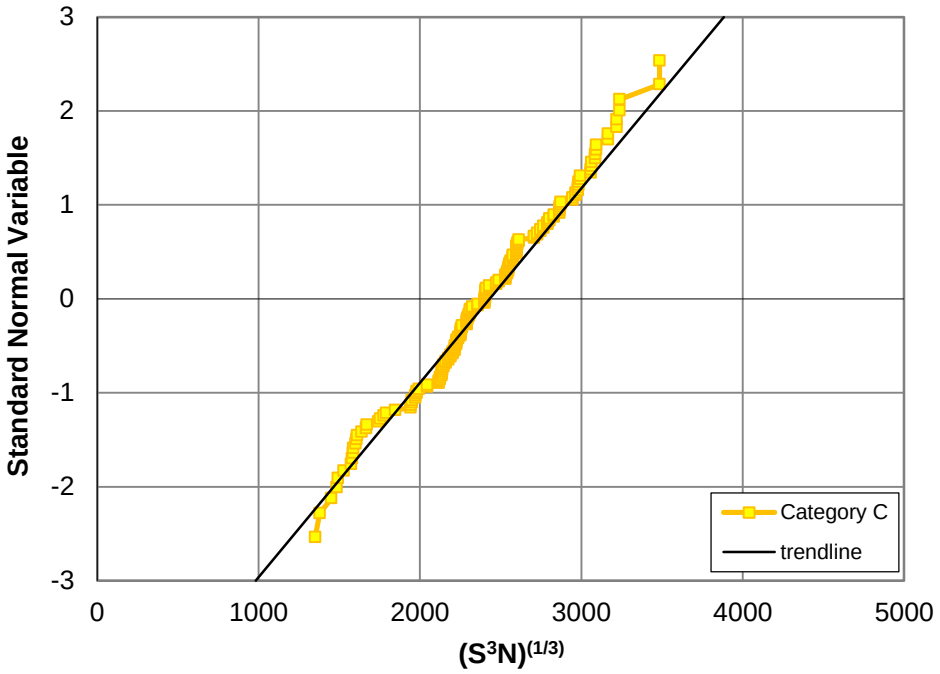

Figure D.3 CDF of fatigue resistance for Category C

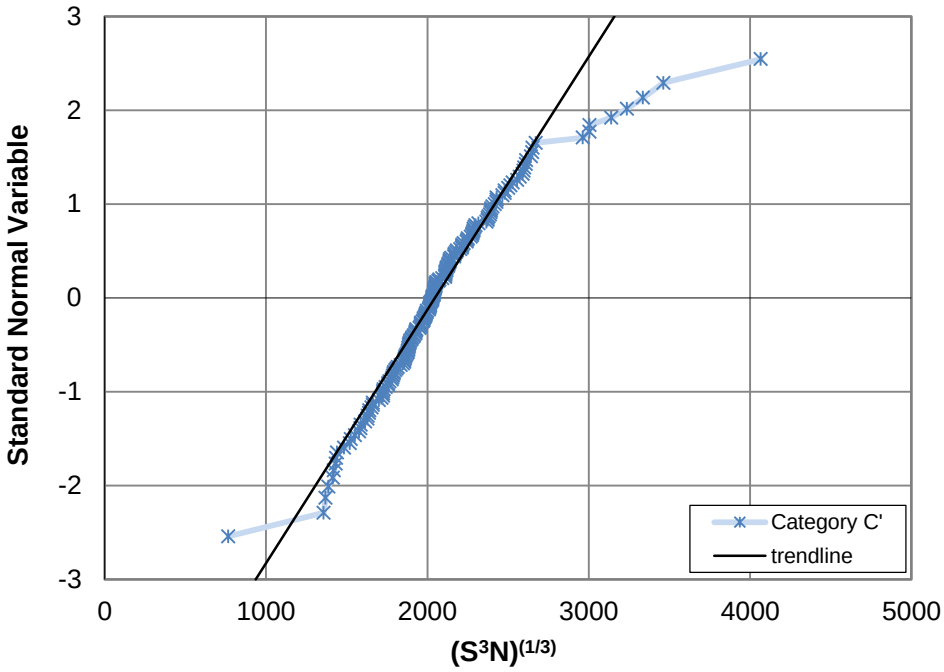

Figure D.4 CDF of fatigue resistance for Category C'

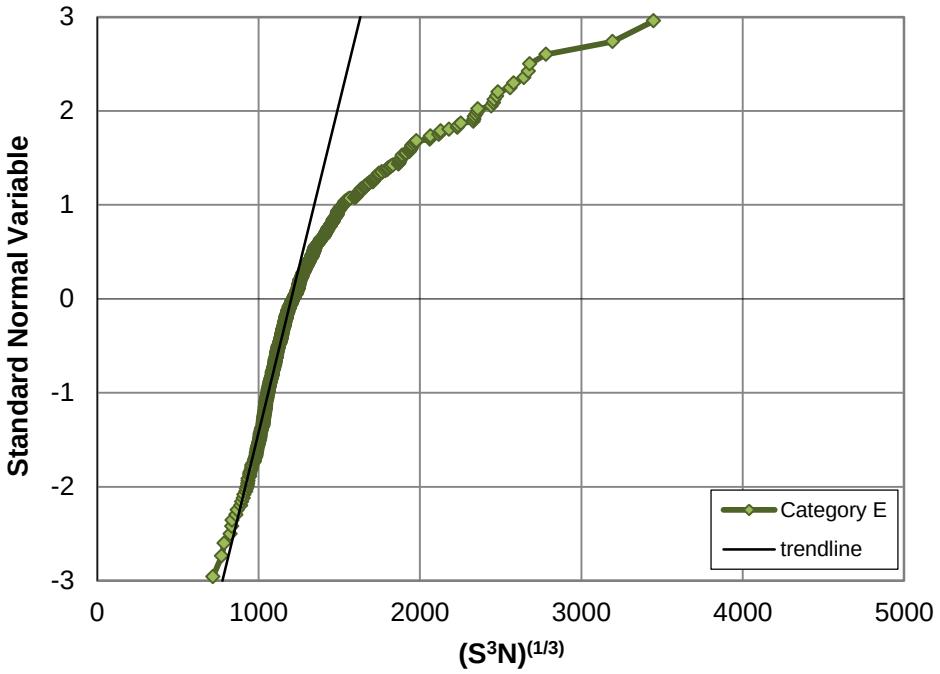

Figure D.5 CDF of fatigue resistance for Category E

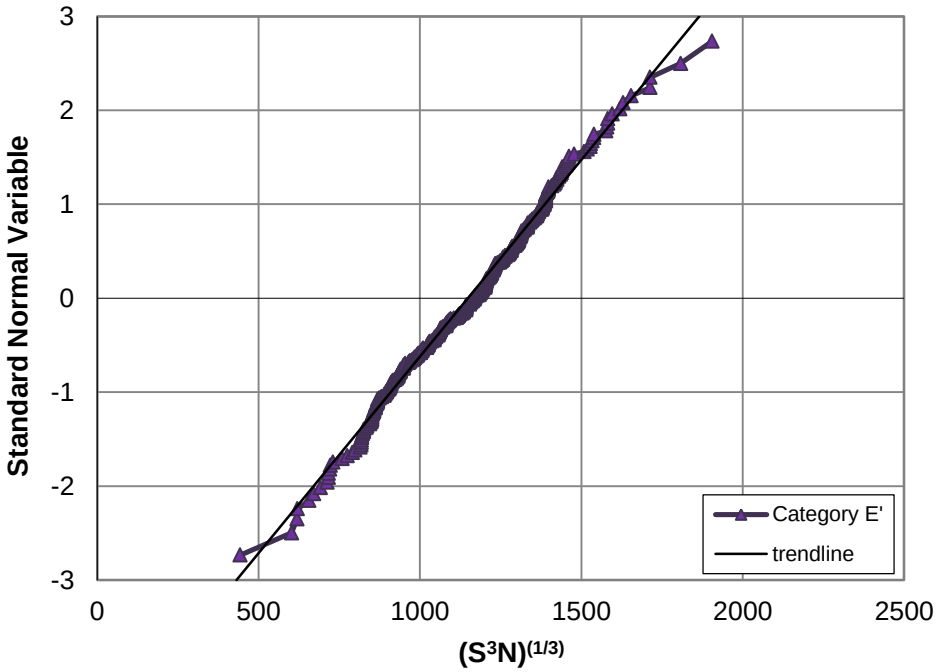

Figure D.6 CDF of fatigue resistance for Category E'

Appendix E Stress Histories for Bridge #1

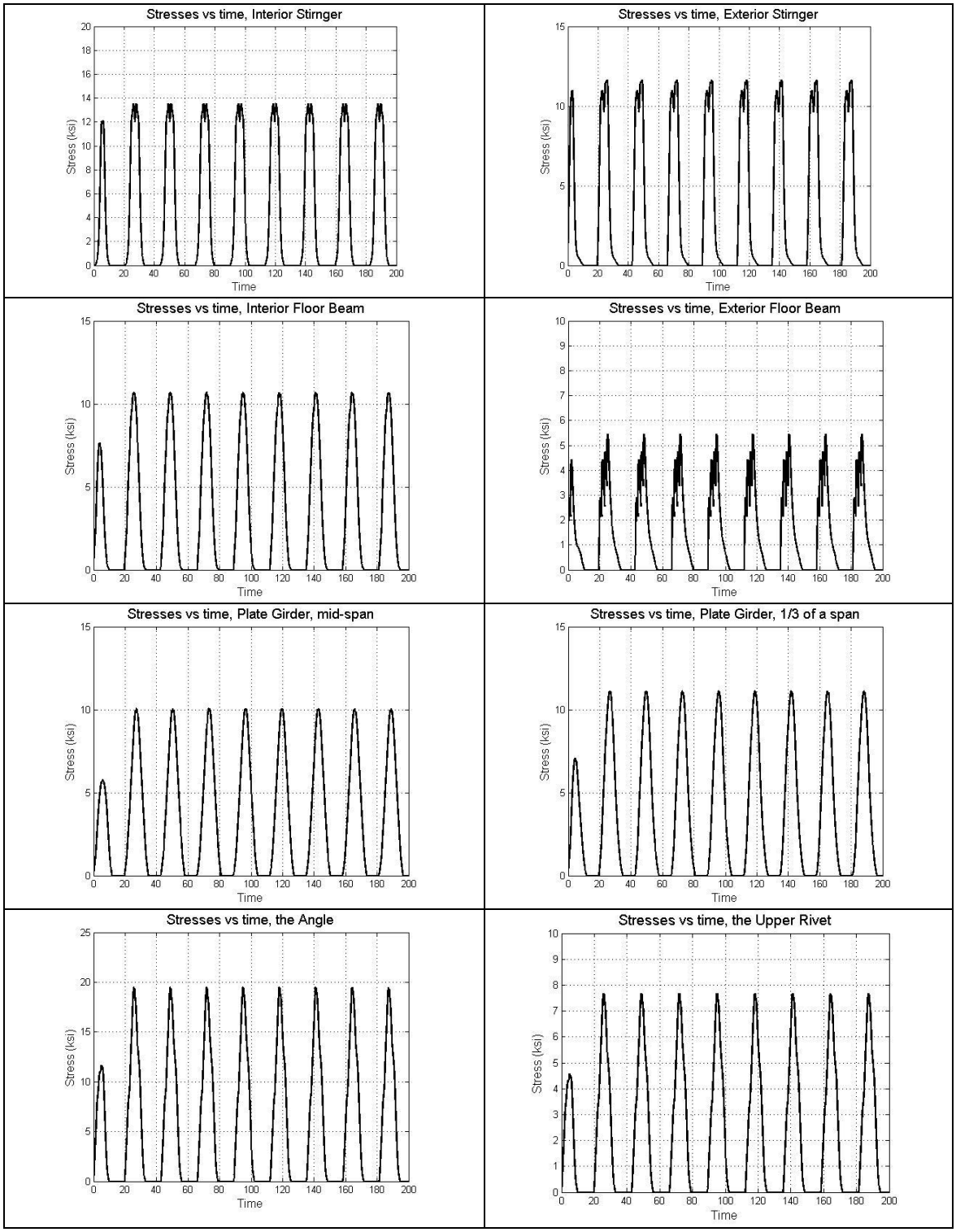

Figure E.1 Line graphs of part of stress-time histories for individual components of Bridge #1 under Train 1

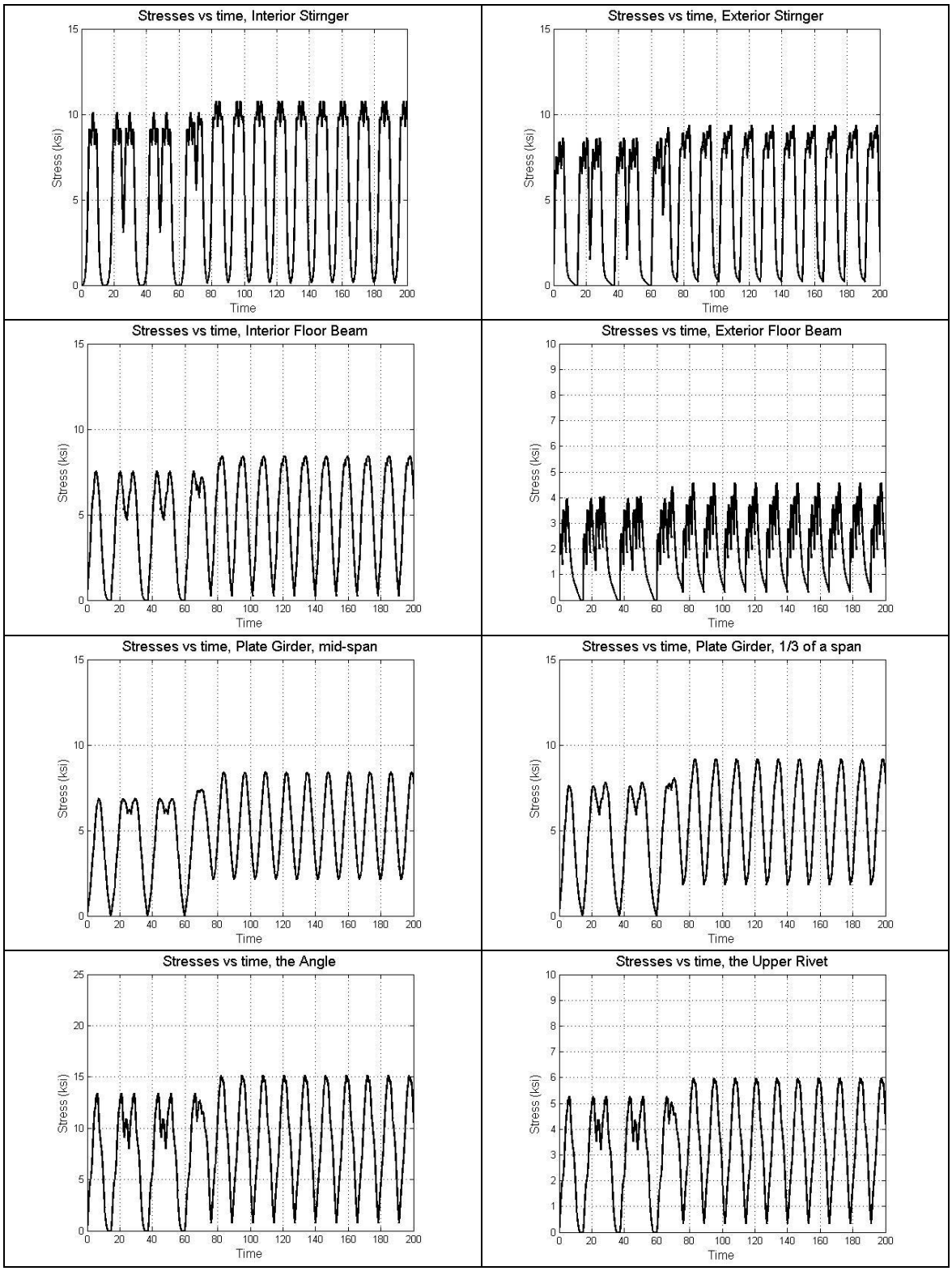

Figure E.2 Line graphs of part of stress-time histories for individual components of Bridge #1 under Train 2

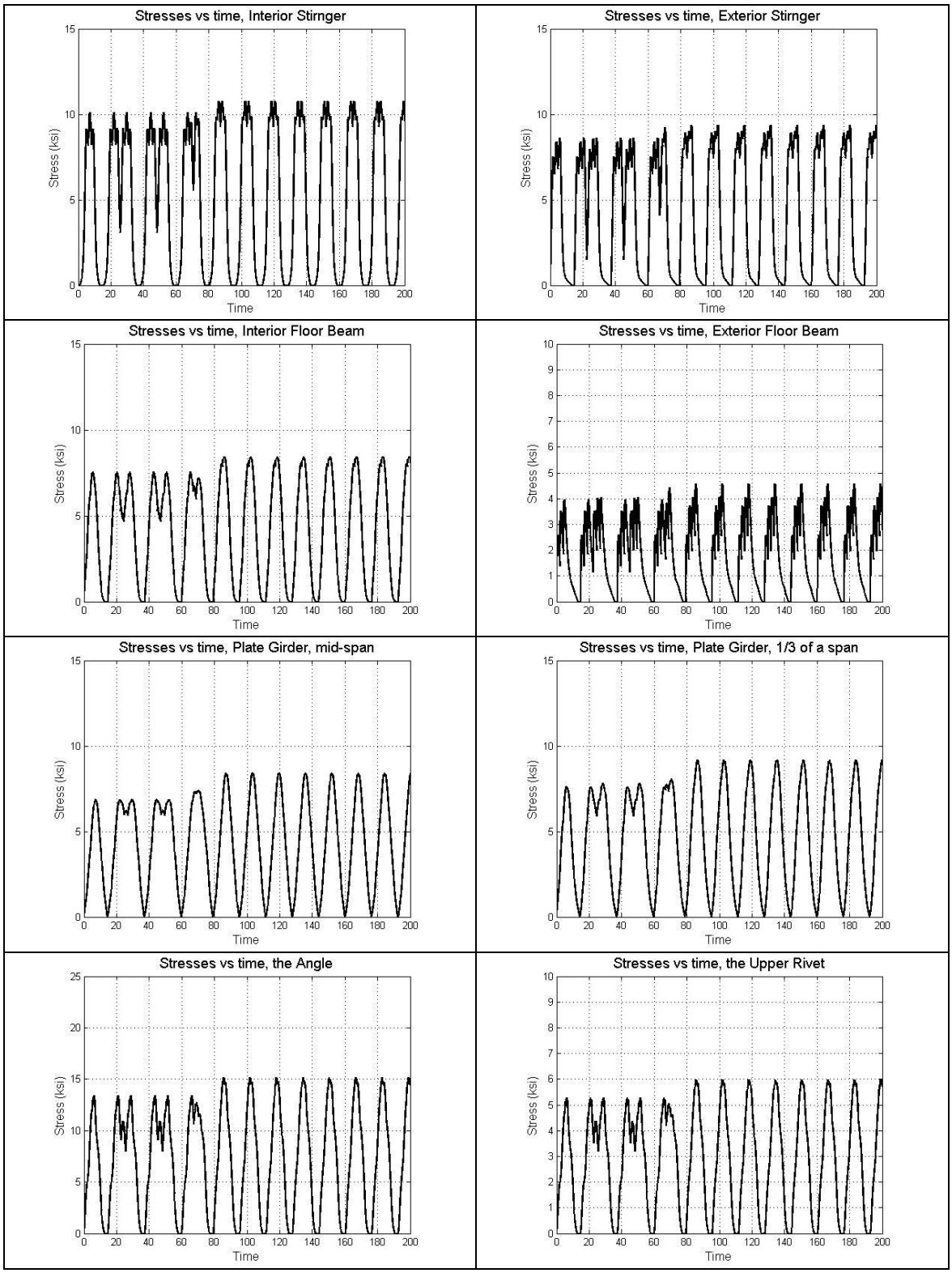

Figure E.3 Line graphs of part of stress-time histories for individual components of Bridge #1 under Train 3

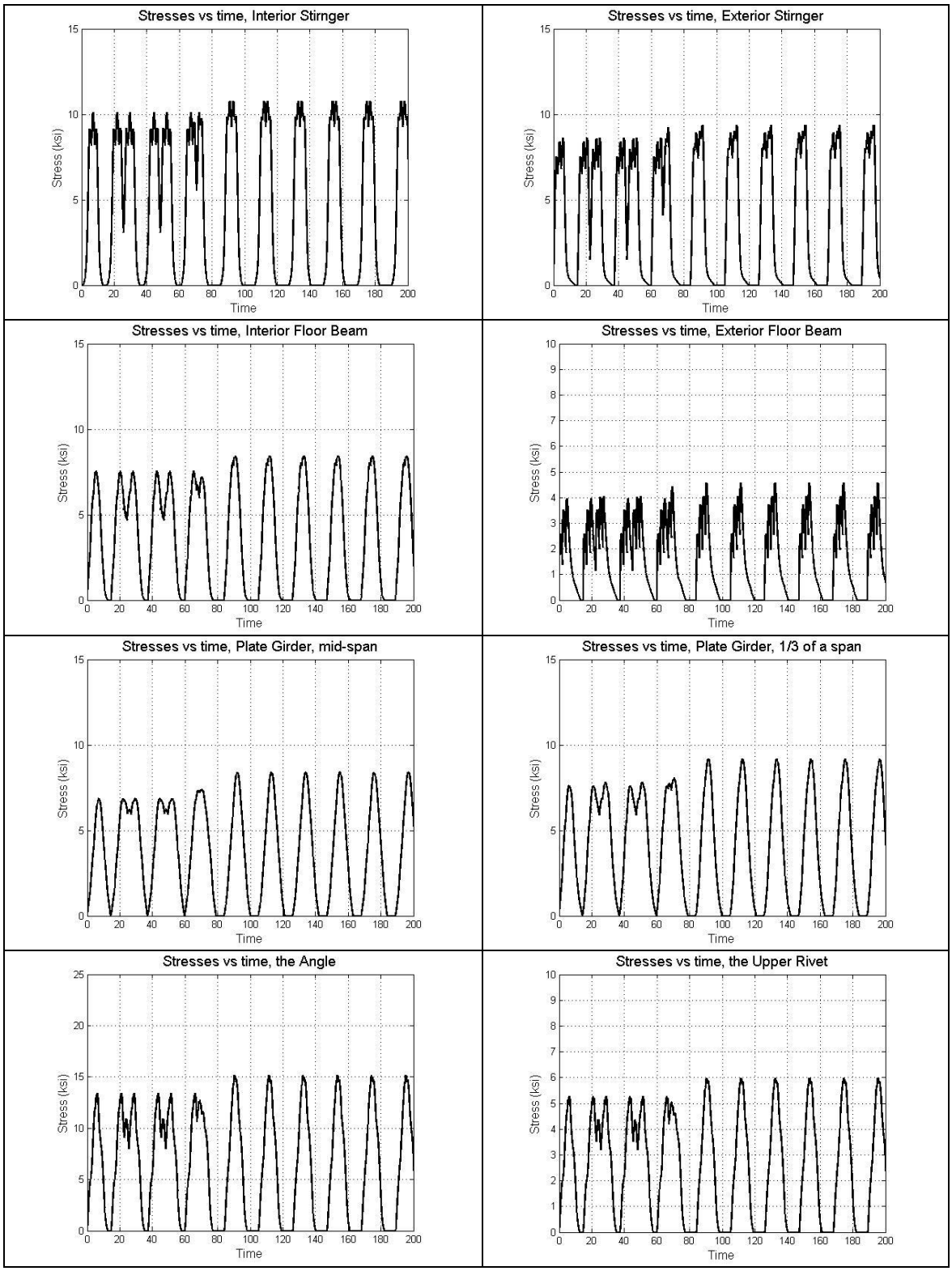

Figure E.4 Line graphs of part of stress-time histories for individual components of Bridge #1 under Train 4

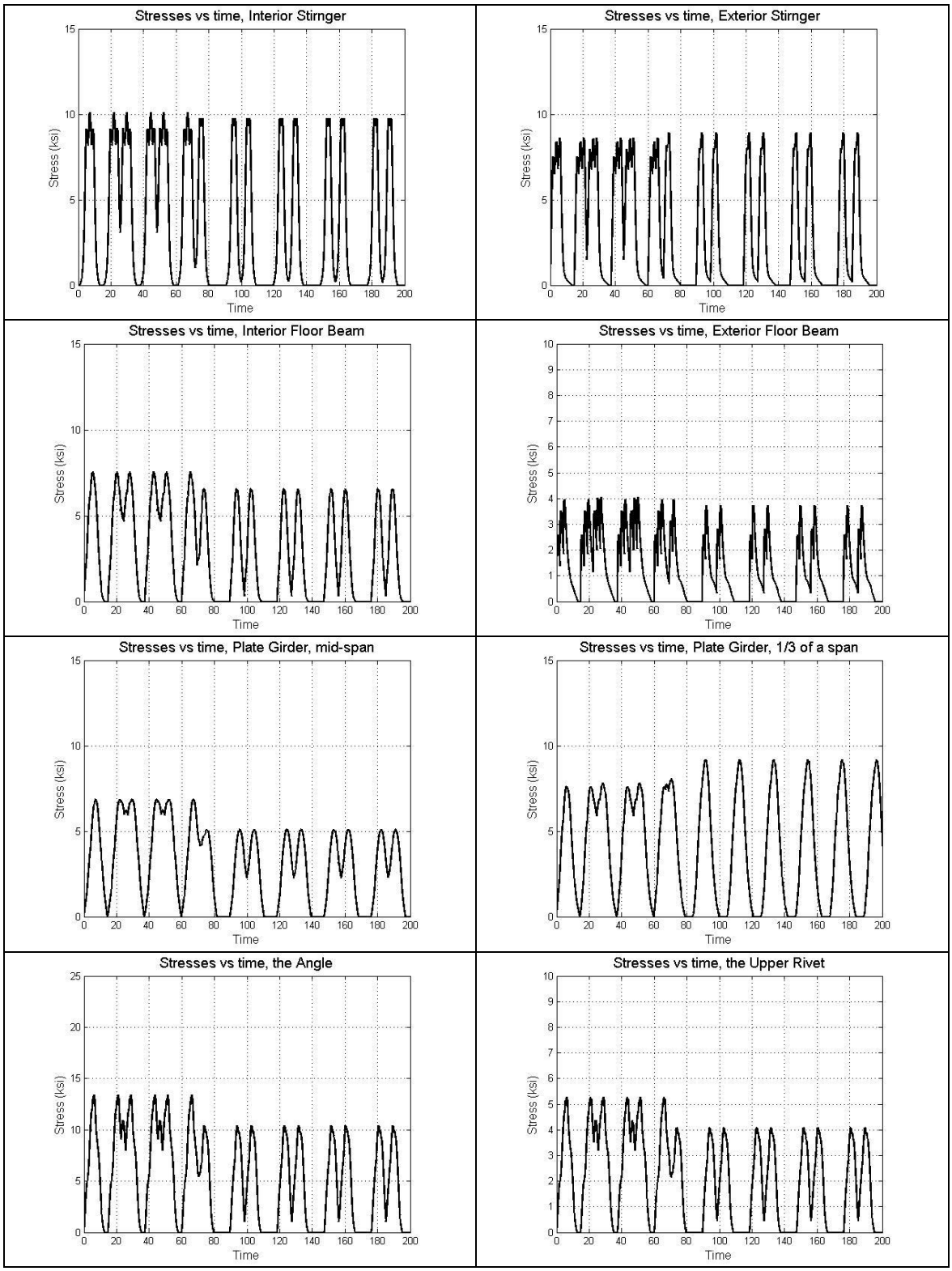

Figure E.5 Line graphs of part of stress-time histories for individual components of Bridge #1 under Train 5

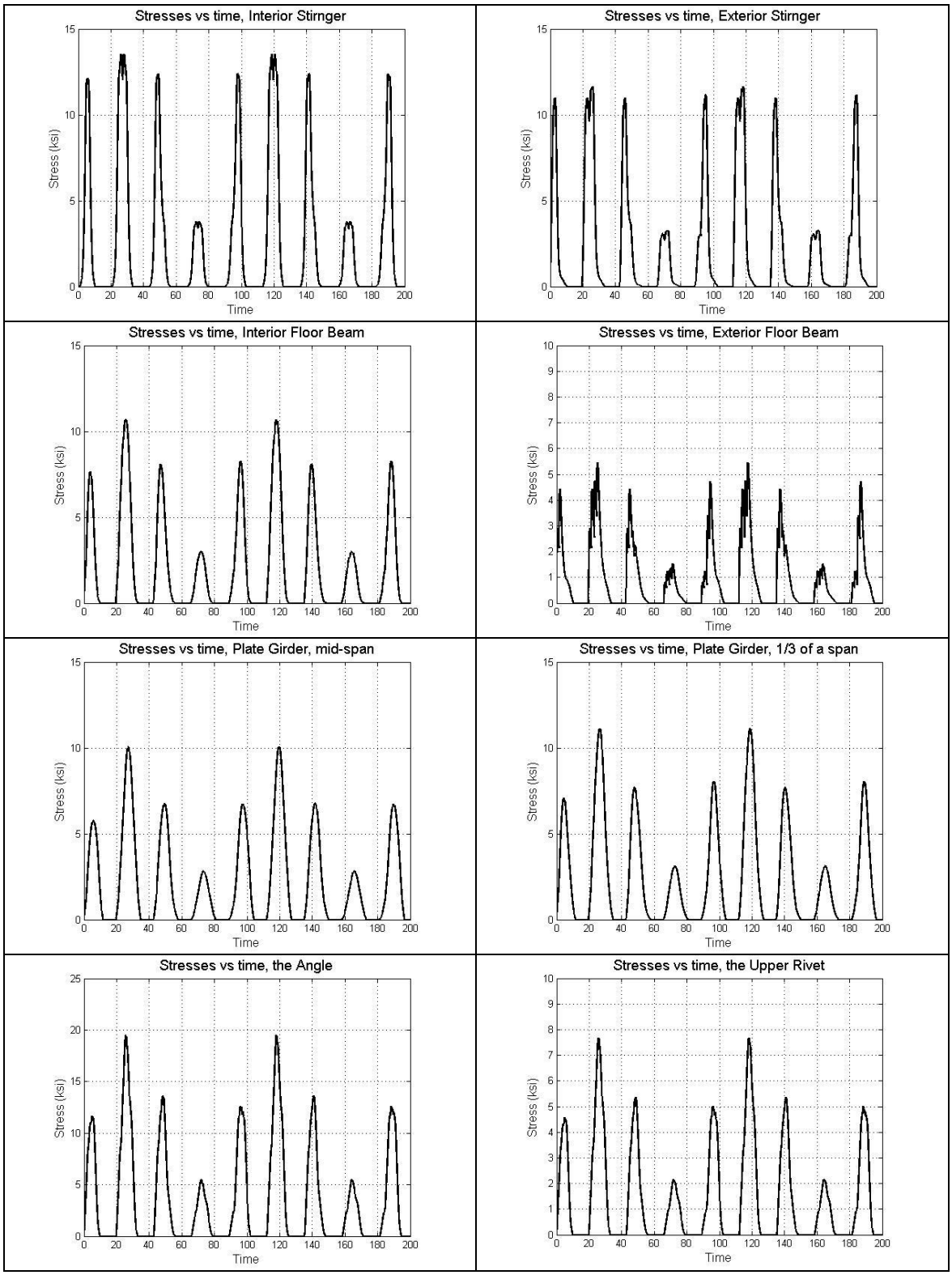

Figure E.6 Line graphs of part of stress-time histories for individual components of Bridge #1 under Train 6

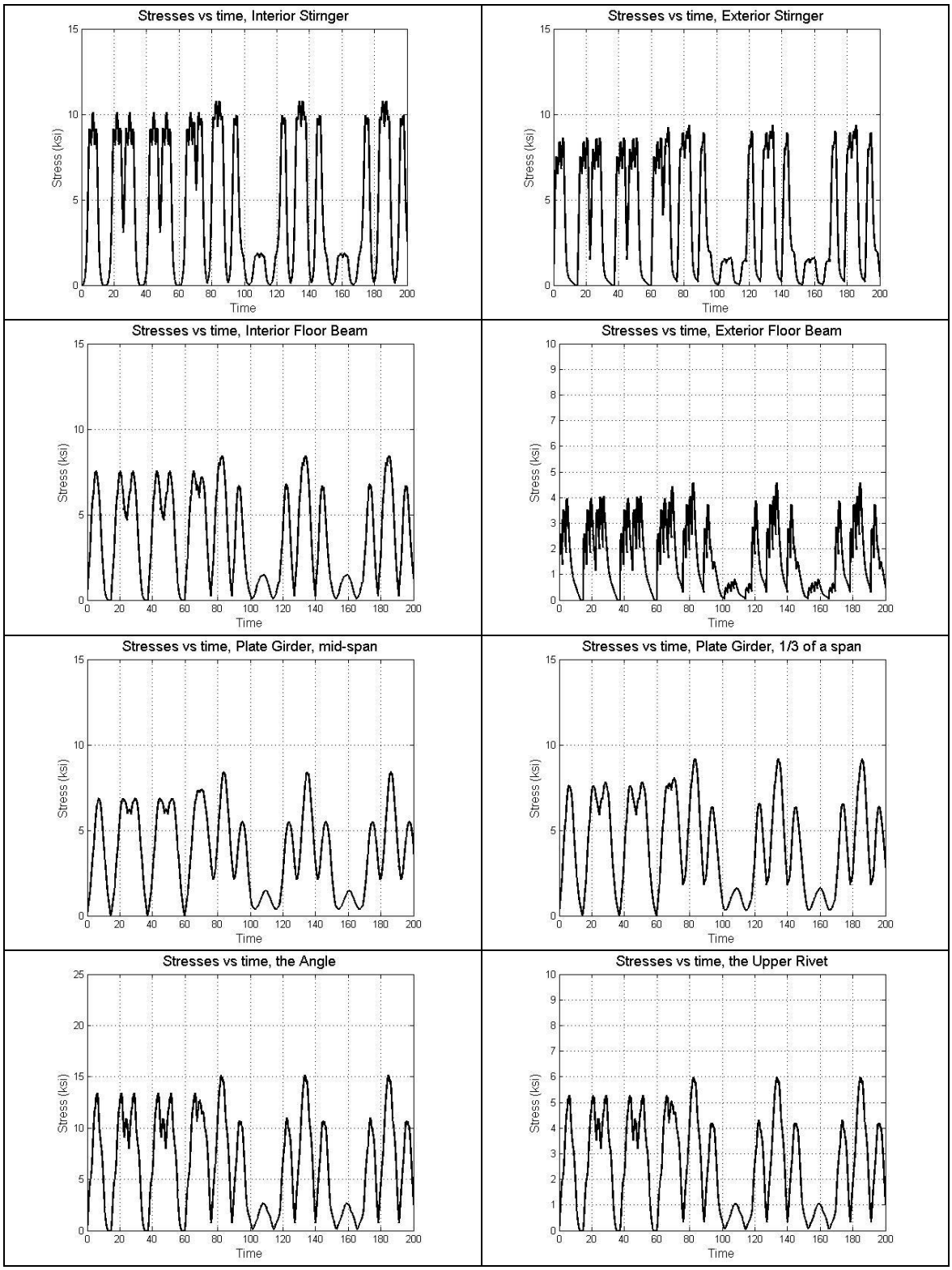

Figure E.7 Line graphs of part of stress-time histories for individual components of Bridge #1 under Train 7

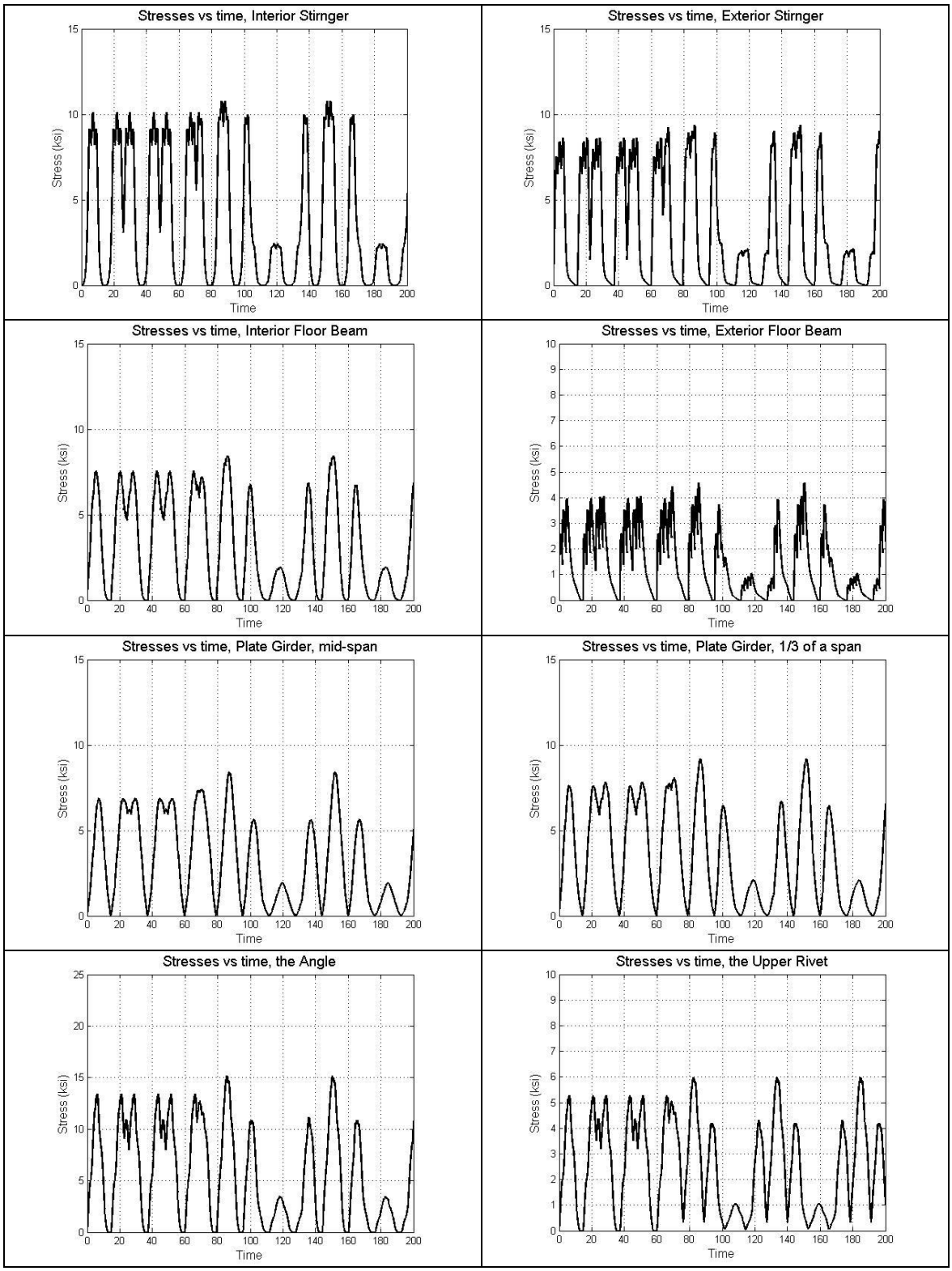

Figure E.8 Line graphs of part of stress-time histories for individual components of Bridge #1 under Train 8

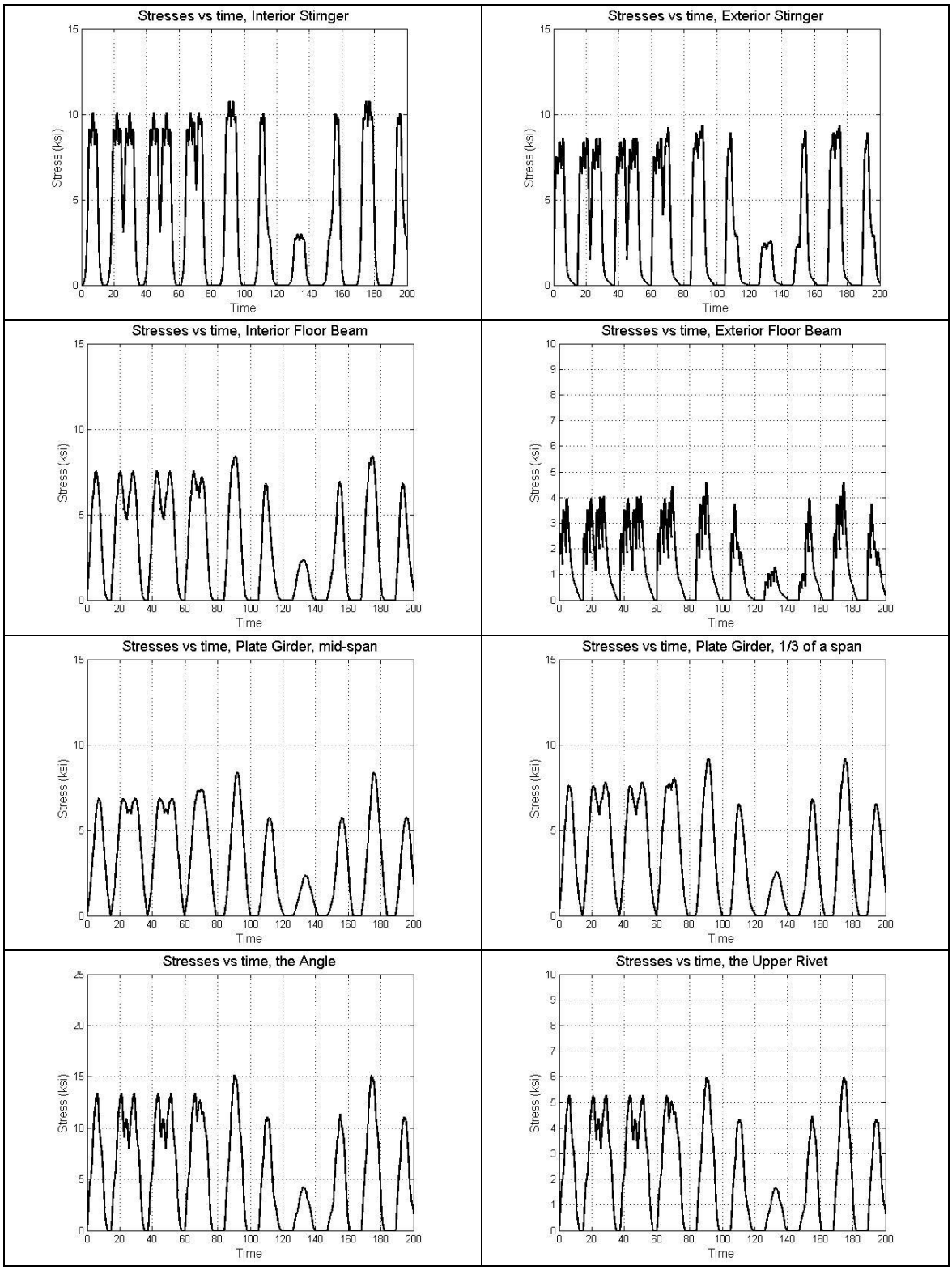

Figure E.9 Line graphs of part of stress-time histories for individual components of Bridge #1 under Train 9

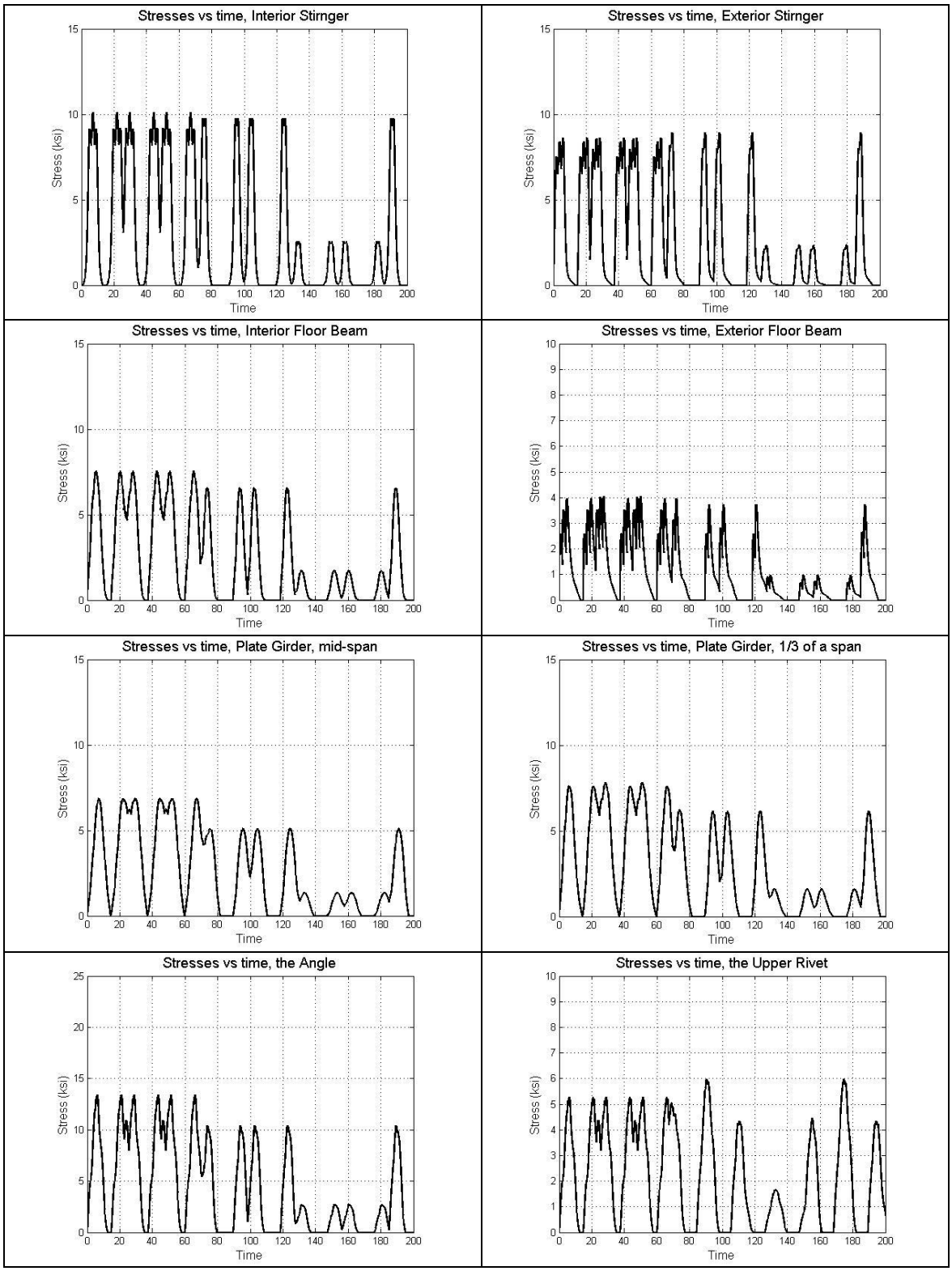

Figure E.10 Line graphs of part of stress-time histories for individual components of Bridge #1 under Train 10

Appendix F Stress Histories for Bridge #2

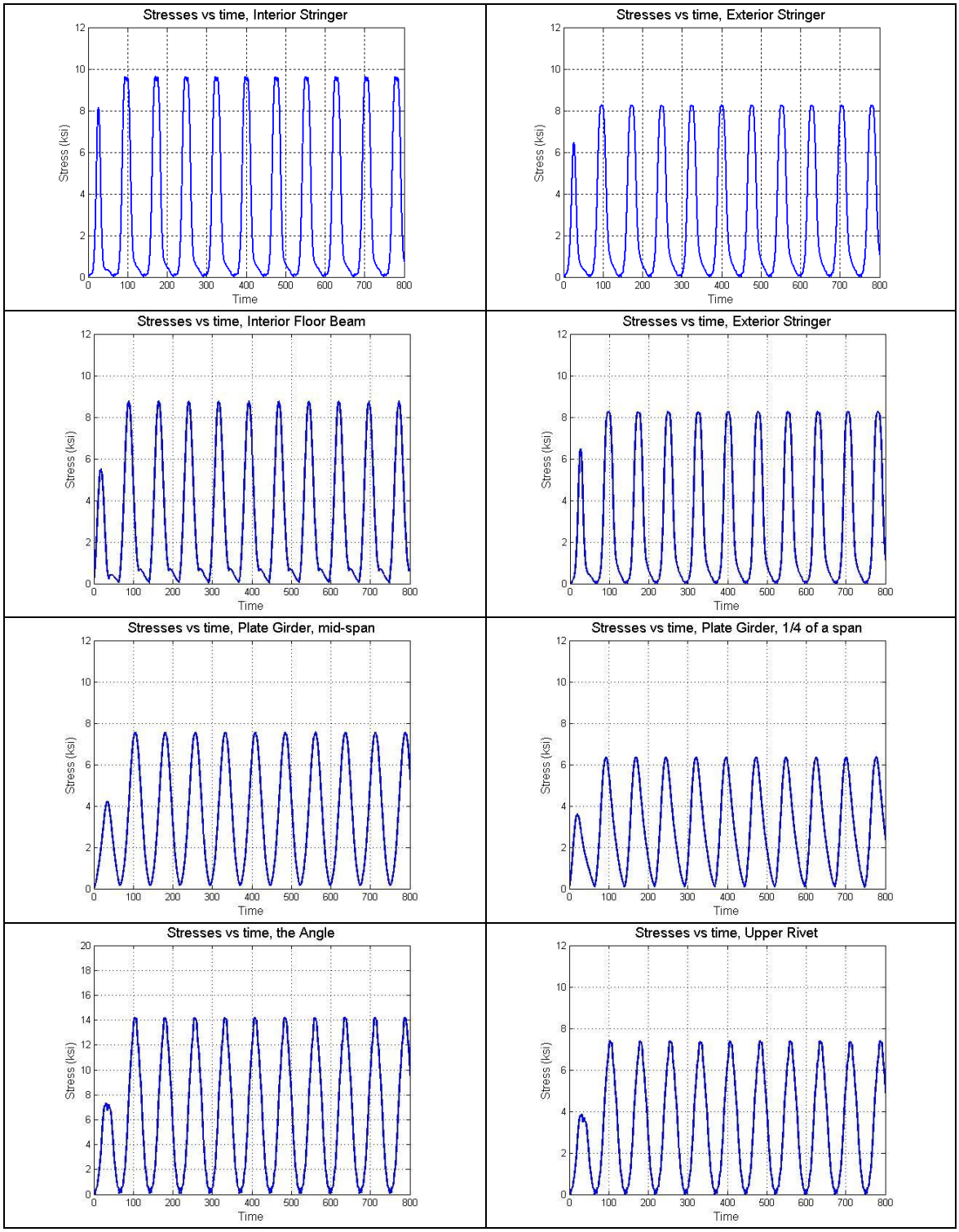

Figure F.1 Line graphs of part of stress-time histories for individual components of Bridge #2 under Train 1

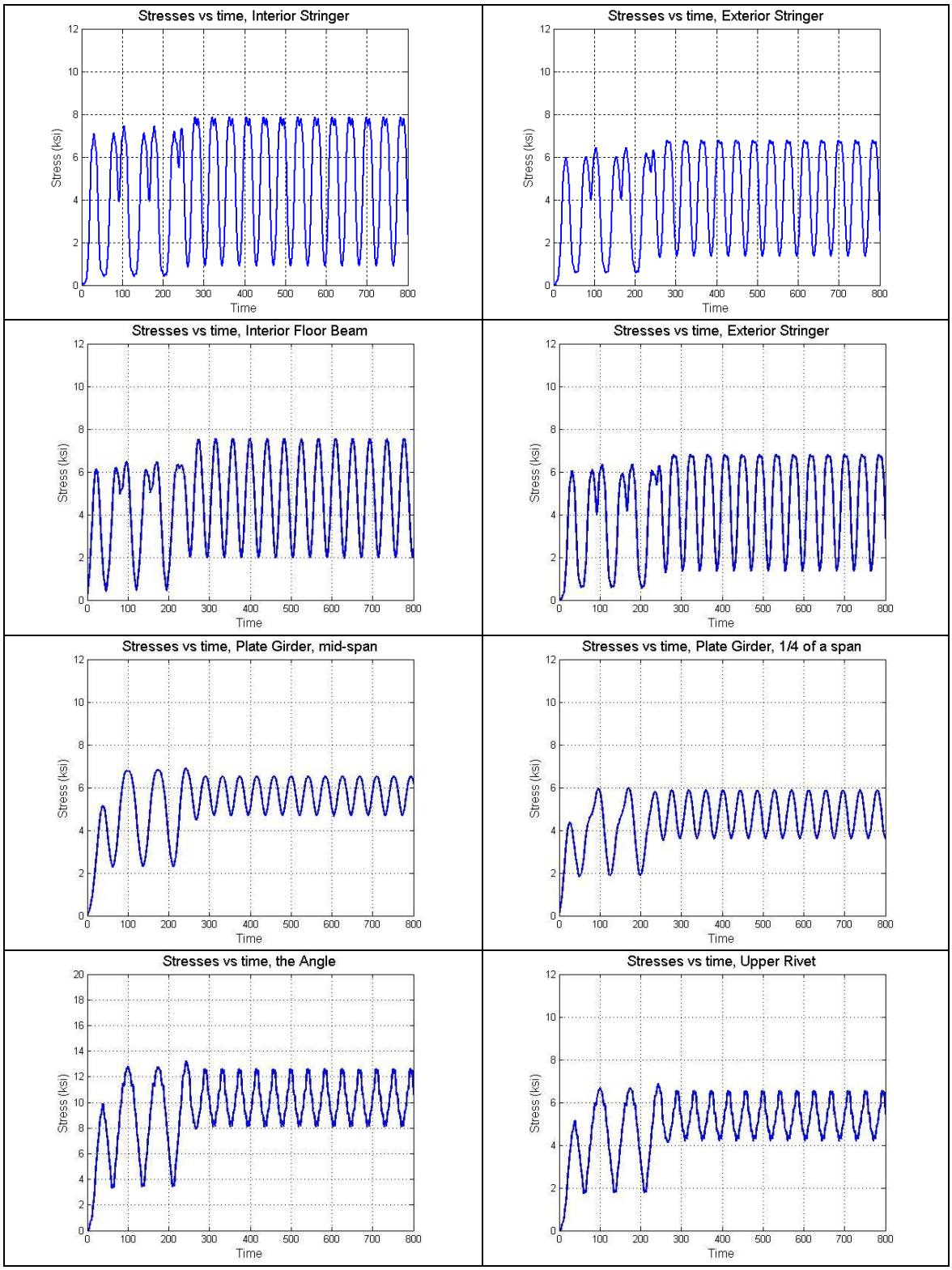

Figure F.2 Line graphs of part of stress-time histories for individual components of Bridge #2 under Train 2

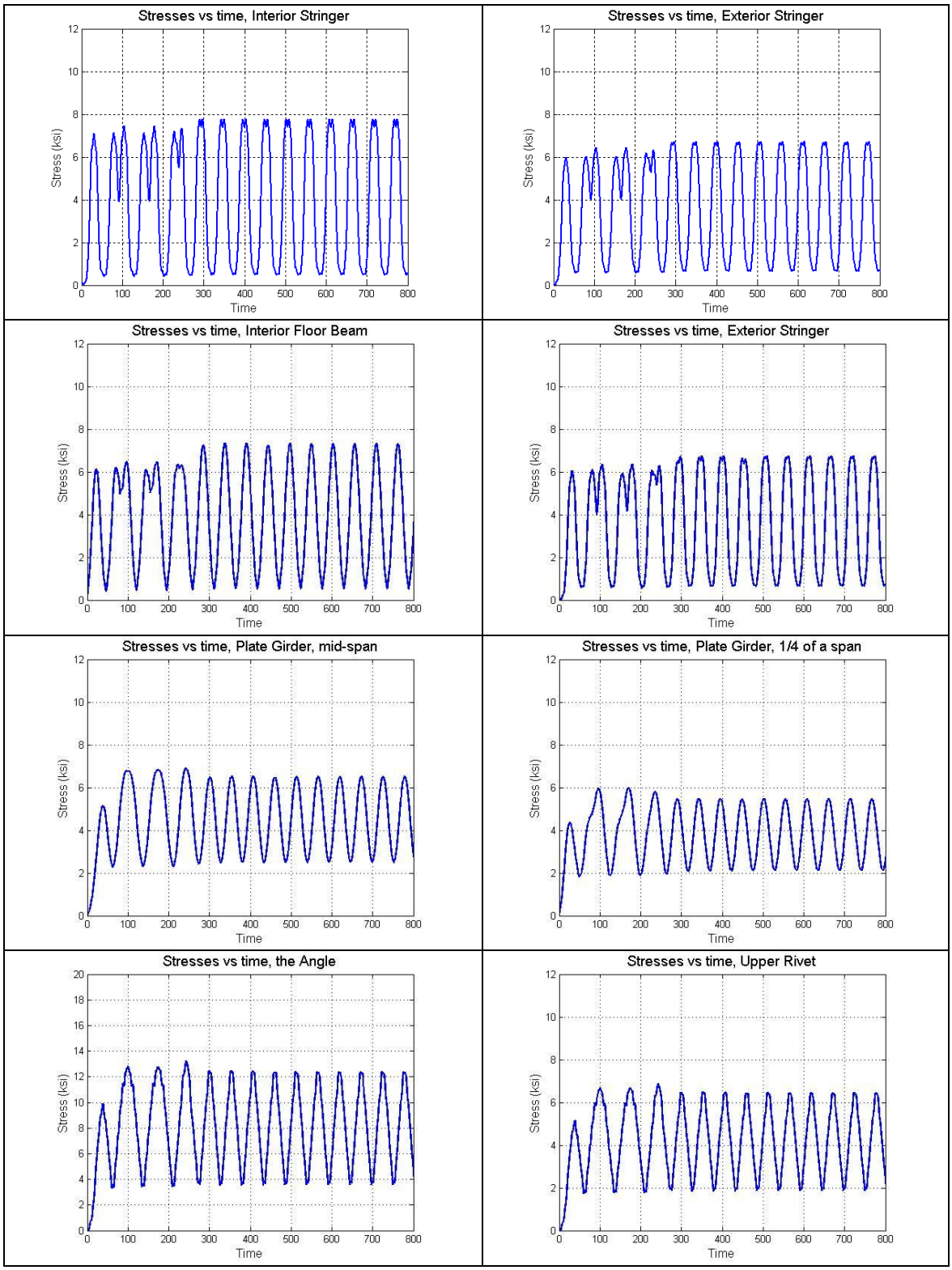

Figure F.3 Line graphs of part of stress-time histories for individual components of Bridge #2 under Train 3

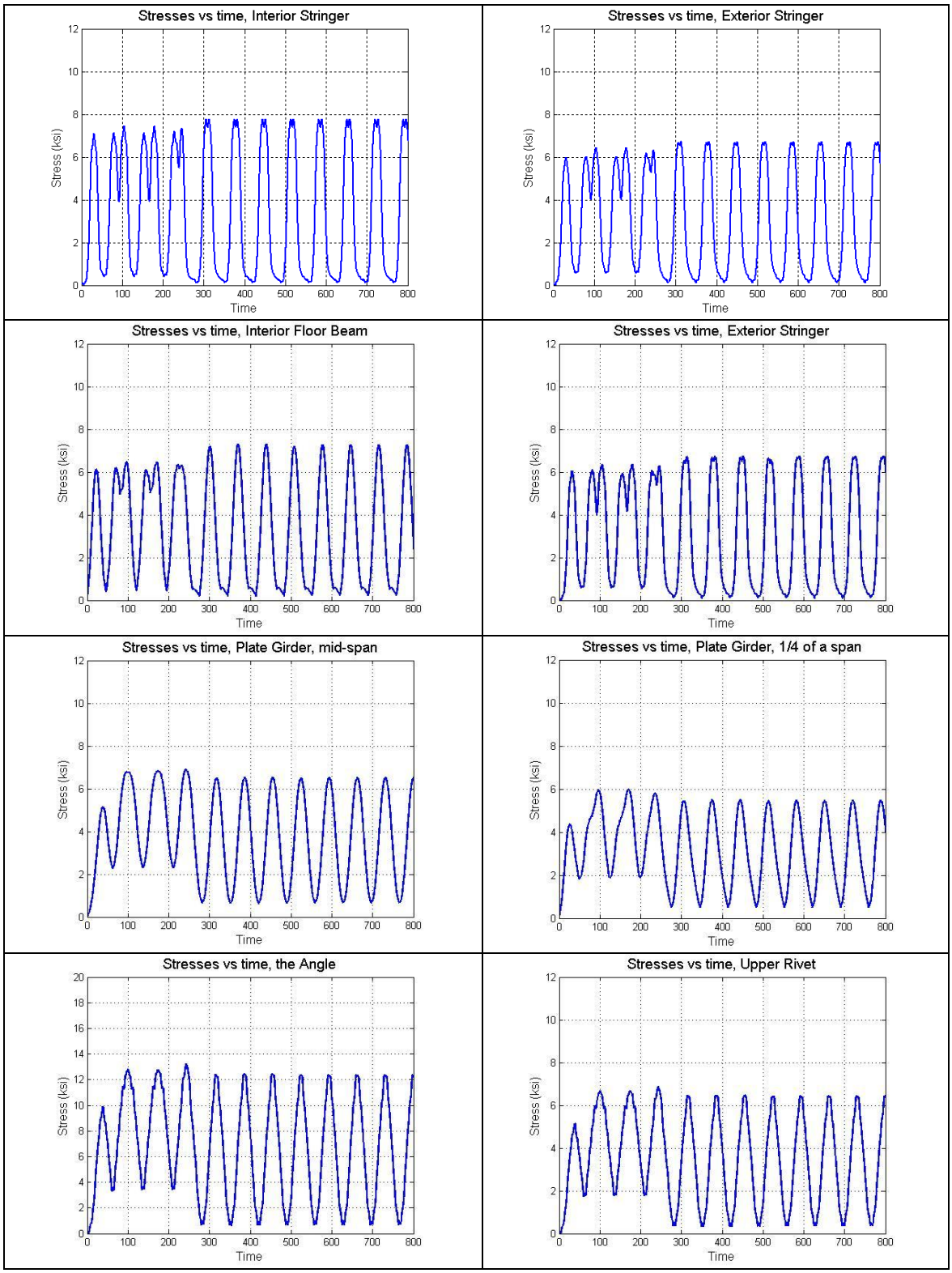

Figure F.4 Line graphs of part of stress-time histories for individual components of Bridge #2 under Train 4

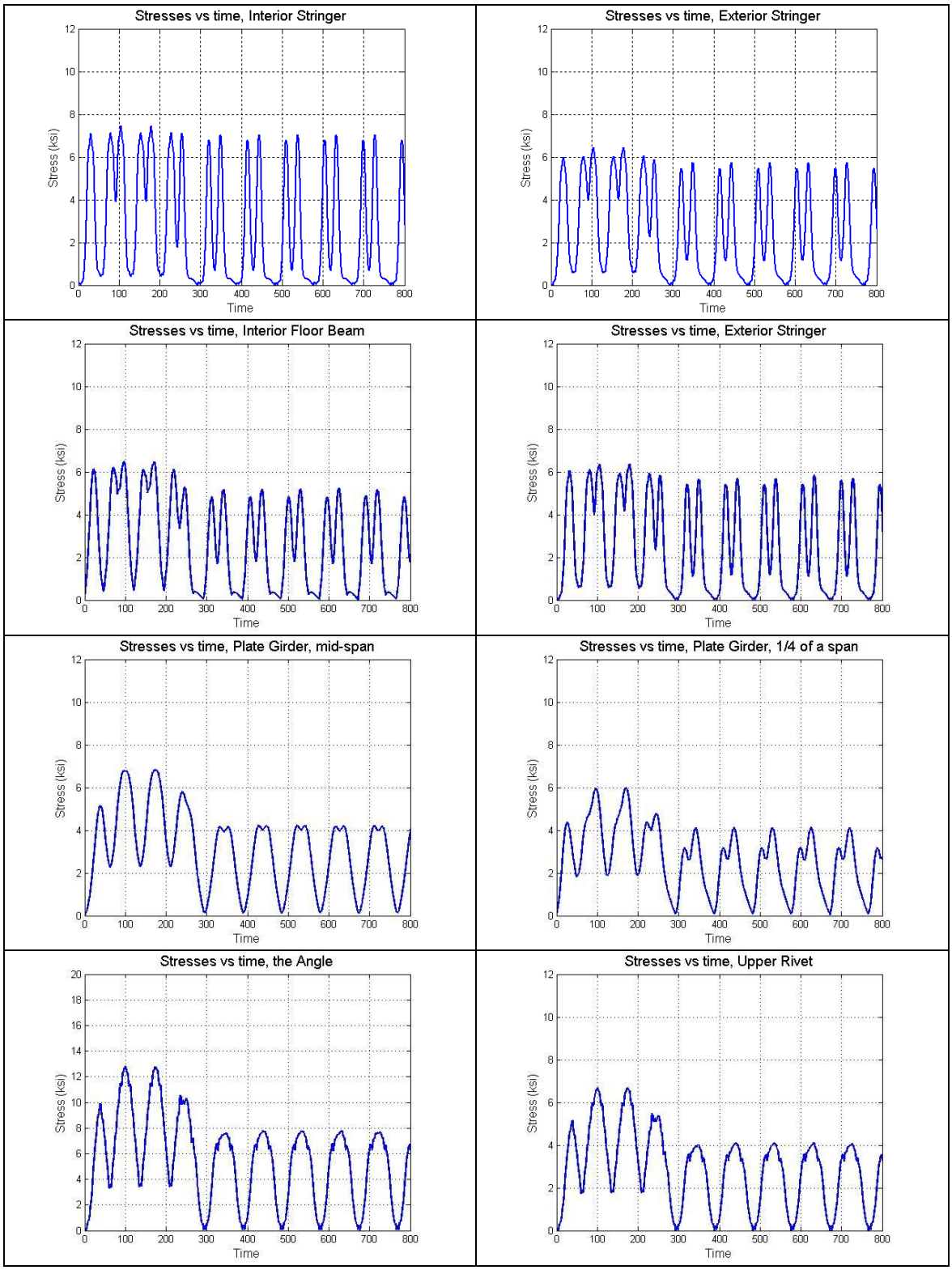

Figure F.5 Line graphs of part of stress-time histories for individual components of Bridge #2 under Train 5

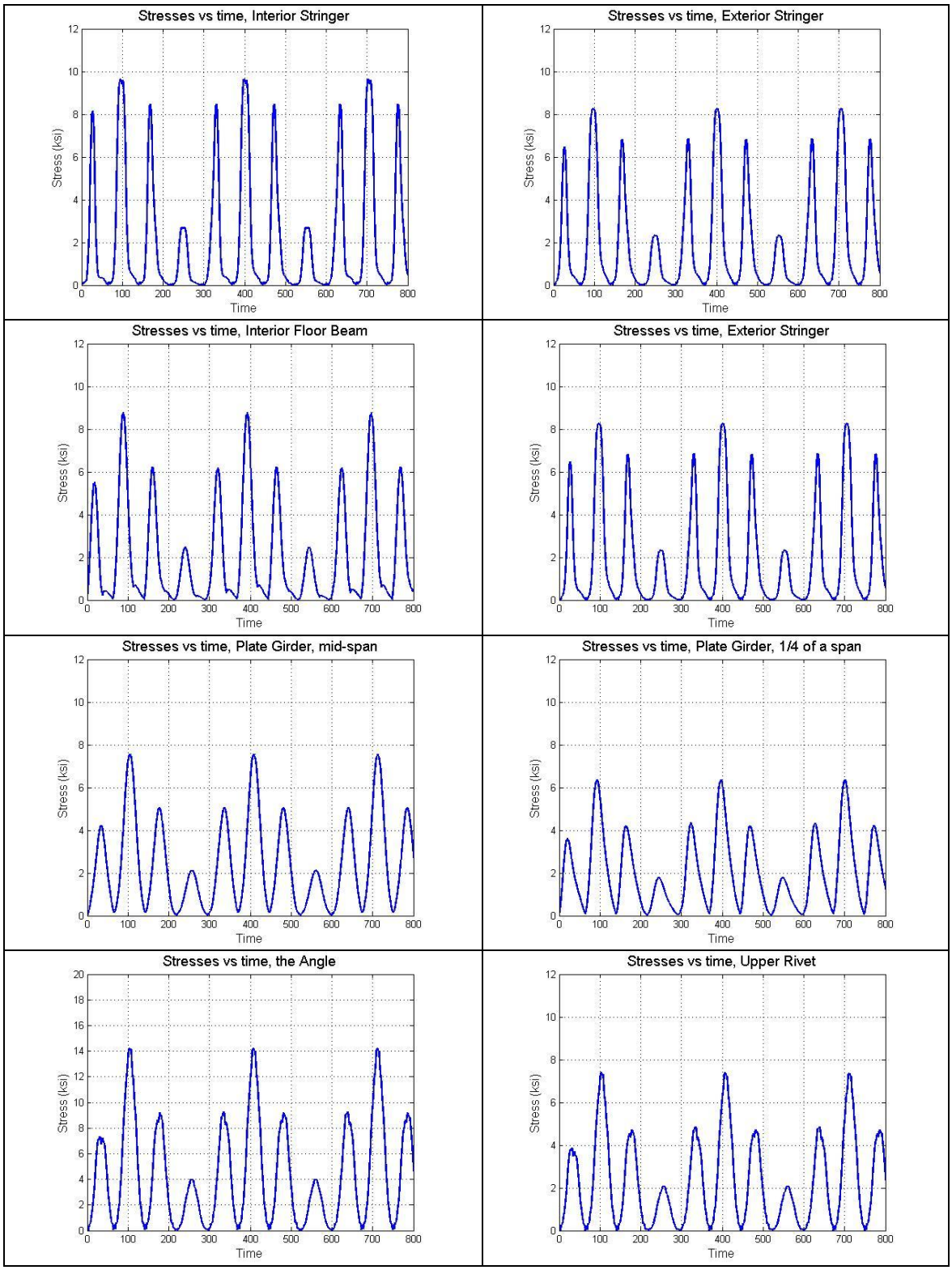

Figure F.6 Line graphs of part of stress-time histories for individual components of Bridge #2 under Train 6

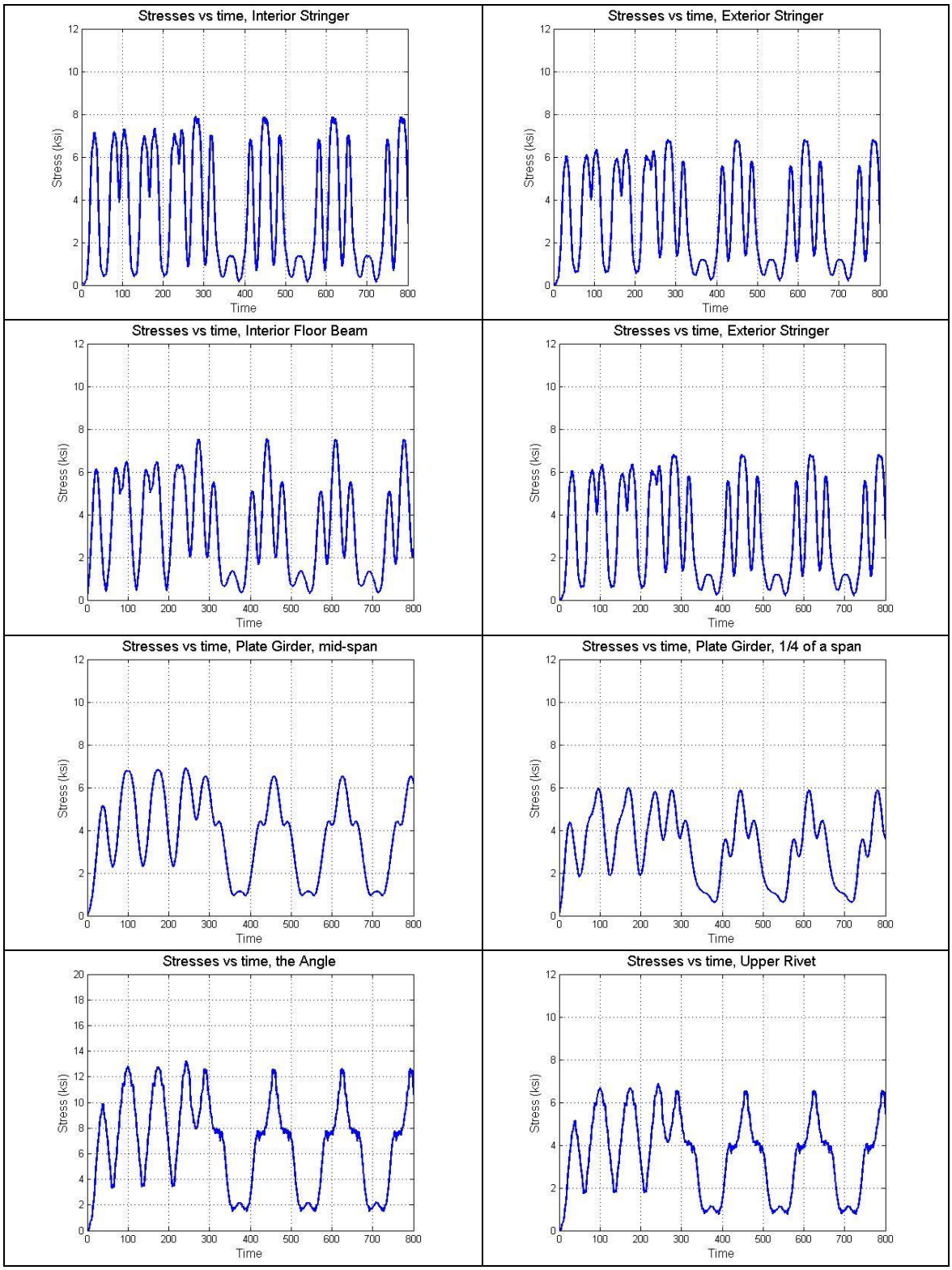

Figure F.7 Line graphs of part of stress-time histories for individual components of Bridge #2 under Train 7

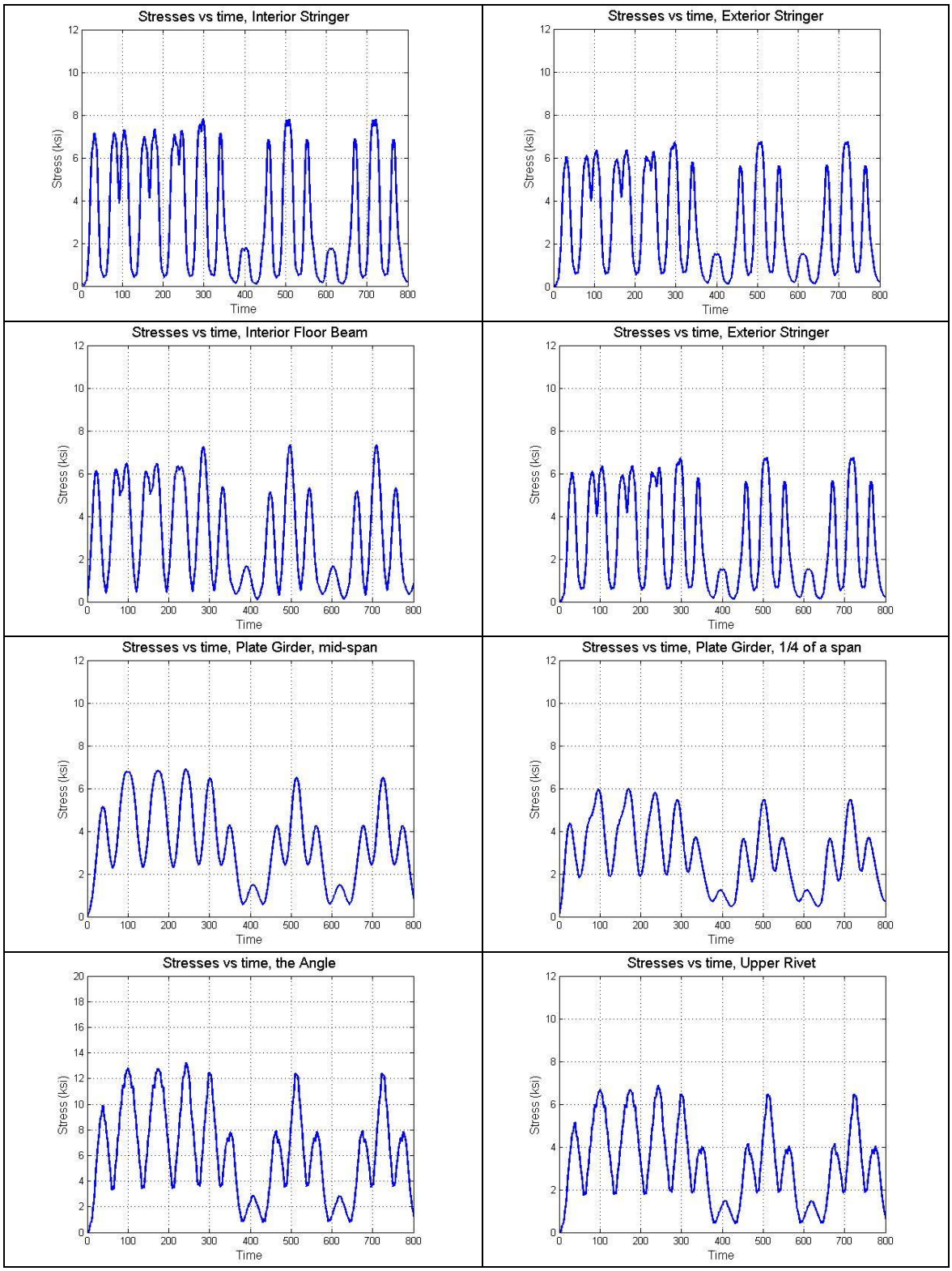

Figure F.8 Line graphs of part of stress-time histories for individual components of Bridge #2 under Train 8

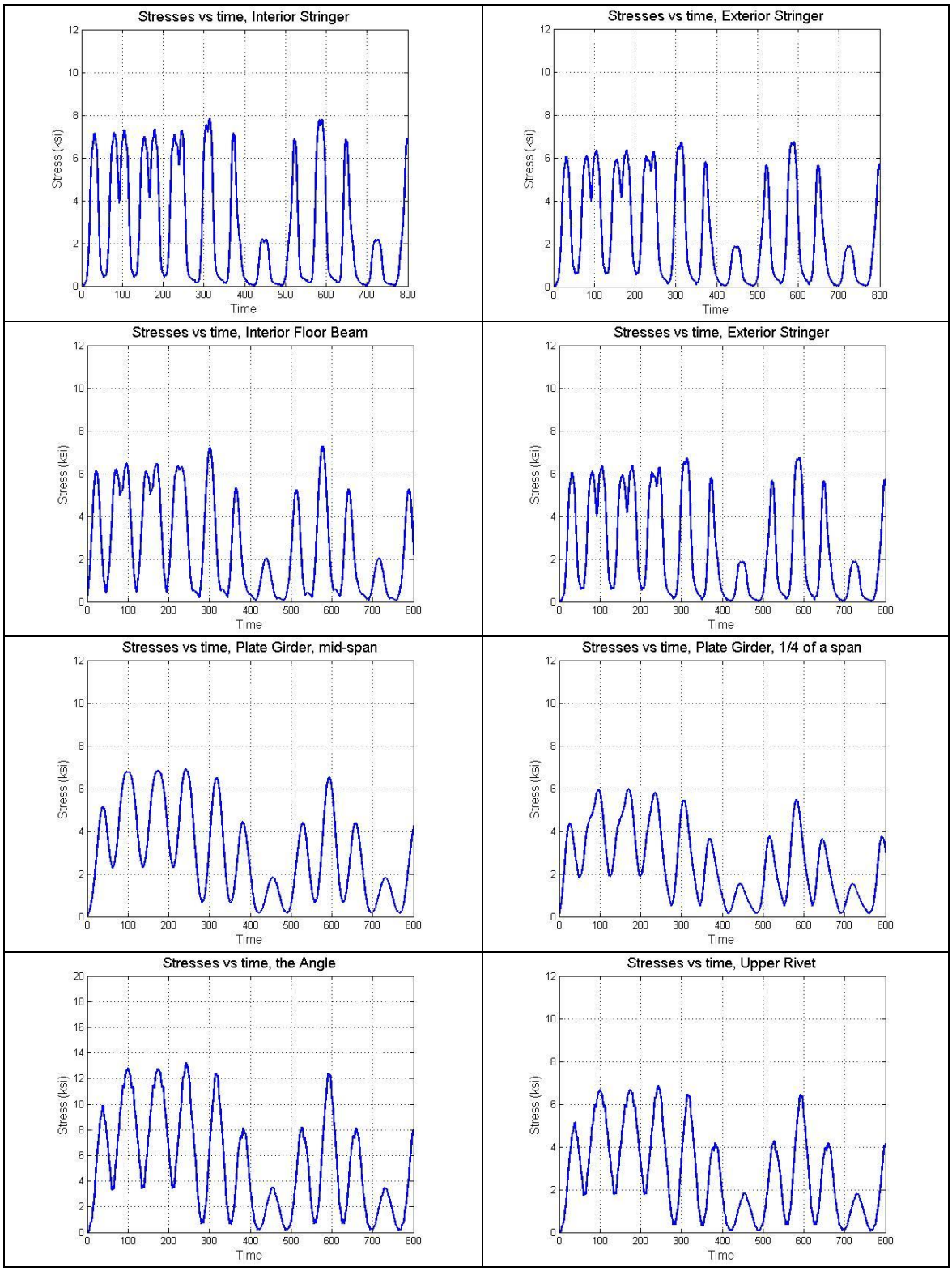

Figure F.9 Line graphs of part of stress-time histories for individual components of Bridge #2 under Train 9

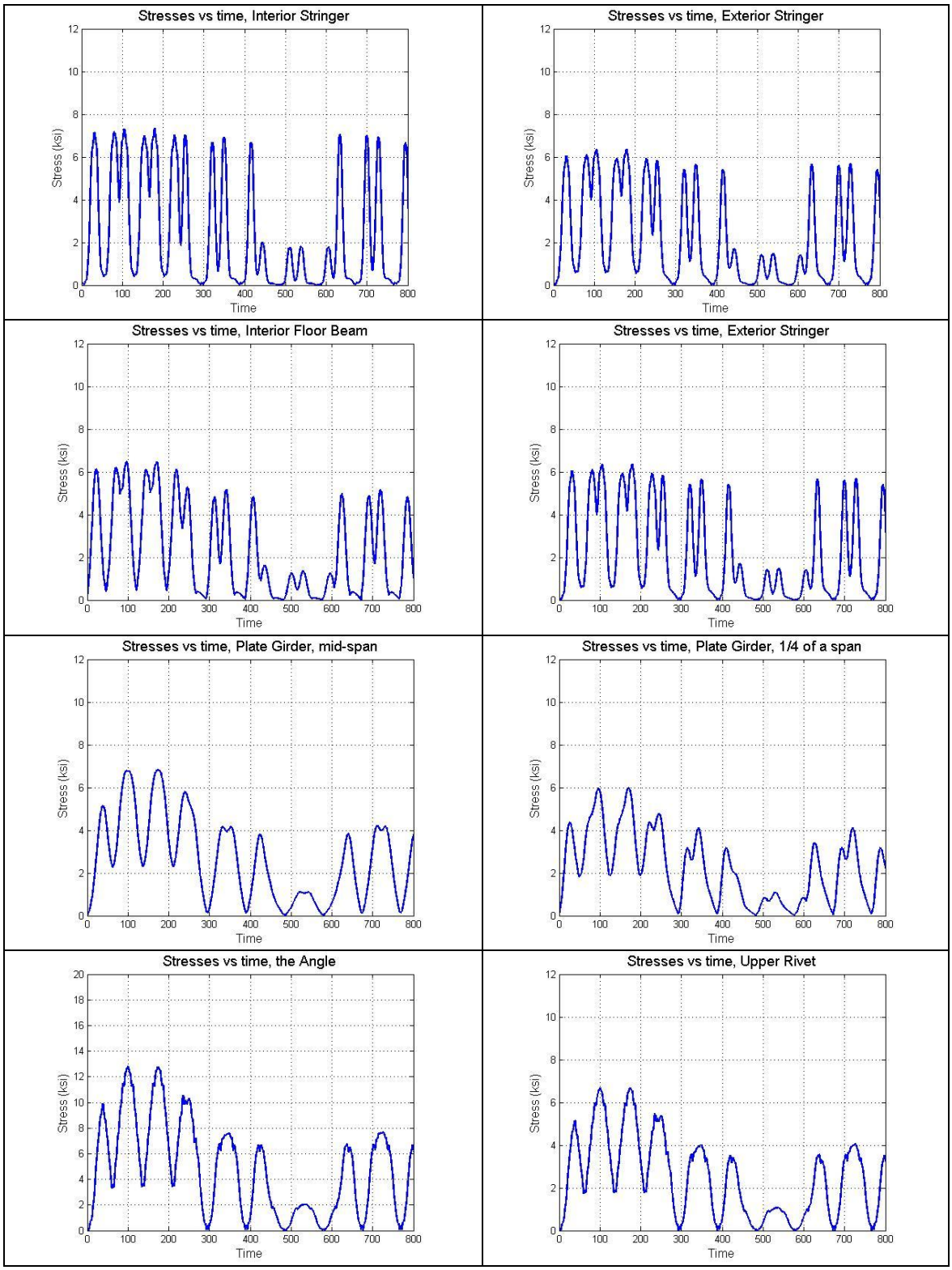

Figure F.10 Line graphs of part of stress-time histories for individual components of Bridge #2 under Train 10

Statistical parameters of resistance

Number of Monte Carlo simulations

$n := 10^6$

$i := 0..n-1$

1. Cross-section (positive moment)

1.1. Girder

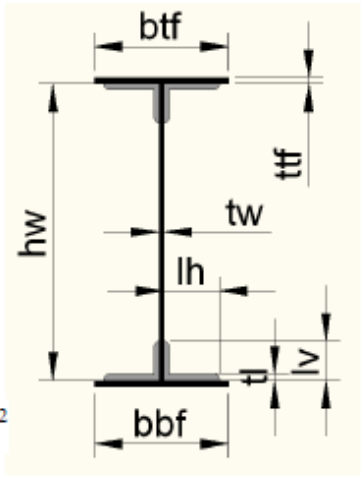

$h_w := 1000mm$

$t_w := 10mm$

$b_{tf} := 250mm$

$b_{bf} := 250mm$

$t_{tf} := 30mm$

$t_{bf} := 30mm$

$a_h := 90mm$

$a_v := 90mm$

$t_a := 10mm$

$y_a := 0mm$

$A_{sl} := (a_h + a_v - t_a) \cdot t_a$

$A_{sl} = 1.7 \times 10^3 \cdot mm^2$

$A_s := h_w \cdot t_w + b_{tf} \cdot t_{tf} + b_{bf} \cdot t_{bf}$

$A_s = 2.5 \times 10^4 \cdot mm^2$

$A_{stot} := A_s + 4 \cdot A_{sl}$

$A_{stot} = 3.18 \times 10^4 \cdot mm^2$

Spacing between girders

$S := 3.3m$

Span

$L := 10m$

1.3. Moment of inertia:

$A_1 := b_{tf} \cdot t_{tf}$ $\quad A_1 = 7.5 \times 10^3 \cdot mm^2$

$A_2 := h_w \cdot t_w$ $\quad A_2 = 1 \times 10^4 \cdot mm^2$

$A_3 := t_{bf} \cdot b_{bf}$ $\quad A_3 = 7.5 \times 10^3 \cdot mm^2$

$A_4 := (a_h - t_a) \cdot t_a$ $\quad A_4 = 800 \cdot mm^2$

$A_5 := a_v \cdot t_a$ $\quad A_5 = 900 \cdot mm^2$

$S_1 := A_1 \cdot \left(\frac{1}{2} \cdot t_{tf} + h_w + t_{bf}\right)$ $\quad S_1 = 7.837 \times 10^6 \cdot mm^3$

$S_2 := A_2 \cdot \left(\frac{1}{2} \cdot h_w + t_{bf}\right)$ $\quad S_2 = 5.3 \times 10^6 \cdot mm^3$

$S_3 := A_3 \cdot \left(\frac{1}{2} t_{bf}\right)$ $\quad S_3 = 1.125 \times 10^5 \cdot mm^3$

$S_4 := 2A_4 \cdot \left(h_w - \frac{1}{2} t_a + t_{bf}\right) + 2A_4 \cdot \left(\frac{1}{2} t_a + t_{bf}\right)$ $\quad S_4 = 1.696 \times 10^6 \cdot mm^3$

$S_5 := 2A_5 \cdot \left(h_w - \frac{1}{2} a_v + t_{bf}\right) + 2A_5 \cdot \left(\frac{1}{2} a_v + t_{bf}\right)$ $\quad S_5 = 1.908 \times 10^6 \cdot mm^3$

$S_n := S_1 + S_2 + S_3 + S_4 + S_5$ $\quad S_n = 1.685 \times 10^7 \cdot mm^3$

$$y_s := \frac{S_n}{A_{stot}} \qquad y_s = 530\cdot mm$$

$$I_{s1} := \frac{b_{tf}\cdot t_{tf}^3}{12} + \left(\frac{1}{2}\cdot t_{tf} + h_w + t_{bf} - y_s\right)^2\cdot A_1 \qquad I_{s1} = 1.99\times 10^9\cdot mm^4$$

$$I_{s2} := \frac{t_w\cdot h_w^3}{12} + \left(\frac{1}{2}\cdot h_w + t_{bf} - y_s\right)^2\cdot A_2 \qquad I_{s2} = 8.333\times 10^8\cdot mm^4$$

$$I_{s3} := \frac{b_{bf}\cdot t_{bf}^3}{12} + \left(\frac{1}{2}\cdot t_{bf} - y_s\right)^2\cdot A_3 \qquad I_{s3} = 1.99\times 10^9\cdot mm^4$$

$$I_{s4} := \frac{a_v\cdot t_a^3}{12} + \left(h_w - \frac{1}{2}t_a + t_{bf} - y_s\right)^2\cdot(2A_4) + \frac{a_v\cdot t_a^3}{12} + \left(\frac{1}{2}t_a + t_{bf} - y_s\right)^2\cdot(2A_4) \qquad I_{s4} = 7.841\times 10^8\cdot mm^4$$

$$I_{s5} := \frac{t_a\cdot a_v^3}{12} + \left(h_w - \frac{1}{2}a_v + t_{bf} - y_s\right)^2\cdot(2A_5) + \frac{t_a\cdot a_v^3}{12} + \left(\frac{1}{2}a_v + t_{bf} - y_s\right)^2\cdot(2A_5) \qquad I_{s5} = 7.465\times 10^8\cdot mm^4$$

$$I_n := I_{s1} + I_{s2} + I_{s3} + I_{s4} + I_{s5} \qquad I_n = 6.343\times 10^9\cdot mm^4$$

2. Constructibility (AASHTO LRFD 6.10.3)

area of web $A_w := A_2$ $A_w = 1\times 10^4\cdot mm^2$

area of tension flange $A_{tf} := A_1$ $A_{tf} = 7.5\times 10^3\cdot mm^2$

area of compression flange $A_{cf} := A_3$ $A_{cf} = 7.5\times 10^3\cdot mm^2$

area of angle $A_a := A_4 + A_5$ $A_a = 1.7\times 10^3\cdot mm^2$

minimum yield strenght of flanges

$Nom_{fy} := 207MPa$

$\lambda_{fy} := 1.05$ material factor

$V_{fy} := 0.1$

$\mu_{fy} := \lambda_{fy}\cdot Nom_{fy} \qquad \mu_{fy} = 217.35\cdot MPa$

$\sigma_{fy} := V_{fy}\cdot\mu_{fy} \qquad \sigma_{fy} = 21.735\cdot MPa$

$f_y := rnorm\left(n, \frac{\mu_{fy}}{MPa}, \frac{\sigma_{fy}}{MPa}\right)\cdot MPa \qquad mean(f_y) = 217.341\cdot MPa$

minimum yield strenght of web

$Nom_{fyw} := 207MPa$

$\lambda_{fyw} := 1.05$ material factor

$V_{fyw} := 0.10$

$\mu_{fyw} := \lambda_{fyw}\cdot Nom_{fyw} \qquad \mu_{fyw} = 217.35\cdot MPa$

$\sigma_{fyw} := V_{fyw}\cdot\mu_{fyw} \qquad \sigma_{fyw} = 21.735\cdot MPa$

$$f_{yw} := \text{rnorm}\left(n, \frac{\mu_{fyw}}{MPa}, \frac{\sigma_{fyw}}{MPa}\right)\cdot MPa \qquad \text{mean}(f_{yw}) = 217.366\cdot MPa$$

minimum yield strenght of angle

$Nom_{fya} := 207\,MPa$

$\lambda_{fya} := 1.1$ material factor

$V_{fya} := 0.11$

$\mu_{fya} := \lambda_{fya}\cdot Nom_{fya} \qquad \mu_{fya} = 227.7\cdot MPa$

$\sigma_{fya} := V_{fya}\cdot \mu_{fya} \qquad \sigma_{fya} = 25.047\cdot MPa$

$$f_{ya} := \text{rnorm}\left(n, \frac{\mu_{fya}}{MPa}, \frac{\sigma_{fya}}{MPa}\right)\cdot MPa \qquad \text{mean}(f_{ya}) = 227.688\cdot MPa$$

3. Strenght Limit State (AASHTO LRFD 6.10.6)

top flange	$P_t := f_y\cdot A_{tf}$	$\text{mean}(P_t) = 1.63\times 10^3\cdot kN$
bottom flange	$P_b := f_y\cdot A_{cf}$	$\text{mean}(P_b) = 1.63\times 10^3\cdot kN$
web	$P_w := f_{yw}\cdot A_w$	$\text{mean}(P_w) = 2.174\times 10^3\cdot kN$
angle	$P_a := f_{ya}\cdot A_a$	$\text{mean}(P_w) = 2.174\times 10^3\cdot kN$

Plastic Neutral Axis

Given

$d_{tf}(y) := \frac{1}{2}t_{tf} + h_w + t_{bf} - y \text{ simplify} \rightarrow 1045\cdot mm - y$

$d_w(y) := \frac{1}{2}h_w + t_{bf} - y \text{ simplify} \rightarrow 530\cdot mm - y$

$d_{bf}(y) := \frac{1}{2}t_{bf} - y \text{ simplify} \rightarrow 15\cdot mm - y$

$d_{ta}(y) := h_w - y_a + t_{bf} - y \text{ simplify} \rightarrow 1030\cdot mm - y$

$d_{ba}(y) := y_a + t_{bf} - y \text{ simplify} \rightarrow 30\cdot mm - y$

$P_t\cdot d_{tf}(y) + P_b\cdot d_{bf}(y) + P_w\cdot d_w(y) + 2\cdot P_a\cdot d_{ta}(y) + 2\cdot P_a\cdot d_{ba}(y) = 0$

$y := \text{Find}(y) \rightarrow 530.0\cdot mm$

$\text{mean}(y) = 20.866142\cdot in$

$d_{tf_i} := \left|\frac{1}{2}t_{tf} + h_w + t_{bf} - y\right| \qquad \text{mean}(d_{tf}) = 515\cdot mm$

$d_{w_i} := \left|\frac{1}{2}h_w + t_{bf} - y\right| \qquad \text{mean}(d_w) = 0\cdot mm$

$$d_{bf_i} := \left| \frac{1}{2} t_{bf} - y \right| \qquad \text{mean}(d_{bf}) = 515 \cdot \text{mm}$$

$$d_{ta_i} := \left| h_w - y_a + t_{bf} - y \right| \qquad \text{mean}(d_{ta}) = 500 \cdot \text{mm}$$

$$d_{ba_i} := \left| y_a + t_{bf} - y \right| \qquad \text{mean}(d_{ba}) = 500 \cdot \text{mm}$$

$$M_{p_i} := \frac{1}{2} \cdot \left(P_{t_i} \cdot d_{tf_i} + P_{w_i} \cdot d_{w_i} + P_{b_i} \cdot d_{bf_i} + 2 \cdot P_{a_i} \cdot d_{ta_i} + 2 \cdot P_{a_i} \cdot d_{ba_i} \right) \qquad \text{mean}(M_p) = 1.227 \times 10^3 \cdot \text{kN} \cdot \text{m}$$

$$\text{Nom}_{Mn} := 1.151 \times 10^3 \ \text{kN} \cdot \text{m}$$

$$\lambda_{Mp_i} := \frac{M_{p_i}}{\text{Nom}_{Mn}} \qquad \text{mean}(\lambda_{Mp}) = 1.066$$

$$\text{stdev}(\lambda_{Mp}) = 0.082$$

$$V_\lambda := \frac{\text{stdev}(\lambda_{Mp})}{\text{mean}(\lambda_{Mp})} \qquad V_\lambda = 0.077$$

Profesional and fabrication factors was taken from Ellingwood, and the parameters are:

$$\lambda_P := 1.02 \qquad \lambda_F := 1.00$$

$$V_P := 0.06 \qquad V_F := 0.05$$

so parameters for resistance I calculate from fallowing formulas:

$$\lambda_R := \text{mean}(\lambda_{Mp}) \cdot \lambda_P \cdot \lambda_F$$

$$V_R := \sqrt{V_\lambda^{\,2} + V_P^{\,2} + V_F^{\,2}}$$

$$\lambda_R = 1.087$$

$$V_R = 0.109$$